NOVEL PRODRUGS AND SELF-ASSEMBLING NANOCARRIERS TO IMPROVE DRUG DELIVERY

A DISSERTATION IN
Pharmaceutical Sciences
and
Chemistry

Presented to the Faculty of the University
of Missouri - Kansas City in partial fulfillment of
requirements for the degree

DOCTOR OF PHILOSOPHY

By

ABHIRUP MANDAL

B.S. in Pharmacy, Manipal College of Pharmaceutical Sciences, Manipal University,
India 2013

Kansas City, Missouri
2018

PART I: DIPEPTIDE PRODRUG APPROACH TO IMPROVE INTESTINAL ABSORPTION OF LOPINAVIR

Abhirup Mandal, Candidate for the Doctor of Philosophy Degree

University of Missouri – Kansas City, 2018.

ABSTRACT

Lopinavir (LPV), a highly potent second-generation HIV-1 protease inhibitor, is currently indicated in HIV-1 infection. However, poor systemic exposure following oral LPV dosing is a major concern. One of the major factors limiting intestinal permeability is the high substrate affinity of LPV towards major drug efflux pumps such as P-gp and MRP2. To address these issues, a histidine-leucine-LPV (His-Leu-LPV) dipeptide prodrug was synthesized and evaluated. His-Leu-LPV was identified by 1H-NMR and LCMS/MS techniques. Aqueous solubility generated by this prodrug was markedly higher relative to unmodified LPV. Importantly, His-Leu-LPV displayed significantly lower affinity towards P-gp and MRP2 as evident from higher uptake and transport rates. [3H]-GlySar and [3H]-L-His uptake receded to approximately 30% in the presence of His-Leu-LPV supporting the PepT1/PHT1 mediated uptake process. A steady regeneration of LPV and Leu-LPV in Caco-2 cell homogenates indicated His-Leu-LPV undergoes both esterase and peptidase-mediated hydrolysis. Based on these results, it appeared that histidine based dipeptide prodrug approach might be an alternative to improve LPV absorption across poorly permeable barriers such as intestinal and blood-brain barriers (BBB).

PART II: NANOFORMULATIONS TO IMPROVE OCULAR DELIVERY OF CIDOFOVIR AND OCTREOTIDE

Abhirup Mandal, Candidate for the Doctor of Philosophy Degree

University of Missouri – Kansas City, 2018.

ABSTRACT

Cidofovir (CDF) has demonstrated significant antiviral activity against cytomegalovirus (CMV) and is indicated for the treatment of CMV retinitis. Nonetheless, high water solubility of CDF limits its absorption through passive transcellular transport. While repeated intravitreal (IVT) injections leads to serious adverse events, back of the eye delivery after topical application remains a major challenge. Therefore, a prodrug containing C12 (twelve carbon chain length) lipid linker and biotin (ligand) for targeting sodium dependent multivitamin transporter (SMVT) was formulated with polymeric nanomicelles for topical application. Apart from serving as an inert nanocarrier for hydrophobic therapeutic agents, polymeric nanomicelles being extremely small in size promotes circumvention of mononuclear phagocytic system (MPS) and efflux transporters thereby improving drug bioavailability. Therefore, we prepared polymeric nanomicelles using polyoxyethylene hydrogenated castor oil 40 (HCO-40) and octoxynol 40 (OC-40). In vitro release studies revealed that B-C12-cCDF-loaded nanomicelles released B-C12-cCDF at a faster rate in stimulated tear fluid in comparison to PBS. MTT and LDH assays demonstrated negligible cytotoxicity of B-C12-cCDF-loaded nanomicelles relative to CDF and B-C12-cCDF in D407 (retinal pigment epithelial), SV-40 (immortalized human corneal epithelial) and CCL 20.2 (conjunctival epithelial) cells. Confocal laser scanning microscopy and flow cytometry analyses indicated that B-C12-cCDF-loaded nanomicelles were efficiently internalized into D407 and SV-40 cells in contrast to CDF and B-C12-

cCDF. Moreover, little B-C12-cCDF was also observed in the nuclei after 24 h of incubation. Polymeric nanomicelles carrying the transporter targeted prodrug did not produce any cytotoxic effects and were internalized into the cells effectively. Permeability experiments across SV-40 cells further confirmed significant transport of prodrug loaded nanomicelles and their subsequent uptake into D407 cells. These findings indicate that HCO-40/OC-40 based polymeric nanomicelles could become a promising topical delivery system for ocular administration of anti-viral agents.

Additionally, octreotide, a somatostatin peptide analogue is a promising therapeutic agent for treating proliferative diabetic retinopathy (PDR) by the activation of pituitary somatostatin receptor (SSTR) and inhibition of the GH-insulin-like growth factor (IGF)-1 axis. However, delivery related issues such as short half-life, low stability due to hydrophilicity, high molecular weight and minimal permeability across blood-retinal barrier are some of the major concerns. To overcome these challenges, we developed self-assembling multi-layered nanomicelles composed of two polymers, HCO-40 and OC-40 designed to combine hydrophilic interaction and solvent induced encapsulation of peptides and proteins. HCO-40 and OC-40 polymers are employed to encapsulate peptides and proteins in the core of the organo-nanomicelles with chloroform as a dispersant. The individual organo-nanomicelles are further encapsulated with another layer of the same polymers leading to the formation of an aqueous stable amphiphilic nanomicellar solution. The size of the multi-layered nanomicelles ranged from ~16-20 nm with zeta potential close to neutral (~-2.44-0.39 mV). In vitro release studies revealed that octreotide loaded multi-layered nanomicelles released octreotide at much slower rate in STF (~27 days) compared to PBST (~11 days) in its native form. MTT assay demonstrated negligible toxicity of the multi-layered nanomicelles at lower concentrations in HRPE (Human retinal pigment epithelial, D407), CCL 20.2 (Human conjunctival epithelial) and RF/6A (rhesus choroid-

retinal endothelial) cells. This work demonstrates an efficient peptide delivery platform with significant advantages over existing approaches, as it does not require modification of the peptide, is biodegradable, has small size and a high loading capacity.

APPROVAL PAGE

The faculties listed below, appointed by the Dean of School of Graduate Studies, have examined the dissertation titled "Novel Prodrugs and Self-Assembling Nanocarriers to Improve Drug Delivery", presented by Abhirup Mandal, candidate for the Doctor of Philosophy degree, and hereby certify that in their opinion it is worthy of acceptance.

Supervisory Committee

Ashim K. Mitra, Ph.D., Committee Chair

Division of Pharmacology and Pharmaceutical Sciences

Kun Cheng, Ph.D.

Division of Pharmacology and Pharmaceutical Sciences

Zhonghua Peng, Ph.D.

Department of Chemistry

Russell B. Melchert, Ph.D., R.Ph

Division of Pharmacology and Pharmaceutical Sciences

Xiang-Ping Chu, M.D., Ph.D.

Department of Basic Medical Science

TABLE OF CONTENTS

LIST OF ILLUSTRATIONS

LIST OF TABLES

ACKNOWLEDGEMENTS

I would like to express my immense gratitude for my mentor Dr. Ashim K. Mitra for his exceptional support and motivation during my graduate studies. His guidance was critical in solving a number of scientific challenges. He pushed me to do better, to improve myself, and tested my limits not only as a student but as a whole person. I deeply appreciate him for encouragement and believing in me that helped me to develop critical thinking as an independent scientist. I would also like to extend my gratitude to members of my supervisory committee Drs. Kun Cheng, Xiang-Ping Chu, Russell B. Melchert and Zhonghua Peng for their constant support, discussions on my research and valuable critics on my dissertation. It is my honor to have such extraordinary scientists and researchers as a part of my supervisory committee. I am greatly thankful to Dr. Dhananjay Pal for providing me tremendous training, guidance and support with cell culture techniques, in vitro experiments in the laboratory and scientific discussions. I would also like to extend my appreciation to Mrs. Ranjana Mitra for her continuous support, creating friendly environment in the lab and motherly love during my stay at UMKC. I would like to thank Drs. Mitesh Patel, Nanda Mandava, Varun Khurana, Ravi Vaishya, Kishore Cholkar and Ankit Shah for teaching me several skill sets during the first few years of my Ph.D.

I am greatly thankful to Drs. Sulabh Patel, Mitan Gokulgandhi, Deep Kwatra, Sujay Shah, Animikh Ray, Anwesha Chatterjee, Ramya Vadlapatla, Aswani Dutt Vadlapudi and Rohit Singh Bisht for their valuable suggestions and constructive inputs for successful completion of my Ph.D. I am thankful to my colleagues Akshay Jain, Navid J. Ayon, Pratikkumar Patel, Bhagyesh Sarode, Ashutosh Barve, Mary Joseph, Hoang My Trinh, Vrinda Gote, Sadia Sikder and Vibhuti Agrahari for their timely help and creating such a cheerful environment in the lab throughout my studies. My deepest gratitude to Drs. Ankit Shah, Mitesh Patel and Varun Khurana for not only helping me in professional matters but

also for being persistent in encouraging, for believing in me, and for the many priceless memories along the way.

My heartfelt appreciation to all my close friends Shweta Sood, Rajvinder Kaur, Shivani Gargvanshi, Nitish Chaudhari, Parth Shah, Sameer Patil, Prajakta Kulkarni, Chandramouli Natrajan, Nadish Roy, Saima Subhami, Mohit Jaiswal, Subhradeep Bhar, Aninda Dey, Chayan Bhattacharya, Geetanjali Joshi, Saurabh Rathore and Pranjal Gupta for appreciating the positive influence on my life.

I sincerely appreciate constant support of Joyce Johnson, Sharon Self, Norma Elizabeth Aguirre, Tamica Lige, Shana Eisentrager, Jane Poe, Jana Boschert in administrative assistance throughout my stay at UMKC. I would also like to thank all the faculty, staff and students of Division of Pharmacology and Pharmaceutical sciences for their valuable suggestions during my seminars and for creating a very friendly environment in our division. I would like to thank National Institute of Health and School of Graduate Studies for financial support.

My special gratitude towards my parents Anupama Mandal and Nepal Chandra Mandal and brother Abhishek Mandal for their constant motivation, encouragement and understanding me during my hard times. From weakness to strength, from grass to grace and from nothing to something, the knowledge they have imparted to me has been a great asset throughout my career. Without the inspiration, drive, and support that they have given me, I might not be the person I am today!

Dedicated to My Family

PART I: DIPEPTIDE PRODRUG APPROACH TO IMPROVE INTESTINAL ABSORPTION OF LOPINAVIR

CHAPTER 1

1. EXPANDING ROLE OF PRODRUGS IN HIV/AIDS THERAPY

1.1. Rationale

Prodrug based delivery approaches have been extensively employed to improve pharmacokinetic, pharmaceutical and physicochemical profiles of small molecules. Prodrugs are usually produced by chemically modifying the parent drug with small targeting or non-targeting moieties. In most cases, these compounds are biologically inactive and need chemical and/or enzymatic biotransformation *in vivo* to regenerate parent drug for desired pharmacological response. Depending on the type of the prodrug, nature of the linkage and pro-moiety (targeting vs non-targeting), the rate and site of reversion may be optimized [7-8]. In general, the major principle behind prodrug design and development is to optimize pharmacokinetic properties and improve drug specificity and selectivity. This process in turn promotes drug bioavailability and minimizes unacceptable drug-related toxicities. In the last decade, considerable attention has been paid to the development of prodrugs for improving drug delivery and efficacy. During 2000 to 2008, prodrugs constituted one-fifth of the total approved small molecule drugs [9]. Currently, prodrugs represent about 10% of the clinically available therapeutic agents [9]. Moreover, extensive efforts have been directed in preclinical stages to develop various types of prodrugs capable of generating superior efficacy. In this chapter, an attempt has been made to understand the prevalence and life cycle of HIV-1, challenges associated with current therapeutic regimens and the role of prodrugs.

1.2. Prevalence of acquired immunodeficiency syndrome (AIDS)

AIDS is a life threatening condition triggered by human immunodeficiency virus (HIV-1). HIV-1 invades the body's immune system, specifically the CD4+ T cells, which are

responsible for maintaining the integrity of the immune system to fight off infections. Over time, HIV-1 depletes CD4+ cells to an extent, where a person is more likely to get other opportunistic infections or infection related cancers [10]. Eventually the weak immune system fails to resist secondary infections and diseases, leading to the last stage of the HIV-1 infection, AIDS [11].

HIV/AIDS continues to be a major global public health issue. More than 36.7 million people worldwide were living with HIV/AIDS at the end of 2016 (Figure 1-1). Of these, 2.1 million were children (<15 years old). According to The Joint United Nations Programme on HIV/AIDS (UNAIDS); an estimated 1.8 million individuals worldwide became newly infected with HIV in 2016 – about 5,000 new infections per day. Importantly, 1.1 million adults and adolescents have been estimated to be living with HIV in the United States in 2016. Of those, approximately 18,160 people received an AIDS diagnosis and 6,721 deaths were reported in 2014 due to HIV-related illness [12-13].

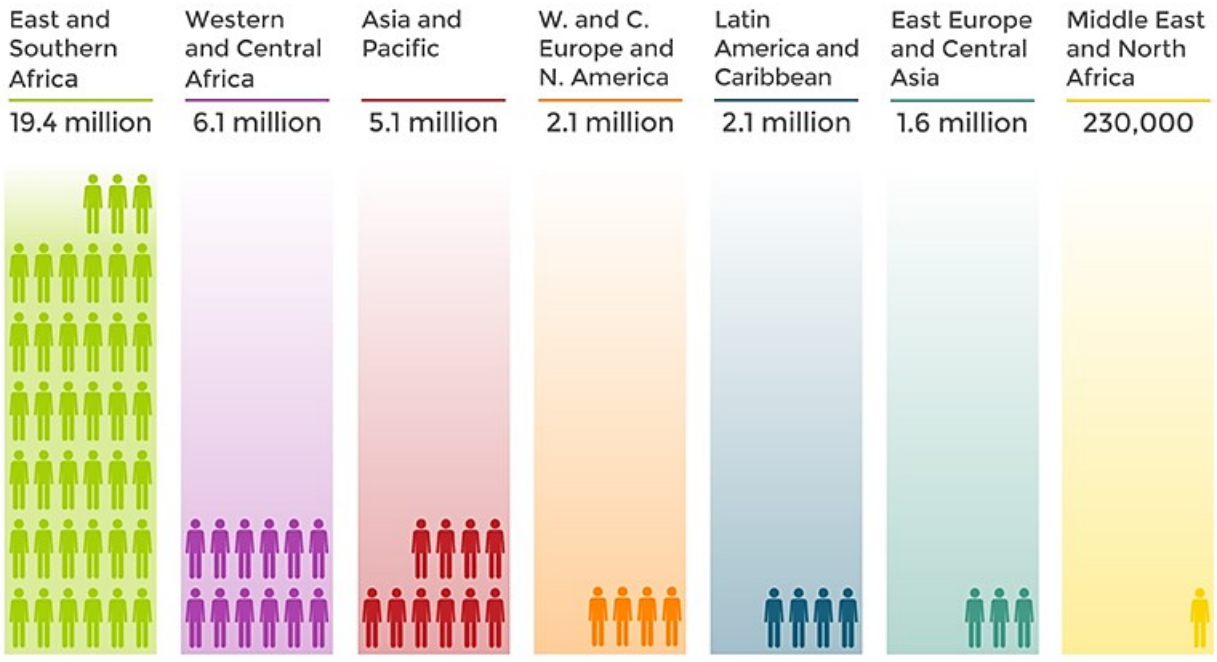

Figure 1-1 Number of people living with HIV in 2016 (UNAIDS Data 2017)

1.3. HIV virus structure and function

HIV type 1 (HIV-1) is an enveloped retrovirus belonging to the lentivirus sub family. It consists of two identical single stranded ribonucleic acid (RNA) molecules in the core of the virus particle, which are reverse transcribed to DNA by the reverse transcriptase enzyme following infection into the host cell [14]. While the genome (a core of RNA) carries the genetic information of the virus, the capsid, a protein component surrounds and protects the genome giving the virus its shape. The HIV-1 genome includes nine distinct genes encoding for three structural proteins: capsid proteins (gag), polymerase gene proteins (pol) and envelope glycoproteins (env); four accessory proteins (Vif, Vpr, Nef and Vpu/p7) and two regulatory proteins (Rev and Tat) [4](Figure 1-2).

The gag gene encodes for the outer core membrane protein (MA, p17), the capsid protein (CA, p24), the nucleocapsid (NC, p7) and a nucleic acid-stabilizing protein (p6) [15-16]. The gag gene is followed by the pol gene, which codes for the enzymes protease (PR, p11), reverse transcriptase (RT, p51) and RNase H (p15) or RT plus RNase H (together p66) and integrase (IN, p31). Adjacent to pol gene, the env gene codes for the two-envelope glycoproteins gp120 (surface protein, SU) and gp41 (transmembrane protein. TM). Additionally, HIV genome codes for other regulatory proteins including Tat (transactivator protein) and Rev (RNA splicing-regulator) that are responsible for initiating HIV replication [17]. Regulatory proteins including Nef (negative regulating factor), Vif (viral infectivity factor), Vpr (virus protein R) and Vpu (virus protein unique) are involved in the promotion of viral replication, propagation, budding and pathogenesis [18]. The presence of Vpx (virus protein X) instead of Vpu in HIV-2 is partially responsible for its reduced pathogenicity [19-20].

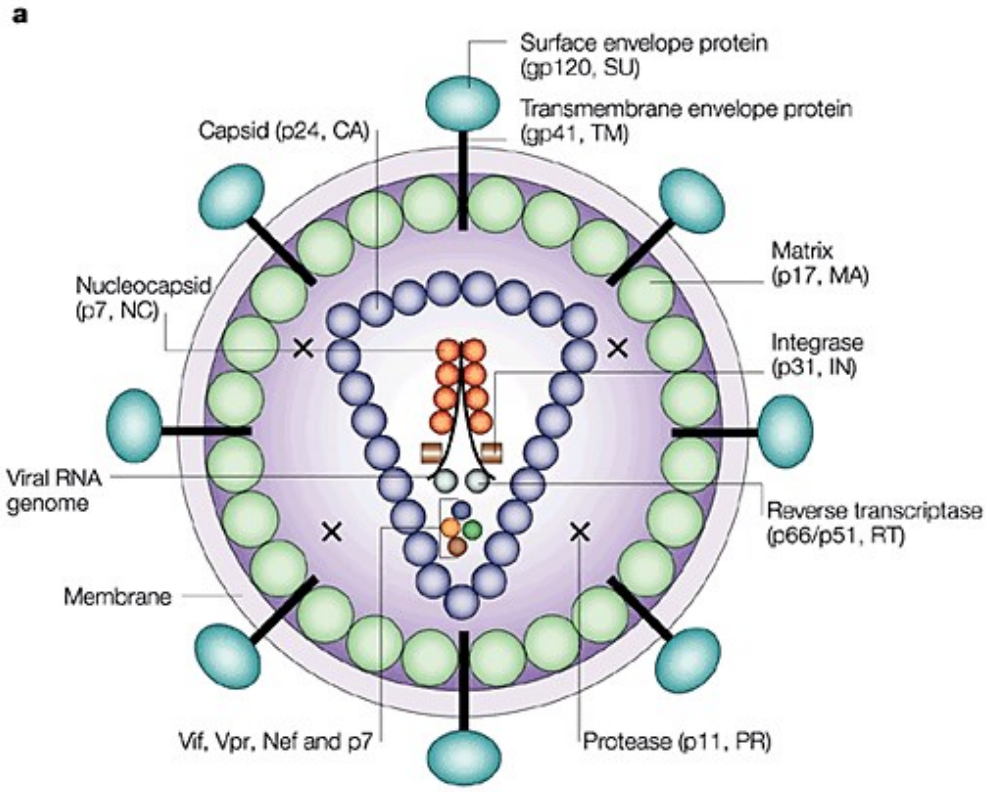

Figure 1-2 Structure of HIV-1 virus. Reporduced with permission from Robinson et al. [4]

1.4. Stages of HIV-1 life cycle

The first step of the HIV-1 replication cycle is the attachment of the viral Env glycoprotein to the CD4 cell surface proteins and a co-receptor {either CC-chemokine receptor 5 (CCR5) or CXC-chemokine receptor 4 (CXCR4)}. HIV-1 co-receptor antagonists can inhibit this process of viral attachment [21]. The second step involves the fusion of the viral and host cell membranes allowing viral capsid entry into the cell, which can be restricted by fusion inhibitors. Once inside the cell, the viral RNA genome is reverse transcribed to double-stranded DNA, which is further integrated into the host genome. Nucleoside analogue reverse transcriptase inhibitors (NRTIs) and non-nucleoside reverse transcriptase inhibitors (NNRTIs)

are generally utilized to inhibit the process of reverse transcription whereas integrase strand transfer inhibitors (InSTIs) and allosteric integrase inhibitors (ALLINIs) can inhibit the viral integrase [22]. Following successful integration, transcription of proviral components yields viral RNAs, which are further translated into viral proteins. Proteolytic processing of viral polyproteins yields mature virions that are capable of infecting new host cells. The maturation step can be blocked by the protease inhibitors which can eventually result in inhibition of reverse transcription and possibly other downstream processes in the HIV-1 life cycle [5](Figure 1-3).

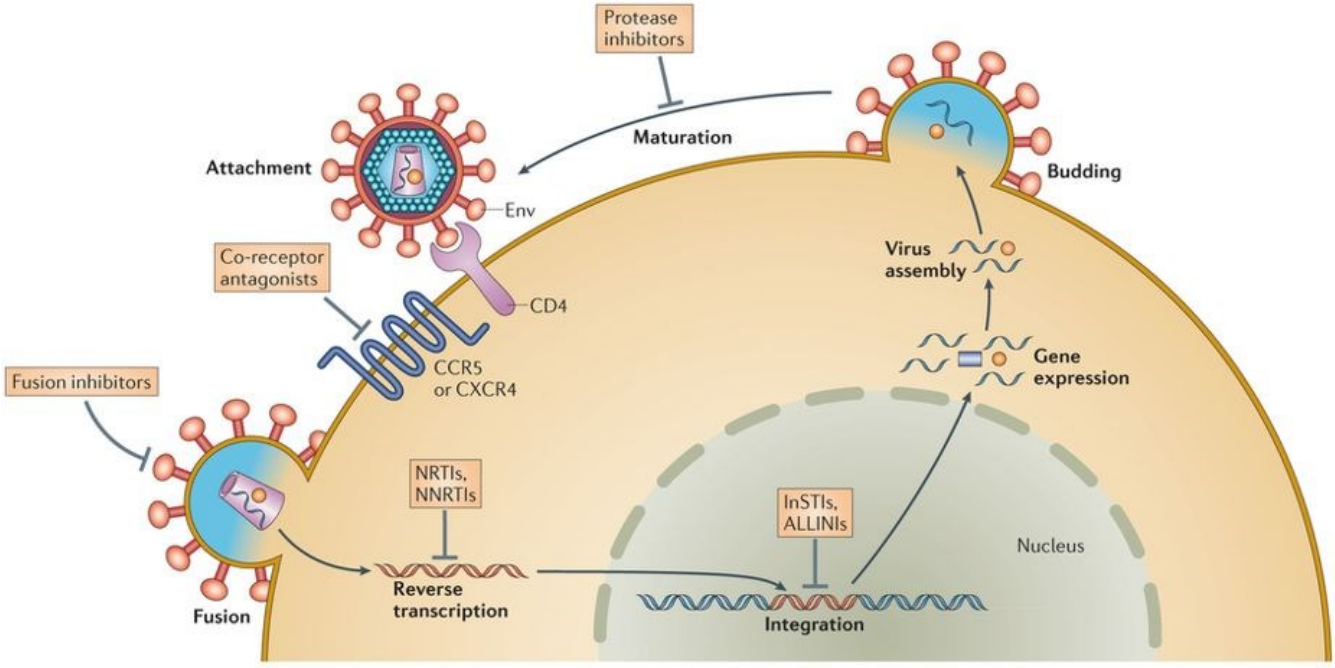

Figure 1-3 Stages of the HIV‑1 life cycle targeted by antiretroviral drugs. Reporduced with permission from Laskey et al. [5]

1.5. Lopinavir (LPV): current issues and challenges

LPV is a second-generation protease inhibitor with high specificity for HIV-1 protease. It is a hydrophobic compound (log P = 3.91) and a very good substrate of efflux proteins (P-

gp and MRP-2) and liver metabolizing enzymes (CYP3A4). LPV has been reported to generate poor oral bioavailability in rats, dogs and healthy volunteers when administered alone. Thus, it is commonly indicated in combination with ritonavir under the trade name Kaletra® for HIV-1 treatment [23]. Ritonavir is responsible for inhibiting the efflux pumps and hepatic metabolism and thus decreases LPV intrinsic clearance. However, such modulation of the endogenous expression and functionality of efflux proteins and/or metabolizing enzymes pose a greater risk of generating adverse side effects [24]. Additionally, the higher expression of efflux proteins on the luminal side of intestinal epithelial cells diminishes LPV intestinal absorption thereby reducing its therapeutic efficacy. A cumulative effect of oxidative metabolism by CYP3A4 and efflux proteins drastically lowers oral bioavailability of LPV.

In fact, LPV being practically insoluble in water is mostly administered in the form of approximately 40% v/v alcoholic solution. Such high alcoholic concentrations could lead to harmful adverse effects in pediatrics and adolescents [25]. Moreover, ethanol consumption has been reported to aggravate CPY3A4 metabolizing activity. Such escalation in CYP3A4 levels might contribute significantly in LPV metabolism and clearance.

1.6. Peptide prodrug approach

The additive effect of poor aqueous solubility and contribution of efflux proteins and CYP3A4 metabolizing enzymes result in low oral and brain bioavailability of LPV. Additionally, higher expression of efflux proteins including P-gp and MRP2 on the intestinal epithelium and the blood-brain barrier (BBB) presents a major challenge in the transport of LPV [26-27]. Hence, we propose to develop amino acid and peptide prodrugs of LPV. We hypothesize that these prodrugs will generate significantly improved systemic and brain concentrations of LPV. The ligand coupled prodrugs are anticipated to permeate intestinal

epithelial and brain capillary endothelial cells by efficiently binding and translocating via influx transporters and simultaneously evading the efflux pumps, P-gp and MRP-2. The hypothetical approach is depicted in Figure 1-4, where LPV, an excellent substrate for efflux pumps, is modified by conjugating a targeting moiety in order to target the membrane influx transporters (peptide and amino acid). The resulting peptide prodrug bypasses the efflux pumps and efficiently translocates across the membrane barriers.

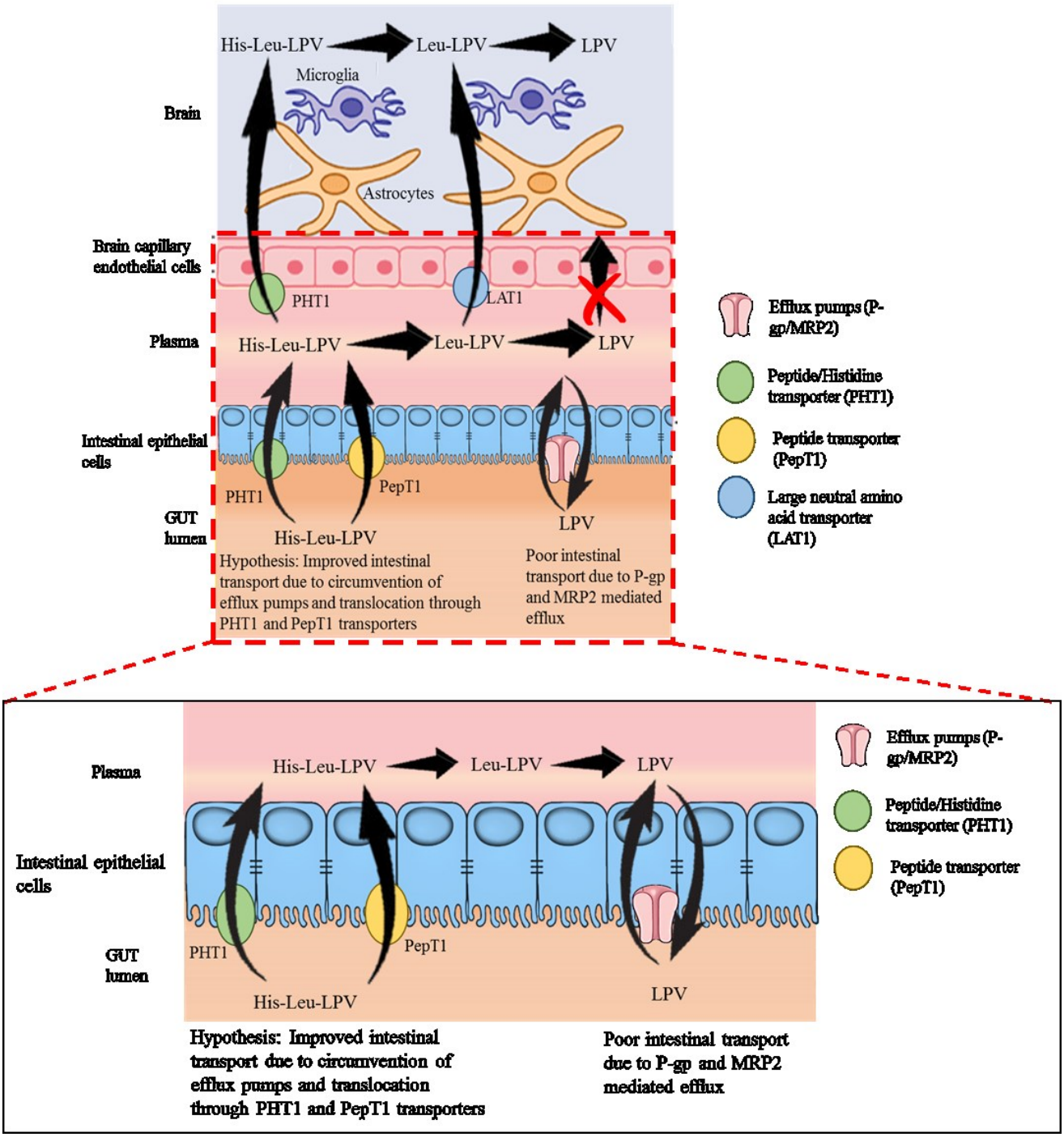

Figure 1-4 Hypothetical mechanisms involved in histidine peptide prodrug approach to improve oral and brain bioavailability, simultaneously

This strategy can also be called as histidine based peptide prodrug approach. Amino acids are selected such that they target specific influx transporters. In this approach, it is hypothesized that following oral administration, histidine based peptide prodrug will target specifically peptide/histidine (PHT1) and peptide influx transporters (PepT1) and simultaneously evade efflux pumps at intestinal epithelium. Such evasion of efflux proteins would allow improved concentration of peptide prodrug (His-Leu-LPV) in the systemic circulation where they may undergo enzymatic hydrolysis to regenerate finite amount of single amino acid prodrug (Leu-LPV) and the parent drug (LPV). Amino acid transporters (LAT1), highly expressed on the BBB, will further recognize systemically regenerated amino acid prodrug and will simultaneously assist in circumventing efflux pumps. Additionally, PHT1 transporters that are also expressed on the BBB can recognize the non-hydrolyzed histidine-peptide prodrug and allow significantly improved LPV transport across the BBB. The most critical advantage of the histidine based peptide prodrug over other peptide prodrugs is the ability to target more than one transporter at the same time expressed on different cell membranes (intestinal and brain capillary endothelial cells). Such targeting using amino acids may aid in circumventing efflux pumps highly expressed on these membranes and generate non-toxic by-products. Designing of such transporter targeted prodrugs capable of targeting two active transport processes, especially PHT1 which is exclusively expressed on the intestinal and brain endothelial cells represent a paradigm shift from traditional delivery approaches. The efflux and influx transporters described in the following chapter are considered especially in the design of such LPV prodrugs.

CHAPTER 2

2. ROLE OF TRANSPORTERS IN DETERMINING CELL PERMEABILITY IN DRUG DELIVERY

2.1. Rationale

Transporter studies for drug development and delivery is a rapidly growing field. It has contributed largely towards better understanding of cell permeability and drug disposition. So far more than 400 membrane transporters have been identified and classified into two major superfamilies: ATP-binding cassette (ABC) and solute carrier (SLC) [28]. Transporter expression, particularly in epithelia of intestine, liver and kidney as well as endothelium of blood-brain barrier are the major determinants of cell permeability which consequently impacts drug pharmacokinetics. Despite the progress, the field suffers from a limited range of integral assays for measuring permeability effects [29]. As a result, conflicting opinions are postulated regarding the importance of transporters on drug disposition.

Drug transport mainly involves three processes: absorption, distribution, and elimination of which diffusion through the bilayer membrane is considered to be the dominant process. Several theories have been proposed to date to understand the mechanism of drug absorption and distribution. Lipinski's rule of five (R05) is one such theory for predicting the permeability of orally administered drugs. The R05 rule states that orally active drugs cannot violate more than one of the following criteria: molecular mass < 500 Daltons, octanol-water partition coefficient log P < 5, number of hydrogen bond donors <5, number of hydrogen bond acceptors <10. These empirical guidelines assist formulators to assess molecular properties of drug molecules for transport of drug across biological membranes and disposition within different organs and tissues [30-31].

However, a few drug classes in spite of violating R05, are highly orally active. These drugs possess unique structural features that allow these molecules to be recognized as substrates by transporters expressed at various biological barriers. Several evidences of such accumulation of drugs are available. Enhanced intracellular uptake of prodrugs with targeting moieties as known substrates carriers have implicated prominent role of carrier-mediated uptake than is assumed to be [32-33]. For instance, Vadlapudi et al. synthesized biotin conjugated prodrugs of acyclovir for targeting sodium dependent multi-vitamin transporter expressed on the corneal epithelium [34].

Furthermore, several transporters belonging to ABC family are also responsible for drug elimination across brush border membrane of proximal tubule and canalicular membrane of hepatocytes. These efflux transporters are usually localized to intestine, liver, kidney, blood-brain barrier, and placenta and are primarily responsible for low absorption and poor drug bioavailability leading to drug resistance [35].

Numerous *in vivo* studies have demonstrated the vital role of transporters in drug disposition, therapeutic efficacy, drug-drug interactions, drug toxicity and adverse drug reactions. Animal models including knockout mice and human genetic variants have indicated the role of transporters in conjunction with drug metabolizing enzymes (DMEs) in drug disposition. Based on current research reports and clinical studies, US Food and Drug Administration (USFDA) has issued several guidelines for conducting research on drug interaction with transporters and metabolizing enzymes [36]. Despite substantial literature and guidance, pharmaceutical scientists are still facing difficulties in conducting *in vivo* studies concerning transporters and metabolizing enzymes in drug development and delivery. In particular, some of the concerns raised are: which transporters are clinically relevant in drug

absorption and disposition? What are the viable methods for studying *in vitro* drug interactions with transporters? What follow-up clinical studies should be conducted and what are the criteria to assess PK-PD relationships?

In this chapter, we will focus on the role of transporters on cell permeability with respect to substrate, inhibitor interactions with a special emphasis on efflux and influx transporters that are critical in the area of drug development and delivery.

2.2. Overview of drug transporters

A prerequisite for orally administered drugs to be effective is to smoothly cross a sequential series of barriers in the intestine, liver and kidney. Systemic bioavailability of orally administered drugs is primarily considered to be a function of intestinal drug absorption and subsequent phase I metabolism in the liver. However, human intestine has been recognized to be a major contributor to first pass extraction. Both influx and efflux transporters primarily belonging to ABC and SLC transporter family are abundantly expressed in human intestine [37]. Additionally, presence of these transporters in kidney also contributes to transport and/or clearance of orally administered drugs. Apart from these barriers, CNS drugs pose further challenge due to the complexity of brain and presence of the blood-brain barrier [38]. Thus, drug transporters are of escalating interest in identifying their role in influencing drug permeability across biological barriers and pharmacokinetics. Figure 2-1 illustrates the localization of various transporters in intestinal lumen, hepatocytes, kidney proximal tubules, brain capillary endothelial cells and tumor and ocular tissues. Table 2-1 summarizes various substrates and inhibitors of efflux transporters, which have been identified in literature to date.

The two major processes involving drug-passage across membranes are carrier-mediated transport and passive diffusion. Carrier-mediated transport can be categorized into: facilitated and active mechanisms. Facilitated transport occurs when nutrients such as glucose, urea and amino acids permeate a bio-membrane without coupling to the breakdown of ATP down the electrochemical gradient. In contrast, active transport involves energy coupling mechanisms to transport molecules against the concentration gradient. It can be either primary which involves energy from ATP hydrolysis or secondary which utilizes previously generated energy by dissipation of ion gradients via ion pumps [39].

2.2.1. Efflux transporters: ATP binding cassette transporters (ABC)

ABC family of efflux transporters are one of the first identified and most investigated transporters expressed at the apical membranes of intestine, liver, kidney and the blood-brain barrier[27]. These include P-glycoprotein (P-gp), multidrug resistance-associated protein (MRP) and breast cancer resistance protein (BCRP). These transporters are expressed abundantly on the apical membranes of these organs in contrast to basolateral side. However, there are several isoforms of MRP (i.e., MRP1, MRP3-MRP6) that are expressed on the basolateral surface of intestine[40]. These transporters play an important role in limiting the absorption of a wide variety of clinically important and frequently prescribed drugs. In fact, intestinal, biliary and urinary secretions of drugs like statins, antibiotics, immuno-suppressants, anti-cancer and cardiovascular drugs are majorly affected by these efflux transporters[41]. Additionally, brain absorption of CNS drugs including HIV protease inhibitors are limited due to the presence of these efflux transporters at the blood-brain barrier. Recently the presence of efflux transporters has been quantified in various organs. Expression and functionality of these efflux proteins can be modulated by various agents which can simultaneously serve as substrate and/or inhibitor

of more than one efflux transporters. Such modulation can lead to altered pharmacokinetics of a broad range of therapeutic agents [42-44]. Moreover, age and sex differences in the expression of transporters are thought to be important determinants accounting for individual disparity in transporter expression. Several transporter genes including ABCA5, ABCB6, MRP1, MRP5, OST-beta, ATP2B2, SLC10A1, SLC6A16, SLC22A12, SLC22A9, SLC31A1, SLC31A2, SLC35F5, SLC43A1, SLC4A1AP, SLC5A10, SLC5A6, and SLC16A11 are highly expressed in males compared to females [45]. Sex differences are also exhibited by the serotonin 5- HT1A receptor and serotonin transporter (5-HTT), a target for psychotic drugs. Women exhibit significantly higher 5-HT1A receptor and lower 5-HTT binding potentials thereby contributing to sex differences in psychiatric disorders [46]. Additionally, transporter genes, ATP7B and SLC9A1 exhibit higher expression in females compared to males. However, few genes (ABCB1, SLC22A2, and SLC25A13) are found to be similarly expressed in both sexes. Aging is another critical factor governing the expression of transporters. Joseph et al. have reported the mRNA expression levels of MRP5, OST-Beta, SLC22A9, SLC31A1, SLC31A2, SLC35F5, SLC43A1, SLC4A1AP, SLC5A6, and SLC16A11 to be higher in age $\geq$ 50 years compared to age <50 years. While, MRP1, MRP5, SLC10A1, SLC6A16, SLC22A2, SLC22A12, and SLC25A13 mRNA expression levels were found to be higher in age <50 years compared to age $\geq$ 50 years, a few of them (ABCA5, ABCB1, ABCB6, SLC5A10, and SLC9A1) were similarly expressed in both age groups.

2.2.1.1. Permeability-glycoprotein (P-gp; ABCB1)

P-gp also known as multi-drug resistance protein 1 (MDR1) is the most important and abundantly expressed efflux transporter on the apical membrane of intestine, liver, and kidney. This efflux pump primarily utilizes ATP as energy source to export xenobiotics back into the

intestinal lumen. It can also expel drugs from hepatocytes to bile ducts. Moreover, this pump can excrete drugs from kidney proximal tubules into urinary ducts and from capillary endothelial cells back into capillaries[47]. The primary isoforms of MDR are abbreviated as mdr1 (a and b) and mdr2/3 in rodents. The class I isoform (mdr1/ABCB1) is largely responsible for drug transport while the class II isoform (mdr2/3/ABCB4) is accountable for efflux of phosphatidylcholine into the bile[48]. Numerous studies have demonstrated the broad substrate specificity of P-gp particularly for hydrophobic and amphipathic molecules. Multiple binding sites on P-gp for substrates/inhibitors have been identified[49]. Hydrogen bonding and partitioning in lipoid membrane are usually the rate-limiting steps [50]. Seelig et al. have reported a general pattern of P-gp recognition by analyzing more than a hundred known substrates [51]. Well-defined electron donor groups (recognition elements) are generally prerequisite for a substrate for P-gp binding. These recognition elements are classified into two groups i.e. Type I and II. Type I units demonstrate two electron donor groups with a spatial separation of 2.5 ± 0.3 Å whereas type II units display two or three electron donor groups with a spatial separation of 4.6 ± 0.6 Å. According to the type and number of recognition elements, drugs can be classified as weak, strong and non-substrates. A series of clinically important drugs including statins (simvastatin lactone, atorvastatin, lovastatin lactone), antibiotics (dicloxacillin, fluoroqinolones, ivermectin), anti-cancer agents (doxorubicin, prazosin, reserpine), anti-HIV agents (indinavir, nelfinavir, saquinavir, darunavir, lopinavir, zidovudine, lamivudine, tipranavir, maraviroc, dolutegravir, raltegravir), tacrolimus, hydrocortisone, talinolol, fexofenadine, colchicine, loperamide, aldosterone, dibucaine and temocapril are known substrates of P-gp. P-gp inhibitors include various immunosuppressive agents and other well-known compounds such as SDZ, PSC833, GF120918 and LY335979[35]. Additionally, statins

(atorvastatin), fluoroquinolones, cyclosporine, quinidine, verapamil and several anti-HIV agents (abacavir, rilpivirine, atazanavir, ritonavir, cobicistat) have shown to inhibit P-gp activity (Table 2-1). In vitro studies have successfully demonstrated the effects of substrates/inhibitors on P-gp. Oral co- administration of doxorubicin with verapamil, resulted in an increase in plasma peak level, elimination half-life, and volume of distribution of doxorubicin [48]. Several factors such as environmental stress, hormones, cell-culture conditions and xenobiotics including rifampicin, St. John's wort, atazanavir, nelfinavir and amprenavir can also induce P-gp transporter expression. One of the most recognized P-gp induction interactions is the co-administration of rifampin with digoxin. A significant reduction in AUC of oral digoxin is further confirmed by a 3.5-fold increase in P-gp expression [52]. Among in vivo studies, mice deficient in mdr1a or mdr1a/b have been selected as powerful models for determining the role of P-gp. Hendrikse et al. demonstrated 7.7 fold-higher accumulation of 11-C-verapamil in mdr1a (-/-) mice relative to mdr1a (+/+) mice. While, 11-C-verapamil accumulation elevated by 5.3 fold in mdr1a (+/+) mice in presence of cyclosporine (P-gp inhibitor), no such increase was reported for mdr1a (-/-) mice [53]. Additionally, studies conducted by Sasongko et al. have shown approx. 2-fold (88 ± 20%) larger AUC brain/AUC blood of 11C-verapamil accumulation in human in the presence of cyclosporine [54].

2.2.1.2. Multidrug resistance-associated protein (MRP; ABCC2)

Until now, nine members have been identified within the MRP family. Among these, MRPs 1-5 can play a significant role in cell permeation. MRPs are mainly responsible for the extrusion of lipophilic, amphipathic anionic molecules[55]. Although, MRP's 1-5 are expressed either on basolateral or apical membranes, MRP2 is considered to be the most abundantly expressed transporter on the apical membrane acting as a major barrier to drug absorption[56].

Clinical importance of MRP2 is attributed to its ability to modulate the pharmacokinetics of various drug molecules [57]. MRP2 was shown to mediate the transport of statins (pravastatin), ceftriaxone, ampicillin, grepafloxacin, vinblastine, irinotecan, SN-38, methotrexate, 7-hydroxymethotrexate, ezetimibe, fosinopril and anti-HIV agents including lopinavir and darunavir[35]. Some other substrates include fexofenadine, sulfasalazine and colchicine. In addition, activity and expression are altered by certain compounds and disease states [58]. Some examples of MRP2 inhibitors include cyclosporine, probenecid, furosemide, ritonavir, saquinavir, lamivudine, abacavir, cidofovir, emtricitabine, adefovir, tenofovir, efavirenz, delavirdine and MK-571. A study conducted by Shibayama et al. demonstrated reduced MRP2 expression levels after induction of cholestasis by 5-FU in vitro [59]. Approximately 3-fold enhanced permeability coefficient (Peff) of sulfasalazine was reported in a recent study following in situ perfusion to rat jejunum in presence of MK-571 (MRP2 inhibitor) [55]. Additionally, Vlaming et al. demonstrated 1.8-fold higher plasma AUC in Mrp2-/- mice (1345 ± 207 versus 734 ± 81 min ·μg/ml) after i.v. administration of [3H] methotrexate (50mg/kg), indicating Mrp2-/- mouse model to be a valuable tool in determining impact of Mrp2 on the disposition of drugs and other toxins [60]. Recent studies have also indicated the efficacy of spironolactone and 1, 25(OH) 2D3 in inducing Mrp2 transporter expression in rats [61].

2.2.1.3. Breast cancer resistance protein (BCRP; ABCG2)

BCRP, a multidrug resistance protein is a member of ABC class of efflux transporters and is also known as “half ABC transporter”. It is primarily expressed on the apical membrane of intestine, liver, kidney and the blood-brain barrier. This efflux protein also plays a vital role in limiting oral as well as brain bioavailability of a broad range of therapeutic agents. The human intestine expresses higher BCRP mRNA levels than any other efflux transporter.

Overlapping substrate specificity of BCRP with P-gp results into a synergistic cumulative effect of the efflux transporters further limiting the absorption of therapeutic agents across various barriers. BCRP transports a highly diverse range of substrates including statins, fluoroquinolones, ciprofloxacin, anti-cancer agents (imatinib, methotrexate, mitoxantrone, SN-38, topotecan, irinotecan, doxorubicin, daunorubicin, gefitinib, tandutinib, ezetinib, lapatinib), cardiac agents (prazosin, dipyridamole) and anti-HIV agents (zidovudine, lamivudine, efavirenz)[35]. Other substrates include glyburide, sulfasalazine and temocapril (Table 2-1). Polarized and non-polarized cell lines including membrane vesicles constitutively expressing BCRP have been utilized as a model for in vitro assays [62]. In vivo studies in Bcrp (-/-) mice demonstrated 10- and 110-folds rise in relative AUCs for topotecan and sulfasalazine respectively. Further studies in patients with solid tumors revealed an increase of approx. 2.5-fold in oral bioavailability and 3-fold in mean Cmax of topotecan in the presence of GF120918 (dual inhibitor of P-gp/BCRP) [63]. Known BCRP inhibitors include estrone, gefitinib, novobiocin, pantoprazole, GG918, cyclosporine, dipyridamole CI1033 and ritonavir[35]. Fumitremorgin C and Ko143 (FTC analog) selectively inhibit BCRP with no overlapping affinity for MRP1 or P-gp (Table 2-1). Efavirenz is a well-known inducer of BCRP and has been reported promote expression of BCRP in the rat intestine [64].

2.2.2. Influx transporters: Solute carrier transporters (SLC; SLCO)

The major influx transporters primarily responsible for xenobiotic transport belong to two solute carrier families: SLC and SLCO. While SLC family members are typically involved in the transport of Type I organic anions, cations and zwitter ions, the SLCO family members are responsible for the transport of Type II organic anions. The members of these families

utilize a variety of porter mechanisms such as uniporter, symporter and antiporter to transport a wide range of substrates including amino acids, vitamins, bile acids and other xenobiotics [65]. The SLC superfamily encompasses a variety of pharmacokinetically important transporters, including organic anion transporters (OAT; SLC22A), organic cation transporters (OCT; SLC22A), electroneutral organic cation transporters (OCTN; SLC22A), equilibrate nucleoside transporters (ENT; SLC29A), concentrative nucleoside transporters (CNT; SLC28A), apical Na+-dependent bile salt transporters (ASBT; SLC10), plasma membrane monoamine transporters (PMAT; SLC29), monocarboxylate transporters (MCT; SLC16A), urate transporters (URAT1; SLC22A12) and peptide transporters (PEPT, SLC15A)[66]. The SLCO superfamily also carries organic anion transporter polypeptide (OATP; SLCO)[67].

2.2.2.1. Peptide transporter (PepT, SLC15)

Peptide transporters including PepT1 and PepT2 are members of the proton-coupled oligopeptide transporter (POT) family and are predominantly expressed on intestinal epithelial cells[68]. The PepT1 acts as a low-affinity/high-capacity transporter and PepT2 as a high-affinity/low-capacity transporter for di- and tripeptides. Peptide transporters can be exploited as potential target for peptide based prodrugs or peptidomimetics as they are highly expressed on intestinal epithelial cells[69]. PepT1 is predominantly expressed on the epithelial mucosa of small intestine and transports peptidomimetics such as β-lactam antibiotics (e.g., penicillin and cephalosporin), angiotensin-converting enzyme inhibitors, aminopeptidase inhibitors, and ester prodrugs. PepT2 is mainly expressed in the kidney and brain with a little expression in other tissues including the enteric nervous system, lung, mammary gland, and spleen and transports many of the same substrates as PepT1[70]. Following transport across intestinal barrier through peptide transporters, the peptide prodrugs may be enzymatically cleaved by esterases

or aminopeptidases to regenerate the active parent drug. Valine-valine peptide prodrugs of Saquinavir (SQV) and Lopinavir (LPV) have demonstrated higher intestinal transport relative to the parent drugs itself [71].

2.2.2.2. Peptide histidine transporter (PHT, SLC15A4)

Peptide/histidine transporters, PHT1 (SLC15A4) and PHT2 (SLC15A3) also belong to the POT family. Recently their splice variants were identified in the rat (rPHT1 and rPHT2) and human (hPHT1 and hPHT2) genome[72]. However, these transporters are less extensively explored for their specific tissue expression, molecular and functional characteristics and cellular localization in contrast to peptide transporters. Some studies have demonstrated the role of hPHT1 in H+-dependent and Na+-independent uptake of histidine and dipeptide carnosine[73-74]. Additionally, valacyclovir, the valine substituted amino acid prodrug of acyclovir, also appeared to be a substrate for hPHT1. Yamashita et al. reported rPHT1 and hPHT1 mRNA expression in the brain, eye, lung, spleen and intestine by Northern blot analysis indicating their potential role in transporting histidine and/or histidine based prodrugs in these tissues[75].

2.2.2.3. Large neutral amino acid transporter (LAT1, SLC3A2/SLC7A5)

Amino acid transporters are highly expressed on brain capillary endothelial cells and can be exploited to improve brain absorption of nutrients, drugs and prodrugs. They can be broadly classified as anionic, cationic and neutral amino acid transporters depending on the charge of the amino acid that is being transported[76]. Large neutral amino acid transporter (LAT) is highly expressed on the luminal surface of brain endothelial cells and assist in the transport of large neutral amino acids with aliphatic and aromatic side chains. Additionally, anionic (system x-), neutral (system A) and cationic (system BO+) amino acid transporters are

also reported to be expressed on the BBB. LAT is primarily responsible for transporting neutral amino acids including phenylalanine, tyrosine, leucine, isoleucine, tryptophan and methionine across the brain[77].

2.3. Summary

Limited quantitative pharmacological evidences for drug uptake and efflux by transporters represents an area of further basic and clinical research. Significant efforts are being made to understand the role of transporters, their iterative interplay with metabolizing enzymes through molecular enzymology, binding and structure-activity relationship studies. While the substrate and inhibitor profiles of transporters are being updated progressively, new transporters are still being discovered. In addition, further research is imperative to develop means of improving transporter utilization or activity that might positively impact drug effects and reduce adverse effects.

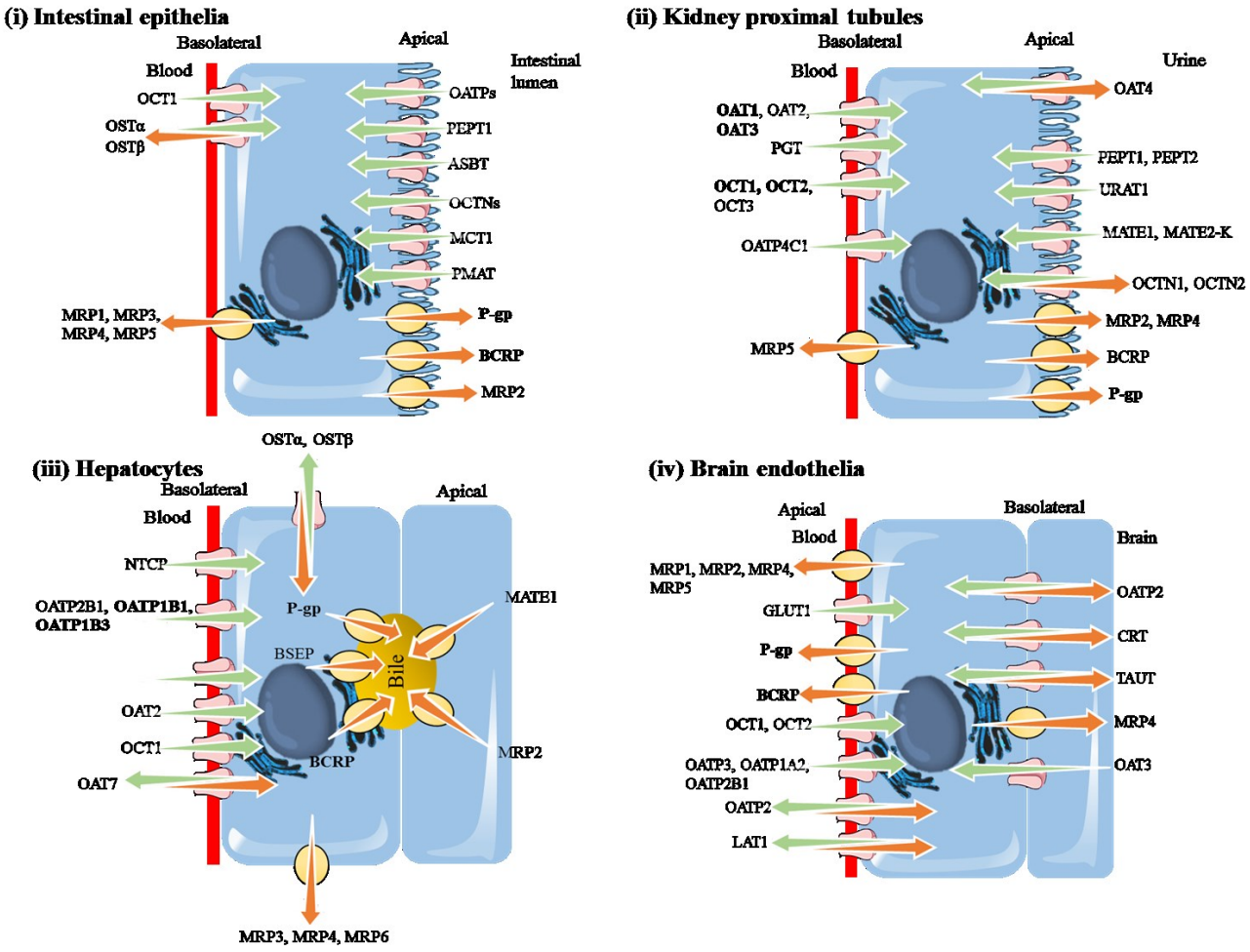

Figure 2-1 Major drug transporters expressed in different tissues: Major transporters in plasma membrane of intestinal epithelia, hepatocytes, kidney proximal tubules, brain capillary endothelial cells and tumor tissues are represented. Orange colored arrows represent efflux while green colored arrows represent influx. Those in Bold letters are discussed in detail

Table 2-1 Drug efflux transporters of emerging importance in drug transport and disposition[35]

Drug Transporter	Gene	Organs/Tissues	Localization	Substrates	Inhibitors	Inducers
P-gp/MDR1	ABCB1	Intestinal enterocytes, Kidney proximal tubules, Hepatocytes, Brain endothelia, placenta, adrenal, testes	Apical	a.	b.	Rifampicin, Monensin, St. John's wort, atazanavir, nelfinavir, amprenavir
BCRP	ABCG2	Intestinal enterocytes, Kidney proximal tubules, Hepatocytes, Brain endothelia, placenta, stem cells, mammary glands	Apical	c.	Estrone, GG918, fumitremorgin C, Ko143, novobiocin, pantoprazole, CI1033, gefitinib, quercetin, cyclosporine, dipyridamole, ritonavir	Efavirenz
MRP2	ABCC2	Intestinal enterocytes, Kidney proximal tubules, Hepatocytes, Brain endothelia	Apical	d.	Cyclosporine, probenecid, furosemide, ritonavir, saquinavir, lamivudine, abacavir, emtricitabine, efavirenz, delavirdine, nevirapine, cidofovir, adefovir, tenofovir, MK-571	Rifampin, spironolactone, 1,25(OH)2D3

a. **Substrates: Statins:** simvastatin lactone, atorvastatin, lovastatin lactone; **Antibiotics:** dicloxacillin, fluoroquinolones (grepafloxacin, levofloxacin and sparfloxacin), erythromycin, cyclosporine, oxytetracycline, doxycycline, valinomycin, ivermectin; **Anti-cancer agents:** doxorubicin, daunorubicin, paclitaxel, vincristine, vinblastine, idarubicin, topotecan, tandutinib, imatinib, methotrexate, mitoxantrone, SN-38, lapatinib; **Cardiac agents:** digoxin, prazosin, reserpine; **Anti-HIV agents:** indinavir, nelfinavir, saquinavir, darunavir, lopinavir, zidovudine, lamivudine, tipranavir, maraviroc,

dolutegravir, raltegravir; **Others:** tacrolimus, hydrocortisone, talinolol, fexofenadine, colchicine, loperamide, aldosterone, dibucaine, temocapril.

b. **Inhibitors: Statins:** atorvastatin; **Antibiotics:** fluoroquinolones (grepafloxacin, levofloxacin and sparfloxacin), cyclosporine; **Cardiac agents:** quinidine, verapamil; **Anti-HIV agents:** abacavir, rilpivirine, atazanavir, ritonavir, cobicistat; **Others:** tariquidar, GF120918, immunosuppressive agents, SDZ, PSC 833, LY335979

c. **Substrates: Statins:** simvastatin lactone, atorvastatin, lovastatin lactone, pravastatin or fluvastatin, rosuvastatin; **Antibiotics:** fluoroquinolones (grepafloxacin, levofloxacin and sparfloxacin), ciprofloxacin; **Anti-cancer agents:** imatinib, methotrexate, mitoxantrone, SN-38, topotecan, irinotecan, doxorubicin, daunorubicin, gefitinib, tandutinib, ezetimibe, 9-aminocamptothecin, lapatinib; **Cardiac agents:** prazosin, dipyridamole; **Anti-HIV agents:** zidovudine, lamivudine, efavirenz; **Others:** glyburide, temocapril, sulfasalazine

d. **Substrates: Statins:** pravastatin; **Antibiotics:** ceftriaxone, ampicillin, grepafloxacin; **Anti-cancer agents:** vinblastine, irinotecan, SN-38, methotrexate, 7-hydroxymethotrexate, ezetimibe**; Cardiac agents:** fosinopril; **Anti-HIV agents:** lopinavir, darunavir**; Others:** fexofenadine, sulfasalazine, colchicine

CHAPTER 3

3. HISTIDINE BASED PEPTIDE PRODRUG: A DUAL TARGETED APPROACH TO IMPROVE INTESTINAL ABSORPTION OF LOPINAVIR

3.1. Rationale

Lopinavir (LPV) is currently indicated in highly active antiretroviral therapy (HAART) in combination with ritonavir [78]. Despite potent efficacy against HIV-1, oral administration results in poor intestinal absorption and negligible LPV levels in the body. One of the major factors that potentially limit intestinal absorption is the high substrate affinity of LPV towards P-gp and MRP2 [79]. P-gp and MRP2 are extensively expressed on the villus tip of enterocytes, the primary absorption site for orally administered drugs [80]. These efflux pumps, limit the entry of harmful substances and xenobiotics and prevent LPV from getting transported across the intestinal epithelium thus secreting it back into the intestinal lumen. Hence, to overcome these efflux pumps, a significantly higher dose of LPV needs to be administered. Although high doses of LPV have made it possible to achieve therapeutic plasma concentrations, at the same time it has resulted in severe cellular and/or systemic toxicities [25, 81].

Combination strategies capable of modulating the expression and functional activity of efflux pumps present a unique approach to improve absorption and efficacy of LPV. However, such strategies may pose a risk of generating serious systemic adverse events [82-84]. For instance, Bertrand et al. reported an excessive increase in vincristine neuropathy when administered along with cyclosporine to modulate MDR [85]. Similarly, Kerr et al. demonstrated an unassuming pharmacokinetic interaction between verapamil (efflux pump inhibitor) and doxorubicin in humans. Although, oral verapamil able to increase the AUC, terminal t1/2 and

volume of distribution of verapamil, the plasma drug clearance significantly dropped due to inhibition of efflux pumps leading to various side effects [86]. In the past few decades, prodrug-based approaches have garnered considerable interest to improve pharmacokinetic as well as pharmacological profiles of poorly permeable therapeutic agents [8, 33]. Interestingly, prodrugs have been designed such that various endogenous transporters, co-expressed with efflux pumps, are targeted to improve drug absorption. In this regard, peptide transporters have been extensively utilized in our laboratory to improve cellular permeability of various antiviral agents such as saquinavir [71, 87], lopinavir [88-89], acyclovir [90-91] and ganciclovir [92]. The peptide prodrug conjugates may extend an additional advantage of generating non-toxic nutrient byproducts at the target site where prodrugs are getting converted to the parent drug and pro-moieties. The binding of a target agent to an influx transporter confers a structural change to the transporter leading to the translocation of molecule across the membrane and thus its subsequent release into the cytoplasm. Moreover, suitable combinations of amino acids in dipeptide prodrugs can modulate physicochemical properties of the parent drug.

Recently, brain and intestinal expression of a peptide/histidine transporter (PHT1, SLC15A4) have been reported [70, 93-95]. Such unique expression renders PHT1 a potential target to improve delivery of P-gp and MRP2 substrates such as LPV. Exploiting the role of peptide/histidine transporter in transporting various P-gp and MRP2 substrates remains elusive.

3.2. Objectives

(i) A histidine based dipeptide prodrug, His-Leu-LPV, was synthesized and evaluated by ^{1}H-NMR and LCMS/MS techniques in the present study.

(ii) Aqueous solubility, buffer stability and cell cytotoxicity of prodrug were examined.

(iii) Uptake and transport studies were carried out in Madin-Darby canine kidney type II (MDCKII) cell lines overexpressing P-gp (MDCKII-MDR1) and MRP2 (MDCKII-MRP2) in presence of efflux inhibitors to determine the affinity of His-Leu-LPV towards these efflux transporters.

(iv) The presence of histidine as a terminal targeting moiety is hypothesized to improve recognition of the prodrug by PHT1[7]. Furthermore, His-Leu-LPV being a dipeptide prodrug is also anticipated to be transported by peptide transporters (PepT1 and PepT2). Such dual recognition of His-Leu-LPV might significantly improve absorption of His-Leu-LPV across poorly permeable membranes. Thus, uptake studies of His-Leu-LPV were carried out in presence of PHT and PepT influx transporter substrates.

3.3. Experimental

3.3.1 Materials

Unlabeled LPV and P-gp inhibitor, GF120918 were generous gift from Abbott Laboratories Inc. (North Chicago, IL, USA). [3H]-LPV (0.5 Ci/mmol), [3H]-glycylsarcosine (3H-GlySar) (29.4 Ci/mmol) and [3H]-Histidine (3H-His) (47.7 Ci/mmol) were purchased from Moravek Biochemicals (Brea, CA, USA). Streptomycin, penicillin, HEPES (4-(2-hydroxyethyl)-1-piperazineethanesulfonic acid), triton X-100, D-glucose, sodium bicarbonate ($NaHCO_3$), MK571, Boc-histidine, Boc-leucine, ethyl acetate, dichloromethane (DCM), dicyclohexylcarbodimide (DCC), 4-(N,N-dimethylamino)pyridine (DMAP), glucose, sodium chloride (NaCl), potassium chloride (KCl), calcium chloride ($CaCl_2$), sodium phosphate (Na_2HPO_4), potassium phosphate (KH_2PO_4), magnesium sulfate ($MgSO_4$) and Amberlyst® A21 resin were obtained from Sigma Chemical Co. (St. Louis, MO, USA). HPLC grade methanol and DMSO were purchased from Fisher Scientific Co. (Pittsburgh, PA, USA). Trypsin-EDTA solution, Dulbecco's modified Eagle's medium (DMEM) were purchased from Invitrogen (Carlsbad, CA, USA). Fetal bovine serum (FBS) was obtained from Atlanta Biologics (Lawrenceville, GA, USA). Premium siliconized microcentrifuge tubes were procured from MIDSCI (St. Louis, MO, USA). Uptake plates and Transwell® inserts were obtained from Corning Costar Corp. (Cambridge, MA, USA). All other chemicals were of analytical reagent grade procured from Thermo Fischer Scientific or Sigma Aldrich and were utilized without any further purification.

3.3.2. Synthesis of His-Leu-LPV

3.3.2.1. Synthesis

His-Leu-LPV was synthesized according to a protocol previously published from our laboratory with minor modifications [89]. His-Leu-LPV synthesis included two steps (a) coupling of leucine to LPV through an ester bond to produce Leu-LPV (b) coupling of histidine to Leu-LPV intermediate via an amide bond to generate His-Leu-LPV. Leu-LPV was synthesized using a procedure published from our laboratory[88]. To synthesize His-Leu-LPV, commercially available Boc-His-OH (341mg, 1.35mmol) and DCC (420 mg, 2.025 mmol) were dissolved in DCM (6 mL) in a round bottom flask. The mixture was stirred for 1h at 0ºC in an ice bath (mixture 1). In a separate round bottom flask, Leu-LPV (500 mg, 0.067mmol) was dissolved in DCM and triethylamine (2 mL) was added to the resulting solution (mixture 2). Mixture 2 was stirred for 30 min at room temperature (RT) under nitrogen atmosphere and added dropwise to the mixture 1. The reaction mixture was stirred for 24h at RT while monitoring every 6h with TLC and LCMS/MS. The reaction mixture was filtered and DCM was evaporated at RT under reduced pressure to obtain crude product. The product Boc-His-Leu-LPV was purified using silica column chromatography with 5% methanol/dichloromethane (MeOH/DCM) as an eluent.

3.3.2.2. Deprotection of the N-Boc group

Boc-His-Leu-LPV was dissolved in 60% trifluoroacetic acid (TFA) in DCM and stirred at 0ºC for 1h in order to remove the N-Boc protecting group. The mixture was evaporated to obtain a solid form of TFA salt of His-Leu-LPV. The TFA salt was further dissolved in anhydrous DCM and mixed with Amberlyst® A21 resin (weakly basic resin) for 15-30 min. The mixture was filtered and quickly evaporated under reduced pressure and the final product

was obtained following recrystallization in cold diethyl ether. The final product was stored in -20ºC until any further use. Reaction scheme for synthesis of Leu-LPV and His-Leu-LPV has been depicted in Figure 3-1.

3.3.3. Identification of the prodrugs

Leu-LPV and His-Leu-LPV were characterized by ^{1}H-NMR analysis. Spectra was recorded on Varian Mercury 400 Plus spectrometer using tetra methyl silane. Chemical shifts (δ) are reported in parts per million relative to the NMR solvent signal (CD_3OD, 3.31ppm for proton and 49.15ppm for carbon NMR spectra). Mass analysis was carried out using LCMS/MS spectrometer with electron-spray ionization (ESI) as an ion source in positive mode.

Leu-LPV: Low melting point solid; LC/MS (m/z): 742.6; ^{1}H NMR (400 MHz, chloroform-d) δ ppm 0.78 (br. s., 3 H) 0.93 (br. s., 5 H) 1.22 (br. s., 5 H) 1.95 (br. s., 2 H) 2.09 (d, J=10.54 Hz, 4 H) 2.57 - 2.75 (m, 12 H) 2.80 (br. s., 2 H) 3.17 (br. s., 1 H) 3.31 (br. s., 1 H) 4.05 (d, J=12.10 Hz, 1 H) 4.17 (d, J=15.23 Hz, 1 H) 4.26 - 4.70 (m, 7 H) 4.81 (br. s., 1 H) 5.01 - 5.14 (m, 1 H) 6.93 (d, J=10.54 Hz, 2 H) 7.04 - 7.30 (m, 7 H).

His-Leu-LPV: Low melting point solid; LC/MS (m/z): 879.7; ^{1}H NMR (400 MHz, chloroform-d) δ ppm 0.65 - 0.96 (m, 5 H) 1.06 - 1.40 (m, 11 H) 1.51 - 1.61 (m, 2 H) 1.70 (br. s., 2 H) 1.77 - 1.95 (m, 3 H) 2.12 (s, 2 H) 2.56 - 2.76 (m, 21 H) 3.12 - 3.28 (m, 8 H) 4.82 (br. s., 11 H) 6.71 (d, J=7.03 Hz, 3 H) 7.15 - 7.29 (m, 3 H) 8.18 (d, J=6.25 Hz, 3 H).

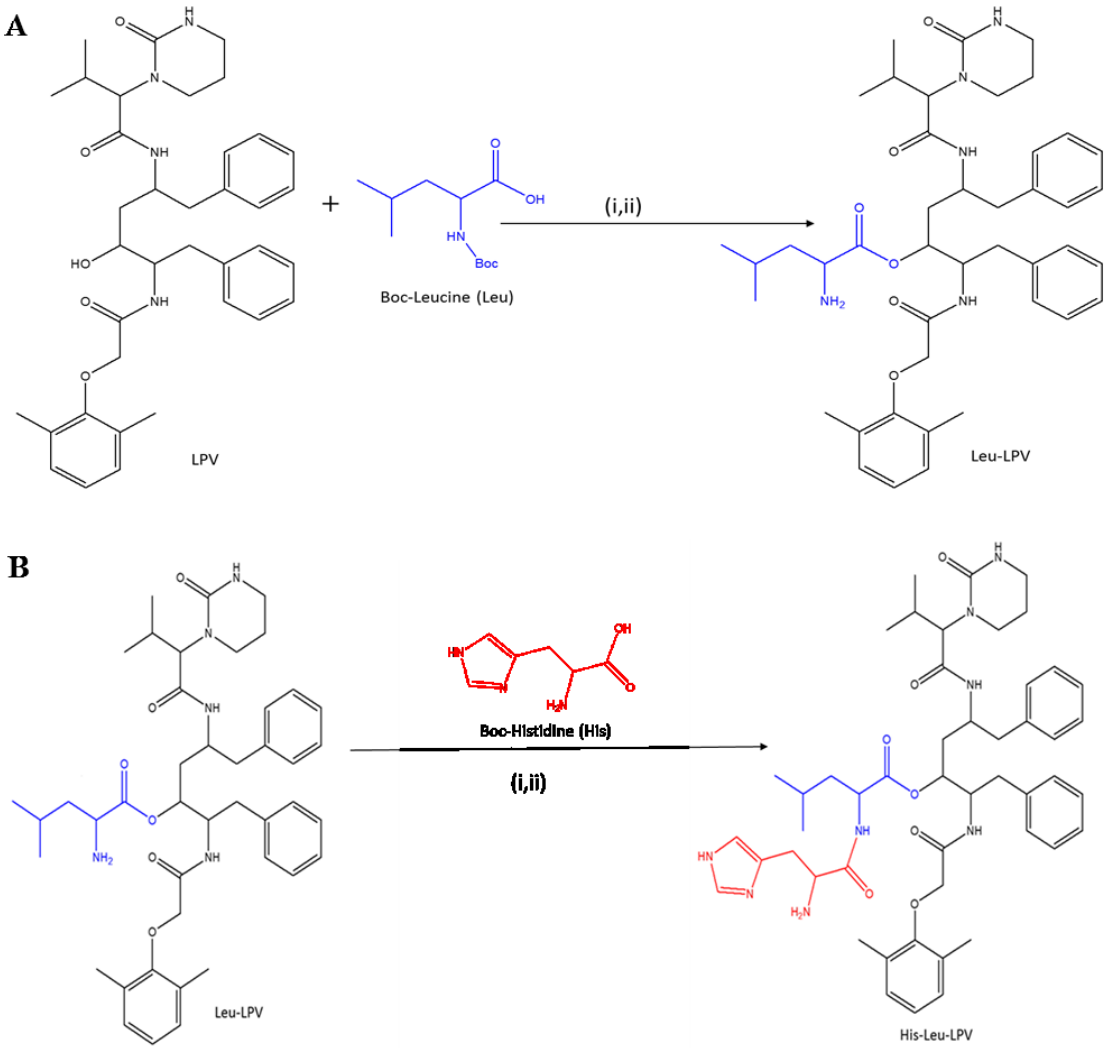

Figure 3-1 (A) Synthesis of Leu-LPV: (i) Boc-Leucine, DCC in DCM: 1h at 0°C; LPV, DMAP in DCM: 15min at RT and mixture stirred for 48h at RT. (ii) 60% TFA in DCM: 1 h at 0°C (B) Synthesis of His-Leu-LPV: (i) Boc-Histidine, DCC in DCM: 1h at 0°C; Leu-LPV, DCM, TEA: 30 min at RT and mixture stirred for 24h at RT. (ii) 60% TFA in DCM: 1 h at 0°C

3.4. Methods

3.4.1 Cell culture

Human P-gp/MDR1 cDNA transfected MDCKII cells (MDCKII-MDR1; passages 5-25) and human MRP2 cells (MDCKII-MRP2; passages 5-25), wild-type MDCKII cells (MDCK WT; passages 50-53) were generously provided by Drs. A. Schinkel and P. Borst (Netherlands Cancer Institute, Amsterdam, The Netherlands). Human derived colon carcinoma cells (Caco-2; passages 20-30) were obtained from ATCC (Manassas, VA, USA). All these cell lines were cultured in T75 flasks in DMEM containing high glucose and glutamine concentrations. The culture medium contained 10% FBS (heat-inactivated), 1% nonessential amino acids, 100 IU/ml streptomycin and 100 IU/ml penicillin. The pH of the medium was maintained at 7.4. Cells were maintained at 37ºC in an atmosphere containing 5% CO_2 and 90% relative humidity. The medium was replaced on alternate days until cells reached 80-90% confluency (5-7 days for MDCKII and 19-21 days for Caco-2 cells).

3.4.2. Solubility studies in distilled deionized water (DDI)

Aqueous solubility studies of LPV, Leu-LPV and His-Leu-LPV were performed according to a previously published protocol from our laboratory [89]. Briefly, saturated solutions of LPV, Leu-LPV and His-Leu-LPV were freshly prepared in DDI in siliconized tubes and placed in a shaker bath for 24h at RT. At the end of 24h, tubes were centrifuged for 10min at 10,000 rpm to separate the undissolved drug. Supernatants were carefully separated and filtered through 0.45 μm membrane filter (Nalgene syringe filter). Samples were further diluted appropriately and analyzed by HPLC.

3.4.3. Buffer stability studies

The extent of chemical hydrolysis of Leu-LPV and His-Leu-LPV was assessed according to a previously published protocol from our laboratory [82]. Degradation rate constants (k x 10^{-4}) and half-life (t1/2) values were determined at pH 4, 5.5 and 7.4. Leu-LPV (50 μM) and His-Leu-LPV (50 μM) were dissolved in 1.5 mL DPBS in siliconized tubes and placed in a shaker bath maintained at 60 rpm at 37ºC. Aliquots (100μL) were withdrawn at predetermined time points for 24hr and stored at -80ºC until further analysis by HPLC. Prodrug concentrations were plotted against time to determine degradation rate constants at different pH values.

3.4.4. Cytotoxicity studies

Cytotoxicity of LPV, Leu-LPV and His-Leu-LPV was determined in MDCKII-WT cells (passage 52) with MTT based cytotoxicity assay kit (Promega Co., Madison, WI). Briefly, cells were seeded in 96 well tissue culture plates at a density of 20,000 cells per well and maintained overnight at 37ºC in an atmosphere of 5% CO_2 and 90% relative humidity. The medium was aspirated the following day and replaced with 100 μL of serum free medium containing various concentrations of LPV, Leu-LPV and His-Leu-LPV (6.25-200 μM). After 4hr incubation at 37ºC, 20 μL of MTT stock solution was added to each well. Cells were kept for incubation for 4h at 37ºC. Cell viability was assessed by measuring absorbance at 485 nm with a microplate reader (BioRad Hercules, CA, USA).

3.4.5. Uptake studies

For cellular uptake studies, cells were seeded at a density of 3 X 10^6 cells in 12 well culture plates and maintained until they achieved 80-90% confluency (6-7 days). The uptake assay was carried out according to previously published protocol from our laboratory [96].

Briefly, medium was aspirated and cell monolayers were washed three times with 2 mL of DPBS (pH 7.4) at 37ºC (each wash of 10 min). Studies were initiated by incubating cells with radioactive solutions in DPBS at 37ºC for 30min. Following incubations, radioactive solutions were immediately aspirated and plates were washed with ice-cold stop solution to arrest the uptake process. Lysis buffer (1mL, 0.1% Triton-X solution in 0.3% NaOH) was added to each well and plates were stored overnight at RT. Following day, 500 µL solution from each well were transferred to scintillation vials containing 3 mL of scintillation cocktail and assayed with a scintillation counter (Beckman Instruments Inc., Model LS-6500; Fullerton, CA, USA). The uptake rate was normalized to protein count, which was further quantified using a BioRad protein estimation kit (BioRad protein; Hercules, CA). For studies involving efflux inhibitors, cells were pre-incubated with 2µM GF 120918 (MDCK-MDR1) or 75µM MK 571 (MDCK-MRP2) at 37ºC for 30 min prior to imitation of uptake studies.

3.4.6. Transport studies

Transepithelial transport studies were performed according to protocol published previously from our laboratory with minor modifications [82]. Briefly, Transwell® inserts (0.4 µm pore size, 12 mm) were coated with type 1 rat tail collagen (100 µg/cm^2) and placed inside a vessel under ammonia vapor for 45 min to promote binding of collagen to the polyester membrane. Cells were seeded at a density of 250,000 cells per insert. Following confluency, medium was removed and cell monolayers were washed three times with DPBS at 37 ºC (each wash of 10 min). Cell monolayer integrity was evaluated by measuring transepithelial electric resistance (TEER) using EVOM (epithelial volt ohmmeter from World Precision Instruments, Sarasota, FL, USA), prior to initiation of transport studies. Cell monolayers exhibiting TEER values >250 Ω*cm^2 were utilized for the transport studies. For A-B (absorptive direction)

permeability studies, 0.5 mL of test solution (25 μM) was added to the apical membrane of 12-well Transwell® plates. At predetermined time points, 100 μL sample from basolateral chamber of each well was withdrawn and replaced with fresh DPBS in order to maintain sink conditions. Studies were carried out for a period of 3 h at 37ºC. Samples were stored at -80 ºC until further analysis using LCMS/MS. For studies involving efflux inhibitors, cells were pre-incubated with 2μM GF 120918 (MDCK-MDR1) or 75μM MK 571 (MDCK-MRP2) at 37ºC for 30 min prior to initiation of transport studies.

3.4.7. Caco-2 cell homogenate studies

Cell homogenate studies were carried out according to protocol previously published from our laboratory. Briefly, confluent Caco-2 cells (passage 25) were washed three times with DPBS. Then cells were collected with a mechanical scrapper in two volumes of DPBS. Multipro variable speed homogenizer (DREMEL, Racine, WI) was used for cell homogenization. The homogenate was centrifuged at 12,500 rpm for 10min. The supernatant was collected and protein content was assessed using BioRad protein estimation kit. Suitable dilutions were made in DPBS (pH 7.4) to achieve a final protein concentration of 0.5 mg/mL. Aliquot (1 mL) of cell homogenate was incubated with His-Leu-LPV at 37ºC in a shaker bath (60 rpm) to achieve a final concentration of 40 ug/mL. At predetermined time points, 100 μL samples were collected and equal volumes of ice-cold acetonitrile:methanol (5:4) mixture was added to terminate enzymatic hydrolysis. Studies were carried out at pH 7.4 for a period of 4 h. Samples were then stored at -80 ºC until further analysis by LCMS/MS.

3.5. Sample and data analysis

3.5.1. Sample preparation for HPLC analysis

Aqueous solubility and buffer stability studies were analyzed by an HPLC technique. Briefly, samples were freshly prepared in DDI or buffer with pH 4, 5.5 and 7.4 in siliconized tubes and placed in a shaker bath maintained at 60rpm for 24 h at 37ºC. Tubes were centrifuged for 10 min at 10,000 rpm. The supernatants were carefully separated and filtered through 0.45µm membrane filter (Nalgene syringe filter). Further appropriate dilutions of the filtrate were made in acetonitrile (50%) and water (50%) containing 0.1% trifluoroacetic acid. Samples (20µL) were injected into HPLC for analysis.

3.5.2. HPLC analysis

Reverse phase HPLC was employed to analyze aqueous solubility and buffer stability of samples. The system comprised of a Waters 515 pump (Waters, Milford, MA, USA) with a C (18) Kinetex column (100 mm X 4.6 mm, 2.6 m; Phenomenex, Torrance, CA, USA) and a UV detector (Absorbance Detector Model UV-C, RAININ, Dynamax, Palo Alto, CA, USA, wavelength 210 nm). Acetonitrile:water (1:1) with 0.1% trifluoroacetic acid was selected as a mobile phase with 0.4 mL/min as flow rate. LPV, Leu-LPV and His-Leu-LPV eluted approximately at 13.62, 8.14 and 6.79 min respectively.

3.5.3. Sample preparation for LCMS/MS analysis

Transport and cell homogenate samples were analyzed utilizing a sensitive LCMS/MS technique according to a method previously published by our laboratory [89]. Briefly, samples were subjected to liquid-liquid extraction with water saturated ethyl acetate (10% water) as extracting solvent. About 50 µL of amprenavir (2.5µM) was employed as internal standard (I.S.). Samples were extracted with 800 µL water saturated ethyl acetate by vigorously

vortexing for 2.5 min. Samples were centrifuged at 10,000 rpm for 7min and aliquots (600µL) were collected and dried under reduced pressure for 45 min. Samples were reconstituted in 100 µL of acetonitrile (70%) and water (30%) containing 0.1% formic acid. The reconstituted samples (20µL) were injected into LCMS/MS for analysis.

3.5.4. LCMS/MS analysis

QTrap® 3200 LCMS/MS mass spectrometer (Applied Biosystems, Foster City, CA, USA) connected to Agilent 1100 Series quaternary pump (Agilent G1311A), vacuum degasser (Agilent G1379A) and autosampler (Agilent G1367A, Agilent Technology Inc. Palo Alto, CA, USA) was employed for sample analysis. Acetonitrile (70%) and water (30%) containing 0.1% formic acid was used as mobile phase at 0.3 mL/min. An XTerra1MS C18 column (50 mm X 4.6 mm, 5.0 mm, Waters, Milford, MA, USA) was employed for analyte separation. Chromatograms were obtained over 5 min. LPV and amprenavir eluted at 3.05 and 2.28 min respectively. Leu–LPV and His-Leu-LPV eluted at 1.60 and 1.18 min respectively.

Positive mode of electro spray ionization was employed and analytes of interest were detected in multiple-reaction monitoring (MRM) mode. Precursor and product ions generated for LPV and amprenavir were +629.30/155.10 and +506.20/245.20 respectively. Precursor/product ions for Leu-LPV and His-Leu-LPV were obtained at +742.30/155.10 and +879.40/155.10 respectively. Turbo ion spray setting and collision gas pressure were also optimized (IS Voltage: 5500V, temperature: 500 ºC, nebulizer gas: 60 psi, curtain gas: 60 psi). Other ion source parameters employed were declustering potential 66V, collision energy 60V, entrance potential 8V, and collision cell exit potential 4V. The peak areas for all components were integrated automatically using Analyst™ software. The lower limits of quantification were found to be 5 ng/mL for LPV and 15 ng/ml for Leu-LPV and His-Leu-LPV.

3.5.5. Permeability analysis

Cumulative amounts of LPV, Leu-LPV and His-Leu-LPV generated during transport were plotted against time. Linear regression of the amount transported as a function of time generated the rate of transport (dM/dt). Ratio of transport rate to the cross sectional area (A) further yielded the steady state flux as shown in Eq. (1).

$$\text{Flux} = \frac{dM/dt}{A} \qquad \text{Eq. (1)}$$

Transepithelial permeabilities were calculated by normalizing the steady state flux to the donor concentration (Cd) of the drug or prodrugs as shown in Eq. (2).

$$\text{Permeability} = \frac{\text{Flux}}{Cd} \qquad \text{Eq. (2)}$$

3.5.6. Statistical analysis

All experiments including uptake, transport, buffer and enzymatic stability were conducted at least in triplicate and results were expressed as mean ± S.D. Student t-test was employed to determine statistical significance between groups. A value of $p \leq 0.05$ was considered to be statistically significant.

3.6. Results

3.6.1. Solubility studies in distilled deionized water

Aqueous solubility values of Leu-LPV and His-Leu-LPV were found to be 600 ± 42 and 481 ± 82 µg/mL relative to 49 ± 3 µg/mL for LPV. The solubilities of Leu-LPV and His-Leu-LPV were respectively 12 and 9.8 times higher relative to LPV.

3.6.2. Buffer stability studies

Chemical hydrolysis of Leu-LPV and His-Leu-LPV was determined in DPBS adjusted to varied pH values i.e., 4, 5.5 and 7.4. Degradation rate constants and half-lives of prodrugs at pH 4, 5.5 and 7.4 values are reported in Table 3-1. Degradation half-lives exhibited by Leu-LPV and His-Leu-LPV at pH 4 were approximately 1.9 and 8.7 fold higher relative to pH 7.4.

Table 3-1 Leu-LPV and His-Leu-LPV degradation rate constants and half-lives at various pH values

Prodrug	**pH 4**		**pH 5.5**		**pH 7.4**	
	k x 10^{-4} (min)	$t_{1/2}$ (h)	k x 10^{-4} (min)	$t_{1/2}$ (h)	k x 10^{-4} (min)	$t_{1/2}$ (h)
Leu-LPV	3.90±0.06	29.6±0.4	5.78±0.09	20.0±0.3	7.53±0.14	15.4±0.3
His-Leu-LPV	2.92±0.03	39.6±0.5	6.21±0.15	18.6±0.5	25.5±2.4	4.6±0.5

3.6.3. Cytotoxicity studies

Cytotoxicity profiles of LPV, Leu-LPV and His-Leu-LPV were assessed in MDCK-WT cells using MTT assay, prior to initiation of uptake and transport studies. Serum-free medium was employed to avoid interference of proteins with MTT reagents. Medium containing no test compounds and 0.1% Triton-X were selected as a negative and positive

control, respectively. Medium containing 2% and 10% methanol was also examined for cytotoxic effects. As depicted in Figure 3-2, medium containing 2% methanol did not exhibit any cytotoxicity effects while medium with 10% methanol showed significant cytotoxicity. Triton-X resulted in about 70% decrease in absorbance compared to negative control. LPV produced no cytotoxic effects in the range of 5-50 µM however, was cytotoxic at 100 and 200 µM. Approximately 13 and 36% reduction in number of viable cells were observed at 100 and 200 µM LPV concentration. Similarly, the prodrugs (Leu-LPV and His-Leu-LPV) were non-toxic in the concentration range of 5-50 µM. Both prodrugs generated significant cytotoxicity at much higher concentrations. Leu-LPV and His-Leu-LPV reduced cell viability by 37% and 33% at 200 µM concentrations.

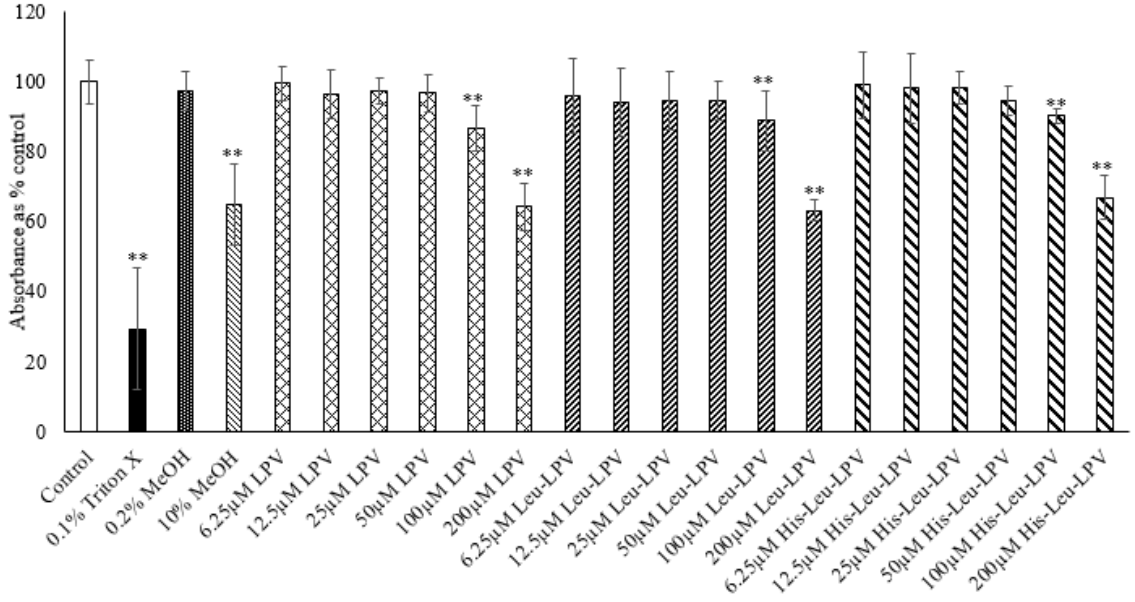

Figure 3-2 Cellular cytotoxicity studies of LPV, Leu-LPV and His-Leu-LPV in MDCK-WT cells after incubation for 4h. Data represent mean ± S.D (n= 8). **P<0.05 compared with the control group

3.6.4. Cellular uptake studies

To study the interaction of LPV with P-gp and MRP2, [3H]-LPV uptake was carried out in MDCK-MDR1 and MDCK-MRP2 cells in presence of efflux inhibitors. As depicted in Figures 3-3 A and B, approximately 4.5 and 2.9-fold rise in LPV uptake was observed in the presence of GF 120918 (2μM) and MK-571(75 μM).

To further confirm the extent of interaction and affinity of LPV, Leu-LPV and His-Leu-LPV with P-gp and MRP-2, concentration dependent uptake studies were performed in MDCK-MDR1 and MDCK-MRP2 cells. Uptake of [3H]-LPV (0.5 μCi/mmol) was carried out in presence of increasing concentrations of unlabelled LPV, Leu-LPV and His-Leu-LPV. [3H]-LPV uptake dramatically elevated with rise in unlabelled LPV concentrations in both MDCK-MDR1 and MDCK-MRP2 cell lines indicating improved interactions of LPV with MDR1 and MRP2 efflux proteins. However, [3H]-LPV uptake remained unaltered with increasing Leu-LPV and His-Leu-LPV concentrations (Figures 3-4 A, B and C) further signifying the ability of the prodrugs in circumventing the efflux proteins.

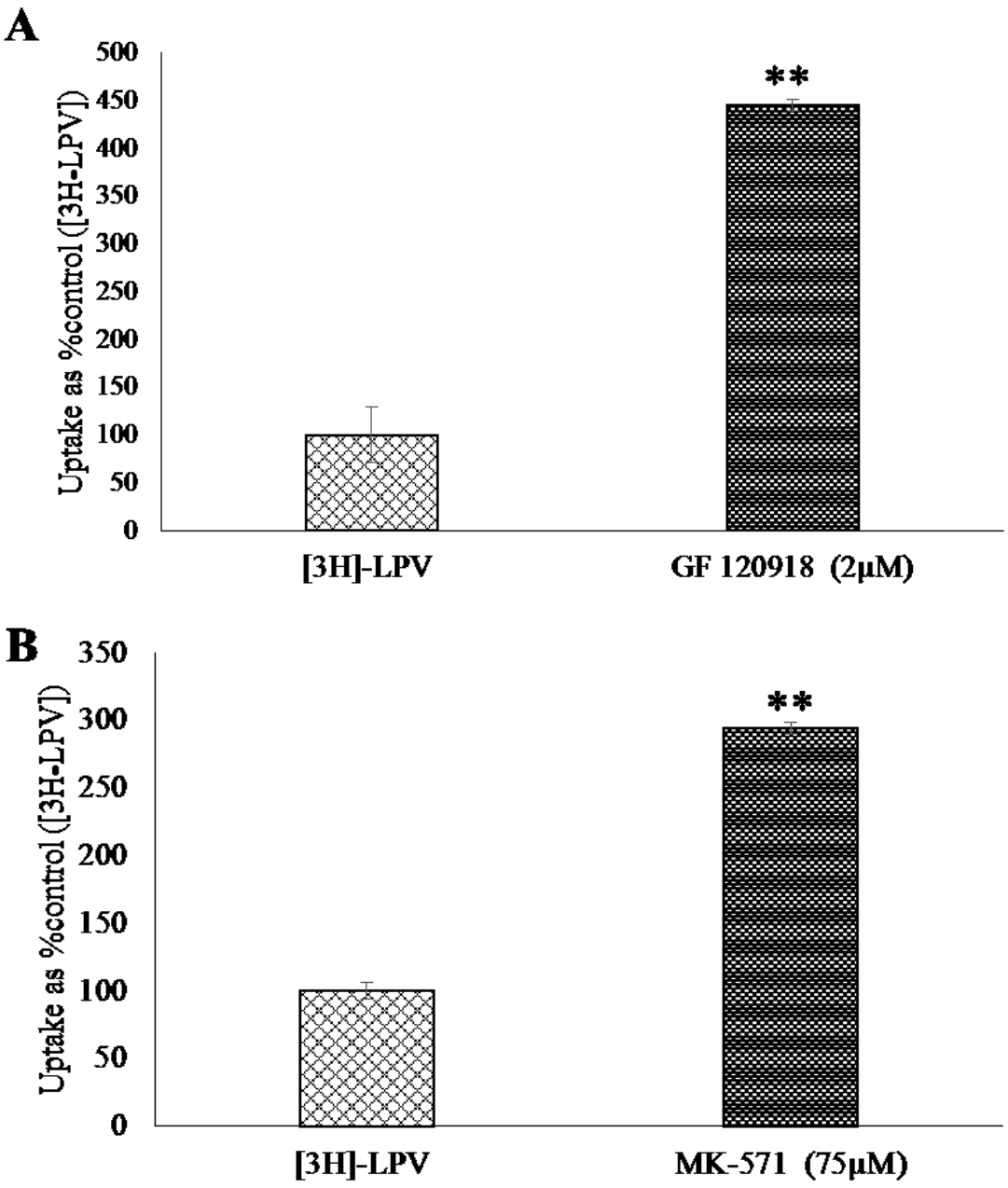

Figure 3-3 Cellular uptake studies of [3H]-LPV (1.5µM) (A) in absence and presence of GF 120918 (2 µM) in MDCK-MDR1 cells and (B) in absence and presence of MK 571 (75 µM) in MDCK-MRP2 cells. Data represent mean ± S.D (n= 4). **P<0.05 compared with the control group

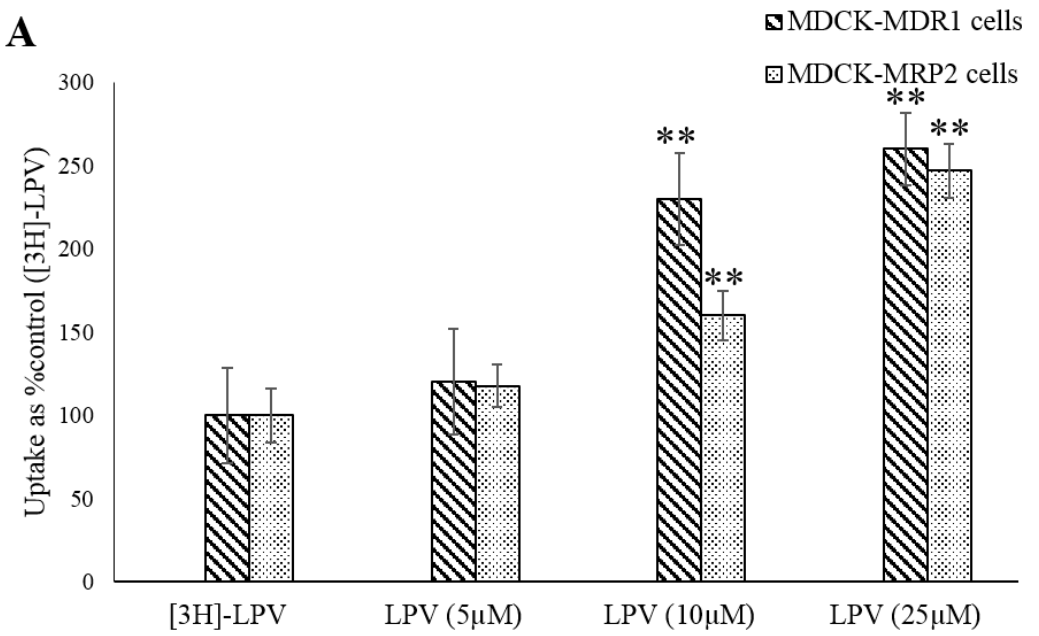
A
MDCK-MDR1 cells
MDCK-MRP2 cells
Uptake as %control ([3H]-LPV)
300
250
200
150
100
50
0
**
**
**
**
[3H]-LPV
LPV (5μM)
LPV (10μM)
LPV (25μM)

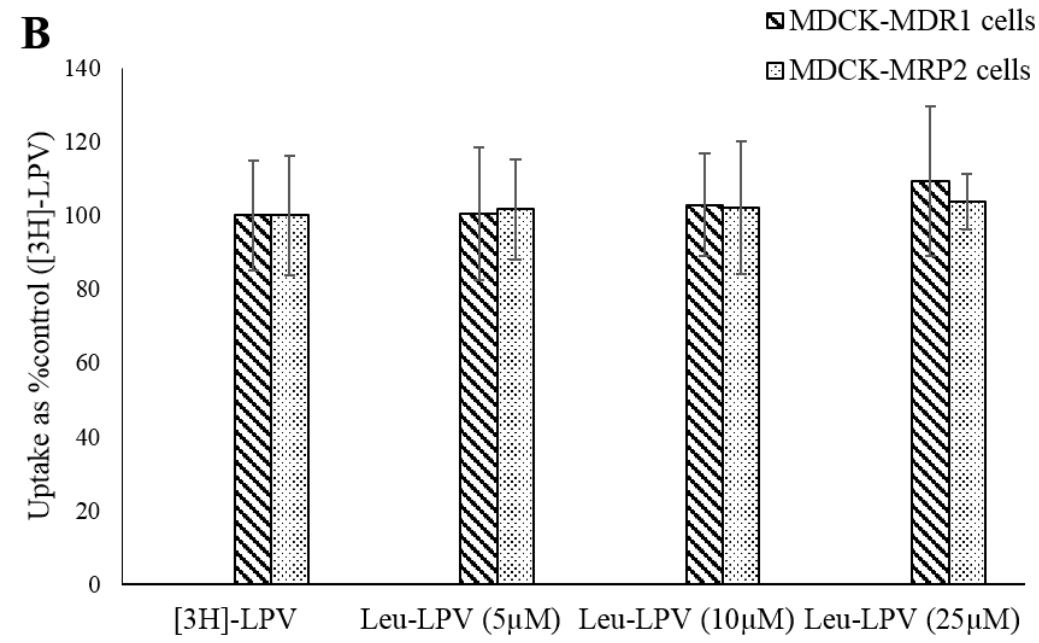
B
MDCK-MDR1 cells
MDCK-MRP2 cells
Uptake as %control ([3H]-LPV)
140
120
100
80
60
40
20
0
[3H]-LPV
Leu-LPV (5μM)
Leu-LPV (10μM)
Leu-LPV (25μM)

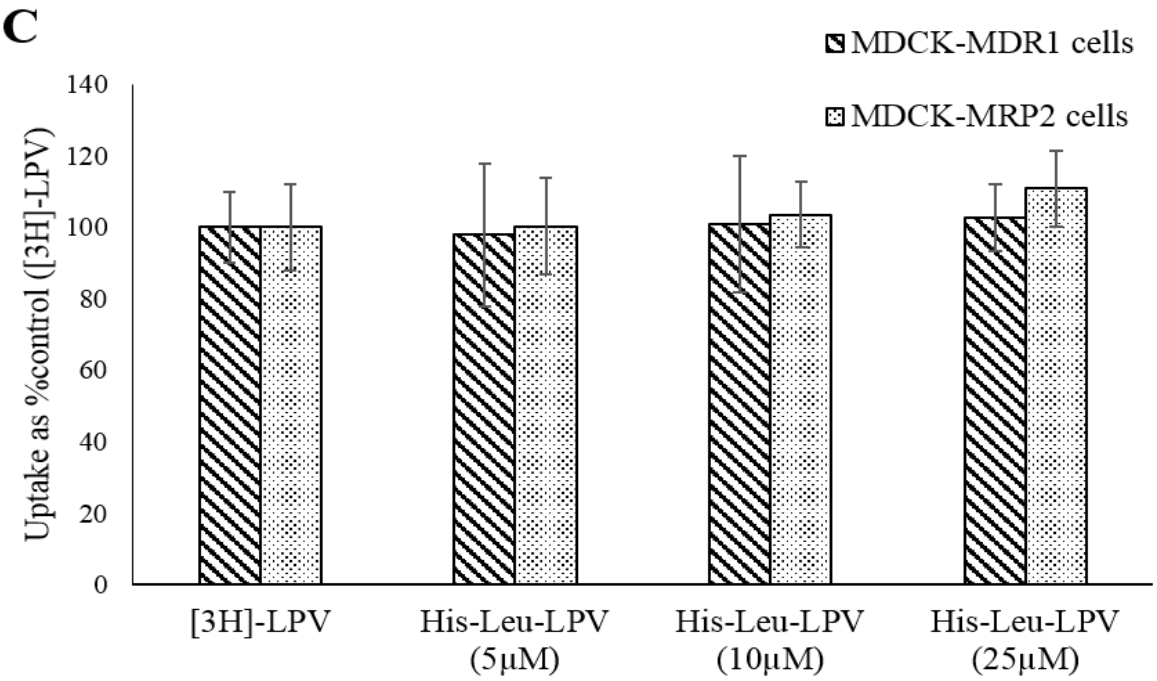

Figure 3-4 Cellular uptake studies of [3H]-LPV (1.5µM) in presence of increasing concentrations of (A) cold LPV, (B) cold Leu-LPV and (C) cold His-Leu-LPV in MDCK-MDR1 and MDCK-MRP2 cells. Data represent mean ± S.D (n= 4). **P<0.05 compared with the control group

3.6.5. Transepithelial transport studies

Transpeithelial studies of LPV, Leu-LPV and His-Leu-LPV were carried out in absorptive direction (A-B) in MDCK-MDR1 and MDCK-MRP2 cells. Results obtained from these studies are presented in Figure 3-5. A-B permeability rate of LPV drastically elevated in both MDCK-MDR1 and MDCK-MRP2 cell lines in the presence of efflux inhibitors. A-B permeability rates generated by LPV in the presence of GF120918 and MK571 were 3.4 ± 0.3 x 10^{-6} cm/s and 3.1 ± 0.2 x 10^{-6} cm/s, respectively. Leu-LPV generated A-B permeability rates of 3.5 ± 0.4 x 10^{-6} cm/s and 3.3 ± 0.7 x 10^{-6} cm/s, a 2.3 and 2.2-fold increase in comparison to LPV, 1.6 ± 0.5 x 10^{-6} cm/s and 1.5 ± 0.3 x 10^{-6} cm/s. A-B permeability rates displayed by His-Leu-LPV in MDCK-MDR1 and MDCK-MRP2 were 6.72 ± 0.67 x 10^{-6} cm/s and 6.10 ± 0.45

x 10^{-6} cm/s. Approximately 4.3 and 4.1-fold enhancement in the A-B permeability rates were observed for His-Leu-LPV relative to LPV in MDCK-MDR1 and MDCK-MRP2 cells respectively. The significant improved permeability of His-Leu-LPV prodrug indicate its ability to circumvent efflux pumps and at the same time recognition and permeation through the influx transporters.

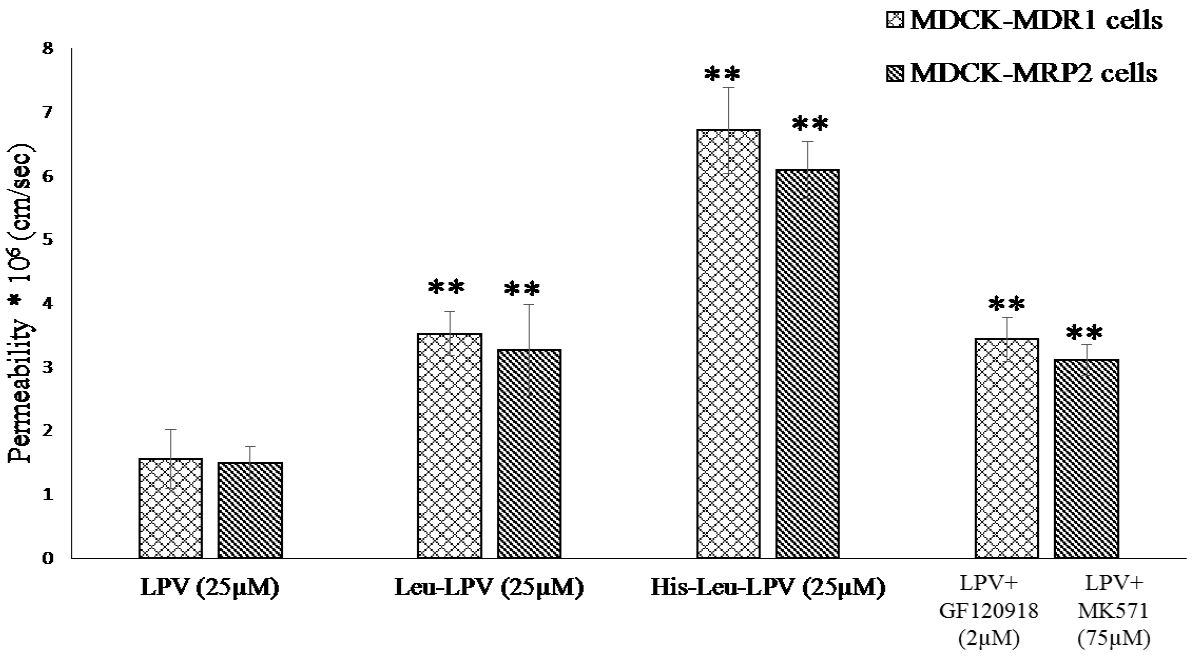

Figure 3-5 A-B permeability of LPV, Leu-LPV, His-Leu-LPV and LPV in presence of GF120918 and MK571 across MDCK-MDR1 and MDCK-MRP2 cells respectively. Data represent mean ± S.D (n= 4). **P<0.05 compared with the control group

3.6.6. Interaction with peptide/histidine transporter (PepT1 and PHT1)

To study the interaction of LPV, Leu-LPV and His-Leu-LPV with PepT1 and PHT1 influx transporters, uptake studies were performed in MDCK-MDR, MDCK-MRP2 and Caco-2 cell lines. Glycylsarcosine (GlySar) and Histidine (His) were used as model substrates for peptide (PepT1) and histidine transporters (PHT1) respectively. Uptake of [3H]-GlySar (0.5

μCi/mmol) was performed in presence of cold GlySar, LPV, Leu-LPV and His-Leu-LPV to determine extent of prodrug interaction with peptide transporters (PepT1). Results obtained from this study demonstrating [3H]-GlySar uptake are depicted in Figure 3-6 A. Approximately 35% reduction was observed in uptake of His-Leu-LPV in all the cell lines in contrast to 75% reduction in presence of cold GlySar indicating that the PepT1 transporters are highly functional in these cell lines and improved affinity of His-Leu-LPV towards PepT1 influx transporters. Furthermore, [3H]-His uptake (0.5 μCi/mmol) was performed in presence of cold His, LPV, Leu-LPV and His-Leu-LPV in MDCK--MDR, MDCK-MRP2 and Caco-2 cell lines to determine prodrug interaction with peptide/histidine transporter (PHT1). [3H]-His uptake results have been demonstrated in Figure 3-6 B. Approximately 30% reduction was observed in uptake of His-Leu-LPV in all the cell lines in contrast to 90% reduction in presence of cold His indicating the functionality and improved interaction of His-Leu-LPV with PHT1 influx transporters.

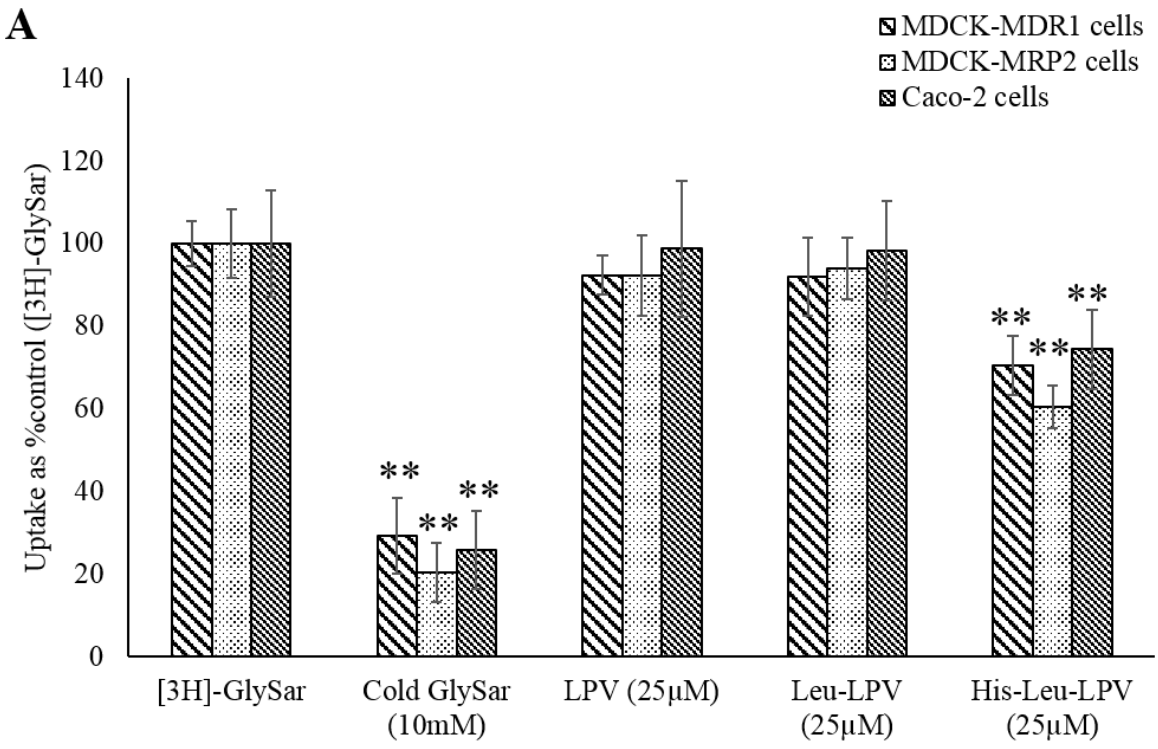
A
MDCK-MDR1 cells
MDCK-MRP2 cells
Caco-2 cells
Uptake as %control ([3H]-GlySar)
140
120
100
80
60
40
20
0
**
**
**
**
**
**
[3H]-GlySar
Cold GlySar (10mM)
LPV (25µM)
Leu-LPV (25µM)
His-Leu-LPV (25µM)

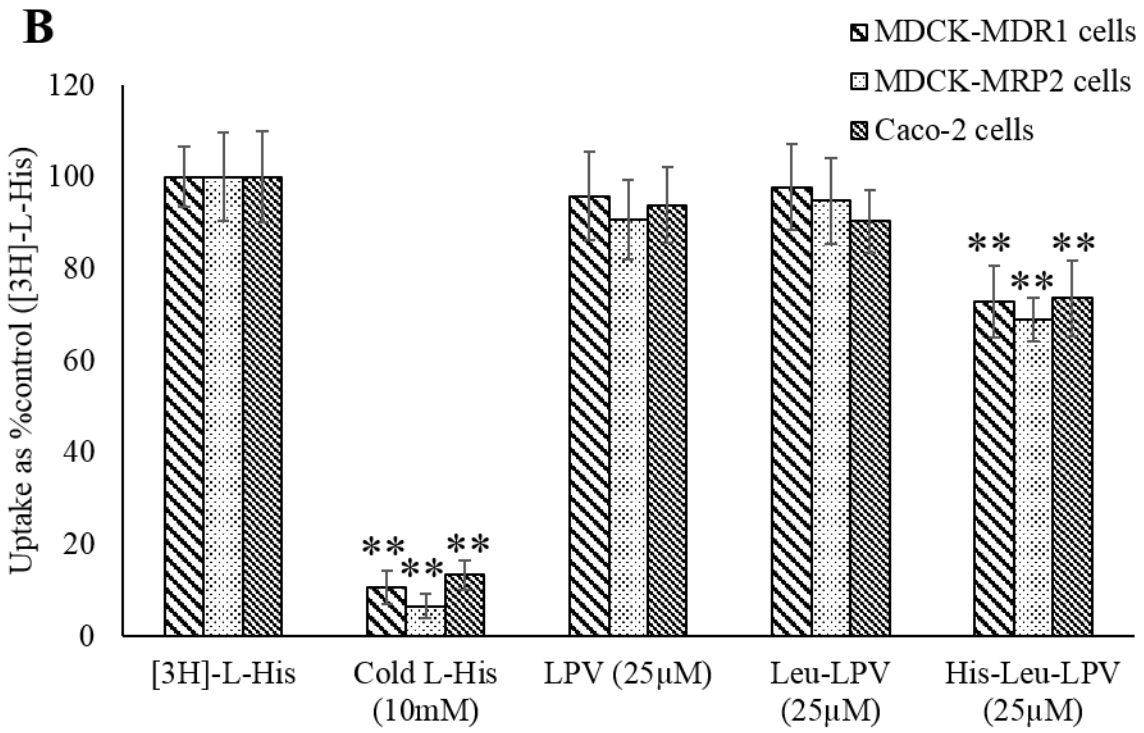

Figure 3-6 Cellular uptake studies of [3H]-GlySar (17nM) (A) and [3H]-L-His (10.5nM) (B) in presence of cold GlySar/ cold L-His (10mM), LPV, Leu-LPV and His-Leu-LPV (25µM) in MDCK-MDR1, MDCK-MRP2 and Caco-2 cells. Data represent mean ± S.D (n= 4). **P<0.05 compared with the control group

3.6.7. Caco-2 cell homogenate studies

Enzymatic hydrolysis of prodrugs were also determined in Caco-2 cell homogenate at pH 7.4 for a period of 4h (Figure 3-8). As depicted in Figure 3-9, intact His-Leu-LPV, both intermediate amino acid prodrug (Leu-LPV) and regenerated parent drug (LPV) from His-Leu-LPV were detected in homogenate samples. The degradation of His-Leu-LPV was found to be rapid in cell homogenates. At the end of 4h, approximately 6% of His-Leu-LPV was detected. Degradation rate constant and half-life of His-Leu-LPV were found to be $5.38 \pm 0.13 \times 10^{-3}$ min^{-1} and 2.15 ± 0.06 h, respectively. Figure 3-7 depicts concentrations of regenerated LPV and Leu-LPV from His-Leu-LPV in Caco2 cell homogenates. Leu-LPV degradation rate

constant and half-life values were also determined and observed to be $1.37 \pm 0.07 \times 10^{-3}$ min^{-1} and 8.5 ± 0.4h, respectively (Figure 3-9).

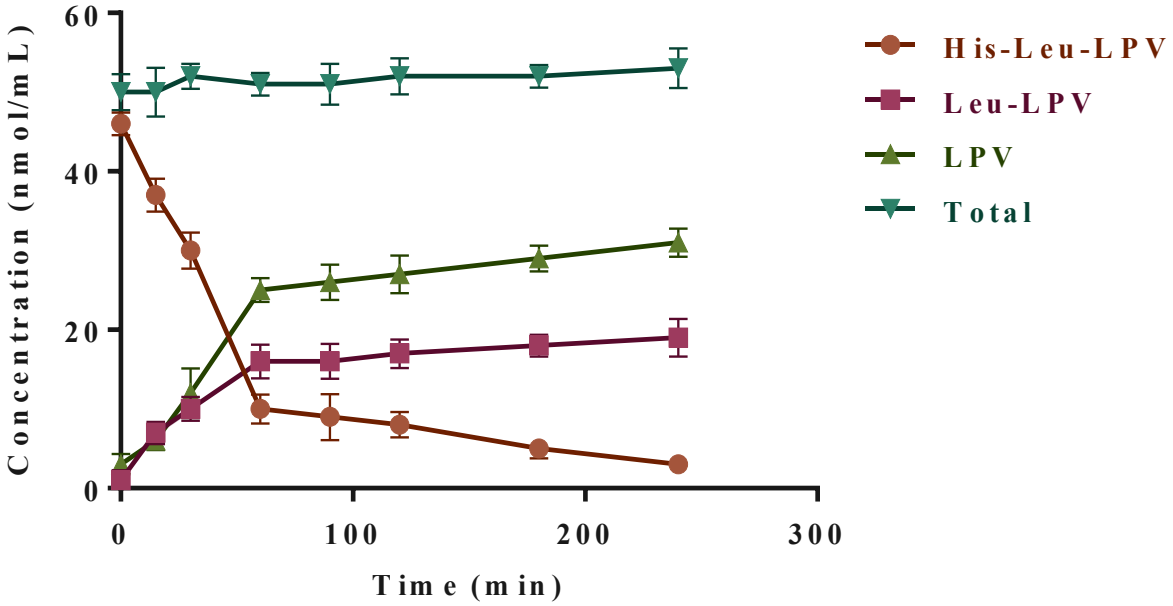

Figure 3-7 Degradation profile (nmol/ml of drug vs time) for His-Leu-LPV in Caco-2 cell homogenate. Data represent mean ± S.D (n= 4).

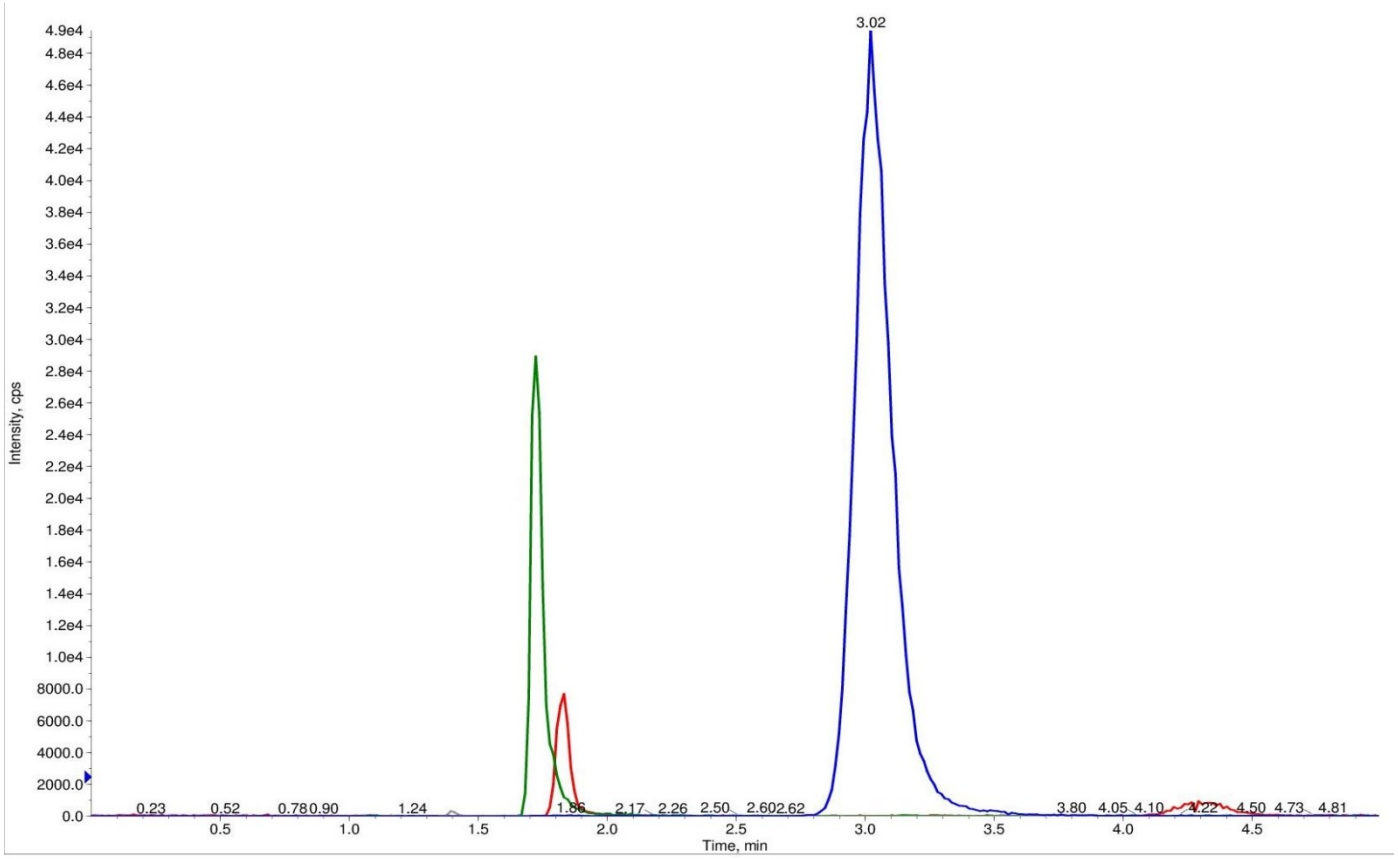

Figure 3-8 Overlaid MRM chromatograms for His-Leu-LPV (red), Leu-LPV (green) and LPV (blue)

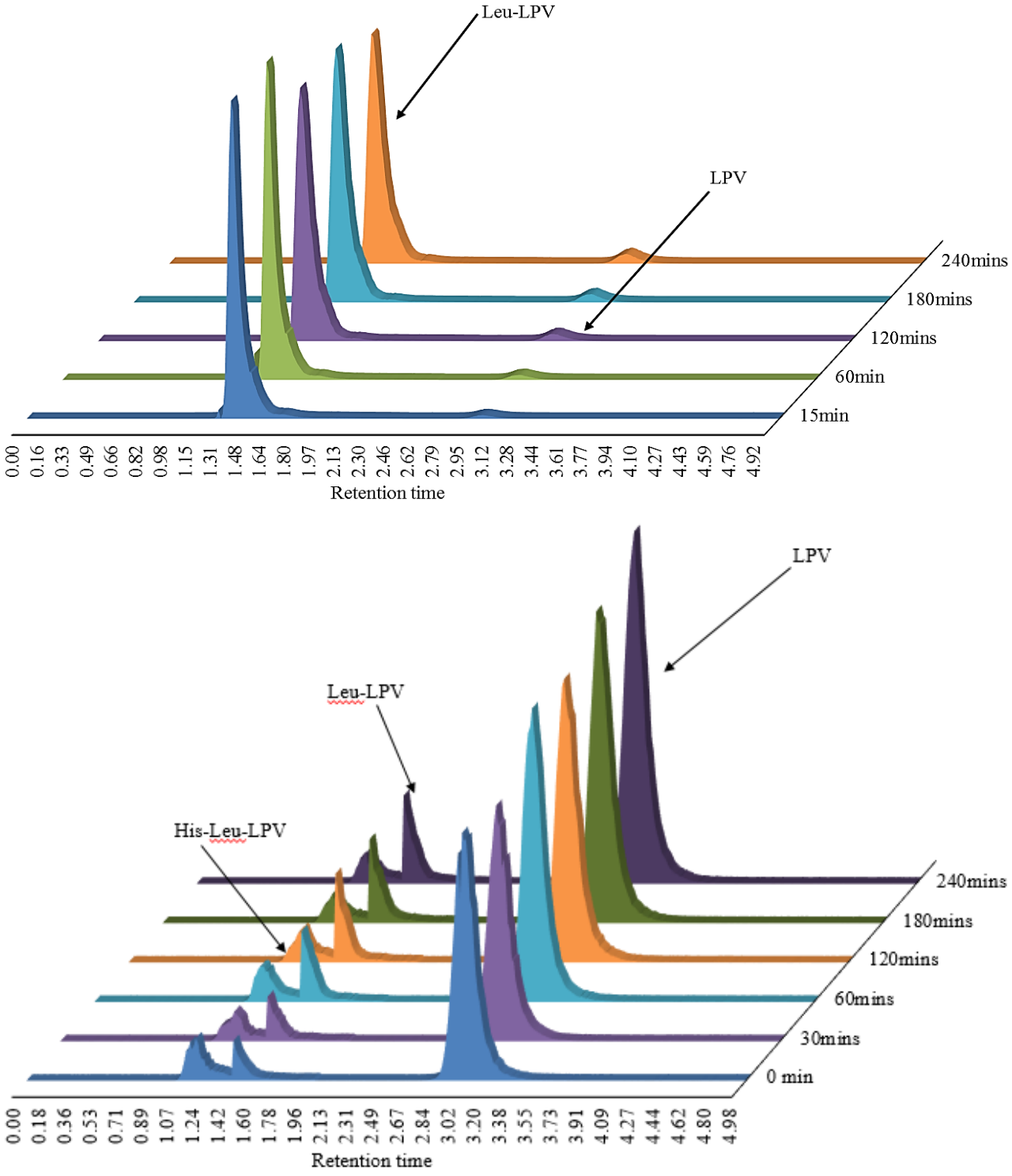

Figure 3-9 LCMS/MS (MRM mode) spectra of Leu-LPV and His-Leu-LPV in Caco-2 cell homogenate at various time points as indicated in the figure

3.7. Conclusion

Poor aqueous solubility and higher affinity towards drug efflux pumps and metabolizing enzymes (CYP3A4) pose a major challenge to LPV delivery. The present study demonstrates the potential of a prodrug approach to improve LPV absorption across P-gp and MRP2 overexpressing polarized membranes. Prodrugs, Leu-LPV and His-Leu-LPV, developed in this study were more water soluble relative to LPV. Moreover, these compounds possessed lower affinity towards P-gp and MRP2 relative to LPV indicating their true potential in circumventing efflux pumps. The higher affinity of LPV towards P-gp and MRP2 is evident from its improved permeation in presence of efflux pump inhibitors. His-Leu-LPV exhibited both PepT1 and PHT1 transporters mediated cellular uptake, which further substantiates improved interaction of His-Leu-LPV with the influx transporters. Thus there is tremendous potential of generating higher systemic as well brain concentrations of LPV through His-Leu-LPV administration.

In future studies, prodrug (a) competitive bidirectional transport in presence of PepT, and/or PHT substrates across blood-brain barrier (BBB), (b) metabolism in presence of esterase and protease inhibitor cocktails and human microsomes, (c) quantification of known CYP3A4 LPV metabolites, (d) plasma protein binding, (e) chemical stability studies in buffers with adequate buffer capacity at different pHs and (f) oral absorption studies in rats will be reported.

PART II: NANOFORMULATIONS TO IMPROVE OCULAR DELIVERY OF CIDOFOVIR AND OCTREOTIDE

CHAPTER 4

4. POLYMERIC NANOMICELLES FOR IMPROVED OCULAR DRUG DELIVERY

4.1. Rationale

The past decades have witnessed significant progress in the development of nano-sized (1-200 nm) ocular drug delivery systems. Such increasing interest in nanomedicine may be attributed to the tremendous advances in nanotechnology, polymer chemistry and chemical engineering [97-98]. However, additional research is required in the area of ocular drug delivery, particularly with regards to the delivery of hydrophobic compounds, nucleic acids and proteins, in order to improve their therapeutic outcomes and thus the quality of life for patients [99-100]. Hydrophobic NSAIDs such as indomethacin, ibuprofen, and diclofenac, indicated for inflammatory disorders, are an excellent example to demonstrate the need for improved ocular delivery. Although, in-vitro studies have suggested their pharmacological effectiveness, studies involving animal models and patients generally fail to achieve sufficient therapeutic activity [101-102]. Such failure is most likely due to insufficient retention and accumulation at the target site resulting in suboptimal therapeutic levels. Additionally, significant amounts of intravitreally administered drugs accumulate inside healthy ocular tissues and can potentially lead to serious side effects, discomfort and blurred vision [103-104].

Several nanomedicines have been formulated and evaluated for ocular drug delivery over the years. The most relevant formulations are depicted in Figure 4-1. All of these have been designed keeping the following two key characteristics of nanomedicines in mind: (i) stable, efficient and reversible drug loading, as well as (ii) prolonged retention and circulation time. In the case of age-related macular degeneration (AMD), for instance, NSAIDs such as

indomethacin and ibuprofen are known to be extensively utilized to reduce inflammation and cystoid macular edema [105]. However, because of their high hydrophobicity, both intravenous and intravitreal administrations are problematic and complicated. They are thus generally administered in combination with solublization enhancers, such as hydroxypropyl-β-cyclodextrin, diethylene glycol monoethyl ether (Transcutol P), n-octenylsuccinate starch, α-tocopheryl polyethylene glycol succinate, polysorbate 80 and tromethamine [106-109].

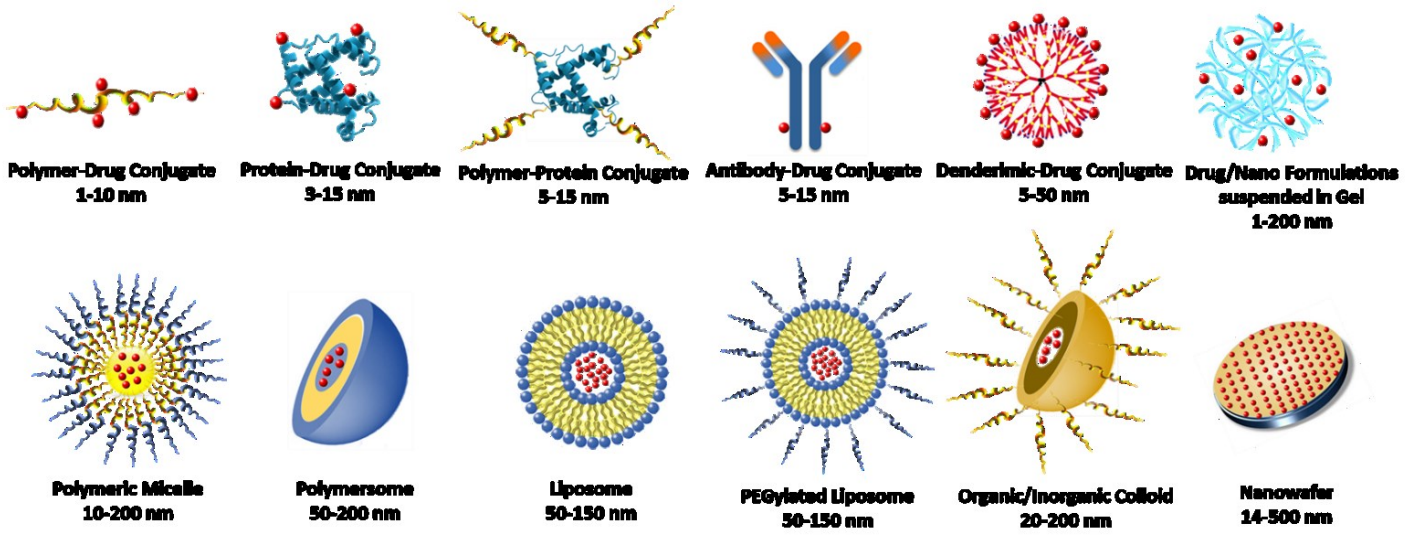

Figure 4-1 Schematic depiction of the most relevant nanomedicine formulations for ocular delivery

FDA approved polymeric implants for posterior segment drug delivery include Vitrasert® (for CMV retinitis), Retisert® (for uveitis), Iluvien® (diabetic macular edema) and Ozurdex® (for macular edema associated with uveitis and diabetes). Vitrasert® and Retisert®, based on the same delivery platform but with Retisert® being slightly smaller in size, require sclerotomy at the pars plana region for implantation. On the other hand, Iluvien® and Ozurdex® are injected into the vitreous cavity via a 23-25 gauge needle. Since, Vitrasert®, Retisert® and Iluvien® are non-biodegradable, the drug-depleted devices need to be surgically

removed or may accumulate in the vitreous cavity as in the case of Iluvien®. Taking frequent intravitreal implantation of these devices into consideration, many patients and insurance companies are taken aback by their price tags (USD $20,000 for Retisert® and $2,000 for Ozurdex®)[110]. Additionally, intravitreal administration of these implants requires skilled professional execution while carrying the risk of side effects potentially requiring patients to undergo cataract and/or glaucoma surgery as well as treatment with pressure lowering medications [11, 12]. Thus, exploring the feasibility of topical administration to deliver drugs to the posterior segment may drastically improve drug delivery in coming years, while minimizing costs and potential complications.

In this chapter, we describe the clinical manifestation of cytomegalovirus (CMV) retinitis, challenges associated with current therapeutic regimen, targeted lipid ester prodrugs, basic principles for the preparation of commonly used polymeric micelles for ocular drug delivery and a combination of prodrug-nanomicellar approach for the treatment of CMV retinitis. Together, the insights obtained indicate that polymeric micelles are highly effective delivery systems for intraocular drug delivery, (i) facilitating the formulation and entrapment of highly hydrophobic drugs, (ii) aiding drug administration, (iii) enabling controlled drug release kinetics, (iv) enhancing therapeutic efficacy, (v) reducing side-effects and and (vi) improving the in-vivo stability.

4.2. Cytomegalovirus (CMV) retinitis

CMV retinitis is a disease caused by an enveloped ds-DNA virus, CMV belonging to the Herpesviridae family and occurs primarily in immunocompromised individuals. CMV retinitis is the most common opportunistic ocular infection in patients with AIDS with CD4 T

lymphocyte counts <50 cells per microliter [111]. CMV retinitis typically initiates in the peripheral region of the retina and centrifugally progresses towards the posterior region ultimately leading to retinal necrosis and thus visual impairment. Other clinical manifestations involve dense, full-thickness areas, yellowish-white lesions, irregular granules at the border, retinal vasculitis and hemorrhage on the retinal surface (Figure 4-2) [112].

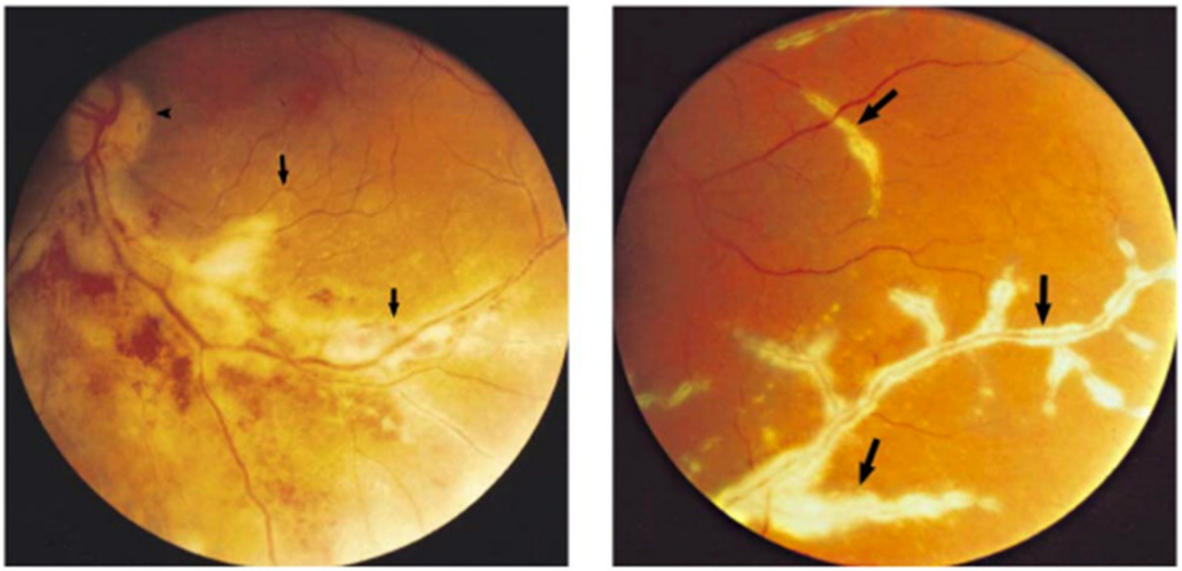

Figure 4-2 White wedged area, hemorrhage representing necrosis (left) and white sheathing along the blood-vessels (right) characteristics of CMV retinitis. Reprinted with permission from Keunen et al. [2], Copyright Massachusetts Medical Society

4.3. Current therapeutic regimen and associated challenges

Currently available therapies for CMV retinitis include ganciclovir (GCV), foscarnet, cidofovir (CDF) and valganciclovir [113]. Most of these therapies are given by intravenous and/or intravitreal injections, which are associated with poor patient compliance and adverse side effects. An oral prodrug form of ganciclovir, valganciclovir (Valcyte®, Roche) has been approved for the treatment of CMV retinitis. Once-daily administration of valganciclovir (900mg) produced GCV systemic exposure equivalent to once-daily IV administration of GCV

(5mg/kg) and 1.7 fold greater than oral GCV (1000mg) given thrice daily [114-115]. However, local delivery of therapeutic agents including implants (Vitrasert®, Bausch and Lomb) to the ocular tissues have been found to be more effective compared to systemic therapy.

Among these ART therapies, CDF (S-1-(3-hydroxy-2-phosphonylmethoxypropyl)cytosine; HPMPC), an antiviral nucleoside phosphonate has demonstrated significant therapeutic activity against CMV and other herpesviruses [116]. Unlike other nucleoside analogues such as acyclovir and GCV, CDF only needs two phosphorylation steps and is not phosphorylated by viral kinase i.e. is not dependent on viral-encoded enzymes in order to be converted to active diphosphate form. CDF undergoes phosphorylation to CDF-monophosphate (CDF-MP) and CDF-diphosphate (CDF-DP) by pyrimidine nucleoside monophosphate and diphosphate kinases respectively [117]. CDF-DP acts as a chain terminator of DNA synthesis and alternative substrate with respect to dCTP (deoxycytidine triphosphate) for DNA polymerase (Figure 4-3). The long half-life of the active diphosphate form and lower chances of viral resistance offers additional advantages to CDF therapeutically. Currently CDF is marketed only as an IV formulation with recommended dose of 5mg/kg once a week for two consecutive weeks followed by 5 mg/kg once every 2 weeks (maintenance phase) [118]. However, the major limitation of CDF is severe renal toxicity[119]. Additionally, CDF is highly hydrophilic and a good substrate of efflux pump, MRP2 which leads to low bioavailability [120].

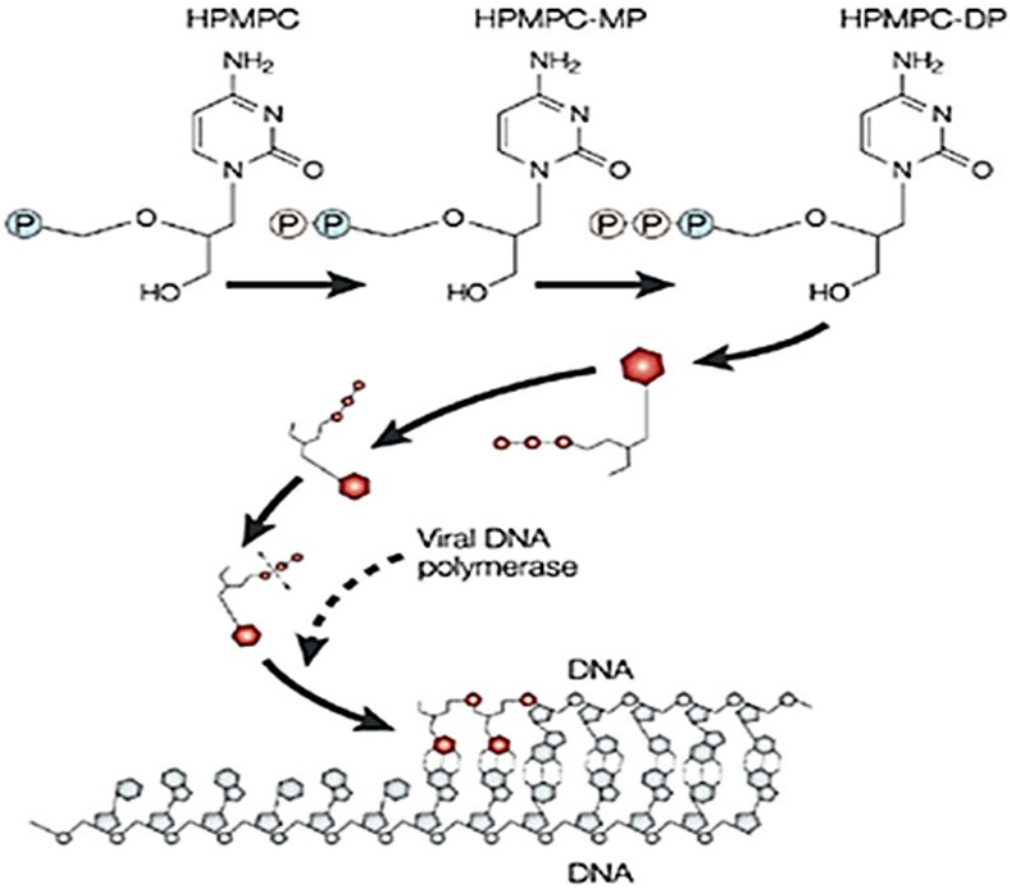

Figure 4-3 Mechanism of action of cidofovir (HPMPC). Reproduced with permission from Clercq et al.[6]

4.4. Challenges to ocular drug delivery

Efficient drug delivery to the ocular tissues faces a number of challenges due to the dynamic anatomy and the blood-ocular barriers (including blood-aqueous and blood-retinal barrier). From a drug delivery perspective, the eye can be divided into four parts: (i) the pre-corneal area (conjunctiva, eyelids); (ii) the cornea; (iii) the anterior segment (iris, ciliary body, lens) and (iv) the posterior segment (retina, vitreous cavity) [121].

The tear drainage rate constant from the pre-corneal area is 1.45 min^{-1} which results in 500 to 700 times greater drug loss from the ocular surface in comparison to the drug absorption rate

into the anterior chamber [122]. This process eventually leads to less than 5% of the topically applied dose reaching the intraocular tissues. Additionally, the complex anatomy of the tear film with its outer oily layer retarding water evaporation, further impedes drug absorption into the cornea and sclera [123].

The cornea is an important route for drug absorption after topical application. It consists of five different layers, namely epithelium, Bowman's membrane, stroma, Descemet's membrane, and endothelium. The corneal epithelium plays a major role in limiting trans-corneal drug absorption with a drug permeability rate of only 10^{-7}-10^{-5} cm s^{-1} [124]. While small lipophilic drugs are passively transported via the transcellular pathway, hydrophilic drugs undergo restricted permeation through tight junctions via the paracellular pathway. The corneal stroma being hydrophilic, impedes transport of lipophilic drug molecules while hydrophilic molecules generally diffuse freely through the stroma. Overall, the efficacy of the trans-corneal route is limited by the relatively low absorption rate constants (1-5 x 10^{-3} min^{-1}) [125-126], with a molecular weight cut-off of 400-600 Da also playing an important role in the corneal permeability of drug molecules [127].

The high permeability of the human conjunctiva, on the other hand, can be attributed to its 17-fold larger surface area in comparison to the human corneal membrane. The larger paracellular spacing in conjunctival tissue (230 times greater than in the cornea cornea) facilitates passage of large hydrophilic molecules [128]. These characteristics have established the importance of the conjunctival-scleral pathway for intraocular delivery of macromolecules including proteins, peptides and nucleic acids. The trans-scleral route may also be utilized for the delivery of large molecules to the retina and vitreous, if suitable drug-delivery systems are

employed. However, lymphatics and blood vessels present in the conjunctiva eliminate significant amounts of therapeutics via the systemic circulation [129].

Similar to the corneal stroma, hydrophilic drugs permeate through scleral matrix pores readily in comparison to lipophilic drugs. The molecular radius and charge of the drug molecule also greatly control the permeability across the sclera. Positively charged molecules appear to permeate the sclera poorly presumably due to their binding with the negatively charged scleral matrix [130]. Additionally, the blood ocular barriers contribute majorly, limiting drug entry into the posterior segment following systemic and periocular administration. The blood-aqueous barrier (BAB) is present in the anterior segment of the eye and restricts drug entry from the blood into the aqueous humor. However, the BAB is not considered a complete barrier because of the fenestrated capillaries present in the ciliary body stroma. These fenestrated vessels being the secondary source of plasma protein leakage to the iris also allow passage of small molecules to enter the iridial circulation [131]. The blood-retinal barrier (BRB) present in the posterior segment is further divided into inner and outer BRB. The inner BRB is composed of tight junctions between retinal capillary endothelial cells and is anatomically similar to the blood-brain barrier (BBB). The outer BRB is formed by the tight junctions between retinal pigment epithelial (RPE) cells. The greater density of tight junctions and pericytes in comparison to the BBB as well as the presence of glial cells, render the inner BRB highly effective in limiting transport of drugs from the blood into the retina [132-133].

4.5. Lipid ester prodrug approach

Prodrugs have been categorized in various classes which include carrier linked vs bioprecursor, site of conversion/metabolism (intracellularly vs extracellularly) and mixed prodrugs (prodrugs belonging to multiple classes) [134-135]. Lipid prodrugs, a type of carrier linked prodrugs, are typically designed to elevate the lipophilic characteristics of hydrophilic drugs thereby promoting passive diffusion (Figure 4-4). Hydrophilic drugs usually generate poor cellular transport due to high polarity and low passive permeability. Transport of these agents may be enhanced by masking the ionizable or polar groups [135-136]. However, it is extremely important to maintain a balance between the lipophilic and hydrophilic properties in order to generate optimal transcellular diffusion and aqueous solubility [136]. The type of the linkages that can be selected for synthesizing prodrugs mainly depends on the nature of functional groups in the parent drug structure.

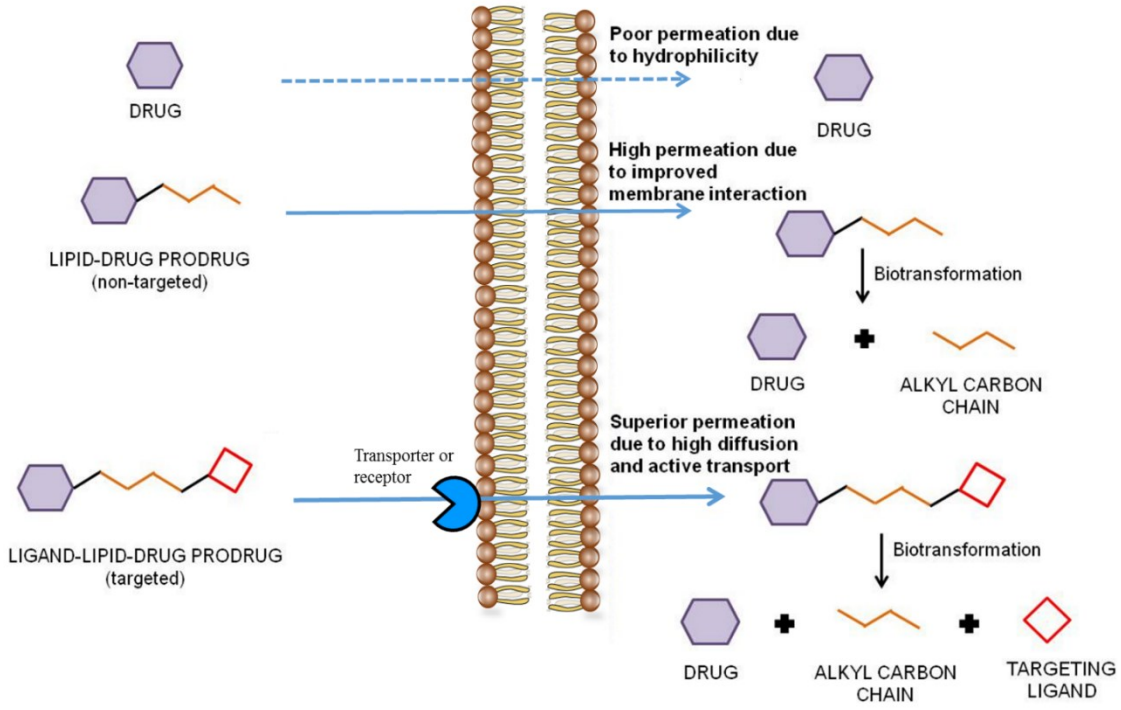

Figure 4-4 Basic cellular uptake mechanism of two types of lipid linked prodrugs extensively employed to improve absorption of hydrophilic drugs

Hydrophilic drugs containing carboxylic acid or hydroxyl groups may be formulated in the form of ester prodrugs by covalently linking suitable pro-moieties. An appropriate geometry and size of the alkyl carbon chain may be optimized to produce stable lipophilic prodrugs, *in vivo*. Such prodrugs can generate higher cellular permeation relative to unmodified parent drug due to improved interaction with absorptive membranes. Following cellular entry, these compounds may undergo enzymatic degradation by esterase class of enzymes to regenerate parent drug and pro-moiety [137]. An important advantage of generating ester prodrugs is the ubiquitous expression of esterase class of enzymes in humans. Hence, prodrugs can be designed such that these compounds are cleaved in blood, liver and other intended target tissues. A careful selection of pro-moiety is highly important so as to render the process of prodrug development more feasible. Ideal properties of pro-moiety include non-immunogenicity, optimal stability at physiological temperature and biological conditions, degradation to non-toxic and inactive metabolites, ease of synthesis and cost effectiveness [7, 9, 138]. Despite potential advantages, ester prodrugs are highly susceptible to enzymatic hydrolysis and may generally yield lower half-lives *in vivo*. In such conditions, carbamate ester prodrugs may be preferred over carboxyl ester prodrugs to impart higher *in vivo* stability and longer half-lives [7].

Amide prodrugs are also generally employed to improve drug absorption due to higher stability relative to ester prodrugs. However, such prodrugs are commonly used for improving tissue specificity and minimizing dose-related toxicities. Some of the amide prodrugs have been evaluated for their potential to improve drug accumulation and efficacy in target tissues [139-140]. Furthermore, disulfide, oximes, imines and thioether linkages have also been explored for prodrug development [7-8, 141-143]. Various types of linkages that can be produced depending

on the presence of a specific functional group in the parent drug structure have been extensively discussed previously [8, 135]. However, considerable attention should be paid to prodrug design in early development phases as these compounds can significantly modulate the pharmacokinetic, toxicokinetic and efficacy profiles of a parent drug.

Recently, transporter targeted lipid prodrug design has emerged as an interesting strategy to improve drug absorption and efficacy [34, 144-149]. In this approach, prodrugs are produced by covalently linking lipid raft as well as a membrane transporter or receptor targeting moiety (Figure 1-1). Lipid rafts would impart lipophilicity whereas targeting moiety may enhance site specificity and selectivity. Such prodrugs generate significantly higher cellular accumulation due to synergistic effects of lipid rafts and transporter or receptor targeting pro-moieties. The presence of lipid may dramatically increases prodrug interaction by facilitating docking of the targeting pro-moiety to the binding domain of membrane transporter or receptor [34]. Subsequently, prodrugs are rapidly translocated across cell membrane and enzymatically cleaved in cytoplasm to yield the parent drug. Such strategy may be employed to improve tissue absorption and specificity of various hydrophilic therapeutic agents such as nucleosides, nucleotides, genes, siRNA, oligonucleotides, peptides, proteins and other macromolecules.

4.6. Targeted lipid ester prodrugs

Membrane transporter or receptor targeted lipid prodrugs presents an innovative approach to improve drug delivery and specificity. Cumulative effects of high passive diffusion, transporter recognition and reduced efflux by targeted lipophilic prodrugs may significantly improve drug efficacy and overcome development of resistance. Vadlapudi et al. have developed a series of sodium dependent multivitamin transporter (SMVT) targeted and

non-targeted lipid prodrugs (Figure 4-5) of acyclovir [144]. These include biotin-ricinoleic acid-acyclovir, biotin-12-hydroxy stearic acid-acyclovir, ricinoleic acid-acyclovir and 12-hydroxy stearic acid-acyclovir. Ricinoleic acid and 12-hydroxy stearic acid were employed as lipid rafts. Biotin was selected to target SMVT. B-R-acyclovir and R-acyclovir have generated about 10 and 4-fold higher cellular uptake in MDCK-MDR1 cells relative to parent drug. Interestingly, biotin-acyclovir has generated about 6-fold higher cellular accumulation relative to unmodified acyclovir. Based on these results, it is apparent that the incorporation of lipid raft as well as transporter targeting moiety in the prodrug construct (B-R-acyclovir) can significantly improve cellular accumulation relative to parent drug (acyclovir), lipid prodrug (R-acyclovir) and transporter targeted prodrug (B-acyclovir). Importantly, cellular accumulation of B-R-acyclovir and B-12HS-acyclovir was significantly diminished in the presence of unlabeled biotin, a potent substrate of SMVT [96, 150-154]. Considerable uptake inhibition clearly indicates that these prodrugs possess higher affinity towards SMVT. Moreover, the half-maximal inhibitory concentration (IC_{50}) values exhibited by B-R-acyclovir (8.04 ± 0.07 μM) and B-12HS-acyclovir (8.17 ± 0.09 μM) were significantly lower relative to B-acyclovir (14.84 ± 0.10 μM). This result further supports the contributory role of lipid raft in generating higher and tighter prodrug binding with SMVT. Similarly, B-R-acyclovir and B-12HS-acyclovir produced about 10 and 8-fold higher cellular uptake relative to unmodified acyclovir in human Caco2 cells.

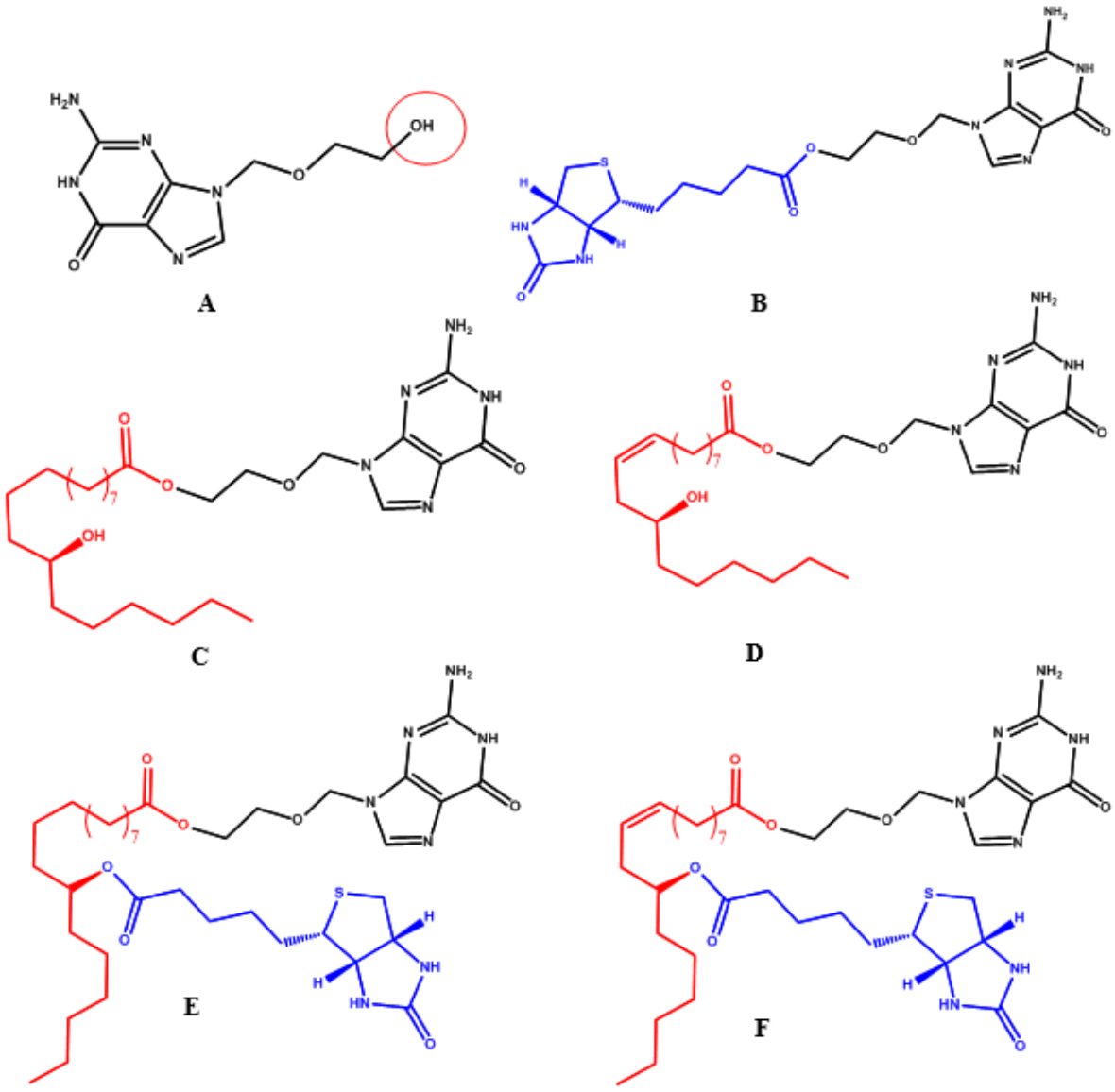

Figure 4-5 Structure of acyclovir (A), B-acyclovir (B), 12-HS-acyclovir (C), R-acyclovir (D), B-12HS-acyclovir (E) and B-R-acyclovir (F). Modifications with lipid rafts and biotin are shown with red and blue color, respectively

Vadlapudi et al. have also investigated the potential of B-R-acyclovir and B-12HS-acyclovir to improve corneal absorption of acyclovir [34], since SMVT is reported to be highly expressed on the apical surface of corneal epithelial cells [150, 155]. B-R-acyclovir and B-12HS-

acyclovir have displayed about 13-fold higher uptake relative to acyclovir in human corneal epithelial cells (HCEC). Moreover, transepithelial transport of [3H]-biotin was significantly abolished in the presence of both prodrugs confirming SMVT involvement in the prodrug translocation across freshly excised rabbit cornea. Docking analysis revealed superior binding affinity towards SMVT for B-R-acyclovir and B-12HS-acyclovir compared to B-acyclovir. Docking scores for B-R-acyclovir, B-12HS-acyclovir and B-acyclovir were -7.5, -7.9 and -6.6, respectively.

Biotin-lipid prodrugs also possessed superior antiviral activities against herpes simplex viruses (HSV-1 and HSV-2) and Epstein Barr virus (EBV) relative to acyclovir itself. B-12HS-acyclovir (EC_{50} = <0.096 μM) has generated 36 and 62-fold higher antiviral potency relative to unmodified acyclovir (EC_{50} = 3.43 and 5.98 μM) against HSV-1 and HSV-2 viruses, respectively. B-R-acyclovir (EC_{50} = 0.27 μM) has produced 22-fold higher antiviral activity against HSV-2 relative to parent drug (EC_{50} = 5.98 μM). Moreover, this prodrug (EC_{50} = 12.4 μM) has demonstrated about 6-fold higher antiviral activity against EBV relative to acyclovir (EC_{50} = 2.1 μM). However, antiviral efficacy of B-R-acyclovir (EC_{50} = 70 μM) and B-12HS-acyclovir (EC_{50} = >300 μM) against human cytomegalovirus (HCMV) was observed to be significantly lower relative to ganciclovir (EC_{50} = 0.21 μM). Importantly, B-R-acyclovir and B-12HS-acyclovir were found to be highly selective and generated negligible cell cytotoxicity as demonstrated by neutral red dye uptake and CellTiter Glo (Toxicity) assays. These results clearly indicate the feasibility of using SMVT targeted lipid prodrugs for the treatment of ocular infections such as herpes keratitis. Investigators also mentioned that these compounds are currently being examined for antiviral efficacy in virus infected animal models by NIH/NIAID.

Recently, Gokulgandhi et al. have designed and developed a series of transporter targeted and non-targeted lipid prodrugs to improve absorption of cidofovir in ocular tissues [145]. Prodrugs synthesized were C6-cidofovir, C12-cidofovir, biotin-C2-cidofovir, biotin-C6-cidofovir and biotion-C12-cidofovir (Figure 4-6), where n denotes number of carbons in lipid chain. Prodrugs were highly lipophilic relative to cidofovir. Significant enhancement in the lipophilicity may improve prodrug diffusion in ocular tissues relative to cidofovir upon topical or systemic administration. [3H]-biotin uptake was diminished significantly with increase in lipid carbon chain length in prodrug structure. B-C12-cidofovir has produced 73% inhibition in [3H]-biotin uptake rate relative to 50% by B-C2-cidofovir. Moreover, affinity of B-C12-cidofovir (IC_{50} = 2.9 μM) towards SMVT was significantly higher compared to B-C2-cidofovir (IC_{50} = 31.4 μM). B-C12-cidofovir reduced [3H]-biotin transport (70%) across MDCK–MDR1 cells relative to B-C2-cidofovir (44%). This study indicates that substrate affinity of prodrugs towards SMVT increase significantly with rise in lipid carbon chain length. Importantly, B-C2-cidofovir (3-fold), B-C6-cidofovir (5-fold) and B-C12-cidofovir (10-fold) prodrugs were observed to partition into the retina–choroid tissue at significantly higher levels relative to cidofovir. This result indicates that intravitreal injection of SMVT targeted lipid prodrugs may be a viable approach to treat infections affecting posterior segment tissues of the eye.

Antiviral efficacy of cidofovir and prodrugs have also been investigated against HCMV, HSV-1 and 2, VZV, EBV, BK and JC viruses, Vaccina (VACV) and Cow pox viruses (CXPV) [156]. B-C12-cidofovir has displayed superior antiviral efficacy against HCMV (EC_{50} = 0.57 vs 1.24 μM), HSV-2 (EC_{50} = 2.16 vs 54.41 μM) and BK (EC_{50} = 13.8 vs 28.6 μM) viruses relative to parent drug. EC_{50} values generated by this prodrug were approximately 2 to 25-fold lower relative to cidofovir. B-C6-cidofovir has displayed excellent antiviral activity against

HCMV (EC_{50} = 1.03 vs 1.24 μM) and HSV-2 (EC_{50} = 12.16 vs 54.41 μM) relative to cidofovir. Interestingly, C12-cidofovir has generated about 3 to 30-fold higher antiviral efficacies against HSV-2 (EC_{50} = 2.09 vs 54.41 μM), BK (EC_{50} = 1.4 vs 28.6 μM), JC (EC_{50} = 0.23 vs 6.61 μM), VACV (EC_{50} = 1.5 vs 9.08 μM) and CXPV (EC_{50} = 1.44 vs 4.25 μM) viruses relative to unmodified cidofovir. Therefore, it appears that biotin lipid prodrug approach may markedly improve delivery as well as efficacy of antiviral drugs. Since, SMVT is highly expressed in intestinal epithelial cells [151, 157-158], lipid prodrugs targeted toward this influx transporter can be explored to improve oral absorption of acyclovir and ganciclovir.

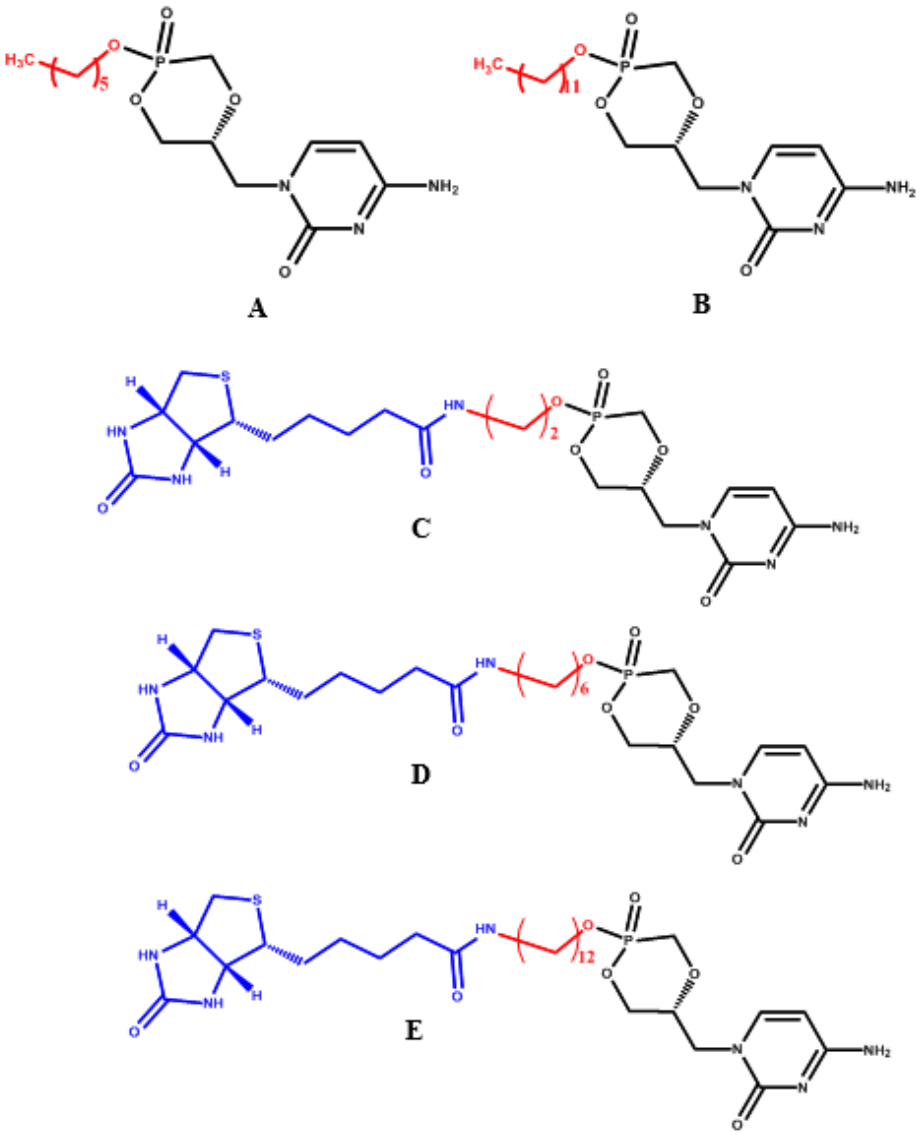

Figure 4-6 Structure of C6-cidofovir (A), C12-cidofovir (B), B-C2-cidofovir (C), B-C6-cidofovir (D) and B-C12-cidofovir (E). Modifications with lipid rafts and biotin are shown with red and blue color, respectively

4.7. Polymeric micelles

The physicochemical nature of nano-sized micelles also termed as “nanomicelles” consisting of a hydrophobic core and a hydrophilic shell, renders these spherical vesicles

highly acceptable for passive drug delivery of hydrophobic compounds. Polymeric micelles (10-200 nm) are based on amphiphilic molecules or block copolymers which can generally self-assemble into organized core-shell/supramolecular structures in aqueous media at concentrations exceeding their critical micellar concentrations (CMC) [159]. On the other hand, low-molecular weight surfactant-based micelles exhibit higher CMC in contrast to polymeric micelles, leading to diminished stability and potential side effects. The potential of polymeric micelles to solubilize and stabilize hydrophobic compounds leads to their prolonged retention thereby improving therapeutic outcomes [160]. Nevertheless, micelle-based nanomedicines suffer from a myriad of problems when employed in *in vivo* systems. Dilution in the blood stream as well as interactions with blood components (including plasma proteins such as albumin, fibrinogen, prothrombin and gamma globulins) lead to their premature disintegration in the systemic circulation. This substantiates the primary reason for the limited improvements in therapeutic efficacy of micellar nanomedicines in clinical trials when administered systemically [161-162], while such issues would be minimal for topical ocular administration.

4.7.1. Principles of micelle formation

The polymeric units self-assemble into a nanoscale aggregates (10-200 nm), known as micelles having a hydrophobic core and a hydrophilic corona. Such self-assembly is favored by a thermodynamic process. The hydrophilic chains cover the hydrophobic core to avoid their direct contact with water and thus reduce the interfacial free energy of the polymer-water system. Micellar formation confides upon the reduction of the interfacial free energy [163-164]. The degree of self-aggregation generally depends on the polymer chain concentration, the properties of the drug or any targeting agents, and the mass and composition of the copolymer

backbone [165]. Depending upon the molecular weight of the block copolymers, micelles can have different shapes including spherical, cylindrical and star-shaped structures [166-167].

4.7.2. Critical micelle concentration (CMC): a key factor in micellization

The minimum polymer concentration required to form micelles is termed as CMC. Below the CMC, insufficient numbers of polymeric chains are uniformly distributed in the solution as monomers[168]. With an increase in the concentration, more polymeric chains are absorbed at the interface. The concentration, at which the interface becomes saturated with polymeric chains is known as the CMC. Above this point, an increase in the polymer concentration in solution results in the formation of micelles [169-170]. Polymeric micelles (10^{-6}–10^{-7} M) usually exhibit CMC values 1000 times lower than that of low-molecular-weight surfactant based micelles (10^{-3}–10^{-4} M), with a low CMC value indicating increased stability of the micellar structure in an aqueous solution [171-172]. For topically administered micellar ophthalmic formulations, the CMC is a critical factor. It regulates the chances of premature drug release from the formulation due to constant tear dilution and nasolacrimal drainage[173]. Dispersity (D), also known as polydispersity index (PDI), is another important factor that can influence the shape, stability and overall performance of the micellar formulation[174]. The kinetics of copolymers which exist between the micellar and non-micellar state are also influenced by the dispersity of the polymers. Therefore, block copolymers with monodisperse core-shell structures having a low dispersity ($D<1.2$) are preferred for the development of controlled release systems [175-176].

4.7.3. Polymeric micelle structures

The preparation of polymeric micelles can be divided into three categories namely (i) polymer–drug conjugates, (ii) drug-encapsulated carriers and (iii) polyion complex micelles.

4.7.3.1. Polymer–drug conjugates

Micelle forming polymer-drug conjugates are developed through hydrolysable chemical bonds between the functional group(s) of the polymeric backbone and the drug. To date, poly(ethylene oxide)-b-poly(ester) and poly(ethylene oxide)-b-poly(amino acid) block copolymer based conjugates have been extensively studied for effective drug delivery applications. Thes polymers may have several functional groups providing various sites for the conjugation of a number of drug molecules to one polymeric chain allowing efficient delivery of therpeutic doses. [177-181].

4.7.3.2. Drug-encapsulated carriers

The solublization and stable encapsulation of drug into polymeric micelles can primarily be achieved by chemical and physical methods. Chemical methods involve covalent core cross-linking of the drug with the polymers consisting of side-chain or end-group-functionalized block copolymers. An important factor to be considered using chemical methods is that the reactive groups of the polymers should be sufficiently hydrophobic or low in number so that they do not interfere with the formation of monodisperse micelles[182]. The most commonly employed methods for preparing core cross-linked polymeric micelles are: (i) radical polymerization, used for micelles containing polymerizable groups in their core; (ii) addition of bifunctional crosslinkers, used for micelles containing reactive groups in their core; and (iii) disulphide bridges, used for micelles containing thiol groups. The last method allows for stimuli-responsive disintegration and drug release. Although chemical crosslinking allows significant improvements in circulation kinetics, biodistribution and target site accumulation of micelles, the series of chemical reactions involved may sometimes be challenging and complicated. On the other hand, physical methods including (i) direct dissolution, (ii) dialysis,

(iii) oil-in-water emulsion, (iv) solvent evaporation, (v) co-solvent evaporation and (vi) freeze-drying methods (Figure 4-7) are much simpler and practical[183].

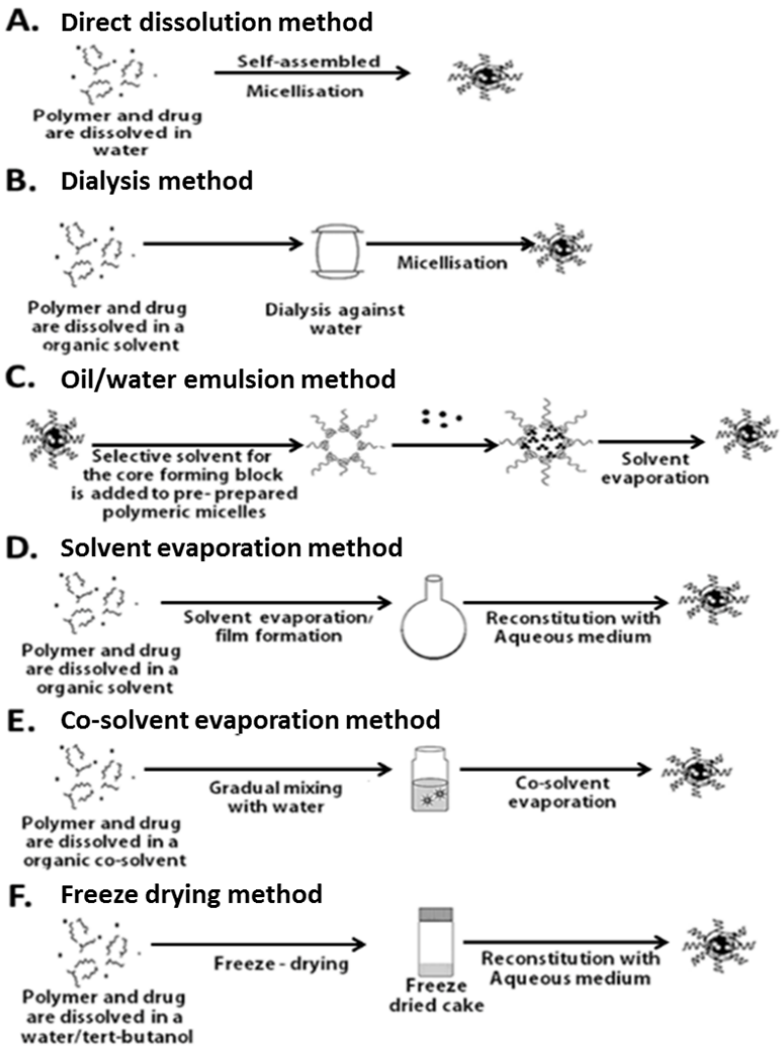

Figure 4-7 Physical methods of drug encapsulation into polymeric micelles: (A) direct dissolution; (B) dialysis; (C) oil-in-water emulsion; (D) solvent evaporation; (E) co-solvent evaporation; (F) freeze-drying

4.7.3.2.1. Direct dissolution method

The direct dissolution method is the simplest technique for the preparation of drug-loaded polymeric micelles. Copolymers along with drugs are mixed in water at or above the CMC to self-assemble into drug-loaded micelles[184]. However, this technique is associated with

low drug-loading which can be enhanced by increasing the temperature of the system before the addition of the copolymer. Preparation of a thin film of drug before the addition of the polymer into the system can also result in higher drug loading (Figure 4-7 A) [185].

4.7.3.2.2. Dialysis method

The drug along with the block copolymer are dissolved in a water-miscible organic solvent (such as N,N-dimethylformamide) and the resultant solution is dialysed against water [186-190] (Figure 4-7 B). During the dialysis process, the organic solvent is replaced by water which induces self-association of block copolymers and the entrapment of drug. The semipermeable membrane of the dialysis bag keeps the drug encapsulated polymeric micelles inside[191]. At the same time unloaded or free drug remains outside the dialysis bag. However, this method is only suitable for lab scale production, while incomplete removal of the free drug from the polymeric assemblies is another drawback. Alternatively, tangential flow filtration (TFF) is a fast and simple method that can be used for scalable manufacturing processes of polymeric micelles [192].

4.7.3.2.3. Oil-in-water emulsion method

The drug is dissolved in a water-immiscible organic solvent (such as chloroform or methylene chloride), followed by addition of this organic to the aqueous phase under vigorous stirring. The polymer may be dissolved in either the organic or the aqueous phase and the organic solvent is then removed by evaporation (Figure 4-7 C) [193-195].

4.7.3.2.4. Solvent evaporation method

Drug and polymer are dissolved in a volatile organic solvent. A thin film of drug/polymer is formed at the bottom of the flask after the evaporation of the organic solvent. This film is then reconstituted in an aqueous phase by vigorous shaking (Figure 4-7 D). This

method can be applied for micelle-forming block copolymers having high hydrophilic lipophilic balance (HLB) values so that the polymer film can be easily reconstituted in an aqueous medium [196-198].

4.7.3.2.5. Co-solvent evaporation method

Drug and polymer are dissolved in a volatile water-miscible organic solvent (co-solvent) followed by addition of the aqueous phase (non-solvent for the core-forming block) which triggers the formation of micelles and drug entrapment. The organic co-solvent is evaporated at the end resulting in drug loaded polymeric micelles (Figure 4-7 E) [199-202].

4.7.3.2.6. Freeze-drying method

This method is applicable for freeze-dryable organic solvents such as tert-butanol which can dissolve the polymer and the drug. The drug/polymer solution is then mixed with water, freeze-dried and reconstituted with isotonic aqueous media. This method is suitable for large scale production. However, it is applicable only to block copolymers and drugs that can be solubilized in tert-butanol (Figure 4-7 F) [203].

4.7.3.3. Polyion complex micelles

Electrostatic interactions between oppositely charged polymer/drug combinations result in polyion complex micelles. This method is suitable for different therapeutic moieties that carry charge including peptides and DNA. Upon neutralization of the charge, the core-forming segment of the block copolymer can induce self-assembly of the polyion complex and further stabilization of the micelle [204-207].

4.8. Ocular delivery pathways of micelles

After topical application of an eye drop, a drug is anticipated to follow either the corneal or the conjunctival-scleral pathway to reach posterior segment tissues [208]. The hydrophilic stroma which constitutes 85-90% of the cornea, acts as a rate limiting barrier for topically applied hydrophobic drugs [209]. Such limitation can be overcome by encapsulating hydrophobic drugs into the lipophilic cores of highly water soluble polymeric micelles. Polymeric micelles, being extremely small, can penetrate through the cornea and/or the alternative conjunctival-scleral pathway after topical application. The higher conjunctival-scleral surface area allows lateral diffusion of such polymeric micelles to reach the posterior segment of the eye [210]. Nano-sized micelles with their hydrophilic corona assist in scleral transport of the micellar-drug construct through the aqueous pores/channels. In addition, the scleral pathway also minimizes the chances of drug washout into the systemic circulation by the conjunctival blood circulation and lymphatics. From the posterior segment, the polymeric micelles may be further engulfed by RPE cells by endocytosis to generate therapeutic concentrations in posterior ocular tissues [211-213]. Such tissue absorption and cellular uptake depend on the surface charge and size of the micelles [214]. Figure 4-8 shows a schematic illustration of the penetration of a polymeric micellar formulation applied in the form of a topical eye drop to the posterior ocular tissues.

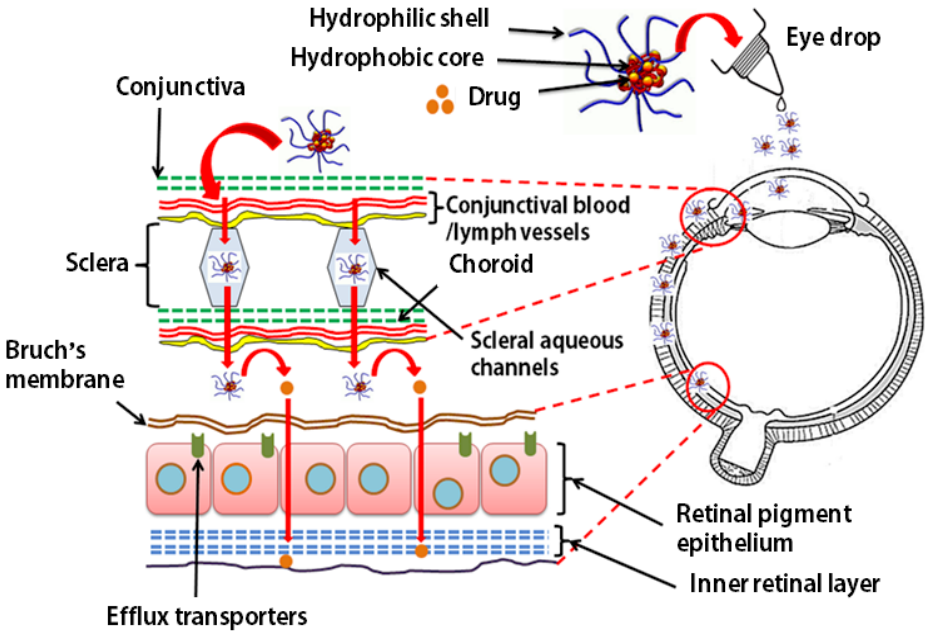

Figure 4-8 Schematic representation of polymeric micelles reaching the posterior ocular tissues via the transcleral pathway after topical application

4.9. Drug release from polymeric micelles

Drug release from polymeric micelles mainly depends upon (i) the design and method used for their preparation; (ii) the structure of the micelle-forming block copolymer and the drug; (iii) their physicochemical properties; and (iv) the localization of the drug in the polymeric micelles. Figure 4-9 shows various modes of drug release from polymeric micelles. Drug release from polymer-drug conjugates generally follows two mechanisms, (i) dissociation of micelles followed by drug cleavage from the polymeric unimers or (ii) drug cleavage inside the micellar structure followed by diffusion out of the carrier[215] (Figure 4-9 A). Drug release from drug-loaded micellar carriers is usually preceded by diffusion (Figure 4-9 B), whereas drug release from polyion complex micelles is triggered via ion exchange in physiological media Figure 4-9 C).

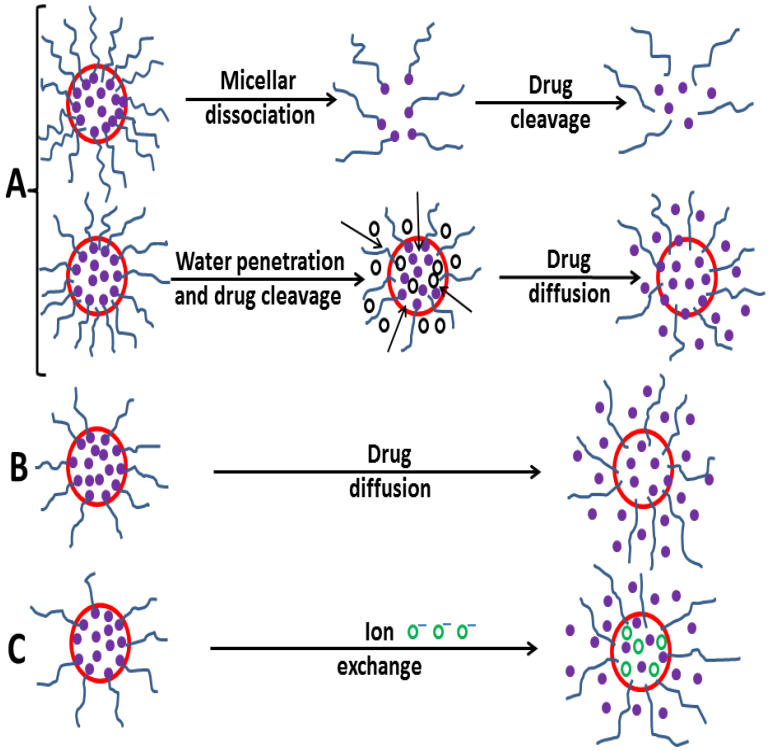

Figure 4-9 Modes of drug release from polymeric micelles. (A) Drug release from block copolymer-drug conjugates, (B) Drug release from drug encapsulated micellar carriers and (C) Drug release from polyion complex micelles

Apart from these basic drug release mechanisms, instant, sustained, pulsed or delayed drug release can be achieved by modifying the chemical structure of the micelle-forming block copolymers which will ultimately modify the physicochemical properties of the core/shell forming blocks. For example, sustained or delayed drug release from the carrier can be achieved by enhancing the hydrophobicity and rigidity of the micellar core which limits the movement of water and free ions to the micellar core in micelle-forming drug conjugates and polyion complex micelles [216-217].

A lower rate of micellar dissociation, the diffusion of drug and the overall drug release from micellar carriers can also be achieved via crosslinking of the micellar core structure and the induction of strong hydrophobic interactions or hydrogen bonds between the core-forming

blocks and the drug [218-220]. The incorporation of hydrophilic or stimuli responsive groups to the core structure may be another avenue to provide an instant or pulsed mode of drug delivery [219, 221-224].

4.10. Potential polymeric micellar formulations for clinical translation

Various polymeric micellar formulations have been patented to date exhibiting great potential for proof-of-concept efficacy and safety as novel ophthalmic micellar formulations. However, for successful clinical translation, a few critical steps are necessary. Obtaining preclinical proof of efficacy and pharmacokinetic data in various animal models is a prerequisite before going into clinical trials[225]. Besides the therapeutic response, systemic exposure and bio distribution in animal models should be reported. Direct head-to-head comparisons of the therapeutic efficacy of various related formulations are strongly recommended. In addition, *in vitro* and *in vivo* safety and tolerability profiles should be generated to determining a safe dose range for clinical evaluation. A thorough characterization including impurity profiling and methods for upscaling production is imperative for successful clinical translation. Table 4-1 lists recent patent inventions related to polymeric micellar formulations for effective ocular drug delivery with most of these still being under preclinical development.

Table 4-1 Summary of recent patented polymeric micelle formulations for ophthalmic applications currently under preclinical evaluation

Patent number	**Year**	**Formulation characteristics**
US8980839 B2	2015	Aqueous nanomicellar ophthalmic solution comprising cyclosporine, a polyoxyl lipid or fatty acid and a polyalkoxylated alcohol
WO2015041520 A1	2015	Peptide-based self-assembling micelles

Patent number	Year	Formulation characteristics
US 9017725 B2	2015	Nanomicelles consisting of dexamethasone, vitamin E TPGS and octoxynol-40.
CN104644550 A	2015	A curcumin micelle drops, comprising curcumin, chitosan micelle drug carriers, surface active agents, surfactants and pharmaceutical purified water.
US 8697098 B2	2014	Prolamine protein conjugated to a polymer, such as a polyethylene glycol (PEG) chain, with conjugates used to prepare micelle assemblies.
US8470371 B2	2013	A polymeric micellar aggregate having a mean particle size between 20 and 500 nm formed from an amphiphilic carbohydrate polymer.
US 20120225834 A1	2012	Ocular iontophoresis consisting of micelles comprising one or more charged surfactants and one or more bioactive agents.
US 20120294945 A1	2012	Micelle consisting of hyaluronic acid and a core region comprising a water-insoluble peptide with a terminal amine group, wherein the water-insoluble peptide is bound to hyaluronic acid or its pharmaceutically acceptable salt.
WO2010144194	2010	Mixed nanomicellar formulations (vitamin E, TPGS, octoxynol-40) of water insoluble drugs.
WO 2011041377 A1	2010	Ocular iontophoresis of charged nanomicelles consisting of alkyltrimethylammonium halide, alkyldimethylammonium halide, alkylmethylammonium halide, alkylethyldimethylammonium halide, alkyldimethylbenzylammonium halide, alkylpyridinium halide, and alkylimidazolium halide, or a mixture of two or more.
WO2008004978 A1	2008	A block copolymer comprising at least a first block and a second block, wherein the first block comprises a range of temperature-sensitive monomeric units, a range of hydrophilic monomeric units

Patent number	Year	Formulation characteristics
		and a range of targeting monomeric units. The second block comprises a range of hydrophobic monomeric units and at least one pH-sensitive moiety.
WO2008017839 A1	2008	Polymeric micellar clusters formed from amphiphilic carbohydrate polymer.
US 20060110356 A1	2006	Micelles with a hydrophilic polymer chain of polyoxyethylene or polyethylene glycol and a hydrophobic polymer chain of polylactone.
EP1609465 A1	2005	Polymer micelle of a block copolymer wherein the hydrophilic polymer chain is polyoxyethylene or polyethylene glycol. The charged polymer chain is a polyamine, a polycarboxylic acid or a polypeptide.
CA 2520525 A1	2004	Polymer micelle of a block copolymer comprising a hydrophilic polymer chain (polyoxyethylene or polyethylene glycol) and charged polymer chain as a core (polypeptide)
US6579519 B2	2003	Micelle solution of block random copolymers of the general formula $(X+Y+Z-)_m$, wherein X is a monomer selected from the vinyl group of compounds, Y is a monomer which will provide thermo-sensitivity of the co-polymer having a general formula R_1-R_2N-(C═O)-CH═CH_2. Z is a monomer selected from acrylate based monomers which will provide mucoadhesiveness and pH-sensitivity.
US5955509 A	1999	Poly(vinyl N-heterocycle)-block-poly(alkylene oxide) copolymer based micelles
US 5766580 A	1998	Micelle comprising ethylene oxide-propylene oxide-ethylene oxide block copolymer.

4.11. Nanomicelles for targeted lipid ester prodrug delivery

Various formulation strategies including polymeric nanoparticles, liposomes, and dendrimers have been developed to improve ocular concentrations of therapeutic agents. However, the majority of these formulations are administered via intracameral, intravitreal and periocular injections to overcome the ocular barriers with frequent injections generally required which may result in adverse effects[226]. Therefore, formulation strategies that are capable of delivering therapeutic agents to the back of the eye after topical application can be highly effective in improving drug efficacy.

Additionally, improving the permeability of hydrophilic agents employing lipid esters and targeting the overexpressed SMVT transporters, has allowed such transporter targeted prodrug approaches to be highly effective in improving permeability and efficacy of hydrophilic therapeutic agents such as CDF.

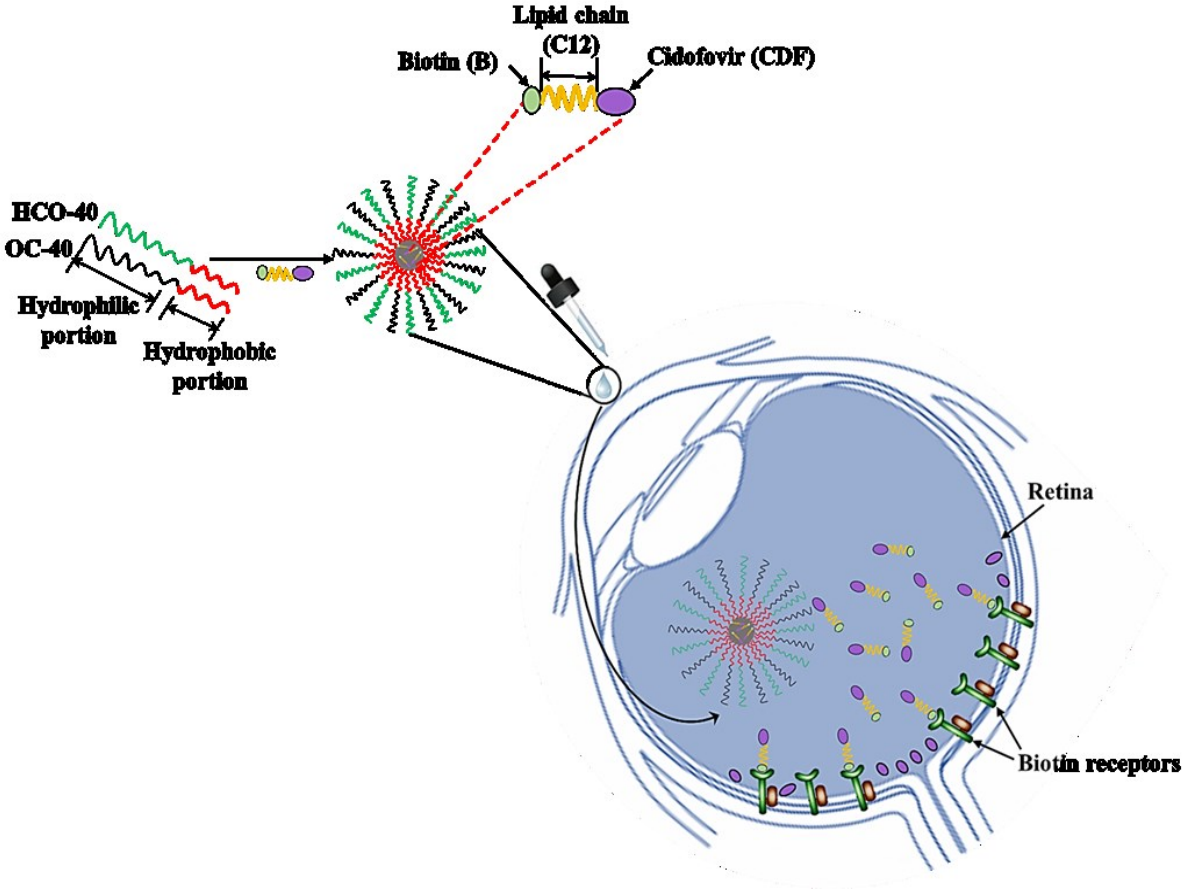

Figure 4-10 Hypothetical mechanisms involved in the transport of B-C12-cCDF prodrug-loaded nanomicelles to improve retinal targetibility and bioavailability, simultaneously

In this approach (Figure 4-10), we have utilized a highly effective prodrug of CDF, B-C12-cCDF that was developed by Gokulgandhi et al. and manufactured in contract with SRI International (Menlo Park, California). We hypothesized that the prodrug would generate improved permeability across ocular barriers in comparison to CDF. The biotin moiety coupled to CDF will allow improved binding and translocation via SMVT transporters simultaneously evading efflux pumps. However, the twelve-carbon chain moiety imparts lipophilicity to the prodrug, which renders it improper for topical application. Hence, we propose to develop a topical aqueous nanomicellar formulation of the lipophilic B-C12-cCDF prodrug. This nanomicellar formulation will allow signficiant entrapment of the lipophilic prodrug into its core. We hypothesize that these nanomicelles being significantly smaller in size (20-80nm) will effectively permeate through the conjunctival scleral pathway and generate improved retinal CDF concentrations over a period for the treatment of CMV retinitis.

CHAPTER 5

5. TOPICAL FORMULATION OF SELF-ASSEMBLED ANTIVIRAL PRODRUG NANOMICELLES FOR TARGETED RETINAL DELIVERY

5.1. Rationale

Cidofovir and its cyclic analogues (cCDF) are indicated in the treatment of cytomegalovirus retinitis (CMV, an infection of retina in the eye in AIDS patients) [113, 227]. However, the biological activity of this compound is dependent on its intracellular accumulation which is hindered by the reticuloendothelial system (RES) as well as various efflux pumps expressed on the corneal and retinal epithelia [228-229]. Self-assembled polymeric nanomicelles have emerged as one of the promising nanocarrier systems [182, 230]. Enhanced aqueous solubility, prolonged circulation time, improved drug bioavailability, reduced toxicity and evasion from RES and efflux pumps render these polymeric nanomicelles superior to other delivery systems [231-232]. The ability to precisely control the chemical composition, molecular weight and size of these polymeric nanomicelles furnishes additional advantages [233-234]. Moreover, slow drug release from these polymeric nanomicelles over a long time period may limit frequent dosing into ocular tissues [183, 235-236].

Remarkably, in contrast to numerous examples of successful delivery of therapeutic agents to ocular tissues with nanocarrier systems [237-239], the development of polymeric nanomicelles for back of the eye delivery has rarely been addressed. However, such a nanomicellar approach may be desirable [240], for instance, in case of a drug such as cidofovir which has lower bioavailability in human ocular tissues following intravenous and/or intravitreal administration [113, 241].

Earlier, we reported on the transporter targeted lipid prodrug of cyclic cidofovir (B-C12-cCDF). This was achieved by conjugating a lipid chain (C-12) and a targeting moiety (biotin) to cCDF. The concept was based on enhanced lipophilicity and melanin-binding in the retina owing to the lipid raft. Better retinal targetability was achieved by conjugating biotin which specifically targets sodium dependent vitamin transporters highly expressed in the retina. By selecting a suitable lipid raft and targeting moiety, it was possible to achieve higher bioavailability in the retina and lower the viral load [145, 242]. Antiviral studies conducted under the contract of the National Institute of Allergy and Infectious Diseases (NIAID) reported that B-C12-cCDF exhibited 2 to 25-fold reduction in EC50 value against HCMV (0.57 μM), HSV-2 (2.16 μM) and BK virus (13.8 μM) relative to the parent drug CDF.

Although we were able to prove that this approach works, the low aqueous solubility of B-C12-cCDF and possibility of getting detected by the RES [243-245] and efflux pumps [246-247] rendered lower drug concentrations in human ocular tissues. Taking all previous results together, further work led to the development of a self-assembled topical nanomicellar formulation of the transporter targeted lipid prodrug of cCDF.

5.2. Objective

(i) In this study, we have developed polymeric nanomicelles based on a blend of polymers, polyoxyethylene hydrogenated castor oil 40 (HCO-40) and octoxynol 40 (OC-40) for the intracellular targeted delivery of B-C12-cCDF to the retina. B-C12-cCDF was manufactured in contract with SRI International. Utilization of such a blend of polymers by our laboratory in the past has resulted into highly stable and water soluble self-aggregating nanomicellar formulations [248-249]. This formulation has recently completed Phase 3 clinical trials and has shown promising results for the treatment of dry eye disease (NCT02254265).

(ii) Physicochemical properties, *in vitro* release and drug loading capacities of polymeric nanomicelles of B-C12-cCDF were evaluated utilizing dynamic light scattering (DLS), transmission electron microscopy (TEM) and ultra-fast liquid chromatography (UFLC).

(iii) The cytotoxicity of prodrug loaded nanomicelles was studied in HRPE (human retinal pigment epithelial, D407), HCE-T (human corneal epithelial) and CCL 20.2 (human conjunctival epithelial) cells by the 3-(4,5-dimethylthiazol-2-yl)-2,5-diphenyltetrazolium bromide (MTT) and lactate dehydrogenase (LDH) assays.

(iv)The uptake behavior and permeability of B-C12-cCDF-loaded nanomicelles were demonstrated in D407 and HCE-T cells using confocal laser scanning microscopy (CLSM) and flow cytometry (FCM).

5.3. Experimental Section

5.3.1. Materials

B-C12-cCDF was obtained from SRI Chemical Synthesis Program (SRI International, Menlo Park, CA). Hydrogenated castor oil-40 (HCO-40) of pharmaceutical grade was procured from Barnet Products, USA and octoxynol-40 (OC-40 or Igepal CA-897) was purchased from Rhodia Inc., New Jersey, USA. Povidone (PVP)-K90 (lot #56943447G0) was obtained from BASF AG (Ludwigshafen, Germany). For buffer and formulation preparation double distilled deionized (DI) water was utilized. HPLC grade DMSO and methanol were purchased from Fisher Scientific Co. (Pittsburgh, PA, USA). TrypLE^{TM} Express Stable trypsin solution, Dulbecco's modified Eagle's medium (DMEM) were received from Invitrogen (Carlsbad, CA, USA). Fetal bovine serum (FBS) was obtained from Atlanta Biologics (Lawrenceville, GA, USA). All other chemicals were of analytical reagent grade procured from Thermo Fischer Scientific or Sigma Aldrich and were utilized without any further purification.

5.3.2. Cell culture

Cell lines D407 and HCE-T transfected with a recombinant SV40-adenovirus vector were kindly provided by Dr. Richard Hunt (University of South Carolina, Columbia, SC, USA) and Dr. Araki-Sasaki (Kinki Central Hospital, Japan) respectively. Mouse macrophage RAW 264.7 cell line and human conjunctival cell line CCL 20.2 were obtained from the American Type Culture Collection (ATCC, Manassas, VA). All cell lines were cultured in T75 flasks in DMEM medium containing high glucose and glutamine concentrations. The culture medium contained 10% FBS (heat-inactivated), 1% nonessential amino acids, 100 IU/ml streptomycin and 100 IU/ml penicillin. The pH of the medium was maintained at 7.4. Cells were maintained at 37 ºC in an atmosphere containing 5% CO_2 and 90% relative humidity. The medium was

replaced on alternate days until cells reached 80-90% confluency (5-7 days for D407, CCL 20.2 and 19-21 days for HCE-T cells).

5.3.3. Synthesis of B-C12-cCDF prodrug

B-C12-cCDF was synthesized by the SRI Chemical Synthesis Program. Briefly, in a flask, CDF (1 equiv), 20 mL of anhydrous N,N-Dimethylformamide (DMF), and 2.1 mL of dry N,N-diisopropylethylamine (DIPEA) were added. The reaction vessel was warmed by a heat gun to facilitate the dissolution of the CDF–DIPEA salt. The solvent was removed under vacuum. The residue, 20 mL of anhydrous DMF, DIPEA (5 equiv), the biotin-conjugated lipid (1.5 equiv) in anhydrous DMF, and benzotriazole-1-yl-oxy-tris-pyrrolidino-phosphonium hexafluorophosphate PyBOP (2.1 equiv) were added, and the reaction mixture was stirred under nitrogen at 45 °C for 48–60 h. The reaction mixture was monitored by ^{31}P NMR, and additional portions of PyBOP were added as necessary. After completion of the reaction, the solvent was removed under vacuum, and the brownish-red residue was purified by repetitive silica gel column chromatography. The product was obtained by a combination of dichloromethane and methanol as the eluent.

5.3.4. Experimental Design

In order to screen the weight percent of polymers, effects of formulation variables on B-C12-cCDF loading, micellar size and polydispersity index (PDI) were evaluated based on a statistical design of experimental (DOE) protocol. Student version of JMP® 10.0 software (SAS institute, USA) was applied to develop the experimental design and analyze the data. Five independent (X1, X2, X3, X4 and X5) and three dependent variables (Y1, Y2, and Y3) were identified. Independent variables X1 through X5 included HCO-40 (wt. %), OC-40 (wt. %), sonication time (min), pH and buffer concentrations (molarity, M), respectively.

Dependent variables Y1, Y2 and Y3 represented the percent drug loading (% w/w), micellar size (nm) and polydispersity index, respectively. The "screening design" in JMP was selected to create the design. A Plackett-Burman design with twelve runs was selected from the "design list" (Table 5-1) and two center points were included. This arrangement resulted in 14 experiments. Coded values −1, 0, +1 were assigned to the weight percent levels for two polymers.

5.3.5. Preparation of polymeric nanomicelles

Nanomicellar formulations of B-C12-cCDF were prepared following solvent evaporation and film rehydration as described previously[248]. Briefly, the experimental procedure was divided into two steps (i) formulation preparation and (ii) rehydration.

(i) **Formulation preparation:** B-C12-cCDF was accurately weighed out and dissolved in ethanol and dichloromethane (DCM) mixture (10:1). Then HCO-40 and OC-40, were weighed out and dissolved separately in ethanol. This solution was stirred and the mixture generated a homogenous solution. The calculated volume of B-C12-cCDF solution was added drop by drop to this solution. The solvent was evaporated under high-speed vacuum (Genevac, Ipswich, Suffolk, UK) overnight (~10 h) to obtain a solid thin film.

(ii) **Rehydration:** The resultant solid thin film was rehydrated in 10 mL of water, and the volume was made up with 2× phosphate/ citrate buffer solution containing 1.2% of PVP K90 (BASF SE, Ludwigshafen, Germany) with varying pH values. PVP was added to increase the viscosity and hence retention of the formulation. The solution was sonicated for an appropriate amount of time. Finally, the formulation was filtered with a 0.2 μm nylon membrane syringe filter (Tisch Scientific, USA) to remove unentrapped drug aggregates and other foreign particulates.

5.3.6. Characterization

Hydrodynamic diameter and polydispersity index (PDI) of nanomicelles were determined in aqueous solution with a Zeta Sizer (Zetasizer Nano ZS, Malvern Instruments Ltd, Worcestershire, UK) at RT. Briefly, 1 ml of nanomicellar solution (2 mg/mL) was placed into a glass cuvette. The samples were measured at a scattering angle of 173 º and 25 ºC. Average values were calculated from three replicate measurements of each sample. The morphology of polymeric nanomicelles was examined with TEM. Typically, a drop of nanomicellar solution was placed on a copper grid. A layer of nitrocellulose and carbon in the evaporator was applied and stained with 1% uranyl formate. Measurements were performed with JEM 1200 EX II TEM at an acceleration voltage of 100 kV.

5.3.7. Critical micellar concentration (CMC)

CMC was determined with iodine as a probe. The polymer concentrations ranged from 3.5 to 1.63 x 10^{-9} wt. %, and the iodine solution was adjusted to a ratio of 0.5:1 (I_2: KI). The absorbance of hydrophobic iodine, I_2, entrapped in the core of polymeric nanomicelles was recorded with a Beckman Coulter (DDX 880). The emission spectrum was recorded from 286 nm to 460 nm at an excitation wavelength of 279 nm. From the iodine emission spectrum, the intensity ratio (I460/I286) was analyzed as a function of polymer concentration. The CMC value was determined at a cross-point by extrapolating the intensity ratio at the polymer concentration regions.

5.3.8. 1H-NMR spectroscopy

To perform ^{1}H-NMR spectroscopy, B-C12-cCDF was dissolved in d6-DMSO. HCO-40, OC-40, Blank and B-C12-cCDF-loaded nanomicelles were prepared in D_2O for NMR

analysis. Spectra were recorded with Varian-400 NMR instrument. NMR data was processed using VNMRJ or ACD labs software.

5.3.9. Entrapment and loading efficiency

The total amount of prodrug entrapped in the formulation was determined by reversed-phase UFLC (RP-UFLC). Ten milliliters of each micellar formulation was collected and centrifuged at 10,000 rpm for 10 min at 4 ºC. One milliliter of supernatant was carefully collected from each centrifuge tube and transferred into fresh vials and lyophilized to obtain a solid pellet. Five hundred microliter of DCM was added to each vial in order to reverse the polymeric nanomicelles and release the prodrug into the surrounding organic solvent. This DCM solution was evaporated under speed vacuum (Genevac Technologies VC3000D, USA) to obtain a solid pellet of reversed micelles. Further, this solid pellet was appropriately diluted in UFLC mobile phase and the amount of prodrug present in the samples was determined. The percent entrapment and loading efficiency of prodrug (B-C12-cCDF) were calculated according to the following formula:

Percent entrapment = (mass of B-C12-cCDF in nanomicelles)/ (mass of B-C12-cCDF added in formulation) x 100 **[Eq. 3]**

Loading efficiency = (mass of B-C12-cCDF in nanomicelles)/ (mass of B-C12-cCDF added + mass of polymers used) x 100 **[Eq. 4]**

5.3.10. In vitro cytotoxicity assay

Cytotoxicity of B-C12-cCDF-free nanomicelles or B-C12-cCDF-loaded nanomicelles against D407, HCE-T and CCL 20.2 cells were assessed *in vitro* by MTT and LDH assays. All three cell lines were seeded into a 96-well plate at a density of $1x10^4$ cells/well in 100 µL

complete DMEM solution containing 10% FBS. Cells were cultured for 1 day at 37 ºC in 5% CO_2 atmosphere. B-C12-cCDF, B-C12-cCDF-free nanomicelles or B-C12-cCDF-loaded nanomicelles were prepared in serum free medium and filtered with 0.22 µm nylon membrane filters under a laminar flow hood. B-C12-cCDF being poorly water soluble was prepared in serum free medium by adding 2-3 drops of DCM. Afterwards, cells were incubated with B-C12-cCDF, B-C12-cCDF-free nanomicelles or B-C12-cCDF-loaded nanomicelles for 24 h at 37 ºC. The concentration of B-C12-cCDF-free nanomicelles (HCO-40/OC-40) ranged from 0.24 to 7.0 mg/mL. B-C12-cCDF-loaded nanomicelles with final B-C12-cCDF-concentrations from 13.95 g/mL to 400 µg/mL were employed. After 24 h of incubation, MTT stock solution (5 mg/mL in potassium phosphate buffer, PBS 20 µL) was added to each well and incubated for 2.5 h. The absorbance was measured with a microplate reader (BioRad Hercules, CA, USA) at 485 nm. Cell viability was expressed according to the following formula:

Cell viability (%) = (Abs of sample- Abs of negative control)/ (Abs of positive control-Abs of negative control) * 100 **[Eq. 5]**

5.3.11. LDH assay

D407, HCE-T and CCL 20.2 cells were seeded into a 96-well plate at a density of $1x10^4$ cells/well in 100 µL of complete DMEM containing 10% FBS. Cells were cultured for 1 day at 37 ºC in 5% CO_2 atmosphere. CDF, B-C12-cCDF, B-C12-cCDF-free nanomicelles or B-C12-cCDF-loaded nanomicelles solutions were prepared as described previously. After 24 h of incubation, plates were centrifuged at 250 x g for 10 min and the supernatant was collected from each well. LDH released into the cell supernatant was quantified with a LDH assay kit (Takara Bio Inc., Japan). The absorbance of the solution was measured using a microplate

reader (BioRad Hercules, CA, USA) at 490 nm. LDH release was expressed according to the following formula:

LDH release (%) = (Abs of sample- Abs of negative control)/ (Abs of positive control- Abs of negative control) * 100 **[Eq. 6]**

5.3.12. In vitro biocompatibility studies

RAW-264.7 cells were seeded into a 96-well plate at a density of $1x10^4$ cells/well in 100 µL of complete DMEM containing 10% FBS. Cells were cultured for 1 day at 37 ºC in 5% CO_2 atmosphere. CDF, B-C12-cCDF, B-C12-cCDF-free nanomicelles or B-C12-cCDF-loaded nanomicelles solutions were prepared as described previously. After 24 h of incubation, plates were centrifuged at 250 x g for 10 min and the supernatants were analyzed for the presence of cytokines i.e., Tumor necrosis factor- α (TNF-α), Interleukin 6 (IL-6) and Interleukin-1β (IL-1β). Lipopolysaccharide (LPS) served as positive control whereas cells without any treatment were considered as negative control. Cytokine levels (in pg/mL) were measured by ELISA according to manufacturer's (e-Biosciences, San Diego, CA) protocol. Standard calibration curves for TNF-α, IL-6 and IL-1β were prepared in the concentration range of 10-750 pg/mL, 5-500 pg/mL and 10-500 pg/mL, respectively.

5.3.13. In vitro release of B-C12-cCDF from B-C12-cCDF-loaded nanomicelles

A fixed volume (1 mg/mL) of B-C12-cCDF-loaded nanomicelles was transferred to a membrane tubing (MWCO 2000 Da, Spectrum labs, CA, USA). The tubing was subsequently immersed in 5 mL PBST (PBS with 0.002 wt. % Tween 20, pH 7.4) or STF (Composition: 2 g $NaHCO_3$, 6.7 g NaCl, 0.08 g $CaCl_2 \cdot 2H_2O$, and deionized water was added up to 1 L, Tween-80 (0.5 wt. %)) solution in a shaking water bath fixed at 60 rpm and 37 ºC to maintain sink condition. At predetermined time points, the entire 5 mL of external buffer were withdrawn

and replaced with 5 mL of fresh buffer solution to maintain sink condition. The amount of prodrug released was determined by RP-UFLC as described below.

5.3.14. Drug Release Mechanism

Drug release parameters were calculated by the following mathematical models: zero order (Eq. 7), first order (Eq. 8), Higuchi (Eq. 9), and Korsmeyer-Peppas (Eq. 10). Release data were fitted into the model equations in order to identify the release mechanism of drug release from formulations.

Zero-order equation: $Q_t = Q_0 + K_0t$ **[Eq. 7]**

First-order equation: $\log Q_t = \log Q_0 + K_1t/2{:}303$ **[Eq. 8]**

Higuchi equation: $Q_t = K_ht^{1/2}$ **[Eq. 9]**

Korsmeyer-Peppas equation: $Q_t/Q_\infty = K_pt^n$ **[Eq. 10]**

5.3.15. FITC labeling of CDF and B-C12-cCDF

Fluorescein isothiocyanate (FITC, Life Technologies, Eugene, OR, USA) was freshly dissolved in DMSO (1 mg/ml) and added to 2 mg/ml of CDF and B-C12-cCDF in 50 mM PBS (final pH 7.6). The final concentration of FITC was 15 μg/ml. The calculated molar ratio of FITC to CDF/B-C12-cCDF was 0.10. After incubation for 16 h in the dark at 4 °C, 50 mM NH_4Cl was added to inactivate the residual FITC. The solution was stored in the dark for an additional 2 h at 4 °C, and stored in aliquots at -20 °C.

5.3.16. Evaluation of cellular uptake by FCM

D407 and HCE-T cells were seeded into 12-well plates at a density of $2.5x10^4$ cells/well in 24 mL complete DMEM containing 10% FBS, and maintained until they achieved 80-90%

confluency (6-7 days) at 37 ºC in 5% CO_2 atmosphere. Afterwards, cells were incubated with FITC-tagged CDF, B-C12-cCDF, B-C12-cCDF-free nanomicelles or B-C12-cCDF-loaded nanomicelles at a final CDF or B-C12-cCDF concentration of 50 μg/mL in serum free medium for predetermined time points at 37 ºC. At each time point, the culture medium was removed and cells were washed twice with DPBS to remove the various treatment groups that were not ingested by the cells. Cells were detached with trypsin for 10 min, and then centrifuged at 1550 rpm for 10 min to obtain a solid pellet. The solid cell pellet was washed twice with DPBS. After removal of the supernatant, the cells were resuspended in 500 μL of 4% (w/v) paraformaldehyde aqueous solution and stored at 4 ºC. The mean fluorescence intensity of FITC-tagged CDF, B-C12-cCDF and B-C12-cCDF-loaded nanomicelles in cells were analyzed by FCM (Becton Dickinson, Franklin Lakes, NJ, USA) with an excitation wavelength of 490 nm for comparative studies.

5.3.17. CLSM observation for cellular distribution

D407 and HCE-T cells were seeded on Nunc Lab-Tek® 8 chambered #1.0 borosilicate cover glass system (Thermo Fisher Scientific, Waltham, MA, USA) at a density of $1x10^4$ cells/well in 2 mL of complete DMEM containing 10% FBS and cultured for 1 day at 37 °C in 5% CO_2 atmosphere. FITC-tagged CDF, B-C12-cCDF, B-C12-cCDF-free nanomicelles or B-C12-cCDF-loaded nanomicelles were added at a final concentration of 15μg/mL, followed by incubation for 2, 12 and 24 h. At each predetermined time point, the culture medium was removed and cells were washed with DPBS (3 x 5 min) to remove the various treatment groups not ingested by cells. Two hundred microliter of cold 4% buffered paraformaldehyde was added to each well to fix the cells and incubated for 10 min at 37 °C. The slides were rinsed with DPBS (3 x 5 min). Finally, the cells were stained with Vectashield Antifade Mounting

Medium with DAPI and stored at 4 °C until examined by CLSM (Leica TCS SP5, Wetzlar, Germany).

5.3.18. Evaluation of cellular transport by FCM

Transwell diffusion chambers (pore-size, 0.4 μm) were utilized for determining *in vitro* permeability of CDF, B-C12-cCDF and B-C12-cCDF-loaded nanomicelles. D407 cells were seeded into 12-well plates (bottom chamber) at a density of $2.5x10^4$ cells/well in 24 mL complete DMEM containing 10% FBS, and maintained until they achieved confluency and developed completely (9-10 days) at 37 ºC in 5% CO_2 atmosphere. Similarly, HCE-T cells were seeded at a density of $1.25x10^4$ cells/inserts (collagen coated, top chamber) until confluency and complete development. Afterwards, the transport experiment was initiated by incubating the HCE-T cells (top chamber) with FITC-tagged CDF, B-C12-cCDF, B-C12-cCDF-free nanomicelles or B-C12-cCDF-loaded nanomicelles at a final CDF or B-C12-cCDF concentration of 50 μg/mL in serum free medium for predetermined time points at 37 ºC. At each time point, the culture medium was removed and the D407 cells (bottom chamber) were washed twice with DPBS to remove the various treatment groups that were not ingested by the cells. The D407 cells were detached using trypsin for 10 min, and then were processed as mentioned in section illustrating the cell uptake of nanomicelles. The mean fluorescence intensity of FITC-tagged CDF, B-C12-cCDF and B-C12-cCDF-loaded nanomicelles in cells were analyzed by FCM (Becton Dickinson, Franklin Lakes, NJ, USA) with an excitation wavelength of 490 nm for comparative studies.

5.3.19. Sample and data analysis

RP-UFLC was employed to analyze in vitro release samples. The system comprised of Waters 515 pump (Waters, Milford, MA, USA) connected to C (18) Kinetex column (100 mm

X 4.6 mm, 2.6 m; Phenomenex, Torrance, CA, USA) and a UV detector (Absorbance Detector Model UV-C, RAININ, Dynamax, Palo Alto, CA, USA, wavelength 280 nm). Acetonitrile:water (4:1) with 0.1% trifluoroacetic acid was selected as a mobile phase with a flow rate of 0.4 mL/min. B-C12-cCDF eluted approximately at 2.61 min. All experiments were conducted at least in triplicate and results were expressed as mean ± S.D. Student t-test was employed to determine statistical significance between groups. A value of $p \leq 0.05$ was considered to be statistically significant.

5.4. Results and Discussion

5.4.1. Formulation Optimization

In this study we selected the Plackett-Burman design to screen essential independent variables for outcomes such as loading efficiency, micellar size and PDI. The results for dependent variables (Y1, Y2 and Y3) from 14 sets of formulations with two center points were subjected to data analysis with the Plackett Burman-Fit Least square analysis via JMP® 10.0 software. Analysis was performed to identify the most pertinent variables for each dependent variable. For data analysis, the main effects of one- and two factor interactions were considered because higher order interactions are less significant. The parameters that showcased the most significant outcomes were selected and processed with a standard least square regression model to fit those parameters. The summary for fit model for loading efficiency, micellar size and PDI are presented in Table 5-1. Further, analysis of variance (ANOVA) for loading efficiency, size and PDI exhibited a non-significant effect with a F ratio (probability > F) of 0.0819, 0.2167 and 0.2997, respectively.

Table 5-1 Experimental design with independent and dependent variables

Pattern	HCO-40 (wt. %)	OC-40 (wt. %)	Sonication time (mins)	pH	Buffer (M)	%Entrapment efficiency	Loading efficiency (%)	Size (nm)	PDI
−+++−	0.5	2	5	7.2	0.01	22.85	1.69	17.33	0.63
++−−−	4.5	2	0	5.5	0.01	61.16	1.83	15.99	0.13
00000	2.5	1.005	2.5	6.35	0.055	90.94	4.64	17.73	0.2
+−−−+	4.5	0.01	0	5.5	0.1	82.75	3.51	16.61	0.06
+−+++	4.5	0.01	5	7.2	0.1	87.57	3.72	16.51	0.06
+++−−	4.5	2	5	5.5	0.01	89.79	2.68	15.47	0.15
−+−−+	0.5	2	0	5.5	0.1	62.84	4.65	12.77	0.47
−−−+−	0.5	0.01	0	7.2	0.01	10.58	2.98	19.26	0.23
−−+−−	0.5	0.01	5	5.5	0.01	21.62	6.09	21.45	0.31
−+−++	0.5	2	0	7.2	0.1	44.39	3.29	17.74	0.46
+−−+−	4.5	0.01	0	7.2	0.01	69.41	2.95	16.56	0.08
00000	2.5	1.005	2.5	6.35	0.055	87.03	4.70	16.22	0.21
+++++	4.5	2	5	7.2	0.1	75.87	2.26	15.18	0.11
−−+−+	0.5	0.01	5	5.5	0.1	15.97	4.50	19.8	0.22

5.4.2. Master formula (Prediction Equation)

The fit model developed by the following polynomial equations for the output are loading efficiency (Eq. 11), micellar size (Eq. 12) and PDI (Eq. 13):

Y1 = Y1= 4.585 + 1.385*X1+ (-1.3375*X2) + 0.2625*X3 + (-0.7125*X4) + (-1.8575*X5) + X1*[X1*(-1.07)] + X1*[X2*(-0.9875)] + X1*[(X3)*1.8775] + X1*[X4*0.0675] + X1*[X5*(-1.1925)] + X2*[X2*0] + X2*[X3*(-0.245)] + X2*[X4*2.525] +X2*[X5*0]+ X3*[X3*0] + X3*[X4*0] + X3*[X5*0] + X4*[X4*0] + X4*[X5*0] + X5*[X5*0] **[Eq. 11]**

Y2= 15.77 + (-0.776)*X1+ (-1.675*X2) - 0.5833*X3 + (-0.0366*X4) + (0.4058*X5) + X1*[X1*(1.2858)] + X1*[X2*(1.1166)] + X1*[(X3)*0.2366] + X1*[X4*(-0.06891)] + X2*[X2*0] + X2*[X3*(-0.1841)] + X2*[X4*0.4833] +X2*[X5*0]+ X3*[X3*0] + X3*[X4*0] + X3*[X5*0] + X4*[X4*0] + X4*[X5*0] + X5*[X5*0] **[Eq. 12]**

Y3= 0.155 + (-0.1617)*X1+ 0.1029*X2 + 0.00256*X3 + (-0.0209*X4) + (0.0399*X5) + X1*[X1*(0.08808)] + X1*[X2*(-0.0387)] + X1*[(X3)*(-0.0234)] + X1*[X4*(0.01851)] + X1*[X5*(-0.0007)] + X2*[X2*0] + X2*[X3*(0.0173)] + X2*[X4*(-0.0416] +X2*[X5*0]+ X3*[X3*0] + X3*[X4*0] + X3*[X5*0] + X4*[X4*0] + X4*[X5*0] + X5*[X5*0] **[Eq. 13]**

where, X1= [HCO-40 (wt. %)-2.5]/2, X2= [OC-40 (wt. %)-1.005]/0.995, X3= [Sonication time (mins)-2.5]/2.5, X4= (pH-6.35)/0.85 and X5= [Buffer (M)-0.055]/0.046

Since the polynomial equations for Y1, Y2 and Y3 fit well with R2 = 0.999, 0.993 and 0.987 respectively, these were used for the optimization process. Therefore, the obtained polynomial equations for loading efficiency (Y1), micellar size (Y2) and polydispersity index (Y3) of input

variables were selected to determine the optimal formula with high loading, small size and narrow PDI.

A Pareto chart was developed for each individual outcome to determine which factors and interactions were relevant. These charts were developed using the absolute value obtained from half the value of the main effects. The bars in the chart that extend past the line indicate values reaching statistical significance ($\alpha = 0.05$). In the case of loading efficiency, individual variables i.e., HCO-40, OC-40 and buffer; two factor-interactions such as OC-40*pH; HCO-40*sonication time and HCO-40*buffer were observed to pass the line indicating their statistically significant effect on loading efficiency (Figures 5-1). However, for micellar size and PDI interactions between the input factors did not cross the line and were thus insignificant (Figure 5-2 and 5-3). These results indicate that only drug loading was dependent on HCO-40, OC-40, buffer concentration and two factor interactions (OC-40*pH; HCO-40*sonication time; and HCO40*Buffer).

A prediction profiler for loading efficiency, micellar size and PDI was also developed (Figure 5-4). This helps to determine the levels of input variables to be adjusted in a combination where the outcome can be predicted. The input variables HCO-40 (2.5 wt. %), OC-40 (1.005 wt. %), sonication time (2.5 min), pH (6.35) and buffer concentration (0.055 M) resulted in high loading efficiency (4.3 ± 0.5 %), which is evident from the results. The prediction profiler and experimental results are in excellent agreement. Therefore, the combination of variables at the above mentioned levels appeared to be the optimal formulation. Also, to determine the effects of input variables on the loading efficiency we developed a contour plot (data not shown) and surface profiles with actual data points (Figures 5-5, 5-6 and 5-7). Contour plots are a three dimensional representation for the outcome where the input

variables are adjusted. From the contour plot one can estimate the levels of input variables and determine the outcome (present on the surface of the box). The shaded region in the contour plot indicates the lower drug loading region. In contrast, the unshaded region represents the higher loading zone. As variables are set at HCO-40 (2.5 wt. %), OC-40 (1.005 wt. %), sonication time (2.5 min), pH (6.35) and buffer concentration (0.055 M), a high loading efficiency can be predicted. Experimental design results and our experimental outcomes suggest that the polymer combination and manufacturing processes kept at a certain level, can yield higher drug loading, small size and narrow PDI. Our experimental results validate the predicted outcome. Taking input levels at adjusted levels, the loading efficiency was predicted to be 4.585 %. We prepared nanomicellar formulation following the procedure described previously and the loading efficiency was determined according to the RP-UFLC method. Results confirmed the average percent drug loading into the nanomicellar formulation to be 4.6 ± 1.8, which is in agreement with the DOE.

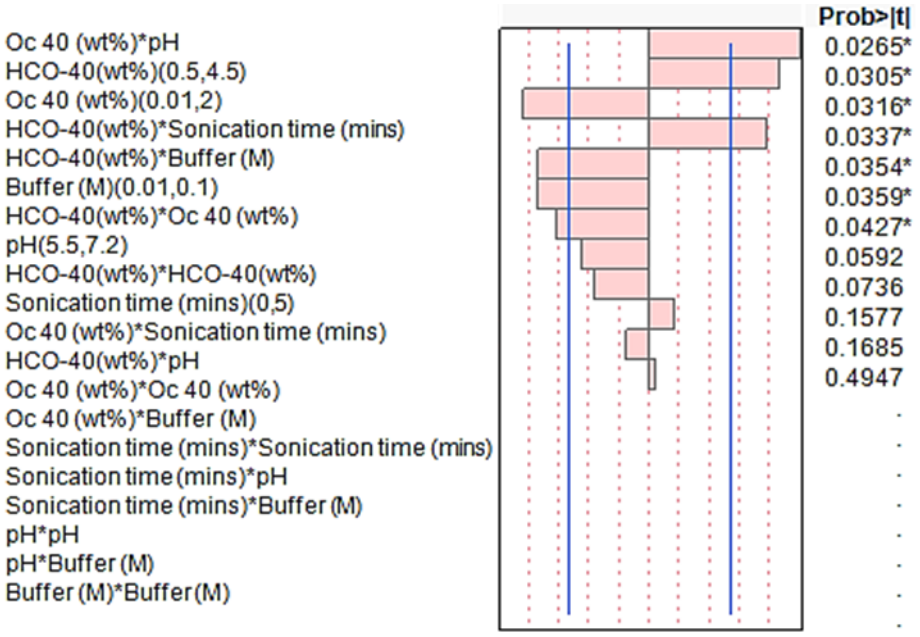

Figure 5-1 Pareto chart for loading efficiency. * next to p-value represents significant term

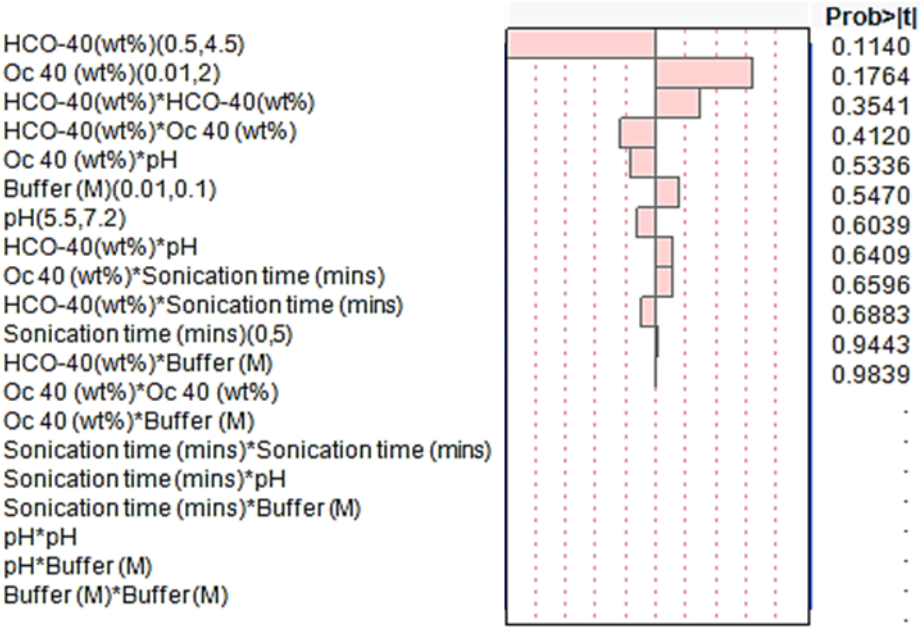

Figure 5-2 Pareto chart for PDI

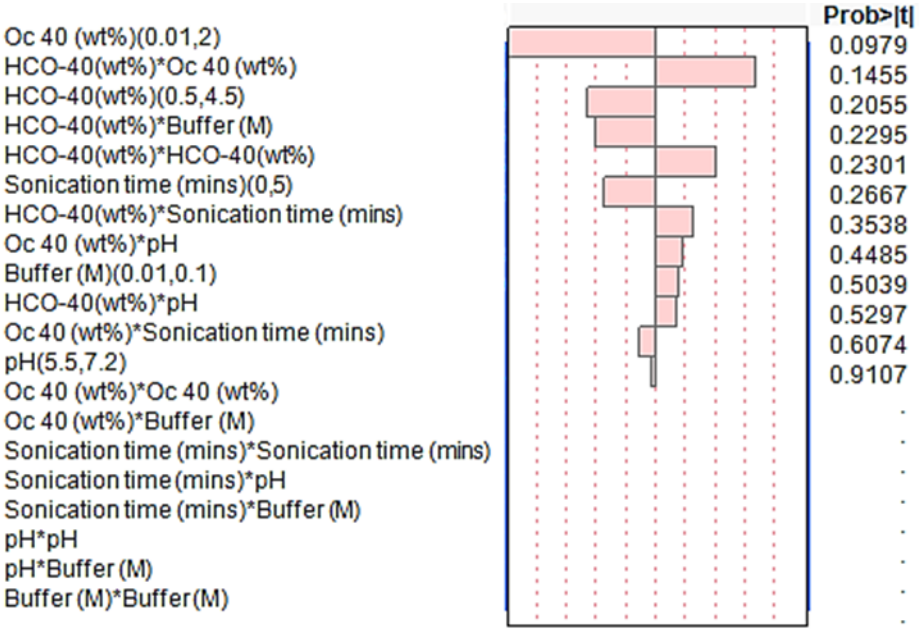

Figure 5-3 Pareto chart for size

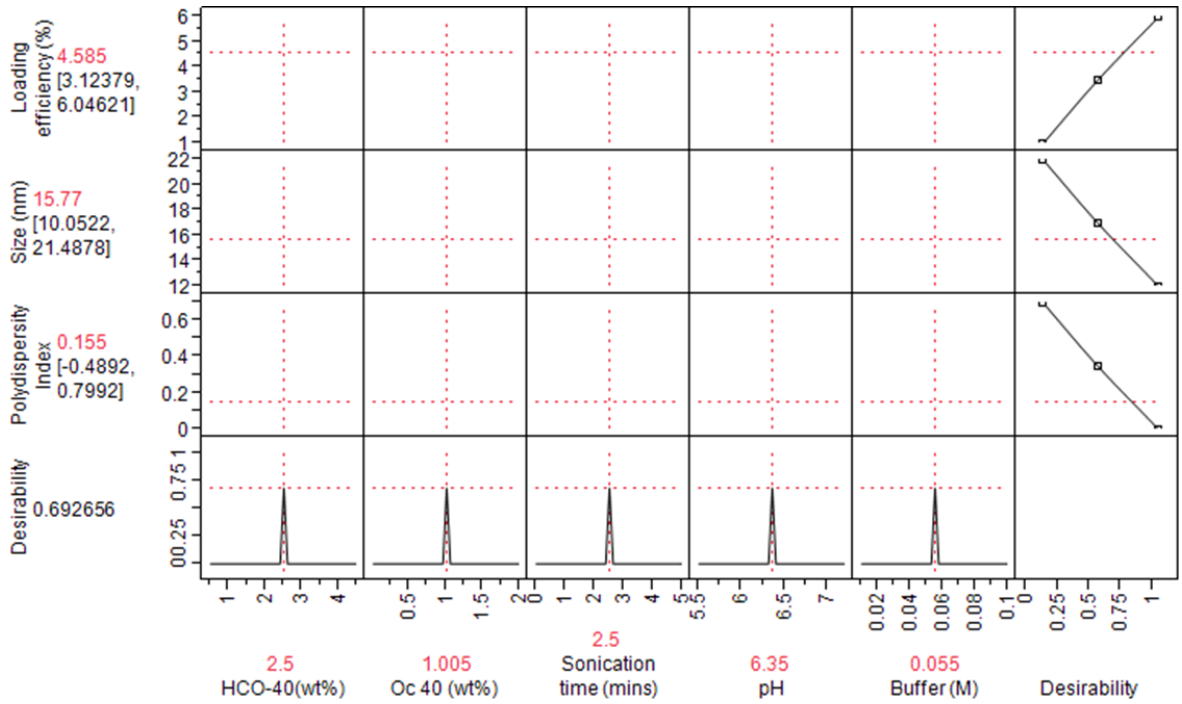

Figure 5-4 Prediction profiler for loading efficiency, size and PDI of B-C12-cCDF-loaded nanomicellar formulation

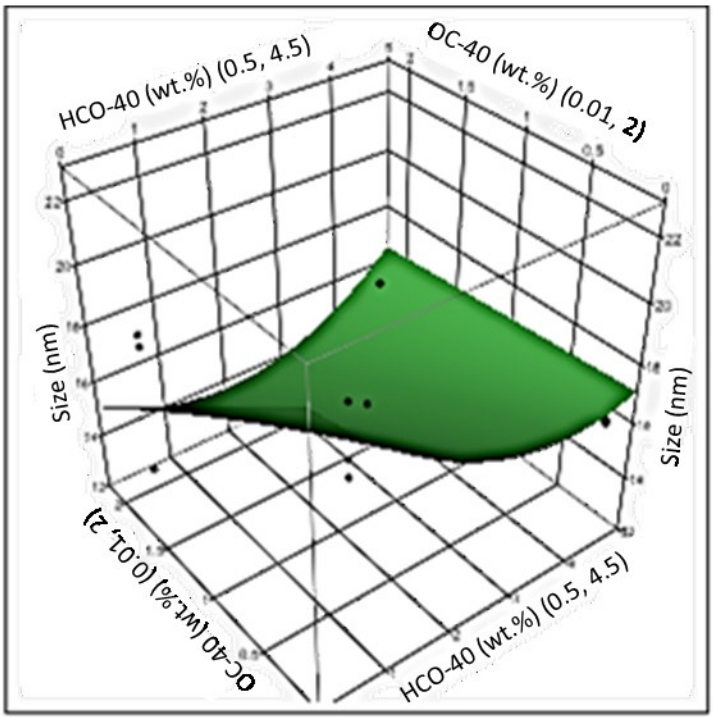

Figure 5-5 Response surface of size. B-C12-cCDF-loaded nanomicelles size is plotted as a function of HCO-40 and OC-40 amounts between -1 and +1

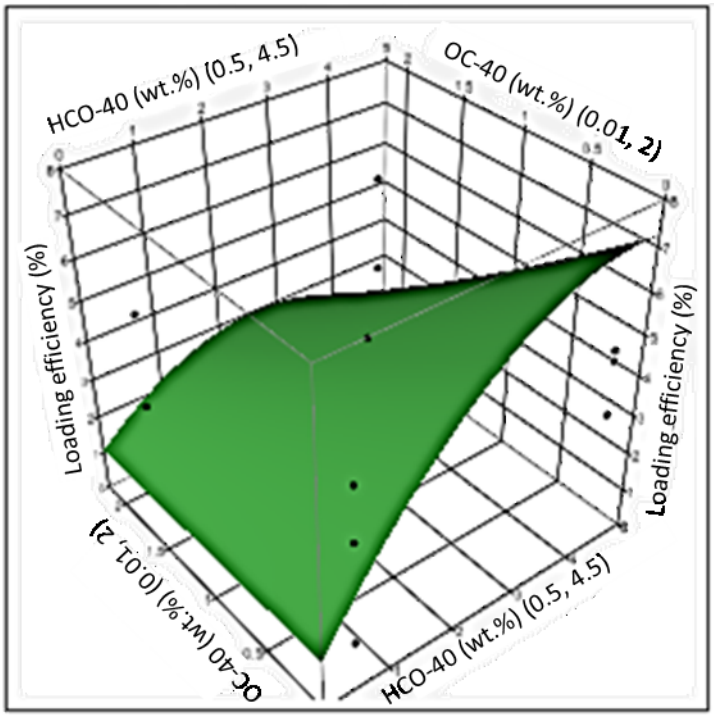

Figure 5-6 Response surface of loading efficiency. B-C12-cCDF-loaded nanomicelles loading efficiency is plotted as a function of HCO-40 and OC-40 amounts between -1 and +1

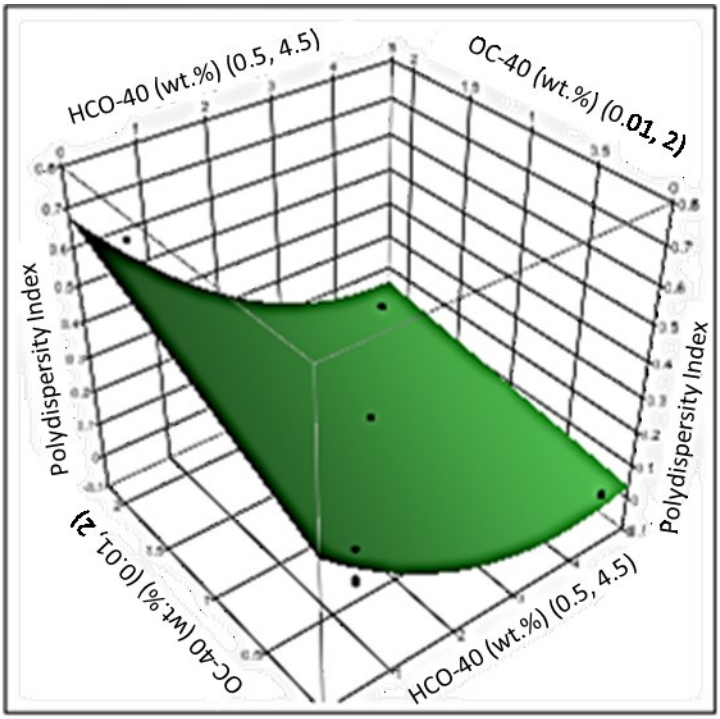

Figure 5-7 Response surface of PDI. B-C12-cCDF-loaded nanomicelles PDI is plotted as a function of HCO-40 and OC-40 amounts between -1 and +1

5.4.3. Entrapment and loading efficiency

B-C12-cCDF entrapment and loading into the polymeric nanomicelles were determined using RP-UFLC. A combination of different wt. % of polymers displayed a range of entrapment and loading efficiencies, which are summarized in Table 5-1. Among the various formulations developed, F3 exhibited the highest entrapment efficiency with optimal drug loading. Formulation F3 was therefore further characterized for size, PDI and surface morphology.

5.4.4. Characterization

Amphiphilic polymers tend to form core-shell structural nanomicelles in water. Herein, nanomicelles of HCO-40 and OC-40 were prepared by the solvent evaporation and film rehydration method. The micellar size is an important parameter for ocular drug delivery because small sized nanocarriers (<1000 nm) are highly effective in maintaining a low-level of RES uptake and minimal renal excretion [250]. Moreover, topically applied therapeutic agents following conjunctival/scleral pathway penetrate ocular tissues by passive diffusion through scleral aqueous channels/pores (ranging from 30 to 300 nm in size) [251-252]. DLS measurements exhibited nanomicelle formation with HCO-40/OC-40 within a size range of 10-30 nm and a PDI of 0.05-0.46. B-C12-cCDF-loaded nanomicelles were slightly smaller than B-C12-cCDF-free nanomicelles. B-C12-cCDF-free nanomicelles (HCO-40:OC-40; 2.5:1.0) and B-C12-cCDF-loaded nanomicelles showed an average size of 19.0 ± 0.5 nm and 17.73 ± 0.3 nm respectively (Figures. 5-8 A and B). The smaller size of B-C12-cCDF-loaded nanomicelles could be attributed to the strong hydrophobic interactions of the hydrophobic prodrug with the hydrophobic chains of the polymers. Additionally, the size and surface morphology of B-C12-cCDF-loaded nanomicelles were also measured and observed by TEM. As shown in Figure 5-8 C, the TEM microscopic image confirmed that polymeric nanomicelles were spherical in shape in aqueous medium with an average diameter close to the result of the DLS measurement. Surface morphology revealed smooth architecture without any nanomicellar aggregation. The size distribution of B-C12-cCDF-loaded nanomicelles and TEM microscopic images are depicted in Figures 5-8 A, B and C.

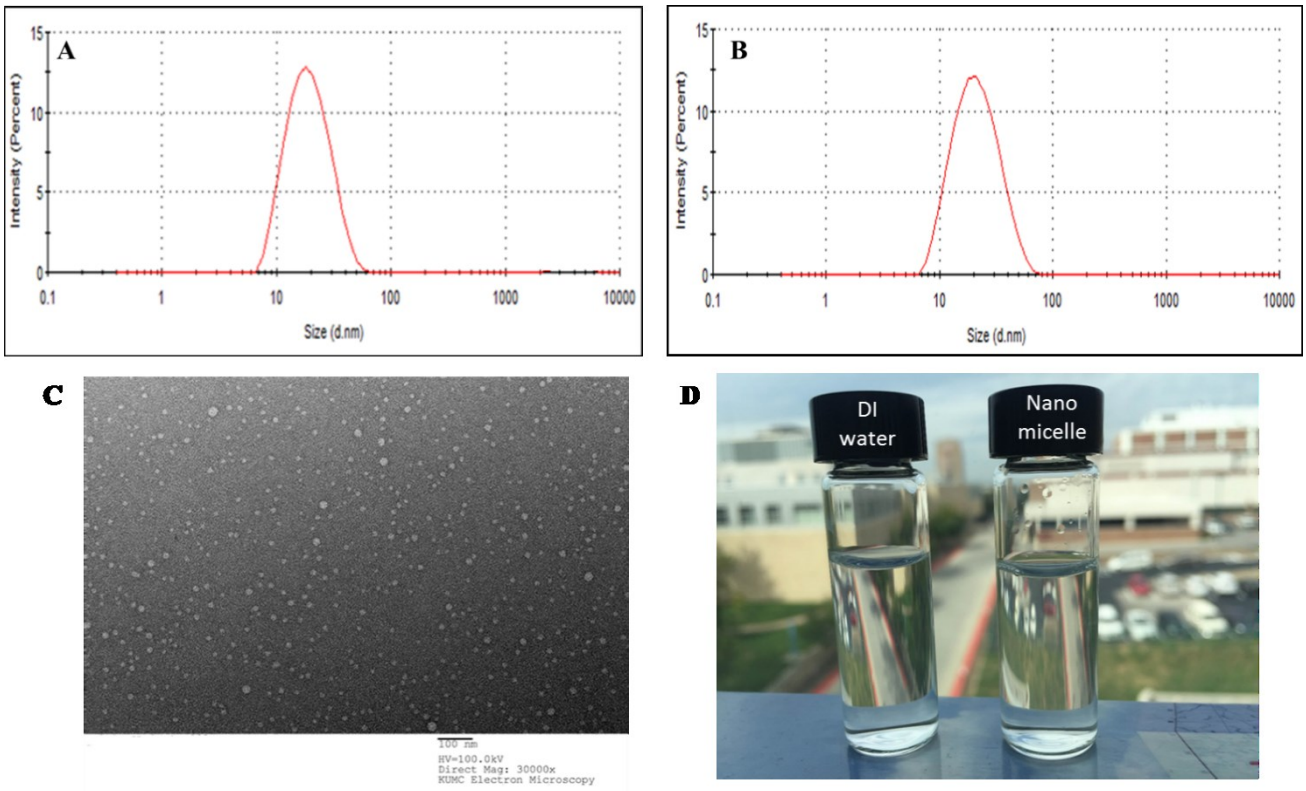

Figure 5-8 The size distribution of (A) B-C12-cCDF-free nanomicelles and (B) B-C12-cCDF-loaded nanomicelles; (C) TEM micrograph of B-C12-CDF-loaded nanomicelles; (D) B-C12-cCDF-loaded nanomicellar formulation compared with DI water

One of the objectives of this study was to achieve a clear aqueous solution of B-C12-cCDF. The optical clarity of the formulation was compared with DI water as blank. As shown in Figure 5-8 D, the formulation clarity is similar to water with no suspended particulate matter in it due to extremely small size of these polymeric nanomicelles.

5.4.5. CMC

CMC is a critical factor which regulates the premature release of topically applied therapeutic agents.[250] Such premature release of drug molecules is due to the presence of several static and dynamic ocular barriers. Tear dilution is one such barrier which contributes majorly to the loss of topically applied drugs [247]. Out of the total dose applied topically, only less than 10% of the formulation is available for absorption. The instilled formulation replaces

the lacrimal fluid in precorneal pocket and occupies the desired space. The precorneal pocket can hold up to 10 µL of tear volume and the tear turnover rate is approximately 0.7 µL/min. Once a formulation is dropped in the cul de sac, it gets continuously diluted by the presence of tears. This may result in disruption of nanocarriers in contact with ocular membranes leading to drug release at the application site itself [253-254]. Low CMC of the formulation is desired to prevent the disruption of nanocarriers including nanomicelles by tear dilution [255]. In order to achieve reduced CMC of polymeric nanomicelles, blends of non-ionic surfactants were applied herein. The CMC of HCO-40/OC-40 polymeric nanomicelle was determined to be 0.033 wt. % measured by fluorescence spectrophotometry with iodine as the probe (Figure 5-9). A low CMC is an indicator of stable formulation.

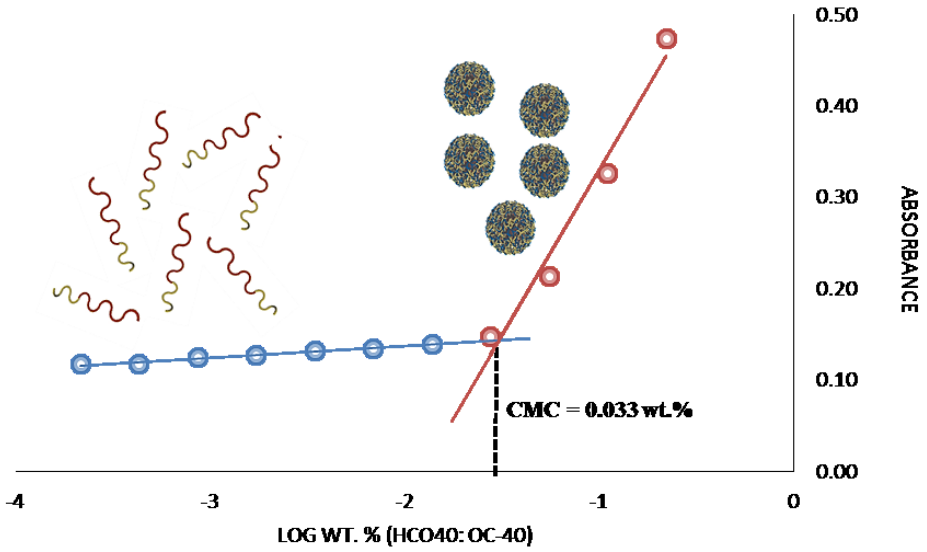

Figure 5-9 Fluorescence intensity ratios of iodine excitation bands (I460 nm/I286 nm) as a function of the concentration of HCO-40 and OC-40 aqueous solutions

5.4.6. ^{1}H-NMR spectroscopy of B-C12-cCDF-loaded nanomicelles

Process of nanomicelle formation and B-C12-cCDF encapsulation in nanomicelle core were studied with proton NMR spectroscopy. Separate 1H-NMR spectra for HCO-40, OC-40 and blank and B-C12-cCDF-loaded nanomicelles were recorded and compared. Sharp 1H-NMR signals from oxyethylene (-CH2-CH2-O) protons (δ=3.8 ppm) and weak signals from methyl (δ=0.9 ppm) and methylene (δ=1.3 ppm) protons of the hydrophobic chain for HCO-40 were recorded (Figure 5-10). Similarly, for OC-40, sharp signals from oxyethylene protons and weak signals from methyl and methylene protons were recorded (Figure 5-11). In addition, aromatic protons (δ=7.3 ppm) on phenyl ring were recorded for OC-40. There was no significant difference observed in the spectra for blank and B-C12-cCDF-loaded nanomicelles (Figures 5-12 and 5-13). Since, the hydrophobic core of the nanomicelle lacks accessibility to polar solvents, no characteristic peaks from B-C12-cCDF were observed in B-C12-cCDF-loaded nanomicelles implying that the drug was molecularly dispersed in the nanomicellar core. D2O peaks (δ=4.8 ppm) were recorded in all the cases except B-C12-cCDF which is in CDCl3 (Figures 5-14 & 5-15).

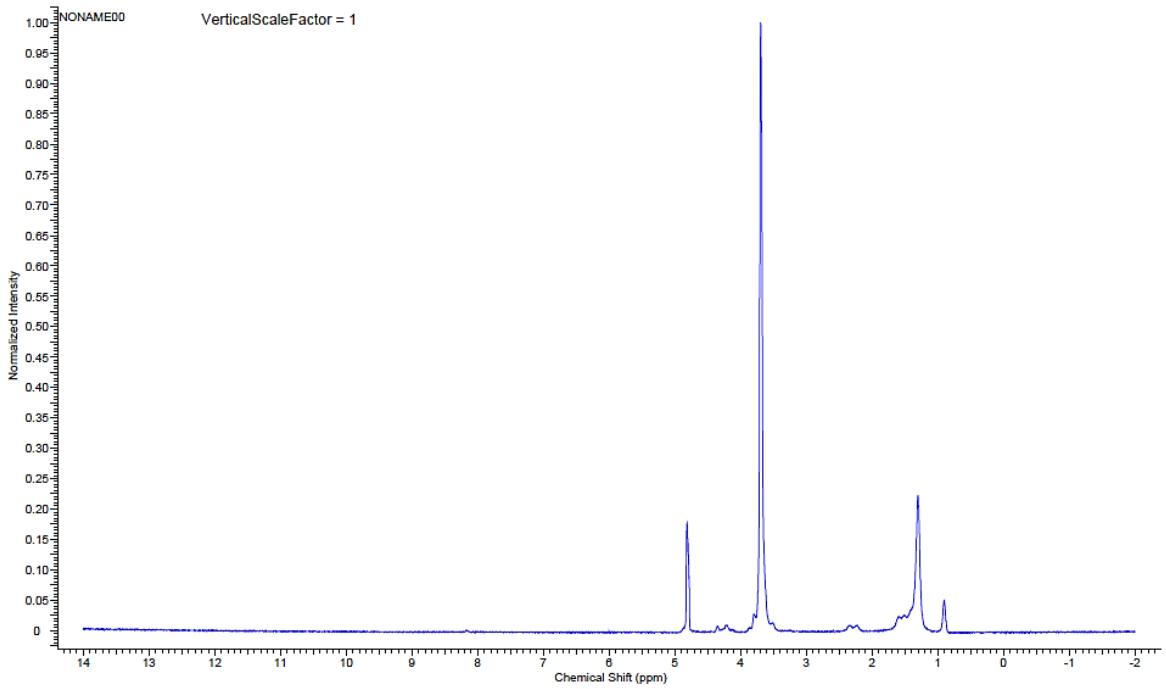

Figure 5-10 ^{1}H-NMR spectra for HCO-40 in D_20

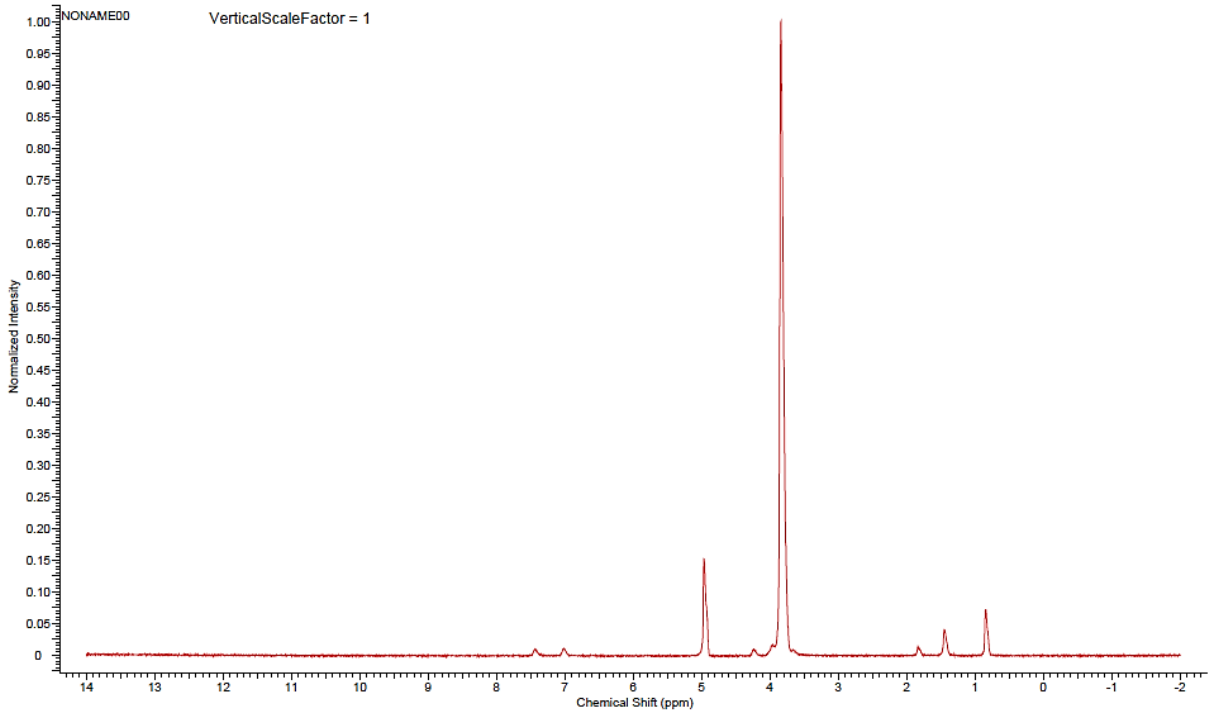

Figure 5-11 ^{1}H-NMR spectra for OC-40 in D_20

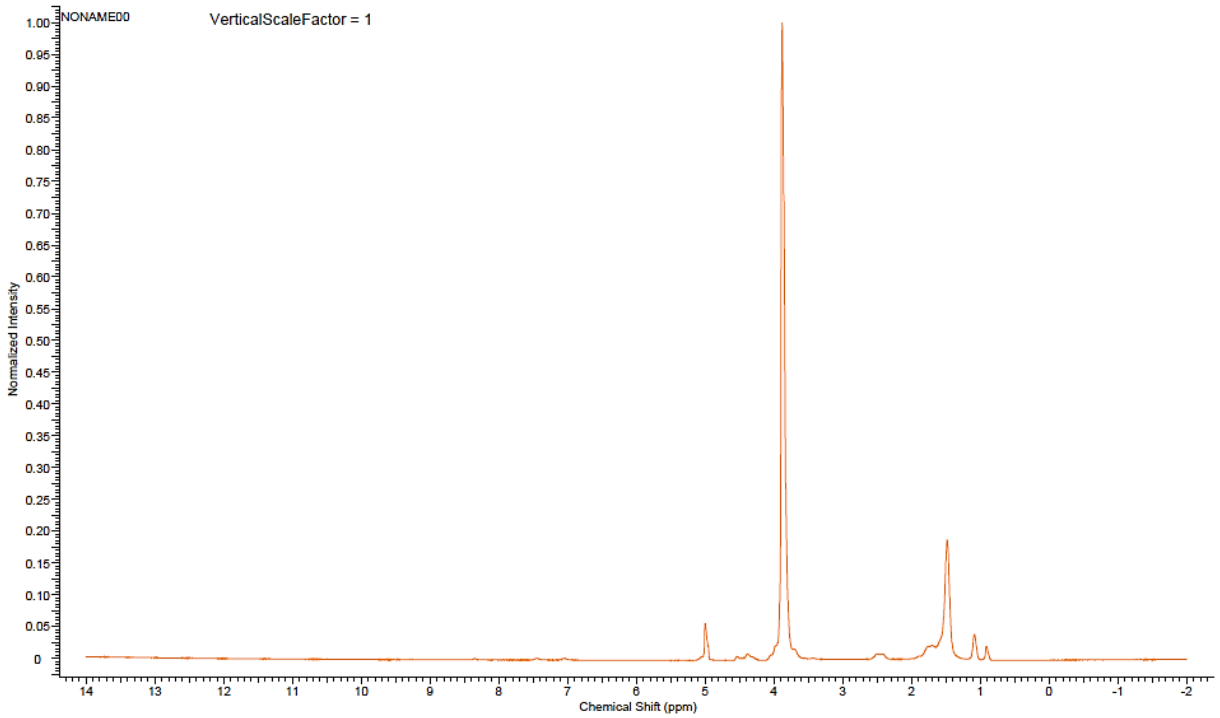

Figure 5-12 ^{1}H-NMR spectra for Blank nanomicelles in D_20

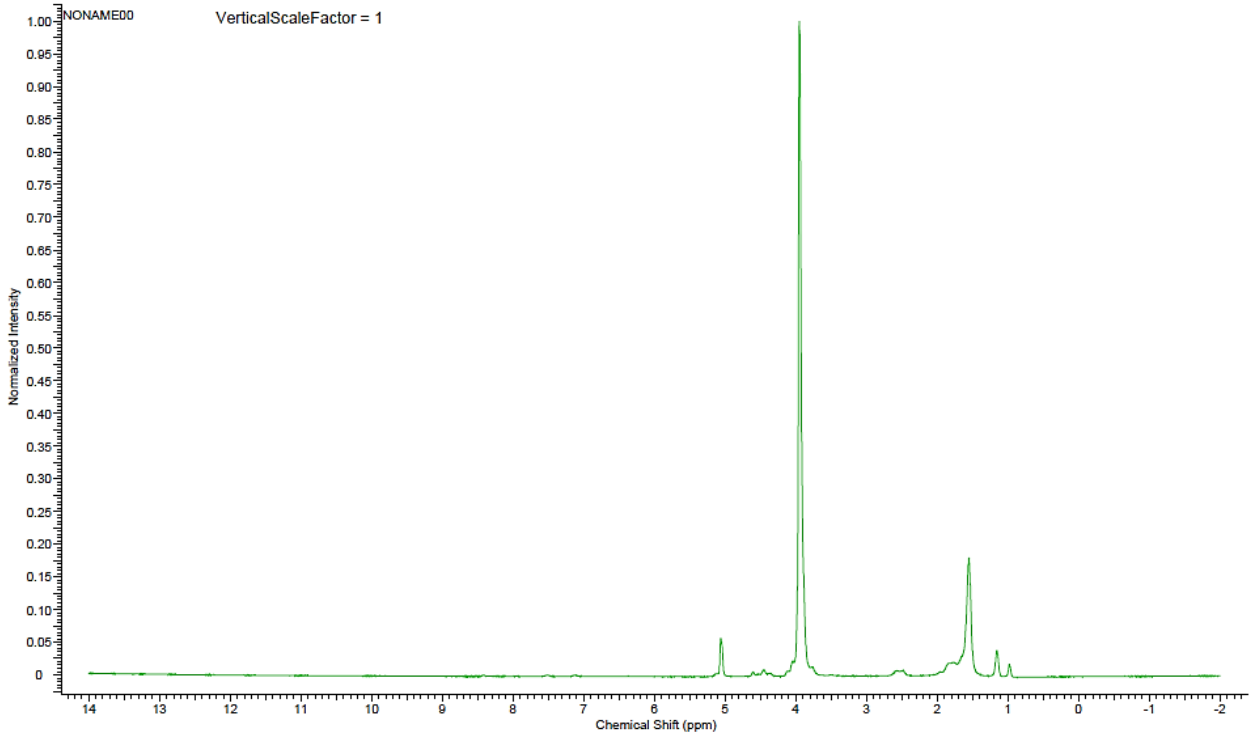

Figure 5-13 ^{1}H-NMR spectra for B-C12-cCDF-loaded nanomicelles in D_20

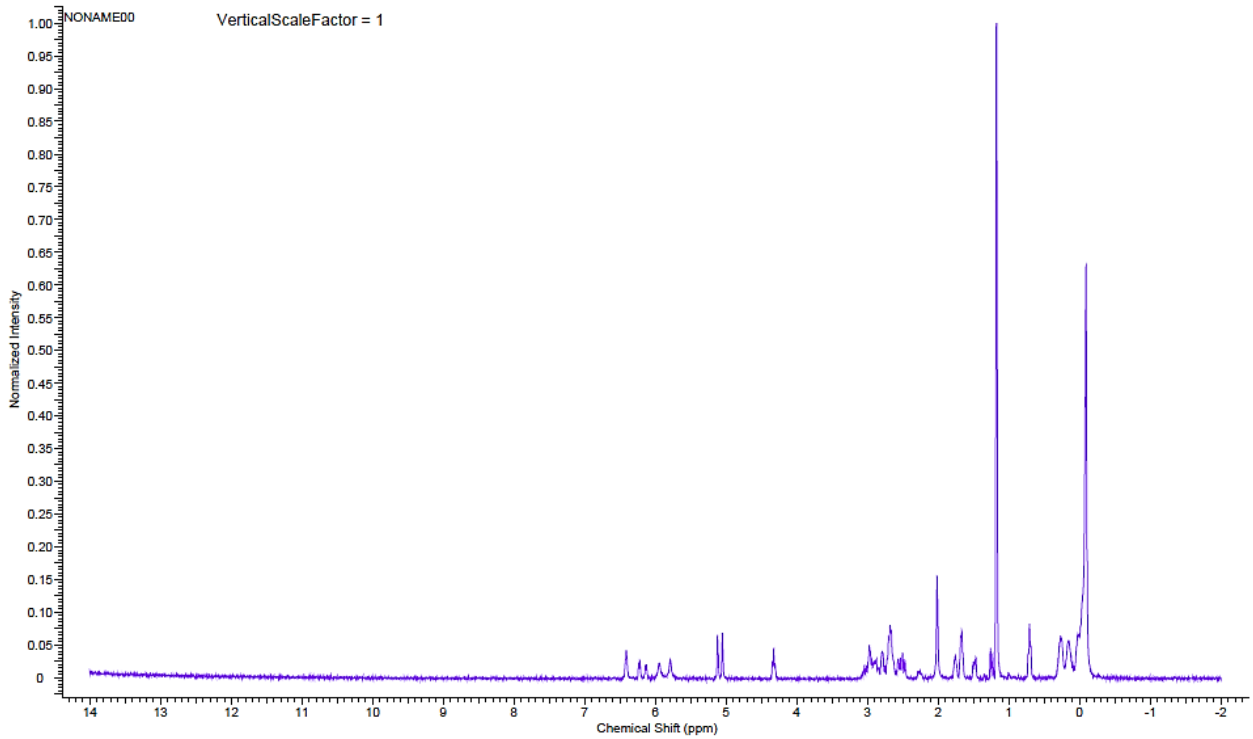

Figure 5-14 ^{1}H-NMR spectra for B-C12-cCDF in d_6-DMSO

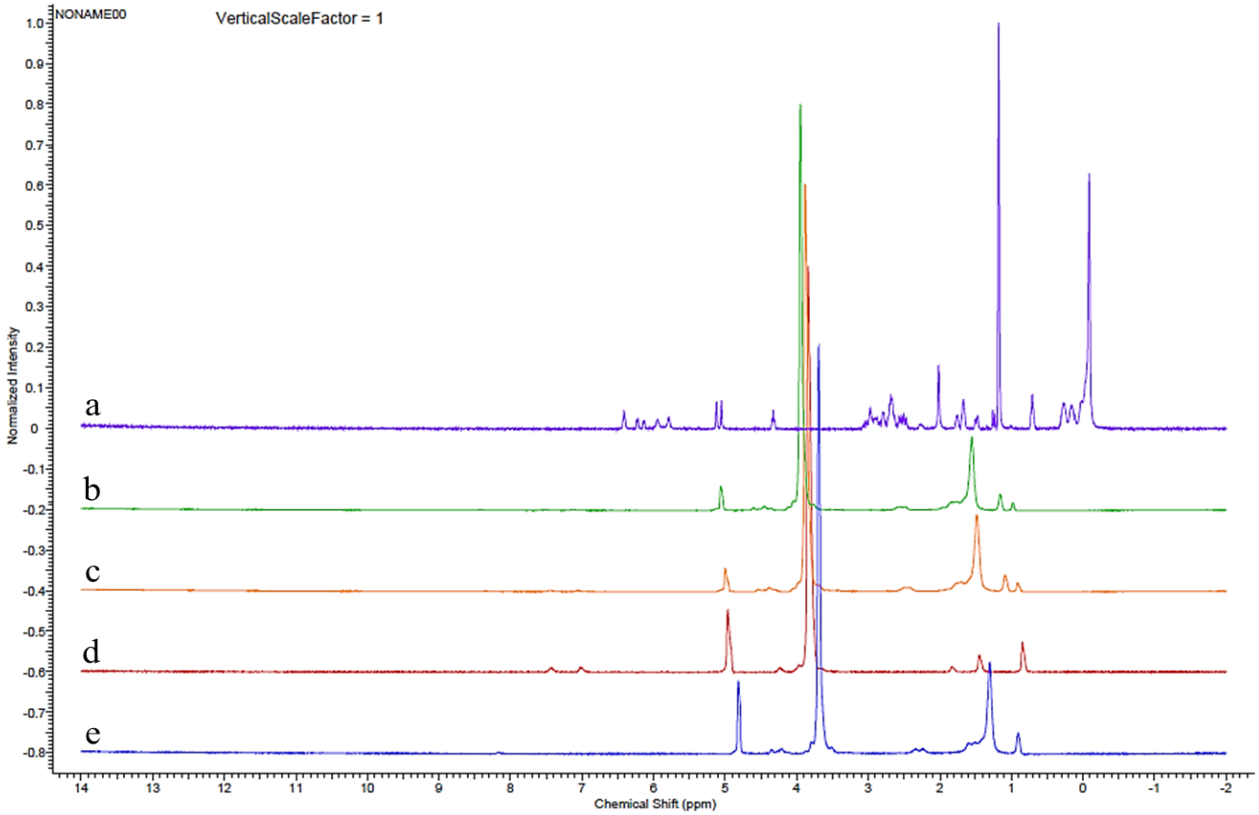

Figure 5-15 ^{1}H-NMR spectroscopies for (a) B-C12-cCDF in d_6-DMSO; (b) B-C12-cCDF-loaded nanomicelles; (c) Blank nanomicelles; (d) OC-40 and (e) HCO-40 in D_20

5.4.7. In vitro B-C12-cCDF release

To investigate the prodrug release behavior from polymeric nanomicelles, we performed B-C12-cCDF release experiments with B-C12-cCDF-loaded nanomicelles in both PBST and STF at 37°C. As shown in Figure 5-16, a sustained release of B-C12-cCDF from the core of polymeric nanomicelles over a period of >1 month was achieved without any significant burst release. In presence of PBST, 75.5% B-C12-cCDF was released over a period of 34 days. However in STF, polymeric nanomicelles rapidly released B-C12-cCDF by 91.09% in 34 days. These results suggest that STF can alter nanomicelle permeability to a larger extent relative to PBST as measured by prodrug release. Thus, it is anticipated that topical application of B-C12-cCDF-loaded nanomicelles will sustain the release of B-C12-cCDF under

physiological conditions leading to therapeutic concentrations in ocular tissues with low dosing frequency. However, one must also take into consideration the presence of the lipid monolayer on top of the tear film and its possible interaction with the polymers. The physicochemical properties and possible tear fluid factor(s) responsible for the observed increase in permeability still remains to be explored. In essence, CDF itself or its prodrug (B-C12-cCDF) can benefit immediately on short-term basis in reducing the viral load, but B-C12-cCDF-loaded nanomicelles may be effective for a longer time period due to slow release of prodrug from nanomicelles. Therefore, higher drug doses in nanomicelles can be administered and at the same time a single dose may produce a therapeutic effect for a prolonged time period given the IC50 of cidofovir to inhibit CMV plaque formation is just 0.9 μg/mL for Davis and 1.6 μg/mL for AD-169 CMV strains, respectively[256]. In contrast, CDF or B-C12-cCDF may require frequent dosing leading to poor patient compliance.

Table 5-2 Summary of fit for kinetic models and associated parameters for release of B-C12-cCDF from nanomicelles

Release medium	**Kinetic and Mechanistic Models**						
	Higuchi Model	**Korsmeyer-Peppas model**		**Hixson-Crowell model**	**Zero Order**	**First order**	
	R^2	**R^2**	**n**	**R^2**	**R^2**	**R^2**	**Rate constant k ($Hour^{-1}$)**
PBST	0.9433	0.9686	1.0085	0.9570	0.8878	0.9169	0.1045
STF	0.9292	0.9888	1.0226	0.9889	0.9169	0.9325	0.1239

The release data was fitted to various mechanistic models including Higuchi, Hixson-Crowell and Korsmeyer-Peppas models to determine the kinetics of B-C12-cCDF release (Table 5-2). The best fit was found with the Korsmeyer-Peppas model with R^2 of 0.9686 for

PBST and Hixson-Crowell model with R^2 of 0.9889 for STF compared to other models. For STF, Korsmeyer-Peppas model also showed high R^2 value of 0.9888 with n value 1.0085 and 1.0226 for PBST and STF respectively. Value of diffusion exponent n >1 for Korsmeyer-Peppas model suggests that mechanism of release followed super case II transport which mainly involves relaxation of polymer chains. The relatively close value obtained from Hixson-Crowell indicates that the drug release might be controlled by diffusion and erosion of polymer to some extent as well. Data was also fitted to zero- and first- order equations to determine the order of release. Process of release followed first order kinetics with R^2 values of 0.9169 and 0.9325 for PBST and STF respectively indicating release rate is proportional to the prodrug concentration. Compared to PBST, release rate was faster in STF, as indicted by first order rate constant which can attributed to the higher concentration of surfactant in STF.

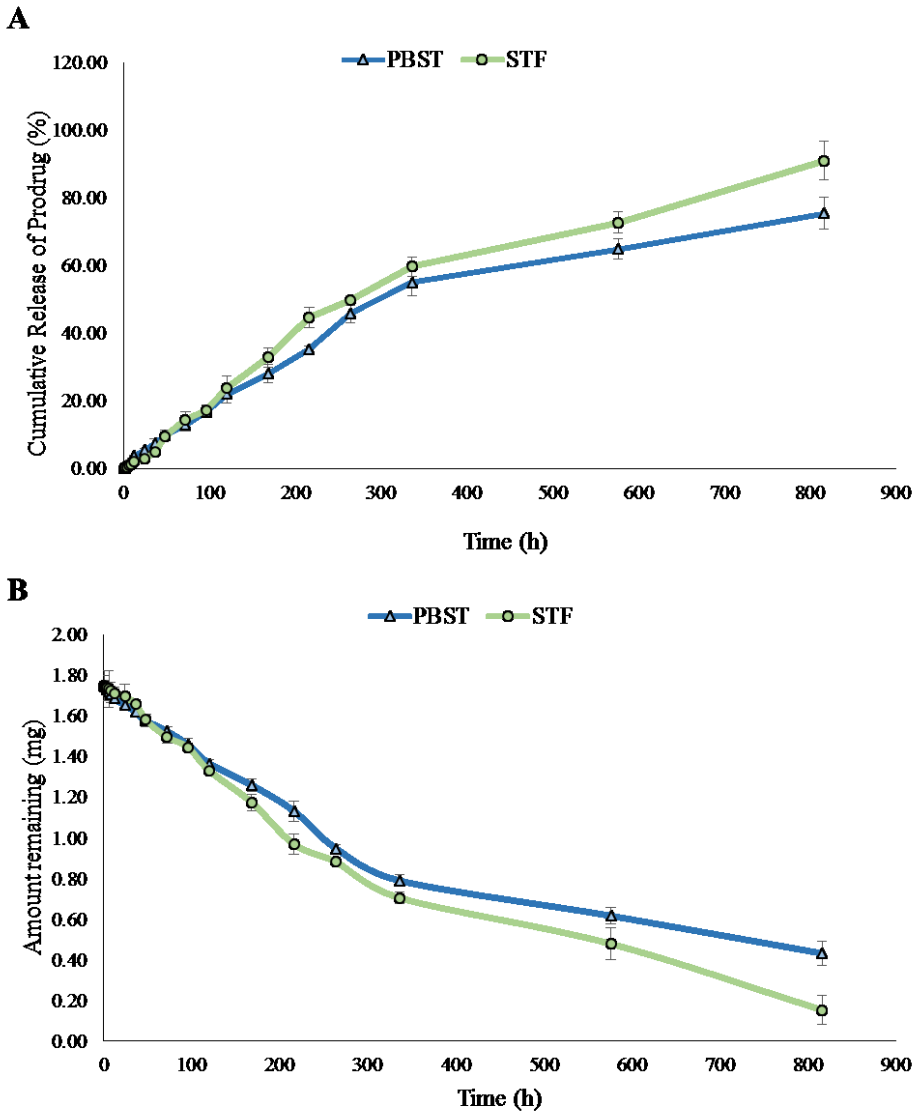

Figure 5-16 (A) Release and (B) amount remaining from B-C12-cCDF from B-C12-cCDF-loaded nanomicelles in PBST and STF (pH 7.4). The standard deviation for each data point was averaged over three samples (n=3)

5.4.8. Effect of molecular weight cut-off (MWCO) on drug release

Apart from the release media, selecting an appropriate molecular weight cut-off (MCWO) for the dialysis membrane is crucial. It is anticipated that the prodrug released from the nanomicelles will diffuse rapidly from the inner compartment, through the dialysis membrane into the outer compartment due to concentration gradient. Although the rationale for selecting a MWCO is rather subjective, a sufficiently high membrane MWCO are often selected for in vitro release studies so that drug transport is not a limiting factor. For instance, a MWCO of 10–14 kDa was used to study drug release of small molecules like risperidone (MW: 410.493 g/mol) and indomethacin (MW: 357.79 g/mol), and a MWCO of 1 kDa for assessing in vitro release of a large molecule, pDNA, and cefuroxime axetil, a cephalosporin antibiotic (MW: 510.474 g/mol)[257]. Herein, results from *in vitro* release studies suggested, dialysis membrane with MWCO 1 kDa proved to be limiting for the diffusion of B-C12-cCDF (<20% released in 34 days). While MWCO of 2 kDa (>75% released in 34 days) was able to sufficiently permit prodrug transport across the dialysis membrane (Figure 5-17).

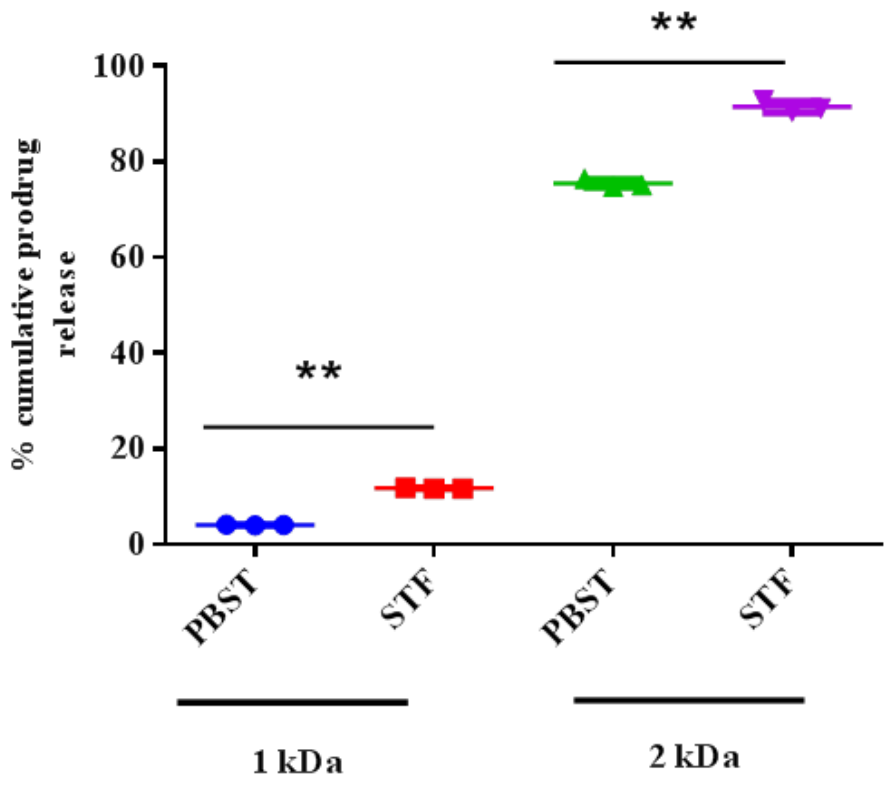

Figure 5-17 Cumulative prodrug release (percentage) from B-C12-cCDF-loaded nanomicelles in PBST and STF (pH 7.4) in 34 days using dialysis membranes with molecular weights 1kDa and 2kDa. The standard deviation for each data point was averaged over three samples (n=3)

5.4.9. In vitro cytotoxicity assay

D407, HCE-T or CCL 20.2 cells were co-cultured with B-C12-cCDF-free nanomicelles (HCO-40/OC-40) at concentrations ranging from 0.24 to 7.0 mg/mL. As shown in Figure 5-18 A, D407, HCE-T or CCL 20.2 cells were not influenced by the addition of nanomicelles at any concentration compared with blank control, demonstrating the non-cytotoxic effect of the polymeric nanomicelles.

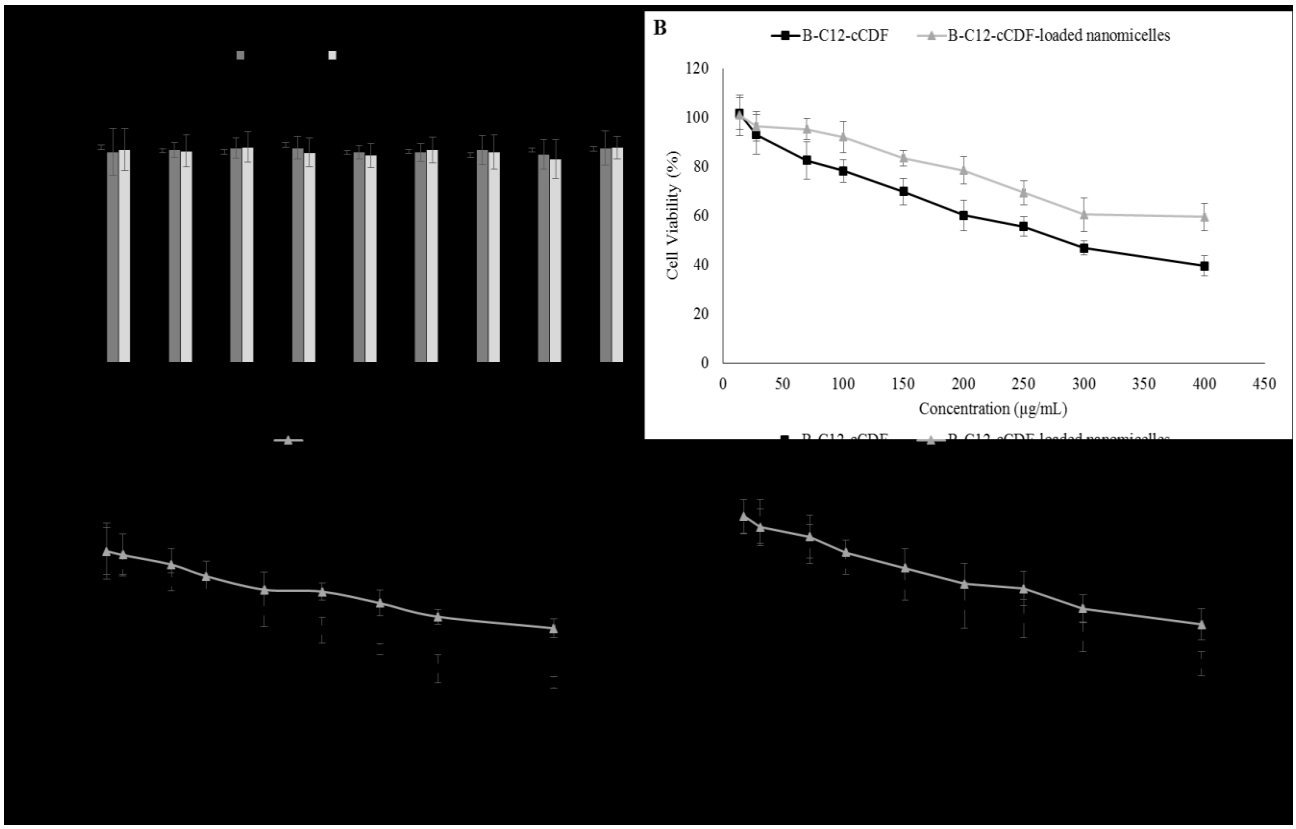

Figure 5-18 (A) MTT assay of HCO-40/OC-40 polymeric nanomicelles in HCE-T, CCL 20.2 and D407 cell lines. Cytotoxicity of B-C12-cCDF and B-C12-cCDF-loaded nanomicelles in (B) D407, (C) HCE-T and (D) CCL 20.2 cell lines

In vitro cytotoxicity of B-C12-cCDF and B-C12-cCDF-loaded nanomicelles against D407, HCE-T or CCL 20.2 cells were determined by the MTT assay. As shown in Figures 5-18 B, C and D, B-C12-cCDF and B-C12-cCDF-loaded nanomicelles demonstrated dose-

dependent cytotoxicity to all cell lines studied. Compared to B-C12-cCDF, B-C12-cCDF-loaded nanomicelles exhibited lower toxicity to D407, HCE-T or CCL 20.2 cells at the same concentration. Both, B-C12-cCDF and B-C12-cCDF-loaded nanomicelles are internalized into cells solely by endocytosis releasing the drug at the target site. More importantly, more rapid release of drug from the prodrug in comparison to B-C12-cCDF-loaded nanomicelles can be the reason for their low cytotoxicity. Toxicity studies for cCDF have been previously reported and showed by our laboratory [145].

In addition, the LDH assay was performed to confirm the results obtained from the MTT assay. Polymeric nanomicelles can interact with the cell membrane and enter into cells through endocytosis [258-259]. Therefore, estimating the amount of LDH released into the surrounding culture medium could be a preferred way to estimate the extent of cell wall damage and thus cytotoxicity of polymeric nanomicelles. The percentage of LDH released from D407, HCE-T and CCL 20.2 cells following 24 h of exposure to B-C12-cCDF, B-C12-cCDF-free and B-C12-cCDF-loaded nanomicelles appeared to be negligible indicating no membrane damage. Approximately 17.16% and 19.01% LDH were released from CCL 20.2 cells treated with CDF 100 μM and 250μM respectively (Figure 5-19). However, prodrug and the prodrug-loaded nanomicellar formulation did not cause any membrane damage or toxicity. Therefore, it appears that this nanomicellar formulation is suitable for ocular application.

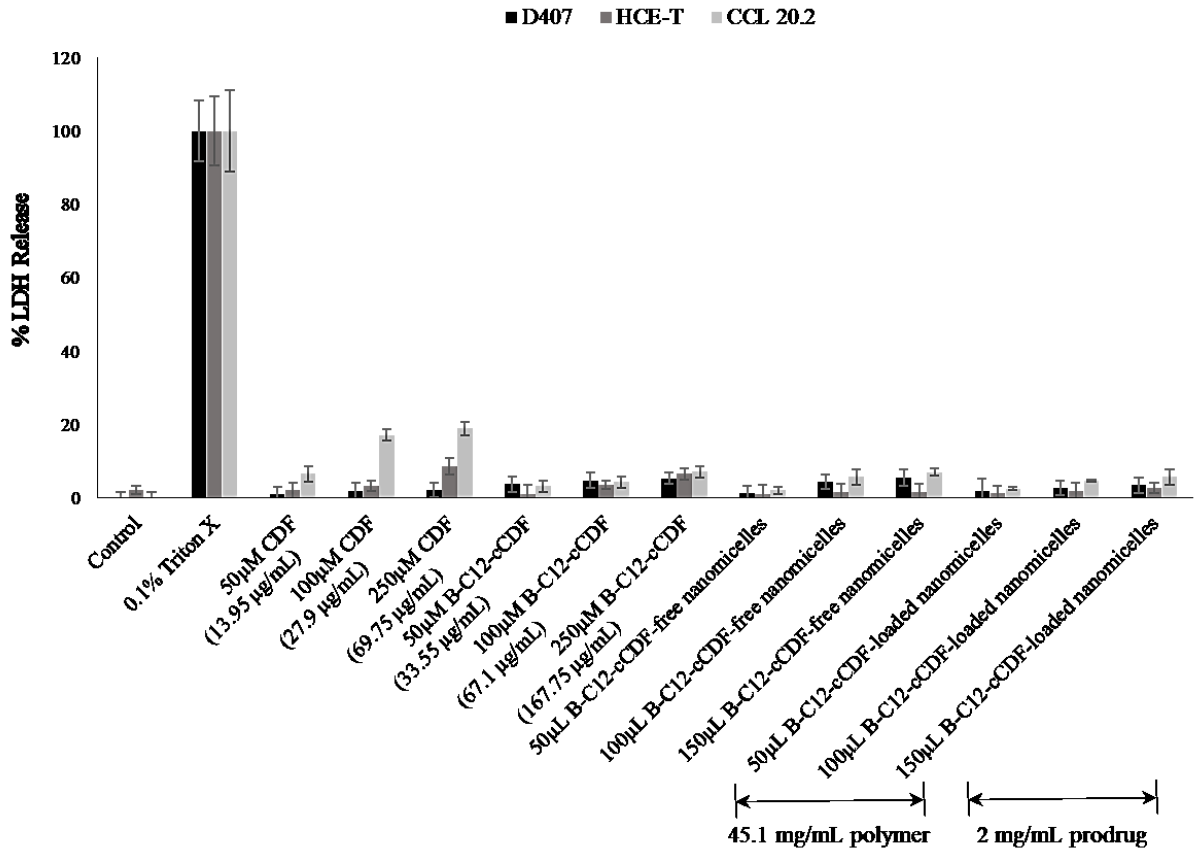

Figure 5-19 LDH assay after 24 h of exposure to CDF, B-C12-cCDF, B-C12-cCDF-free nanomicelles and B-C12-cCDF-loaded nanomicelles to D407, HCE-T and CCL 20.2 cells

5.4.10. In vitro biocompatibility studies

RAW-264.7 cells are widely utilized as *in vitro* cell culture model for determining the biocompatibility of polymeric materials intended for human applications. In this study, we examined the cytokine (TNF-α, IL-6, and IL-1β) release into the culture supernatant following 24 h of exposure to CDF, B-C12-cCDF, B-C12-cCDF-free and B-C12-cCDF-loaded nanomicelles. Samples were analyzed via a sandwich ELISA assay. Results depicted in Figure 5-20, indicate significant release of TNF-α, IL-6, and IL-1β following LPS exposure. However, no significant release of TNF-α, IL-6, and IL-1β was observed when sample were treated with

different concentrations of CDF, B-C12-cCDF, B-C12-cCDF-free and B-C12-cCDF-loaded nanomicelles relative to negative control (cells without treatment). These results suggest that B-C12-cCDF-loaded nanomicelles are suitable for in-vivo applications.

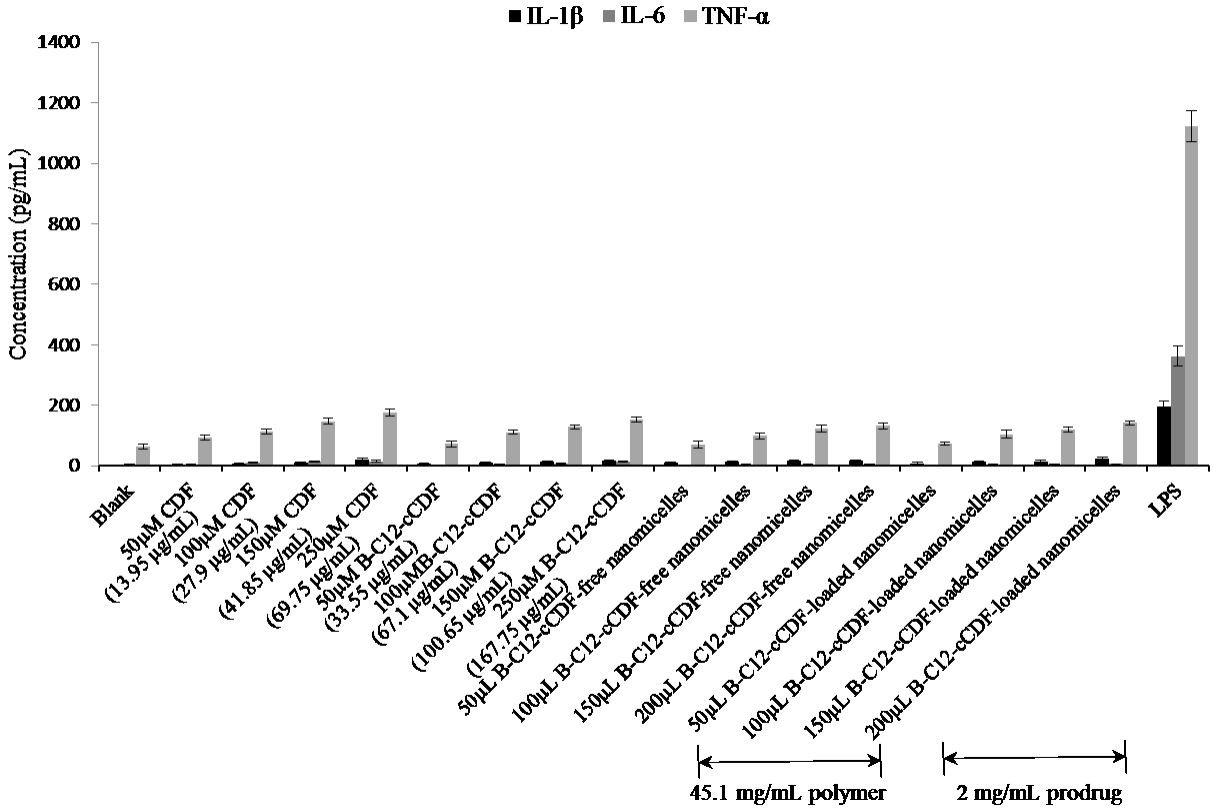

Figure 5-20 *In vitro* release of TNF-α, IL-6, and IL-1β from RAW 264.7 cells following 24 h exposure of CDF, B-C12-cCDF, B-C12-cCDF-free micelles and B-C12-cCDF-loaded nanomicelles. Results are given as mean ± SD, n = 4

5.4.11. In vitro cellular uptake of B-C12-cCDF-loaded nanomicelles

Experiments on cellular uptake and prodrug release from B-C12-cCDF-loaded nanomicelles were performed on D407 and HCE-T cells by FCM and CLSM. To validate cellular uptake, D407 and HCE-T cells were incubated with FITC-tagged CDF, B-C12-cCDF and B-C12-cCDF-loaded nanomicelles for 2, 12 and 24 h and then monitored with CLSM. As

illustrated in Figures 5-21 A and B, B-C12-cCDF-loaded nanomicelles show weak FITC fluorescence in the cytoplasm after 2 h, indicating slow internalization of nanomicelles into the cells. After 12 h of incubation, significant amounts of FITC-tagged B-C12-cCDF and B-C12-cCDF-loaded nanomicelles were observed inside the cell cytoplasm. In contrast, weaker FITC fluorescence was observed in cells treated with FITC-tagged CDF. With further incubation for 24 h, the FITC fluorescence intensity inside the cells increased and the accumulation of FITC-tagged B-C12-cCDF-loaded nanomicelles in the cell cytoplasm and nuclei became more evident. Cells incubated with B-C12-cCDF-loaded nanomicelles exhibited strong FITC fluorescence indicating accumulation of prodrug loaded nanomicelles inside the cells. Consequently, no burst release was observed for B-C12-cCDF-loaded nanomicelles. These results are consistent with the cytotoxicity results for B-C12-cCDF-loaded nanomicelles. These prodrug-loaded nanomicelles showed minimal cytotoxicity because of slow and sustained release of B-C12-cCDF from the hydrophobic core of the nanomicelles. However, relatively lower fluorescence signals of FITC-tagged B-C12-cCDF and B-C12-cCDF-loaded nanomicelles in D407 cells could be attributed to higher expression of tight junction proteins, including zonula occludens-1 (ZO-1), occludin, claudin-1, claudin-2, claudin-3, claudin-4, and claudin-5. Additionally, the trans epithelial electrical resistance (TEER) offered by D407 cell monolayer is ~300 Ωcm^2 which increases rapidly during the initial 7 days of culture unlike HCE-T cells (~300-600 Ωcm^2) [260-261]. The higher resistance offered by D407 cells impedes the penetration of the treatment groups to an extent thus justifying the difference in cellular accumulation of B-C12-cCDF and B-C12-cCDF-loaded nanomicelles in D407 and HCE-T cells.

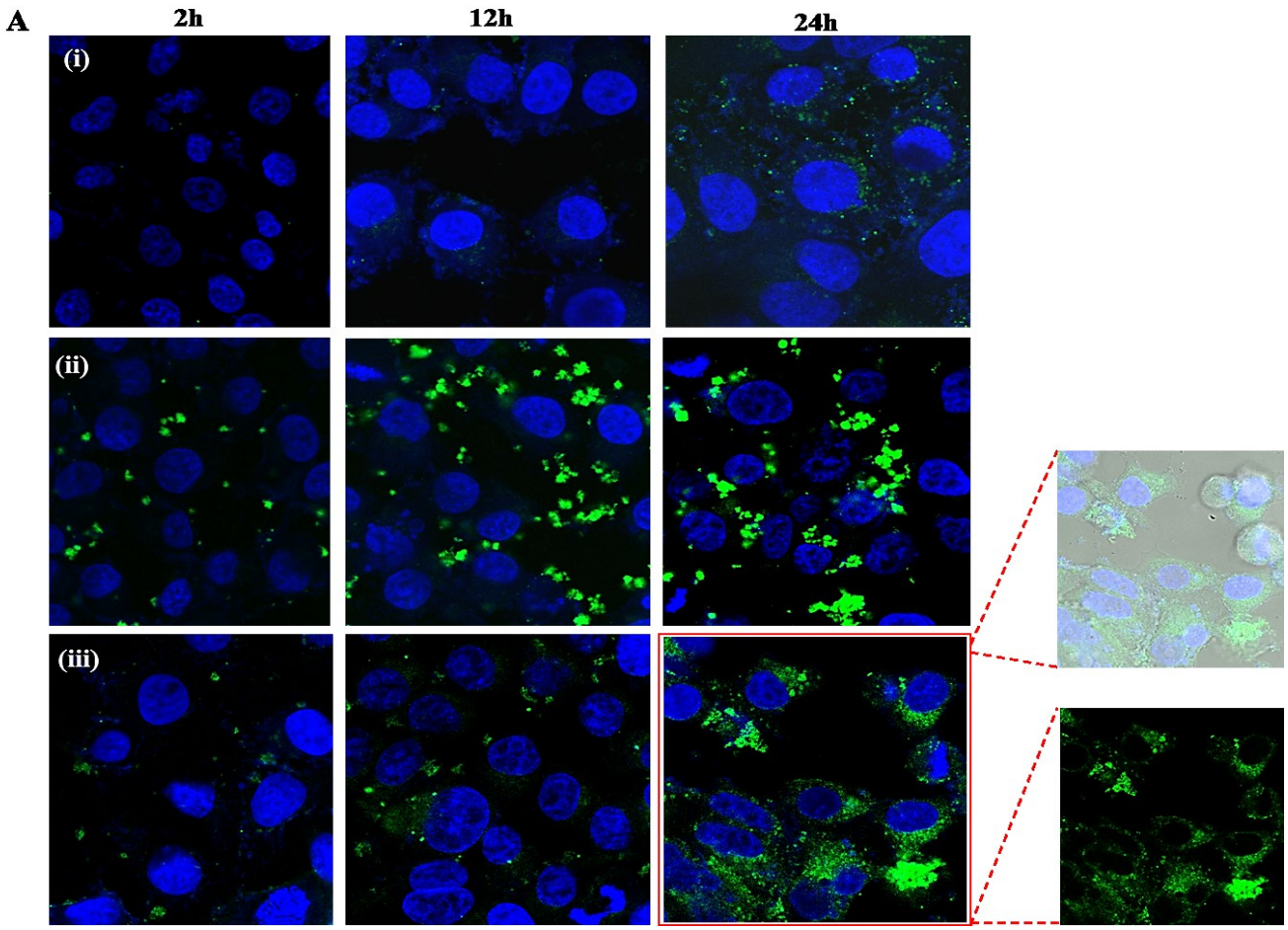
A
2h
12h
24h
(i)
(ii)
(iii)

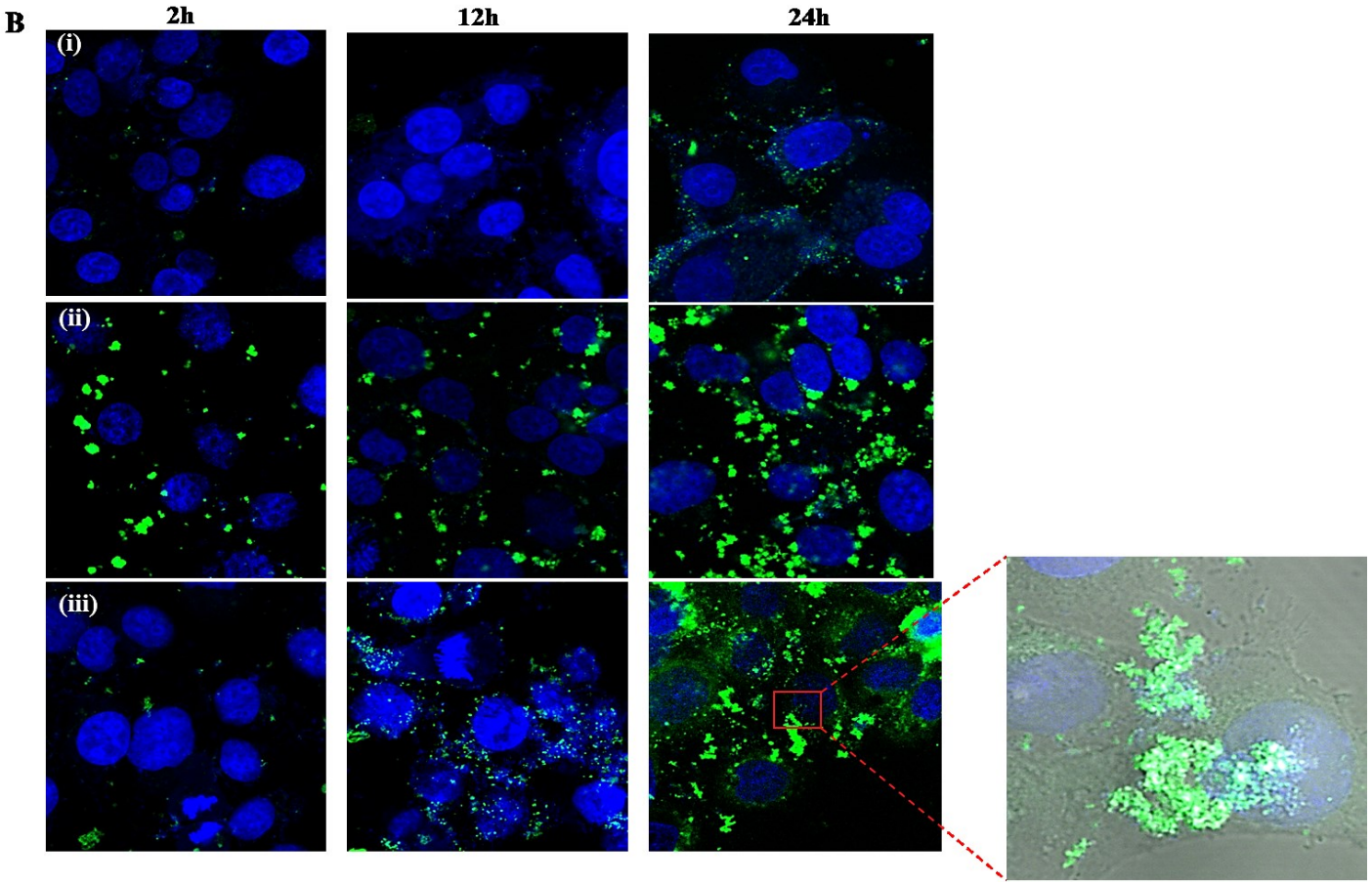

Figure 5-21 Confocal laser scanning microscopy images of (A) D407 and (B) HCE-T cells after incubation with (i) CDF, (ii) B-C12-cCDF and (iii) B-C12-cCDF-loaded nanomicelles. CDF, B-C12-cCDF and B-C12-cCDF-loaded nanomicelles were added at a final concentration of 15 µg/mL. Blue and green fluorescence shows the nuclei and FITC conjugated drug/prodrug respectively. Scale bar is 20 µm

The drug accumulation was further evaluated in D407 and HCE-T cells incubated with FITC-tagged CDF, B-C12-cCDF and B-C12-cCDF-loaded nanomicelles by FCM (Figures 22 A and B). The outcome was consistent with the CLSM results. Figures 23 A and B show the mean FITC fluorescence intensity in D407 and HCE-T cells after incubation with FITC-tagged CDF, B-C12-cCDF and B-C12-cCDF-loaded nanomicelles for 0.5, 2, 6, 12 and 24 h. Mean

fluorescence intensity (MFI) of cells treated with B-C12-cCDF-loaded nanomicelles was higher than cells incubated with CDF and B-C12-cCDF at 24 h. The fluorescence signals are associated with the accumulation of B-C12-cCDF-loaded nanomicelles. Enhanced intracellular fluorescence in cells treated with FITC-tagged B-C12-cCDF-loaded nanomicelles at 24 h was due to higher stability and permeation of nanomicelles across various ocular barriers efficiently. These results are in accordance with our expectation that the blend of polymers can impart higher stability to the prodrug conjugate in the hydrophobic core of the nanomicellar structure and would sustain the release of the prodrug correlating with the CLSM and in vitro cytotoxicity results.

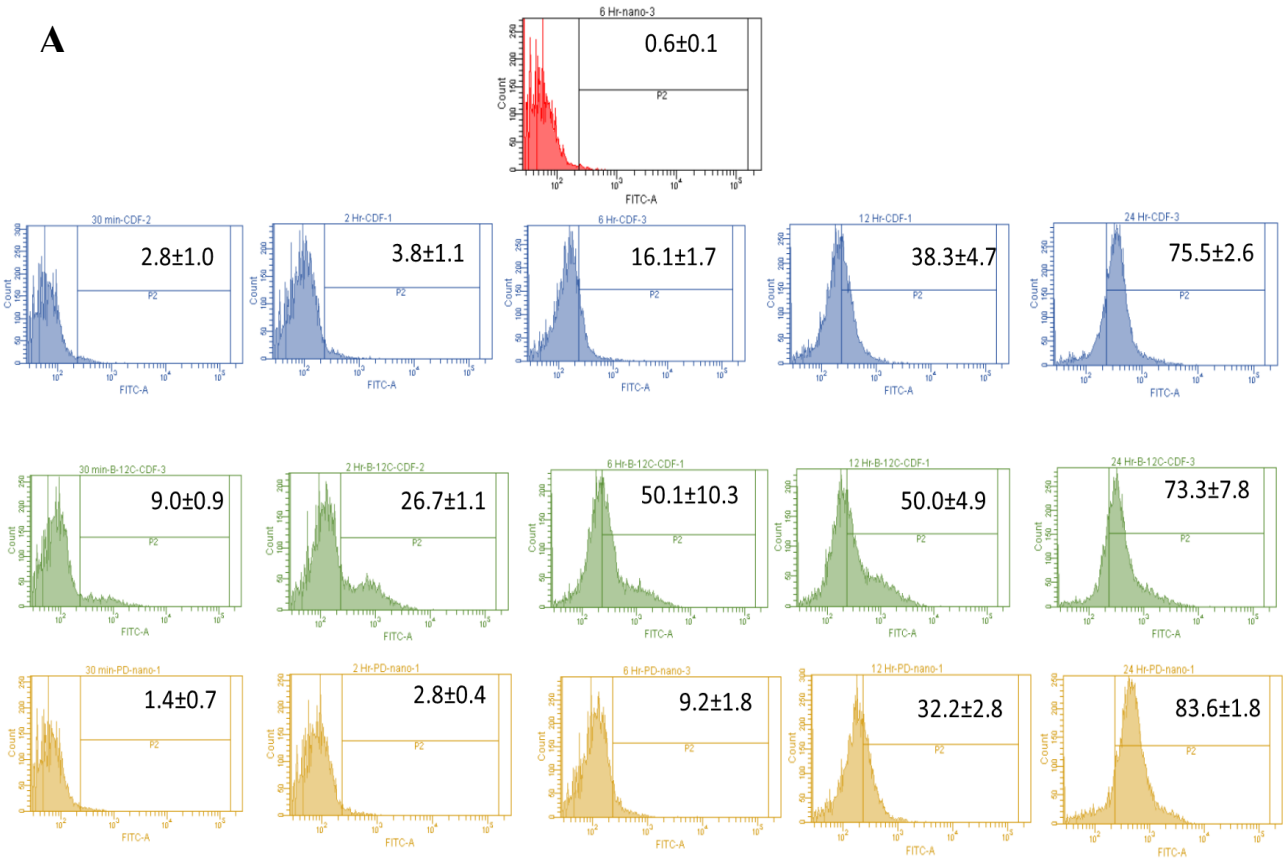

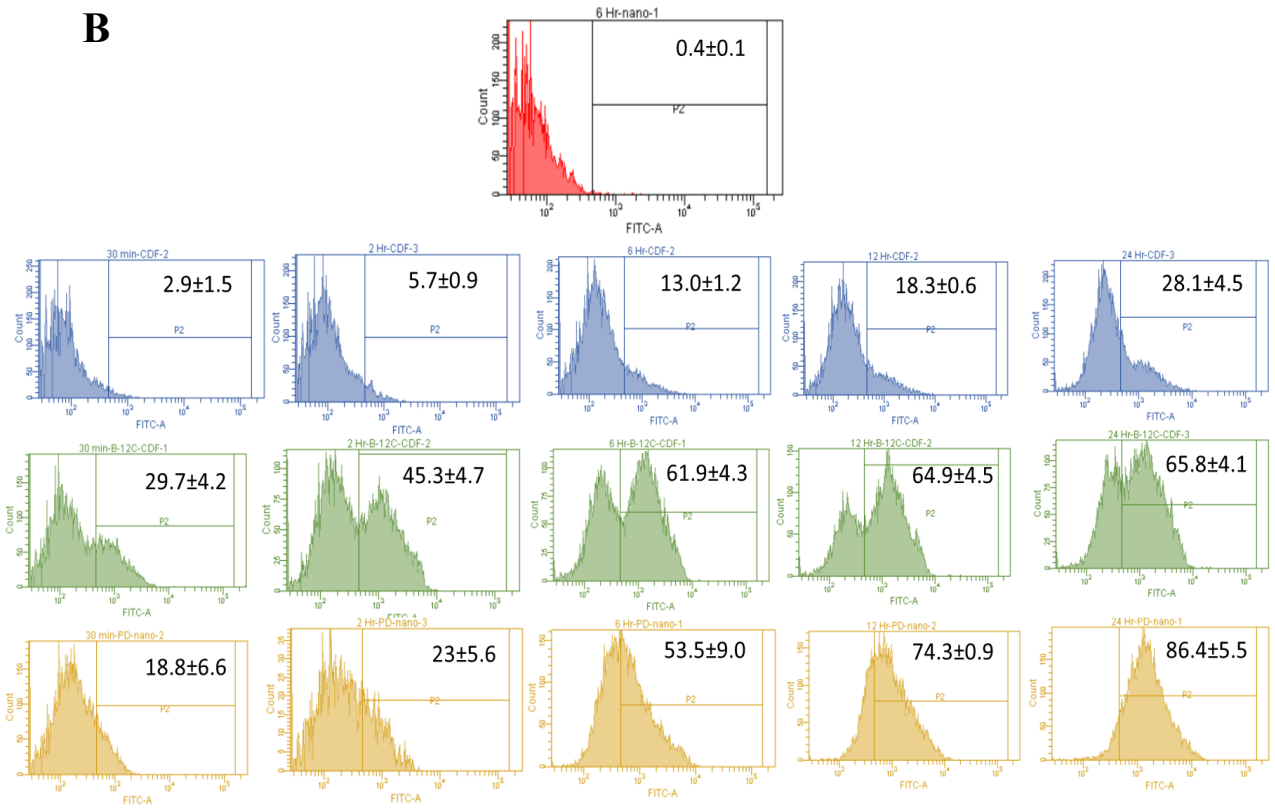

Figure 5-22 FACS analysis of uptake of CDF (blue), B-C12-cCDF (green) and B-C12-cCDF-loaded nanomicelles (yellow) for 0.5 h, 2 h, 6 h, 12 h and 24 h in (A) D407 and (B) HCE-T cell lines. CDF, B-C12-cCDF and B-C12-cCDF-loaded nanomicelles were added at a final concentration of 50 µg/mL. *P ≤ 0.05, compared to corresponding control group (red). #P ≥ 0.05, compared to corresponding control group

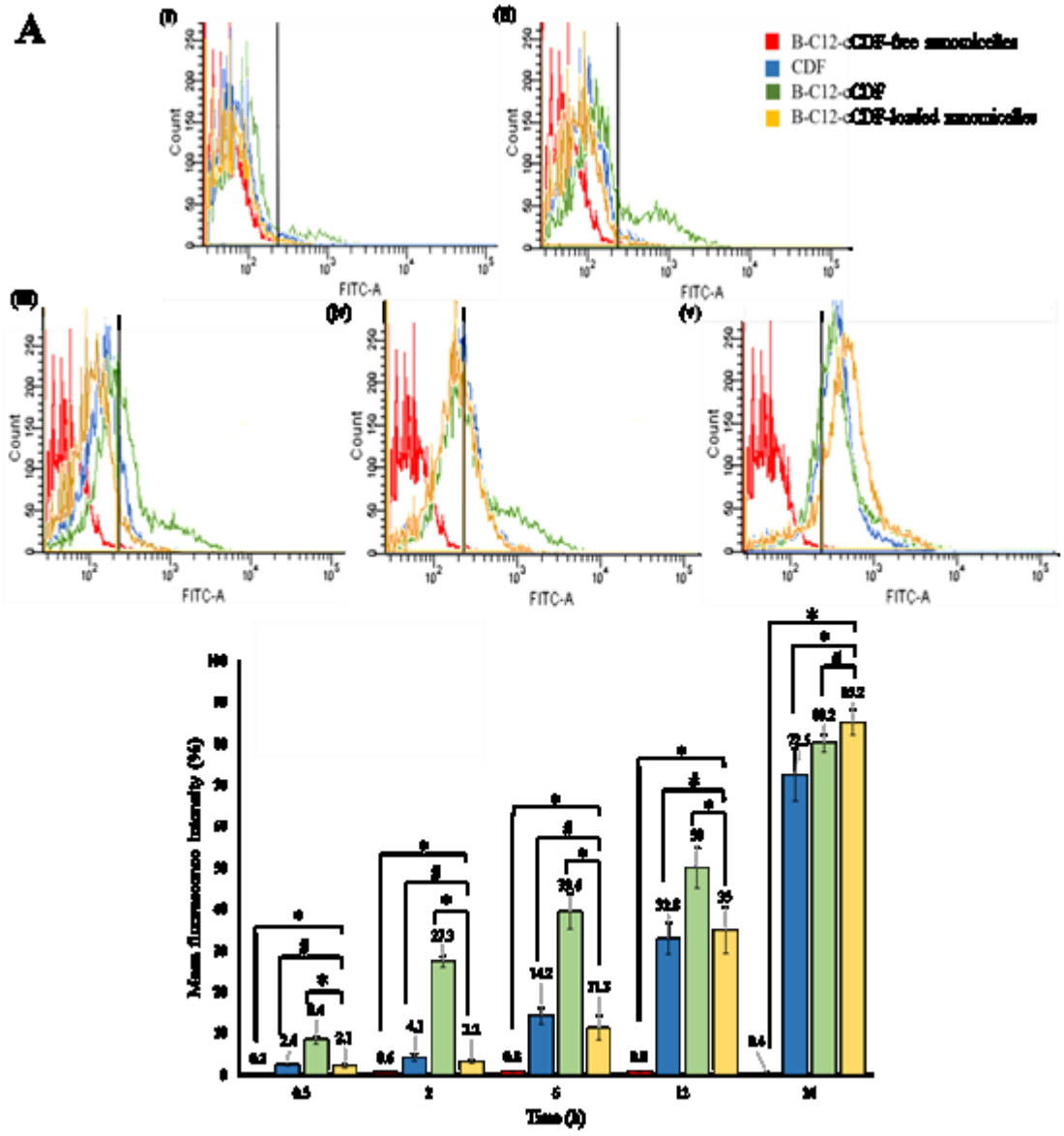
A
(i)
(ii)
(iii)
(iv)
(v)
B-C12-cCDF-free micelles
CDF
B-C12-cCDF
B-C12-cCDF-loaded micelles
Count
FITC-A
Mean fluorescence intensity (%)
Time (h)
0.5
2
6
12
24

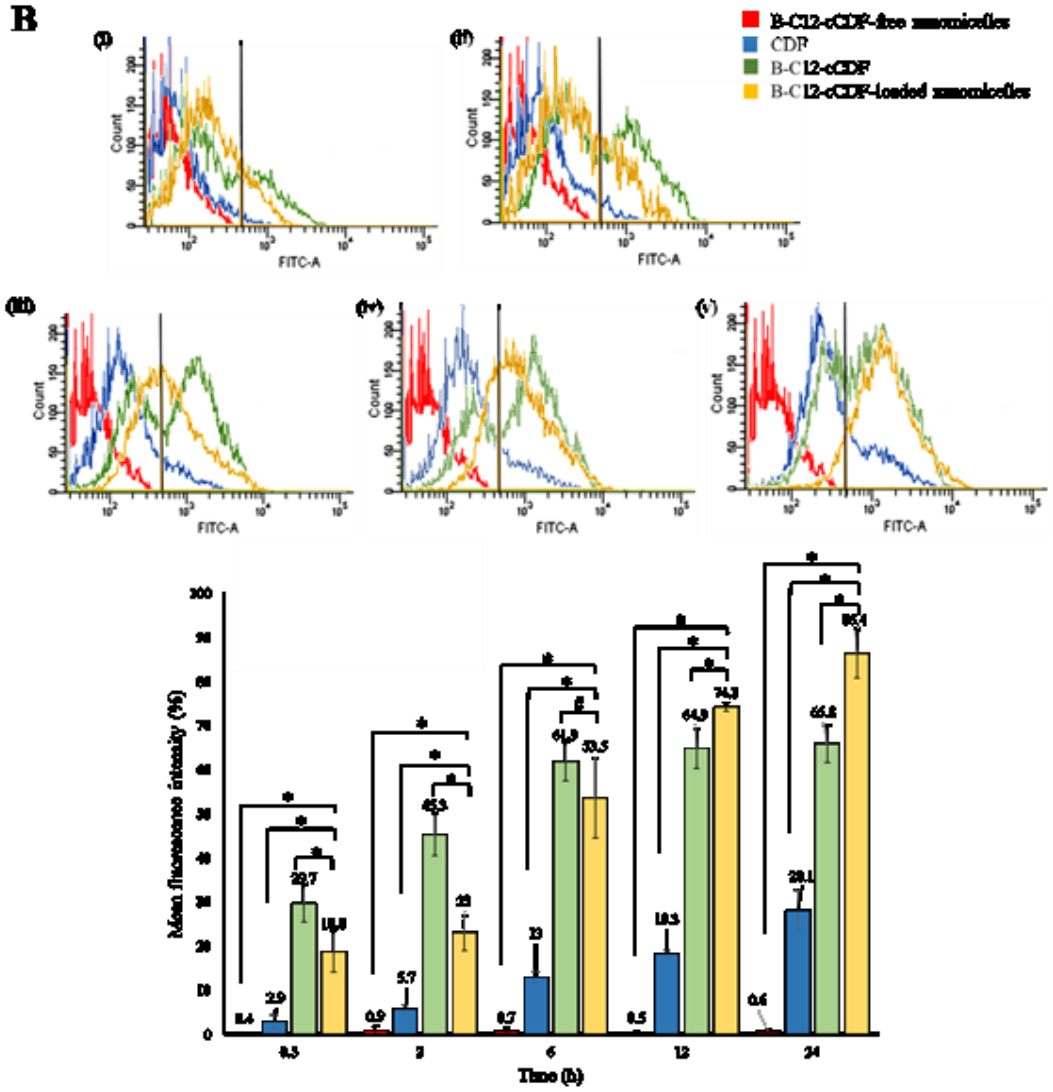

Figure 5-23 Overlay of FACS analysis of B-C12-cCDF-loaded nanomicelles uptake in comparison to CDF and B-C12-cCDF for 0.5 h (i), 2 h (ii), 6 h (iii), 12 h (iv) and 24 h (v) in (A) D407 and (B) HCE-T cell lines. CDF, B-C12-cCDF and B-C12-cCDF-loaded nanomicelles were added at a final concentration of 50 µg/mL. *P ≤ 0.05, compared to corresponding control group. #P ≥ 0.05, compared to corresponding control group

5.4.12. In vitro cellular transport of B-C12-cCDF-loaded nanomicelles

Previous results showed significant uptake of FITC-tagged B-C12-cCDF-loaded nanomicelles at 24 h in both corneal and retinal cell monolayers. However, the question remains whether the drug loaded nanomicelles would be able to permeate corneal layers and reach retinal cells *in vivo*. For a delivery system to be effective to deliver drugs to back of the eye, drug molecules must cross the corneal barriers and reach the retinal cells. Although, corneal permeability of lipophilic drugs has been reported to be greater in comparison to hydrophilic drugs, their poor solubility and chances of getting detected by the RES system render them ineffective.

In this study, we investigated the permeability of B-C12-cCDF-loaded nanomicelles in comparison to CDF and B-C12-cCDF. As shown in Figure 5-24, corneal cells (HCE-T) were grown on transwell filters in the upper chamber while bottom chamber contained retinal cells (D407). FITC-tagged B-C12-cCDF-loaded nanomicelles were added to the upper transwell filters which traversed to the bottom chamber through corneal monolayers reaching D407 cells. In contrast to previous uptake results, transport across corneal cells was negligible at 0.5 and 2 h. However, significant transport was observed at 24 h as evidenced by a 7-fold (MFI) higher fluorescence in D407 cells by FITC-tagged B-C12-cCDF-loaded nanomicelles in comparison to the control group. Additionally, the amount of CDF and B-C12-cCDF transported across HCE-T cells remained almost the same at all-time points probably due to non-specific binding and precipitation of hydrophobic prodrug in the culture medium (Figures 5-25 and 5-26). Hence, these results suggest that HCO-40/OC-40 based polymeric nanomicelles might be a suitable carrier for back of the eye delivery of anti-viral prodrugs (B-C12-cCDF).

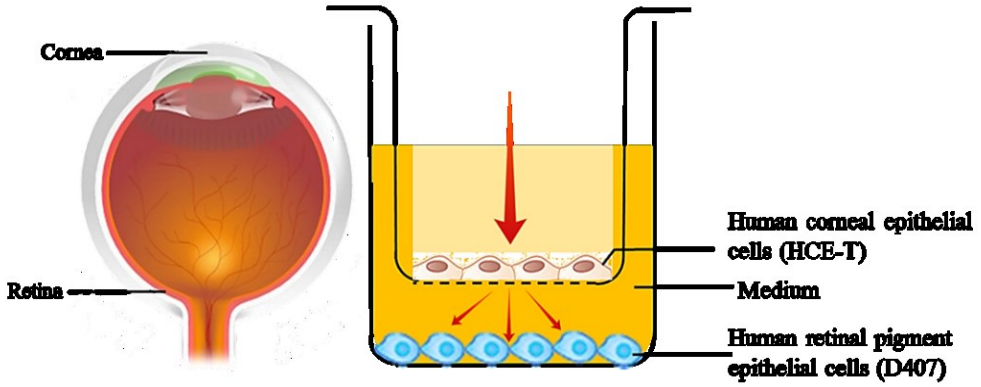

Figure 5-24 Schematic drawing of the preparation of the in vitro corneal-retinal model. Human corneal epithelial cells (HCE-T) were grown for 10 days in the transwell inserts until all the different layers of corneal cells were established completely. Similarly, retinal pigment epithelial cells (D407) were seeded at the bottom chamber of 12-well plates and were grown for 10 days. Cells were grown in DMEM culture medium. Experiments were performed on day 11

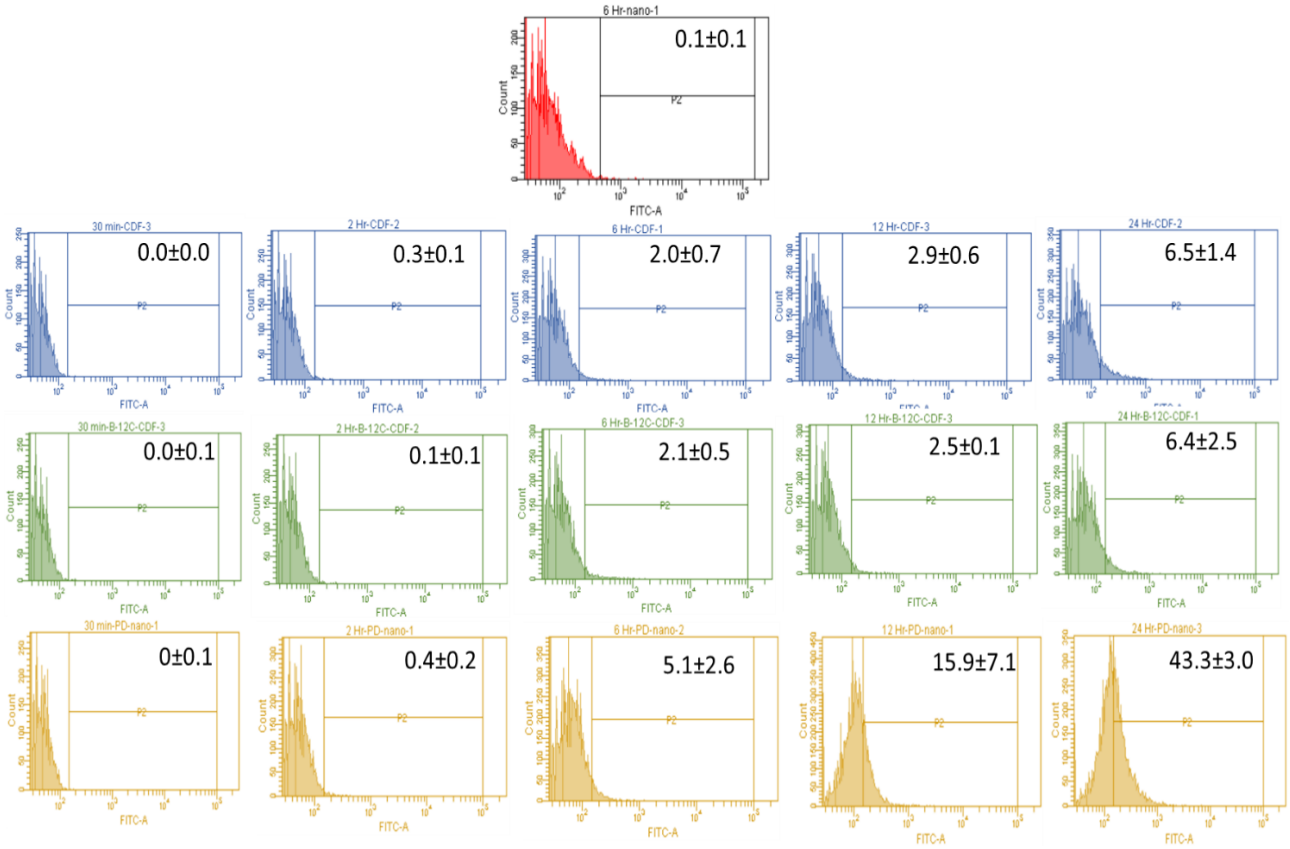

Figure 5-25 FACS analysis of uptake of CDF (blue), B-C12-cCDF (green) and B-C12-cCDF-loaded nanomicelles (yellow) for 0.5 h, 2 h, 6 h, 12 h and 24 h in transwell diffusion chamber with HCE-T & D407 cell lines. CDF, B-C12-cCDF and B-C12-cCD-loaded nanomicelles were added at a final concentration of 50μg/mL. *P ≤ 0.05, compared to corresponding control group. #P ≥ 0.05, compared to corresponding control group

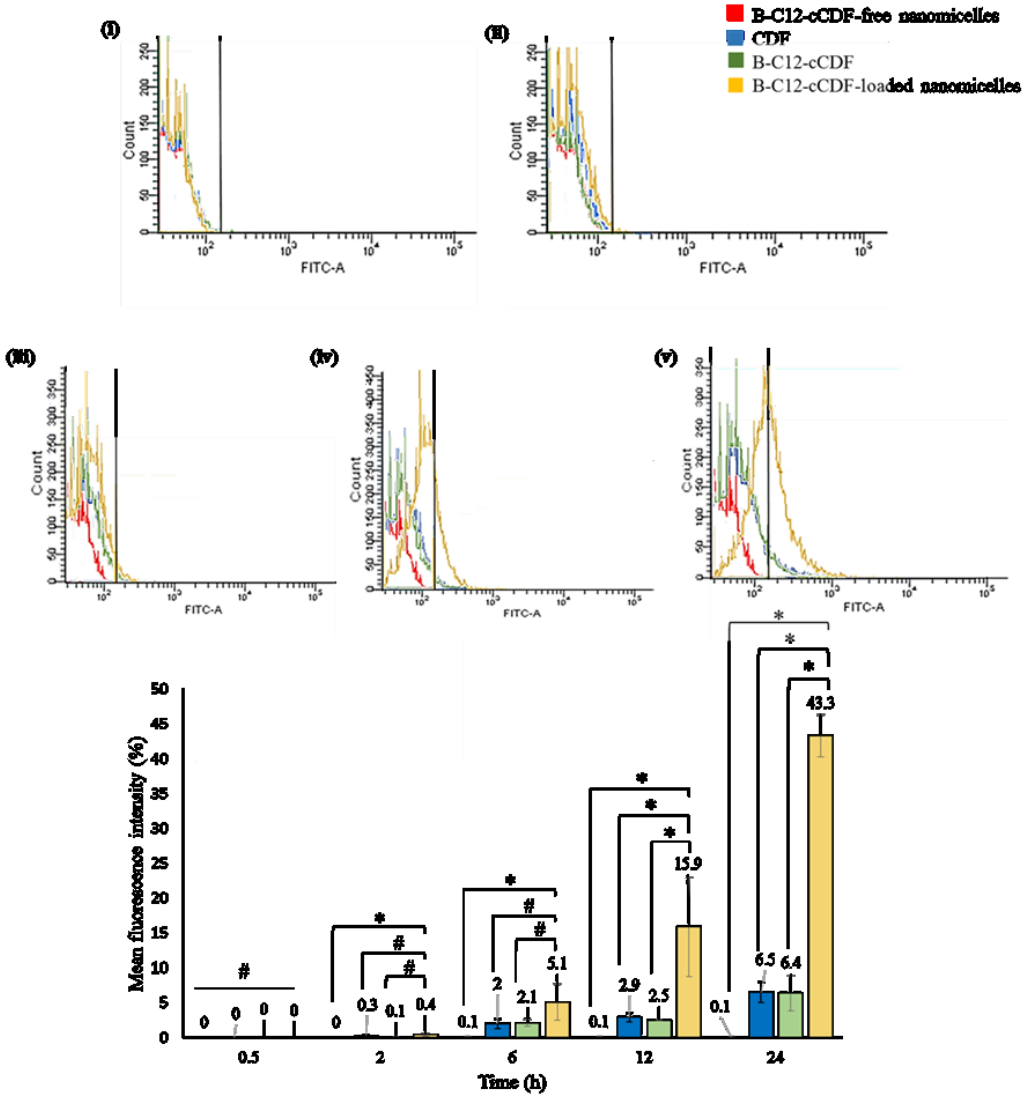

Figure 5-26 Overlay of FACS analysis of B-C12-cCDF-loaded nanomicelles uptake in comparison to CDF and B-C12-cCDF for 0.5 h (i), 2 h (ii), 6 h (iii), 12 h (iv) and 24 h (v) in transwell diffusion chamber with HCE-T & D407 cell lines. CDF, B-C12-cCDF and B-C12-cCDF-loaded nanomicelles were added at a final concentration of 50 µg/mL. *P ≤ 0.05, compared to corresponding control group. #P ≥ 0.05, compared to corresponding control group

5.5. Conclusions

A clear, stable aqueous B-C12-cCDF-loaded polymeric nanomicelle was prepared and optimized by full factorial statistical DOE using JMP. A specific blend of polymers (HCO-40/OC-40) at a wt. % ratio of 2.5:1.0 produced excellent drug entrapment, loading, small size and narrow PDI. In vitro release studies revealed that in the presence of STF, B-C12-cCDF-loaded nanomicelles released B-C12-cCDF more rapidly relative to PBST. Cell experiments showed that self-assembled B-C12-cCDF-loaded nanomicelles were highly stable and able to permeate various ocular barriers efficiently with minimal toxicity in D407, HCE-T or CCL 20.2 cells. Biocompatibility studies further unraveled the non-cytotoxic nature of these polymeric nanomicelles. Cellular uptake studies in D407 and HCE-T cells revealed internalization of B-C12-cCDF-loaded nanomicelles in the cytoplasm and nuclei after 24 h. Permeability experiments across HCE-T /D407 cells further confirmed the potential of B-C12-cCDF-loaded nanomicelles in transporting the prodrug across multiple cell layers. Therefore, HCO-40/OC-40 based polymeric nanomicelles hold potential as promising carriers for the delivery of anti-viral prodrugs such as B-C12-cCDF for a prolonged period of time, affording enhanced CDF effects in the back of the eye.

CHAPTER 6

6. OCULAR DELIVERY OF PROTEINS AND PEPTIDES: CHALLENGES AND FORMULATION APPROACHES

6.1. Rationale

In the past few decades, since the first approval of a protein- based biopharmaceutical in 1982 (Humulin®; recombinant human insulin; Eli Lilly, Indianapolis), the approval rate of protein and peptide based biopharmaceuticals has grown significantly [262]. Of the top 10 pharmaceutical products by sales in 2014, a majority was biopharmaceuticals including recombinant therapeutic proteins, peptides, enzymes, monoclonal antibodies and antibody-drug conjugates. From 1982 to 2014, the total number of licensed biopharmaceutical products advanced from 13 to 246 in the United States (US) and European Union (EU; Brussels). The worldwide sales of biopharmaceutical drugs was estimated to be $289 billion in 2014 and are projected to grow to $445 billion by 2019[98]. Among these, the rapidly growing monoclonal antibody (mAb) therapeutics market itself has currently resulted in global sales of over US$50 billion [263]. Likewise, the ophthalmic protein- and peptide-based biopharmaceutical drug market has witnessed a tremendous growth since the introduction of the anti-vascular endothelial growth factor (anti-VEGF) aptamer in 2004 (Macugen®; Pegatanib sodium; OSI Pharmaceuticals, New York) and monoclonal antibody in 2006 (Lucentis®; Ranibizumab; Genentech, California). The global sales of biopharmaceutical drugs for ophthalmic indications had exceeded $8 billion in 2016, with about 16% annual growth rate (2011-2016)[264]. A recent survey of ophthalmology market research revealed biologics and drug delivery systems to be the sectors that are anticipated to show strong growth in the next five years[265] (Figures 6-1 and 6-2).

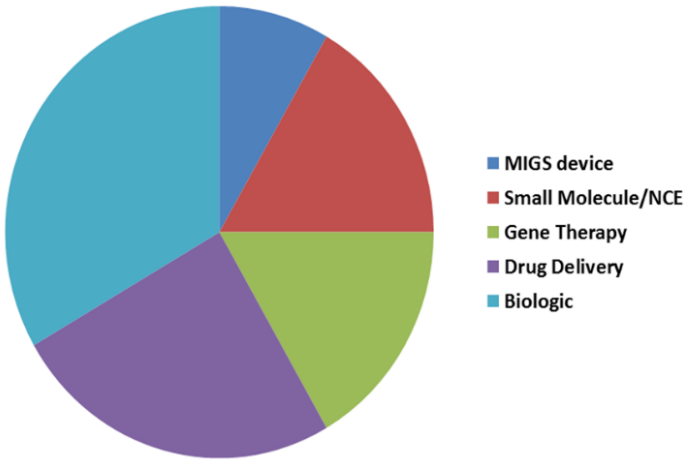

Figure 6-1 Numbers of Phase 3 products by technology type for ophthalmic indications (Till Nov., 2015): MIGS (minimally invasive glaucoma surgery); NCE (New chemical entity).

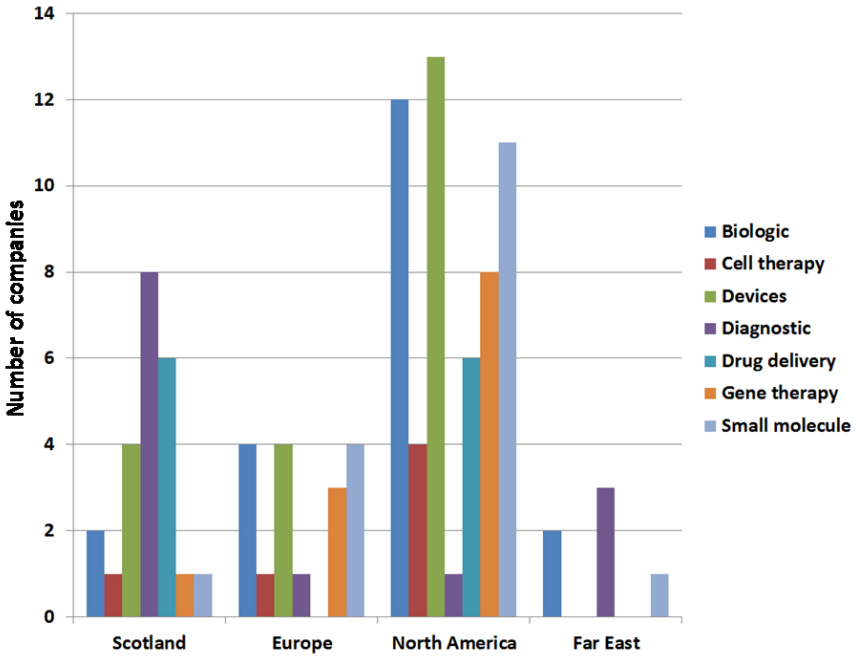

Figure 6-2 Number of companies classified by technology as well as global areas for ophthalmology market: This analysis does not include multinational companies, as these entities cannot be defined by a single technology and any one country. Note that the classification "Europe" excludes Scotland to avoid double counting

In addition to global sales and market, ophthalmology has garnered quite startling investments in terms of research funding in comparison to other disease areas indicating the urgent need for advanced therapeutic approaches for the treatment of chronic ocular diseases[266] (Figure 6-3).

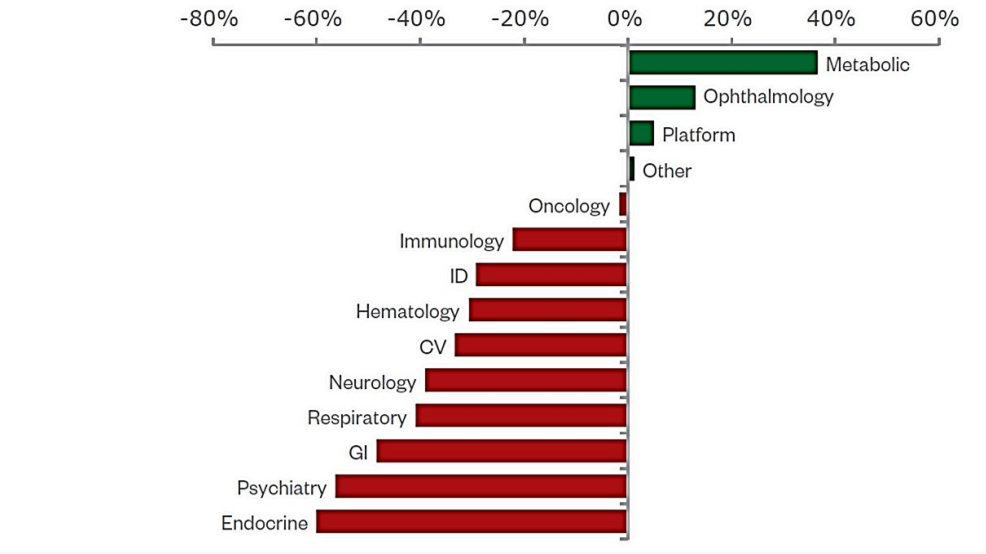

Figure 6-3 Novel drug R&D venture funding by disease area, 2004-2008 vs 2009-2013

While over 900 new biopharmaceutical entities are in pipeline, targeting diseases across a wide range of therapeutic areas, the emergence of biosimilars is anticipated to represent the biggest shift in biologic approval landscape[267]. The U.S. patents for blockbuster Lucentis® will be expiring in 2019 and several biosimilar manufacturers are already targeting that molecule[268]. The current ophthalmic drug delivery technologies are tailored to non-targeted small molecules/drugs.

Biopharmaceuticals including proteins and peptides have shown great promise as novel therapeutics in the treatment of ocular diseases. These large molecules offer several advantages

compared to small molecule drugs with respect to high potency, activity, low unspecific binding, less toxicity, minimization of drug-drug interaction, biological and chemical diversity [269-270]. However, these macromolecules also face various challenges such as physical and chemical degradation, short in vivo half-lives, circulation, and distribution. Additionally, macromolecules lack efficient and specific delivery to the target sites. Besides these, clearance by the mononuclear phagocytes (MPS) of the reticuloendothelial system (RES), risk of immunogenic effect, high molecular weight (MW), structural complexity, and failure to permeate cell membranes further reduce their therapeutic efficacy [271]. For these reasons, there is a need to develop novel ophthalmic biopharmaceutical drugs and delivery systems, ideally targeting these macromolecules to biologically relevant ocular tissues.

In this chapter, an introduction on proliferative diabetic retinopathy (PDR), role and mechanism of action of octreotide in PDR, challenges associated with large molecules and designing ocular formulation, routes of delivery and a multi-layered nanomicelle approach will be discussed.

6.2. Proliferative diabetic retinopathy (PDR)

Diabetes mellitus is an epidemic with global prevalence that is dramatically inflating and is predicted to reach 592 million by 2035 [272]. Diabetic retinopathy (DR) is the most common microvascular manifestation of diabetes significantly affecting visual acuity on a global scale and is the leading cause of blindness in American adults[273]. DR can be broadly categorized into the earlier stage of nonproliferative diabetic retinopathy (NPDR) and the advanced stage of PDR and/or diabetic macular oedema (DMO) [274]. In PDR/DMO, progressive nonperfusion of the retinal vascular bed occurs resulting in regions of ischemia and impaired oxygenation of the metabolically demanding retinal neurons. The resultant ischemic retina is

driven by hypoxia and expression of pro-angiogenic growth factors that further stimulate aberrant new blood vessels formation in the retina protruding into the preretinal space (Figure 6-4). Such retinal neovascularization leads to vitreous hemorrhage or retinal detachment leading to severe vision loss [1].

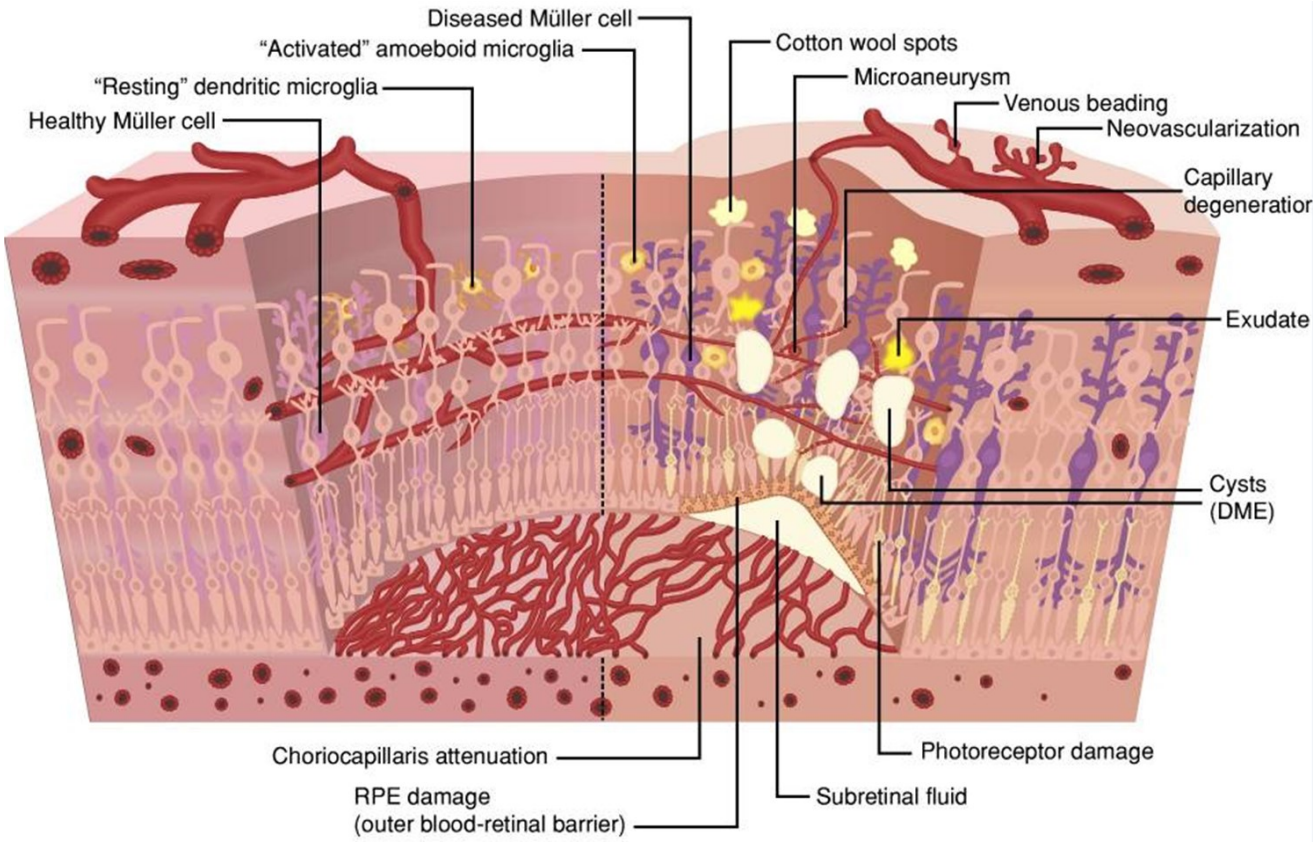

Figure 6-4 An illustrated schematic of normal retina compared with early proliferative diabetic retinopathy (PDR). Reprinted with permission from Duh et al. [1]

6.3. Role of octreotide in PDR

PDR has multifaceted pathogenesis. Thus, pharmacological therapies targeting multiple PDR mechanisms may provide more effective treatment strategies. Currently available therapies include anti-VEGF medication, laser photocoagulation and vitrectomy [275]. With the early identification of role of pituitary gland in PDR, somatostatin, a naturally

occurring pituitary growth hormone (GH) secretion inhibitor was realized to play a potential role in mitigating retinal neovascularization [3]. GH secretion from anterior pituitary results in the synthesis of insulin-like growth factor-1 (IGF-1) that acts as a mediator of GH's mitogenic actions and results in acute retinopathy progression. Octreotide, a somatostatin analog (Figure 6-5) inhibits GH, glucagon and insulin secretion more actively than native somatostatin [276]. Octreotide also acts via G-protein coupled receptors, exerting its direct antiproliferative effect by cell cycle arrest via somatostatin receptor-2 (SSTR2), apoptosis via SSTR3 stimulation and SSTR1-mediated effects on angiogenesis [277-279]. However, poor bioavailability in ocular tissues due to short half-life (2 hours) and large molecular weight (1,019.24 g/mol) has limited its therapeutic success.

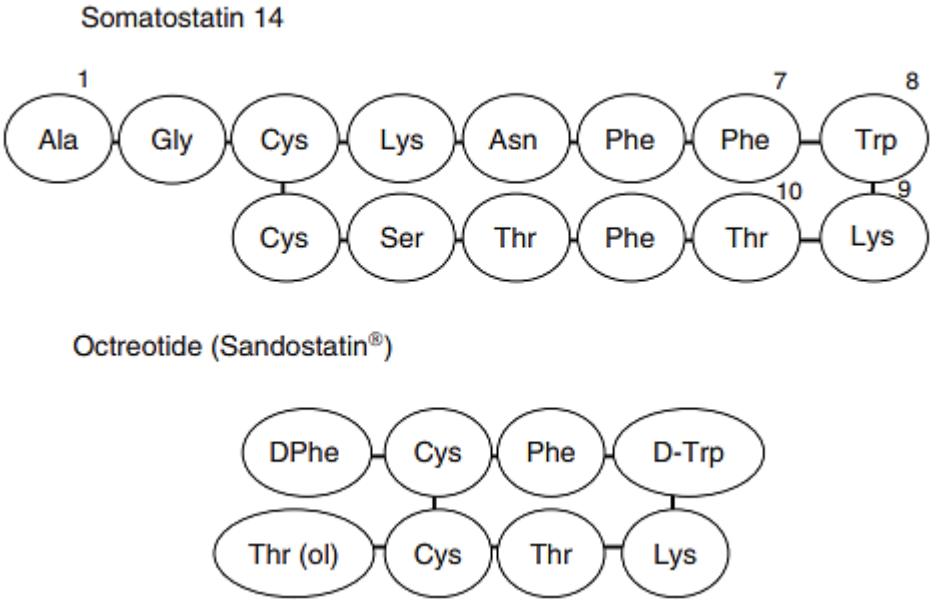

Figure 6-5 Amino acid compositions for both native somatostatin 14 and the synthetic octapeptide analog octreotide. Reprinted with permission from Grant et al. [3]

6.4. Ocular diseases: current biologics based treatments

Millions of people worldwide suffer from a wide variety of ocular diseases. A majority of these pathologies lead to irreversible blindness thereby substantially reducing quality of life. The number of visually impaired people has escalated to 285 million worldwide currently. In the United states alone, one million people were legally blind (visual acuity of 20/200 vision or worse) while 3.2 million suffered from visual impairment and another 8.2 million had vision problems due to uncorrected refractive error in 2015. The number of these conditions are projected to double by 2050[280].

The last few decades have witnessed a considerable growth in the understanding of the pathogenesis and genetics of ocular diseases. Deciphering various compliment pathways, gene associations and pharmacological interventions for retinal diseases have led to substantial development of effective therapies[281]. The major ocular diseases that have significantly impacted vision worldwide include age-related macular degeneration (AMD), cataracts, diabetic retinopathy (DR), dry eye conditions and glaucoma. The treatment market for glaucoma had the largest market share in 2013 with product sales (both branded and generic) exceeding US$ 4.5 billion (£ 2.9 billion) in the United States, Europe and Japan combined. Age related diseases including cataracts, AMD and diabetic retinopathy are expected to become more common with aging populations in developed countries[265]. Table 6-1 lists FDA approved biopharmaceuticals for ocular indications.

Table 6-1 List of FDA approved biopharmaceutical drugs for ocular delivery

Drug	MW (kDa)	Route of administration	Half-life	FDA approval	Indication
Adalimumab (Humira®)	148	Subcutaneous	~2 weeks (human)	July 2016	Uveitis
Aflibercept (Eylea®)	115	Intravitreal	3.63 days (rabbit); 7.1 days (human)	November 2011	Wet AMD
Ranibizumab (Lucentis®)	48	Intravitreal	2.88 days (rabbit); ~9 days (human)	June 2006, August 2012	Wet AMD, DME
Pegatanib sodium (Macugen®)	50	Intravitreal	~10 days (human)	December 2004	Wet AMD
Bevacizumab (Avastin®)	150	Intravitreal	4.32 days (rabbit); 4.9 days (human)	Off-label	Wet AMD

Table 6-2 Proteins and peptides currently in clinical trials for various ocular complications

Protein/peptide drug	Description	MW (kDa)	Target/activity	Half-life	Company	Current indication	Phase	Ref.
AGN-150998 (Abiciparpegol)	Recombinant ankyrin repeat protein	34	VEGF-A	~2 weeks	Allergan	Wet AMD	Phase III	NCT02462486; NCT02462928
ALG-1001 (Luminate®)	Integrin peptide	1	Integrin receptors	~3 months	Allegro Ophthalmics	DME, NPDR	Phase II	NCT02348918
Conbercept (Lumitin®)	Recombinant fusion protein	143	VEGF-A/B, PGF-1	~1 week	Chengdu-Kanghong	Wet AMD, DME	Chinese FDA Phase III/ Phase II	NCT01809236
GSK933776	Anti-amyloid β antibody	NA	Amyloid β fibrils	~12 days	GlaxoSmithKline	Dry AMD	Phase II	NCT01342926
iSONEP™ (Sphingomab™)	Humanized antibody	~49	S1P	More than 4 days	Lpath	Wet AMD	Phase II	NCT01414153
Lampalizumab	Antigen-binding fragment of a	47	CFD	~6 days	Roche	Geographic atrophy	Phase III	NCT02247479

Protein/peptide drug	Description	MW (kDa)	Target/activity	Half-life	Company	Current indication	Phase	Ref.
	humanized monoclonal antibody					secondary to AMD		
RN6G (PF-4382923)	Anti-amyloid β antibody	NA	Amyloid β fibrils	NA	Pfizer	Dry AMD	Phase II	NCT01003691
RTH258 ESBA1008	Antibody fragment	26	VEGF-A	~5 days	Novartis AG	Wet AMD	Phase III	NCT02507388
VGX-300 (OPT-302)	Recombinant fusion protein	NA	VEGF-C/D	NA	Circadian Opthea	Wet AMD	Phase I	NCT02543229
HI-con1	Recombinant fusion protein	NA	Tissue factor	NA	Iconic Therapeutics	AMD	Phase II	NCT02358889
Zimura	Aptamer	~50	Complement factor C5		Ophthotec Corporation	AMD, IPCV	Phase II/III	NCT02686658 NCT02397954

NPDR, nonproliferative diabetic retinopathy; S1P, sphingosine 1-phosphate; IPCV, Idiopathic polypoidal choroidal vasculopathy

6.5. Proteins and peptides: challenges in ocular delivery

Proteins and peptides, as a class of biopharmaceuticals, pose significant challenges owing to their large size, poor permeation and susceptibility to degradation. Understanding the intrinsic properties associated with the complex macromolecular nature of proteins and peptides is often required for achieving high biological activity. However, such structural complexity also renders them as one of the most challenging classes of therapeutics to be formulated and delivered. Short half-lives of peptides and low stability especially of protein drugs at physiological pH and temperature or during storage, leads to loss of activity, thus putting significant burden on formulation technologies (Table 6-2).

6.5.1. Adverse physicochemical properties of proteins and peptides

6.5.1.1. Hydrophilicity

Most of the therapeutic proteins and peptides are highly hydrophilic (log P<0) which hinders their permeability across biological membranes. Bioavailability of proteins and peptides depends on their ability to cross these membranes. Poor membrane permeation of macromolecules often embodies added challenge in development of protein- and peptide-based drug formulations to intracellular target sites. The lipophilic nature of biological membranes restricts these macromolecules from spontaneously entering cells. The absorption of these macromolecules is not governed by simple diffusion or passive absorption. Rather active transport which involves binding to specific receptor, pinocytocis or endocytosis are the major mechanisms responsible for absorption [282-283]. Permeation of hydrophilic molecules is hindered by the tight junctions present in the cornea and the lipophilic nature of the corneal epithelium [284-285] whereas hydrophobic molecules permeate corneal epithelium easily. Additionally, the

collagen fibers present in the hydrophilic stroma may impede penetration of hydrophobic drugs to some extent. Under certain circumstances, small peptides or even small particles are taken from the extracellular space into cells by an active transport mechanism known as receptor-mediated endocytosis [60]. One of the major disadvantages of proteins and peptides entering into the cell via endocytic pathway is their entrapment into the endosomes and eventually in lysosomes, where majority of the degradation processes undergoes by the action of lysosomal enzymes[286]. This leads to only a small fraction of unaffected proteins/peptides appearing in the cytoplasm. So far, multiple and partially successful attempts have been made to deliver protein and peptide based biopharmaceuticals directly into the cell cytoplasm bypassing the endocytic pathway. Mechanical delivery methods like microinjection and electroporation have been used for decades for cell cytoplasm delivery, but are low-throughput and invasive and require specialized equipment to physically puncture membranes[287]. The delivery of biologics via most favored "oral route" is highly challenging due to GI mucosa and degradative acidic environment. A large fraction of approved and investigational protein and peptide molecules are administered via parenteral routes (IV, IM or SC), intravitreal and sub conjunctival injections[288]. However, non-targeted delivery of protein- and peptide-based formulations may lead to distribution into normal tissues requiring large quantities of drug administration, which is often not economical and sometimes complicated owing to non-specific toxicity[289].

6.5.1.2. Large molecular weight

Another major challenge for the delivery of protein and peptide based drugs is their high molecular weight and poor membrane permeability across ocular tissues and barriers. Such challenges have promoted highly invasive intravitreal injection as the primary mode administration for protein and peptide based drugs. The molecular weights of peptides and

proteins are generally > 1000 Da with large hydrogen bonding donor/ acceptor groups [290]. Such large size of macromolecules limits diffusion and renders patient compliant topical treatment highly inefficient (Table 6-3). The cornea, sclera and retina have tight junctions that significantly limits diffusion of hydrophilic large molecules [291-292]. The tight junctional space of conjunctival epithelium is generally wider than cornea, but still insufficient for the penetration of these large molecules [130, 293]. The human retina limits the diffusion of molecules greater than 76 kDa due to the inner and outer plexform layers. Macromolecules greater than 150 kDa fail to reach the inner retina [291]. Additionally, choriocapillaries may wash out the molecules that traverse through choroid thus reducing therapeutic concentrations. The ocular anatomy and tissue barriers are shown in Figure 6-6.

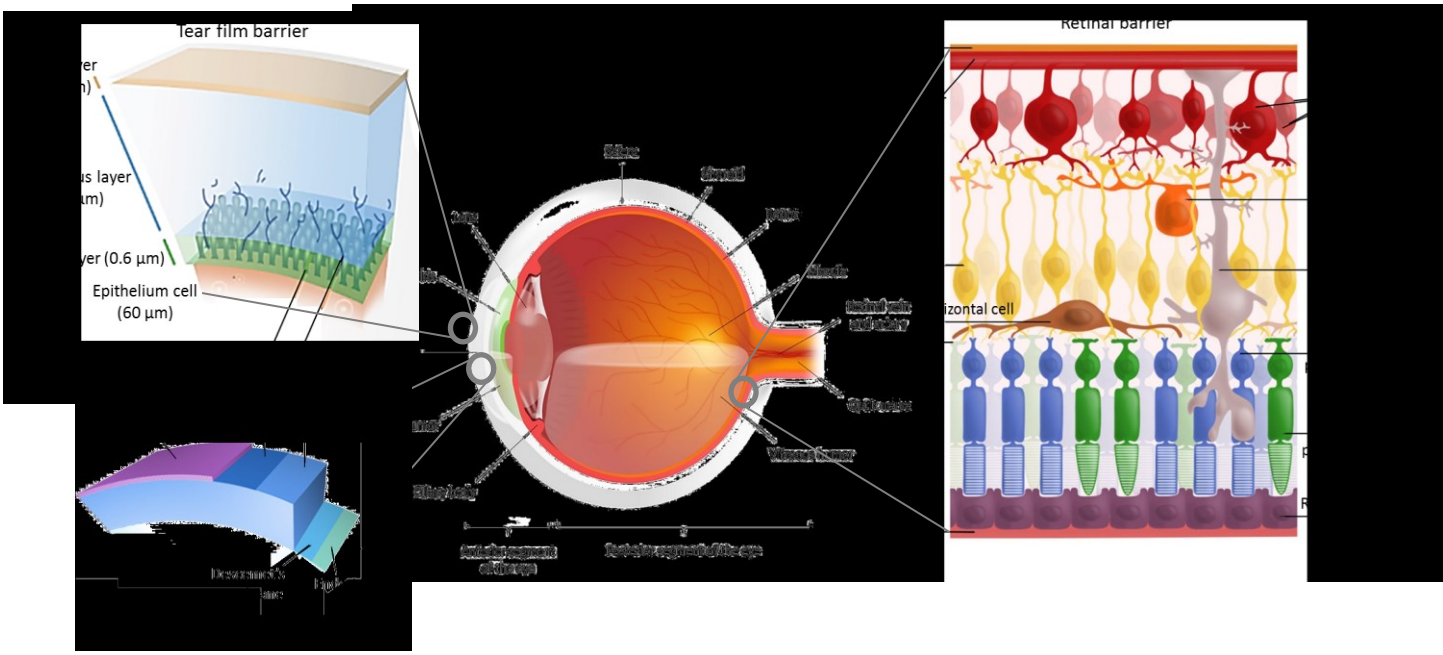

Figure 6-6 Ocular anatomy and tissue barriers

Table 6-3 Permeability of proteins, peptides and macromolecules across ocular barriers [294]

Compound	MW[a] (Da)	Tissue	Animal[b]	Permeability
Serum albumin	66000	cornea	H	5.48E-07
Inulin	5000	cornea	R	5.50E-07
Cyclosporine	1201	cornea	R	1.10E-05
Deoxycorticosterone	330	cornea	R	4.00E-05
Progesterone	314	cornea	R	2.00E-05
Testosterone	288	cornea	R	4.20E-05
Immunoglobulin	140000	stroma	R*	8.00E-09
Hemoglobin	64500	stroma	O	5.70E-07
Serum albumin	65000	stroma	R	1.40E-07
Dextran	75000	endothelium	R	7.50E-07
Serum albumin	65000	endothelium	R	8.30E-09
Poly(vinylpyrrolidone)	45000	endothelium	R	3.80E-07
Dextran	16000	endothelium	R	2.70E-05
Inulin	5000	endothelium	R	1.40E-06
Bevacizumab	145000	sclera	H	5.30E-07
Dextran-70	70000	sclera	H	1.90E-06
Serum albumin	65000	sclera	C	1.30E-07
Hemoglobin	64500	sclera	C	3.60E-07
Dextran-40	40000	sclera	H	4.30E-06
Dextran-10	10000	sclera	H	6.20E-06
Inulin	5000	sclera	C	1.90E-06
Inulin	5000	sclera	H	9.00E-06
Inulin	5000	sclera	R	2.50E-06
Hydrocortisone	362	sclera	C	6.50E-06

Compound	MW[a] (Da)	Tissue	Animal[b]	Permeability
Inulin	5000	conjunctiva	R*	3.80E-06
FITC-dextran	77000	RPE-choroid	C	2.70E-08

a (MW) Molecular weight

b Source of tissue (R) rabbit, (C) cow, (O) ox, (H) human

All permeability measurements were obtained from in vitro experiments except those followed by an asterix (*), which were obtained from in vivo.

6.5.1.3. Metabolic instability

Proteins and peptides also suffer from a number of physical, chemical and biological instability issues due to their complex secondary, tertiary and quaternary structures. Various physical degradation pathways are involved in the instability of proteins and peptides including denaturation, adsorption, aggregation and precipitation. Moreover, conformational transformation of proteins to inactive forms occur due to pH, temperature, high salt concentration; dissociation of subunit proteins; complexation of enzymes and cofactors; non-covalent complexation with ions, proteolytic degradation under the influence of esterases and proteases. Chemical modifications by different compounds (for instance oxidation of SH-groups in sulfhydryl containing enzymes and Fe (II) atoms in heme containing proteins; thiol-disulfide exchange and destruction of labile side-chains of tryptophan and methionine) may also lead to inactivation of various biologically active protein- and peptide-based drugs in ocular tissues [270].

In the body, the chemical degradation pathways of peptides and proteins include deamidation, oxidation and reduction, proteolysis, disulfide exchange and β-elimination [295]. Any alteration in “active” confirmation may lead to loss of activity and irreversible aggregation

of proteins. Vulnerability towards enzymatic degradation under in vivo condition results into shorter half-lives even with parenteral administration. Inside the vitreous humor the half-life of large molecule tends to be in the range of days to weeks [125]. For instance, the average apparent plasma half-life of pegaptanib is 10 days after 3 mg dose whereas ranibizumab remains for 2.88 days in rabbit[296]. Half-life of bevacizumab is 4.32 days with maximum concentration 162 μg/ml in vitreous cavity [297]. In AMD, the vitreous elimination of ranizumab is just 9 days and intrinsic systemic elimination half-life is 2 hours followed by multiple intravitreal injection dose of 0.3-2.0 mg/eye biweekly or monthly [298]. Such short half-lives of proteins requires frequent parenteral administrations to maintain therapeutic levels. Frequent parenteral administrations reduce patient compliance and/or are not well tolerated and often associated with complications including cataract, retinal hemorrhage and detachment [299].

6.5.2. Challenges in designing protein and peptide based ocular formulations

The formulation of protein- and peptide-based bio therapeutics poses unique challenges that are not often experienced with small molecules. Overcoming the instability of protein- and peptide-based agents due to structural properties and environmental factors is one of the key challenges in the development of formulations. Several agents have been incorporated including small sugars (e.g. trehalose) and polysaccharides (e.g. dextrans) to enhance the stability of protein and peptide based biopharmaceuticals [300-301]. Pluronics and non-ionic surfactants such as polysorbates at low concentrations are widely applied to decrease protein and peptide aggregation [302].

Another major drawback of biopharmaceutical drug formulations is high and variable viscosity. For topical ophthalmic formulations, corneal contact time is longer with increased viscosity of formulations up to 20 centipoise (cP) [303]. However, a further increase in viscosity

leads to reflex tearing and blinking in order to regain the original viscosity of the lacrimal fluid (1.05–5.97 cP). With a rise in clinical application of monoclonal antibodies, the need for high protein doses (concentrated formulations) is often crucial. The FDA does not permit the intravitreal injection of large volumes of drug formulations in patients with ocular diseases[239]. Such requirements render formulation of protein- and peptide-based biopharmaceuticals very difficult as solutions with high protein content are exceedingly viscous. High viscosity of protein and peptide based biopharmaceuticals also greatly affects the syringeability (time required to complete the injection) as well as the force required to deliver the solution with appropriate needles (18 mm in length, 27-30G) [269]. Thus, approaches to achieve lower viscosity formulations with hydrophobic/inorganic salts or lysine and arginine may be useful.

It is also important for protein- and peptide-based biopharmaceutical formulations to have the same pH as the lacrimal fluid to achieve maximum activity. However, proteins and peptides are often not stable at physiological pH leading to their folding and aggregation. Additionally, the buffer capacity of such formulations is of equal importance for proper preservation. Although, the buffering action of the tears is capable of neutralizing the effect of topically applied biopharmaceutical formulations[304], intraocular hyperosmotic solutions have been reported to elicit transient desiccation of the anterior chamber tissues while hypotonic solutions may cause edema leading to corneal clouding[305]. For this reason, pH of such formulations are compromised and maintained by buffers to achieve maximum activity and maintain stability[306]. The effect of buffers on tonicity should also be taken into account considering the permissible limits of osmolarity for ophthalmic formulations (171-1711 mOsm/kg). Although many of these agents utilized for maintaining the stability and activity of such protein- and peptide-based biopharmaceutical formulations have been proven to be

effective, their use requires careful consideration in terms of local toxicity and potential immunogenicity.

A better understanding of the viscosities of biological solutions, characteristics of nascent proteins and peptides, dynamics and behavior of protein- and peptide-based topical and injectable formulations is crucial. Towards this goal, utilization of chemical chaperones to inhibit protein misfolding as well as reactivate non-native protein structures,[307-308] and/or co-administration of recombinant human hyaluronidase with drug to degrade hyaluronic acid (a key structural component of tissues) to facilitate protein and peptide delivery may prove to be useful in addressing formulation challenges[309].

6.6. Routes of protein and peptide delivery to ocular tissues

Challenges to ocular delivery of biopharmaceuticals are noteworthy, and considerable opportunities remain to be optimized for delivery approaches, formulation and processing conditions for each peptide- and protein-based therapeutics.

6.6.1. Systemic delivery

Oral administration and parenteral injections are the most common methods of systemic delivery. However, attempts to deliver large hydrophilic protein and peptide based biopharmaceuticals for ocular indications have seen limited success[310]. The small size of the eye and presence of ocular barriers prevent drug partitioning into the eye even for small molecules. Furthermore, dilution effect of the systemic blood volume, first-pass metabolism by the liver and clearance by kidney require larger drug doses which can result in high costs, systemic side-effects and possible toxicity[311].

The integrity of ocular barriers seems to play a major role in the penetration of biopharmaceuticals. A clinical study showed an increase in visual acuity by 14 letters after treatment with 3 doses of systemic bevacizumab (5mg/kg) in patients with classic choroidal neovascularization (CNV) probably facilitated by the compromised RPE layer [312]. Rohrer and co-authors also reported reduced CNV size and preserved retinal function after intravenous administration of fusion protein CR2-fH (where CR2 is complement receptor 2 and fH is factor H) indicating CR2-fH accesses the site of CNV by way of the impaired BRB. CR2-fH plays a critical role in regulating the inflammatory responses by inhibiting complement activation products in AMD [313-314]. Although, no serious ocular or systemic side-effects were observed in both the cases, high concentration of injected drug or fusion proteins should be taken into consideration. Such shortcomings preclude systemic administration of protein- and peptide-based biopharmaceuticals for ocular delivery expensive and rare.

6.6.2. Extraocular delivery

6.6.2.1. Topical delivery

Topical instillation of ophthalmic drops has been the method of choice for administering pharmaceutical agents for the treatment of ocular diseases particularly that manifest on the ocular surface and/or the anterior segment[239]. This route has been extensively utilized clinically for the treatment of diseases affecting cornea, conjunctiva, sclera, iris, ciliary body and aqueous humor. However, the limited capacity of lacrimal fluid and constant tear drainage from precorneal area leads to wash out of a majority of eye drop within minutes[315]. Additionally, only a few experimental studies have demonstrated their efficacy for posterior segment diseases. The properties of corneal barriers allow significant passage of moderately lipophilic small molecules, whereas highly hydrophilic large molecular weight

biopharmaceuticals undergo restricted permeation generating insufficient concentrations for therapy. Nomoto and co-authors demonstrated the incompetence of topical bevacizumab to reach therapeutic concentrations in the iris, choroid, retina and vitreous of rabbits even after aggressive dosing of 1.25mg/0.05mL six times daily for a week [316]. In another study, topical administration of bevacizumab (10mg/kg, 3 times for 7 days) in mice did not generate any appreciable concentrations into the healthy corneal stroma [317]. In a recent study, Moisseiev and group also failed to generate detectable drug levels in both aqueous and vitreous samples of human eyes after topical administration of bevacizumab (25mg/mL, four drops with 10 min interval) [318]. In contrast, Hernandez and coworkers provided the first evidence that somatostatin (SST) reached the retina not through the cornea but by the trans-scleral route following topical administration. Such topical administration of SST prevented retinal neurodegeneration in streptozotocin induced diabetes mellitus (STZ-DM) rats and opened up new preventive pharmacological strategy targeted to early stages of DR. [319].

6.6.2.2. Periocular delivery

6.6.2.2.1. Subconjunctival delivery

An injection into the subconjunctival area i.e. space underneath the conjunctiva is widely used as a route for periocular delivery. The delivery of biopharmaceuticals into the subconjunctival space deep into the bulbar conjunctiva and superficial to the sclera may provide a way to directly deliver therapeutics transscleraly into intraocular tissues. Subconjunctival routes can be used for sustained delivery since a depot can be formed in the space that can expand and accommodate up to 500 µL volume [130]. However, drugs injected into the subconjunctival space are often rapidly cleared via conjunctival blood and lymphatic flow[247]. In addition, pore diameter and intracellular spaces of scleral fiber matrix regulate drug

permeation to a large extent. Longer in vivo half-life in the iris/ciliary body and retina/ choroid after subconjunctival injection of bevacizumab relative to intravitreal injection may possibly be attributed to binding with negatively charged scleral proteoglycans [316]. In another in vivo study, high bevacizumab concentration was detected in the whole cornea 24 h post subcutaneous injection which remained almost unchanged in all layers of stroma over the next 14 days [317]. Various drug delivery technologies including microparticles/nanoparticles may be combined with physical techniques such as ultrasound and iontophoresis to achieve therapeutic concentrations of protein and peptide based biopharmaceuticals following periocular administration [320-321].

6.6.2.2.2. Sub-tenon delivery

Sub-tenon route is widely utilized for administering anesthetics during ocular surgery. It involves the injection of drug into a fibrous membrane, called tenon's capsule which along with the sclera binds the sub-tenon space. Although upto 4 mL of drug formulation could be injected through this route, administration complications including pain, chemosis, subconjunctival hemorrhage, retrobulbar and/or orbital hemorrhage, optic nerve damage, retinal ischemia, orbital swelling and rectus muscle dysfunction limit its use for the delivery of protein- and peptide-based biopharmaceuticals [322-323]. In patients with clinically significant macular edema, sub-tenon's injection of bevacizumab (2.5 mg in 0.1 mm volume) resulted in significant short-term visual improvement in eyes [324]. Thus, sub-tenon's injection may serve as an alternative to intravitreal injection for ocular delivery of biopharmaceuticals.

6.6.3. Intraocular delivery

Intraocular delivery techniques involve direct delivery of therapeutic agents to the target site thus reducing the distance traversed by the drug generating higher local drug concentrations, reducing off-target effects, and bypassing various ocular barriers to improve ocular drug bioavailability.

6.6.3.1. Intrastromal delivery

Intrastromal administration entails direct drug delivery into the corneal stroma to overcome the corneal epithelial barrier along with tear fluid drainage. The densely packed collagen fibrils and proteoglycans hinder the diffusion of proteins and peptides inside the corneal stromal structure allows it to serve as a reservoir for large hydrophilic biopharmaceuticals. Hashemian and co-authors reported that intrastromal injection of bevacizumab (2.5 mg/1 mL) using a hypodermic needle led to regression of corneal stromal vascularization in a patient [325]. Recently, in vivo studies by Kim and group have demonstrated corneal vascular regression after intrastromal administration of bevacizumab (4.4 μg) with microneedles (MNs) [326]. These studies further confirm intrastromal delivery as an attractive modality for delivering biopharmaceuticals directly into the cornea.

6.6.3.2. Intracameral delivery

Intracameral delivery is intended to place the drug solution directly into the anterior segment of the eye. Although, intracameral injection has been extensively explored to improve delivery of biopharmaceuticals to both the anterior as well as posterior segments of the eye, it has not been possible to achieve therapeutic drug concentrations in the posterior segment of the eye following intracameral administration. However, intracameral administration of

antibiotic prophylaxis for cataract surgery to prevent endopthalmitis [327-328] and antifungal agents for deep corneal infections such as fungal keratitis [329] is widely used to deliver drugs to the anterior segment of the eye. Additionally, a combination of intrastromal and intracameral injections was recently shown to be effective in reducing fungal mass not only in the anterior segment but also in the corneal stroma where fungal invasion may lead to corneal perforation [330].

Several *in vitro* and *in vivo* studies have demonstrated the effectiveness of intracameral bevacizumab in treating neovascularization with no effects on corneal endothelial cells or thickness [331-333]. Patients with neovascular glaucoma and iris rubeosis have also responded well to the intracameral bevacizumab therapy and did not show any morphological changes of corneal endothelial cells [334-336]. Intracameral injection of bevacizumab-loaded polymeric delivery systems may sustain drug release into the anterior segment [337]. However, repeated injections to maintain therapeutic concentrations over prolonged time periods and sparse degradation of polymers may obstruct the aqueous flow, thereby elevating intraocular pressure and increasing risk of ocular infections.

6.6.3.3. Intravitreal delivery

To date, intravitreal injection remains the main modality for delivering biopharmaceuticals to the posterior segment of the eye. It is an invasive procedure that involves injection of a drug solution or suspension into the vitreous cavity in the center of the eye after penetrating through all layers of the ocular globe. The vitreous cavity can generally accommodate a volume of 20-100μL drug solution/suspension without adversely affecting the visual acuity[338]. However, various complications associated with the intravitreal injection

include edopthalmitis, retinal detachment, uveitis, iritis, intraocular hemorrhage, cataract and hypotony which may lead to permanent vision loss if untreated[339].

Currently, most of the biopharmaceuticals including pegatanib sodium, ranibizumab, bavcizumab and aflibercept for the treatment of neovascular AMD are given as intravitreal injections. A comparative pharmacokinetic analysis revealed concentration (Cmax) of bevacizumab in retina/choroid after an intravitreal injection (1.25 mg/0.05 mL) to be ~317-fold higher than a subconjunctival injection at 1 week in rabbits [316]. Intravitreal injection of Avastin® generated significant bevacizumab concentrations in the retina, the retinal pigment epithelium, the choroid and particularly the photoreceptor outer segments in cynomolgus monkeys [340]. Although, biopharmaceutical drugs tend to prevent immediate elimination from the vitreous unlike small molecules due to their large molecular weight, their vitreous half-lives of just few days to weeks may not be sufficient to achieve long term therapeutic effect. Therefore, novel delivery methods and/or long-term controlled release formulations for protein- and peptide-based biopharmaceuticals are warranted in order to significantly reduce complications caused by repeated injections.

6.6.3.4. Suprachoroidal delivery

It is often overlooked that the tissue site of action for most of the biopharmaceuticals is not the vitreous but the choroid and retina. Therefore, delivering drug directly in the target tissues (i.e., choroid and retina) may provide more effective therapy to chorioretinal diseases. Suprachoroidal injections, that involve the placement of a drug in the suprachoridal space (SCS), a potential space between the sclera and the choroid, holds potential in achieving higher drug levels in target tissues. SCS can expand to accommodate a drug suspension or solution up to 1 mL [341]. Previously, SCS was accessed surgically with a scleral incision and insertion

of a long cannula or hypodermic needle through the SCS, often leading to SCS collapse due to deformability of the chorioretina and the hydrostatic pressure in the eye. Recent advancements in suprachoroidal delivery using MNs, has enabled higher local drug concentrations in the choroid with fewer side effects and minimal obstruction of the visual axis. However, high blood flow in choriocapillaries render the half-lives of small molecules and biopharmaceuticals in SCS in the order of hours. In fact, sustained delivery systems (20 nm - 10 μm) are retained in the SCS for longer periods indicating the utility of SCS injections [342-343].

Several studies have demonstrated the effectiveness of suprachoroidal injections for localized delivery of therapeutics to the choroid-retina region [344]. Although, intravitreal injections of bevacizumab have been shown to be superior to microcannula suprachoroidal injections in sustaining bevacizumab release for one week [345], MNs have demonstrated potential in delivering bevacizumab (100 μl) to the SCS without any serious adverse effects as noted in Phase I clinical trials [346-347]. Figure 6-7 depicts current and emerging routes for protein and peptide delivery to ocular tissues.

Inflammation, is a common side effect of ocular diseases including neovascularization, significantly affects the integrity of corneal epithelium, choroid and the RPE layer. Such incompetent barrier function allows protein- and peptide-based biopharmaceuticals, that have limited access to the intact eye, to gain significant access through the compromised barriers of inflamed eyes. Several studies to date have shown the effectiveness of systemic, intravitreal and SCS delivery in compromised tissues and confines compelling implications for other biological approaches in the treatment of ocular diseases. Some characteristics of various routes of administration for ocular drug delivery are provided in Table 6-4. Additionally, a list

of controlled-release systems for protein and peptide therapeutics for ocular implications are depicted in Table 6-5.

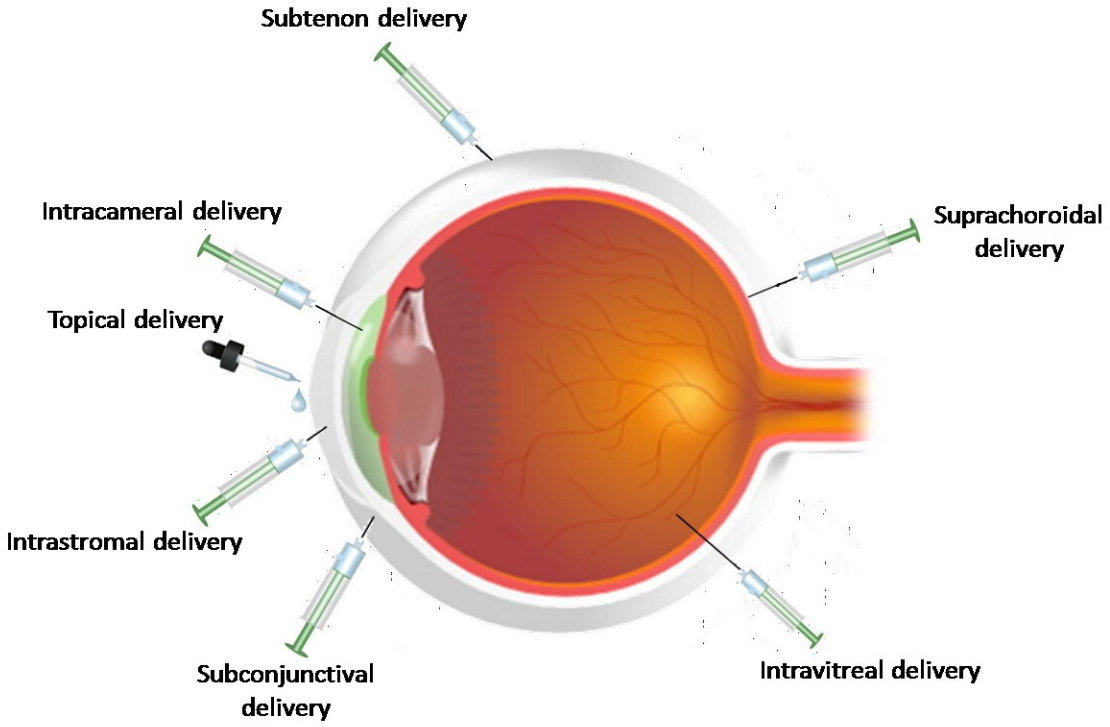

Figure 6-7 Current and emerging routes for protein and peptide delivery to ocular tissues

Table 6-4 Characteristics of various routes of administration for ocular drug delivery[294]

Routes	Notes
Topical	
Drug entry pathways	Corneal, conjunctival, and sclera pathways.
Delivery barriers	Membrane barriers and elimination pathways on the eye surface, cornea, BRB, and tight conjunctions.
Elimination pathway	Tear wash out; nasolacrimal drainage
Advantages	High patient compliance; less systemic side effects; relatively easy and safe to administer.
Limitations	Small retention time of drug or dosage forms; blurring of vision; irritation; precorneal drug losses; drainage through the nasolacrimal duct; low bioavailability; limited volume of administration (approx. 30 μL); fast clearance from ocular surface; metabolism by tear enzymes; nonproductive uptake into systemic circulation via highly vascularized conjunctiva, choroid, uveal tract and inner retina; aqueous humor outflow gradient.
Approaches for improvement in therapeutic efficacy	Bioadhesive formulations may reduce precorneal clearance and increase corneal surface contact time. Positive charge of formulations may enhance the contact time with cornea to interact with negatively charged mucosa. Nanowafers approach may be beneficial for long-term and sustained drug release.
Systemic	

Routes	Notes
Drug entry pathways	Choroid and conjunctiva
Delivery barriers	Choroid and BRB (selectively permeable to highly lipophilic molecules).
Elimination pathway	Hepatic clearance; conjunctival and choroid capillaries and phagocytic clearance.
Advantages	Better patient compliance relative to intraocular injection.
Disadvantages	Low bioavailability due to the BRB, hence higher doses required which may produce systemic side effects.
Approaches for improvement in therapeutic efficacy	Large molecules and/or hydrophilic drugs are able to penetrate the choroid from the systemic circulation, but are unable to cross the inner BRB into the retina. Therefore, drugs must exit the choroidal circulation and permeate the outer BRB.
Intravitreal	
Drug entry pathways	Directly to the vitreous chamber
Delivery barriers	Diffusion through the vitreous chamber, neural retina, and BRB.
Elimination pathway	Movement through aqueous chamber and retina; dynamic clearance mechanisms, such as anterior bulk aqueous flow or posterior vitreoretinal-choroidal flow, and elimination from the site of deposition.
Advantages	Local and direct delivery; high therapeutic concentration; no barrier to reach macula.
Disadvantages	It is necessary to administer the drug frequently to maintain adequate intraocular concentrations; frequent injections have been associated with adverse events especially retinal detachment, cataract, vitreous

Routes	Notes
	hemorrhage and endophthalmitis; linked to degeneration of PRs and cataracts and increase in IOP; only about 50–100 µl is administrable in human via intravitreal; high cost of administration of drugs (anti-VEGF).
Approaches for improvement in therapeutic efficacy	Extended drug release formulation for longer duration and/or drug modifications including specific properties such as size, charge, and lipophilicity; also need stimuli-responsive approach for drug release.
Periocular	
Drug entry pathways	Trans-scleral pathway to effectively deliver drugs next to the choroid.
Delivery barriers	Scleral thickness, choroidal blood circulation and BRBs.
Elimination pathway	Conjunctival and choroidal blood and lymphatic flow; losses from the periocular space, BRB, and choroidal circulation; drug binding to tissue proteins.
Advantages	Less invasive; high therapeutic drug levels; possible repetitive periocular administration under local anesthesia without direct interference with the vision. High volumes of drug solution can be administered in human and can bypass the BRB without intraocular penetration.
Disadvantages	Rapid drug clearance; systemic side effects; tissue hemorrhage; and low retinal bioavailability compared to intravitreal injections; the injected drug still has to traverse the sclera, which is less permeable to larger molecules. The drugs have to pass through several layers including the episclera, sclera, choroid, BM, and RPE-while overcoming choroid circulatory clearance; the delivery is not as effective as intraocular injections in targeting retinal tissue.

Routes	Notes
Approaches for improvement in therapeutic efficacy	Improvements to formulations that either increase residence time or promote diffusion from the middle coat may be effective in overcoming the barriers to periocular delivery; nano-size formulations may provide superior diffusion; charge of formulations determines the interaction or diffusion process.
Suprachoroidal (SC)	
Drug entry pathways	Flow across the sclera is quick along the inner surface of the eye and subsequently into the posterior chamber.
Delivery barriers	Choroid and basement membrane.
Elimination pathway	High blood flow in the chorio-capillaries can wash away therapeutic molecules deposited in the SC space.
Advantages	Preferred site for drug delivery to the posterior tissues such as choroid, RPE and macula, due to its non-interference with the optical pathways and improved diffusional access to the choroid; this allows larger volumes of drugs with minimally invasive procedure; SC space can accommodate up to 1 ml of fluid, which rapidly diffuses into the posterior segment; injections of 10–50 μL into the SC space have been demonstrated to be well tolerated with lower risks for ocular complications.
Disadvantages	Injection of a drug solution into the SC space can result in rapid drug diffusion to cover the entire SC surface which may potentially induce drug-related toxicities of the surrounding tissues; rapid clearance of macromolecules occurs following suprachoroidal administration; postoperative inflammation and choroidal hemorrhage remain a concern and needs to be overcome while injecting into the SC space.

Routes	Notes
Approaches for improvement in therapeutic efficacy	Diffusion kinetics from the SC space could be optimized using sustained release formulations such as nano and microparticles; drug delivery systems that can provide controlled and continuous drug release are likely to minimize side-effects; such controlled devices might help overcome rapid fluctuation of the dosed drugs from conventional injectable solutions into the SC space and hence reduce toxicity to the surrounding tissues; MNs appear to offer a viable option for delivery of drugs to the back of the eye, especially when delivered through the SC route; these needles help to deposit drug or carrier system into sclera or into the SCS which may facilitate diffusion of drug into deeper ocular tissues, choroid and neural retina.

Table 6-5 Controlled-release systems being investigated for protein and peptide therapeutics for ocular implications[294]

Formulation Approaches	Drug	Description	Release	Status
Particulate systems				
Biodegradable polymeric microspheres				
PLGA MPs	Bevacizumab	Fabricated by Double emulsion method; particle size, 2–10 μm	62% released within 91 days	Preclinical, in vitro
PLA NPs within PLGA MPs	Bevacizumab	Fabricated by supercritical infusion and pressure quench technology	67% released within 120 days (4 months)	Preclinical, in vivo, rat model
PLGA MPs	Bevacizumab	Fabricated by solid-in-oil-in-hydrophilic oil method; particle size, 2–7 μm	NA	Preclinical, in vivo, rabbit model
Silicon dioxide MPs	Bevacizumab	Synthesized by electrochemical etching and oxidation of silicon wafer in hydrofluoric acid followed by ultrasonic fracture; particles with a pore size of 100 nm	165 days (5 months)	Preclinical, in vitro
Biodegradable polymeric nanospheres				
PLGA – albumin NPs	Bevacizumab	Fabricated by w/o/w double emulsion in presence of albumin as a stabilizer; particle size ~ 197 nm	165 days (5 months)	Preclinical, in vivo, rabbit model
Liposome	Bevacizumab	EPC-Chol and DPC-chol liposomes formed by dehydration and rehydration method followed by freeze drying	NA	Preclinical, in vivo, rabbit model
Liposome – annexin	Bevacizumab	PC-PS-Chol-Toc liposomes fabricated by dehydration and rehydration method and subsequently coated with annexin; particle size, 100 nm	NA	Preclinical, in vivo, rabbit mode
Biodegradable and non-biodegradable polymeric implants				
ENV705 (intravitreal) Envisia therapeutics	Bevacizumab	Drug dispersed into biodegradable hydrogel-based matrix made by PRINT technology and molded into implants	2 months	Preclinical animal test
Nano-pores film device (intravitreal) Zordera Inc.	Ranibizumab	Biodegradable DDS based on PCL; drug pellet sandwiched between a nanopore and impermeable layer (total thickness 40 mm)	3 months	Under investigation
Posterior micropump system (subconjuctival)	Ranibizumab	Nonbiodegradable refillable DDS drug loaded with preprogrammed micropump; drug delivered in controlled nanodroplets	Long-term (refillable)	Phase I

Formulation Approaches	Drug	Description	Release	Status
Port delivery system (PDS) (subconjuctival) Genentech	Ranibizumab	Semipermeable nonbiodegradable membrane with a refillable port; several exit ports to release drug into vitreous humor	Long-term – 1 year (refillable)	Phase II
Verisome IB20089 (intravitreal) Icon bioscience	Triamcinolone/ ranibizumab	Biodegradable with liquid gel or solid core; liquid injectable formulation; coalesces after intravitreal injections to form spherules	1 year	Phase II
In-situ gelling formulations				
Hyaluronic acid-dextran	Bevacizumab	Catalyst-free chemical crosslinking between vinylsulfone functionalized HA/thiolated dextranin under physiological conditions; transparent gel formed in vitreous after injection; better sustained release observed in vivo compared with in vitro release	6 months	Preclinical, in vivo, rabbit model
Alginate-chitosan hydrogel/PLGA microspheres	Bevacizumab/ ranibizumab	Antibody-loaded PLGA microspheres encapsulated into alginate hydrogels	196 days (6.5 weeks)	Preclinical, in vitro
Silk-based hydrogels	Bevacizumab	On the basis of physically crosslinked silk fibroin heavy chain (Mw = 350 kDa); biocompatible crosslinking reaction	Up to 3 months	Preclinical, in vitro
Diels–alder hydrogels	Bevacizumab	On the basis of PEG macro-monomers, chemically crosslinked by Diels–Alder reaction; mechanical stability enhanced	Up to 6 weeks	Preclinical, in vitro
Poly(2-ethyl-2-oxazoline)-b-poly(caprolactone)-b-poly(2-ethyl-2-oxazoline)	Bevacizumab	Reversible sol–gel transition; good in vitro and in vivo biocompatibility	20 days	Preclinical, in vitro
Poly(n-isopropylacrylamide) pnipaam and poly(ethylene glycol diacrylate) peg-da	Bevacizumab/ ranibizumab	Enhanced mechanical properties; good biocompatibility; thermoresponsive hydrogel; PNIPAAm shows LCST behavior	3 weeks	Preclinical, in vivo, rat model
PEG-poly-(serinolhexamethylene urethane)	Bevacizumab	Sol-to-gel phase transition when kept at in vivo temperatures; good in vitro and in vivo biocompatibility	17 weeks	Preclinical, in vivo, rabbit model
Delivery using living cells				
Renexus NT-501 (surgical) Neurotech Inc.	Cell line secreting CNTF	Nonbiodegradable; cell encapsulated in a semipermeable polysulfone capsule; Phase 2 results not encouraging because of adverse effects	18 months	Phase II/III
NT-503 (surgical) Neurotech Inc.	Cell line secreting VEGFR-Fc	Nonbiodegradable implant; semipermeable hollow fiber membrane encapsulating cells	12 months	Phase I

CNTF, ciliary neurotrophic factor; DDS, drug delivery systems; DPC-chol, 1,2 dipalmitoyl-sn-glycero-3-phosphocholine; EPC-chol, egg phosphatidylcholine-cholesterol; MPs, microparticles; NPs, nanoparticles; PLGA, polylactic-co-glycolic acid; PC-PS-Toc, egg phosphatidylcholine-porcine brain phosphatidylserine-tocopherol; PCL, polycaprolactone; PEG, polyethylene glycol; PLA, polylactic acid.

6.7. A multi-layered nanomicellar approach

Despite the major hurdles in ocular delivery of proteins and peptides, technological breakthroughs in formulation, delivery approaches and manufacturing methods have facilitated the growth and improvement in the biopharmaceutical market. Some of the work with the delivery of biopharmaceutical drugs have shown encouraging results. However, many needs remain unmet for the delivery of relatively smaller biologics, and greater challenges keep arising for developing formulations for larger biopharmaceutical drugs. Current biopharmaceuticals suffer from poor intracellular delivery leading to low ocular bioavailability, reduced stability (including storage, handling and administration), incompetent formulation development strategies and scalability and high manufacturing costs. Developing new biomaterials for effective protection of proteins and peptides and improving intracellular delivery will significantly improve biopharmaceutical delivery. Earlier Nomoto et al. has reported three-layered polyplex micelles for light-induced gene delivery for solid tumors [348]. Similarly, Abebe et al. has reported triblock copolymers based three-layered biodegradable micelles as efficient gene delivery system [349].

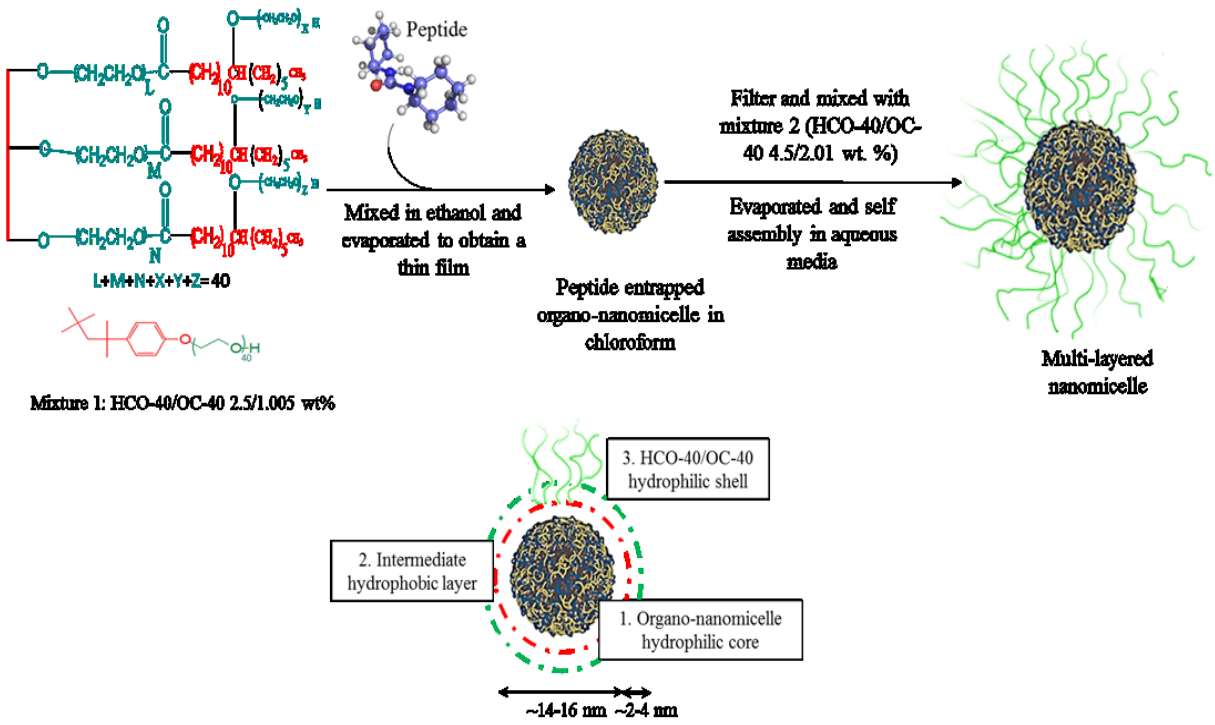

Figure 6-8 A schematic illustration showing the preparation of multi-layered nanomicelles by a modified multi-step solvent evaporation/rehydration method

In this approach, we have developed self-assembling multi-layered nanomicelles composed of two polymers, HCO-40 and OC-40 designed to combine hydrophilic interactions and solvent-induced encapsulation of peptides and proteins. HCO-40 and OC-40 polymers are employed to encapsulate various biologics including octreotide in the core of the organo-nanomicelle with chloroform as a dispersant. The individual organo-nanomicelle is further encapsulated with another layer of the same polymers allowing formation of an aqueous stable amphiphilic nanomicellar solution (Figure 6-8). The multi-layered nanomicelles are hypothesized to permeate through the conjunctival/scleral route similar to nanomicelles. The aqueous nanomicellar formulation with size ranging from ~16-20 nm could be administered topically to generate improved octreotide concentrations in the back of the eye over a period for the treatment of PDR.

CHAPTER 7

7. MULTI-LAYERED NANOMICELLES AS SELF-ASSEMBLED NANOCARRIER SYSTEMS FOR OCULAR PEPTIDE DELIVERY

7.1. Rationale

Peptide engineering, recombinant advancements and hybrid technologies combining solid and liquid syntheses have generated new classes of biologic-based therapeutics with bioactivities significantly higher compared to small molecules [350-351]. A particular success is in the area, where peptides have been engineered to bind to extracellular targets with superior specificity and affinity. At the same time, peptides are relatively safe and well tolerated and thus have shown incredible promise for a variety of indications including ocular and autoimmune diseases, inflammation and cancer [352]. Furthermore, peptide therapeutics are associated with lower production complexity and thus reduced production costs in comparison to other biopharmaceuticals. Despite the successes of peptides, they have several intrinsic weaknesses including poor chemical and physical stability and short circulating plasma half-lives [353]. Peptide engineering is a powerful tool that has facilitated growth of peptide-based therapeutics in clinical trials. However, it requires manipulation of peptide conformations or sequences for therapeutic applications [354]. Arguably, the primary reason there are only a few peptide-based therapeutics in the market, is the unmet challenge in delivering sufficient amounts of functional peptides in their native forms. Successful design and implementation of a functional ocular delivery system that is generally applicable to therapeutic peptides would have significant impact on human health. Such a nanocarrier system may open up a new

paradigm for a host of new peptide-based therapies for the treatment of a wide variety of diseases.

Approaches in the peptide-based biotherapeutics delivery include polymer modifications, encapsulation of divalent cations and chemical modification of peptides at reactive amines to minimize acylation using maleic anhydride and PEG[355]. Alternatives to PEG, the negative charge of sialic acid as well as the glycosaminoglycan hyaluronic acid and hydroxyl ethyl starch also hold potential in prolonging half-lives of peptides[269]. The low pH resulting from degraded products of PLGA polymers was shown to catalyze acylation at the lysine residue of peptides [356]. For instance, more than 60% of octreotide, an octapeptide is released in acylated form over 3 months from Sandostatin LAR® depot. Similar challenges have been reported for other peptides and biologic drugs including bovine serum albumin, human atrial natriuretic peptide, human parathyroid hormone, leuprolide, insulin and salmon calcitonin[357]. Conjugation of maleic anhydride to octreotide has demonstrated to inhibit acylation to less than 10% from PLGA films[358]. Polymer poly(D,L-lactide-cohydroxymethyl glycolide) has been modified to minimize nucleophilic attack of octreotide amine on glycolide and thus reducing acylation up to 30% during in vitro release. Utilization of hydrophobic ion-pairing (HIP) complexation by our laboratory in the past was demonstrated to maintain native chemical structure of octreotide to more than 95% during release from PLGA microparticles-in-gel composite formulation [357]. However, generation of lactic and glycolic acid from PLGA over long term usage may possess potential toxicity concerns. Furthermore, the large size of microparticles may hinder diffusion of peptides across cornea or through conjunctival pathway after topical administration.

In order to overcome these drawbacks, a blend of polymers, polyoxyethylene hydrogenated castor oil 40 (HCO-40) and octoxynol 40 (OC-40) have been utilized to develop a self-assembling nanocarrier for small peptides. A combination of these polymers in the past has resulted into a highly stable and water soluble self-assembling nanomicellar formulation. The formulation has completed Phase 3 clinical trials and has shown promising results as a highly biocompatible nanocarrier for the treatment of dry eye disease (NCT02254265).

7.2. Objective

(i) In this study, we newly designed a multi-layered nanomicellar formulation for topical administration of small peptides. The key to forming three layered compartments within a single nanocarrier platform is the sequential self-assembly of peptide with HCO-40 and OC-40 composed of segments with distinct functionality in an aqueous solution. The nanocarrier thus has a hydrophilic core compartment for stable packaging of peptides, an intermediate hydrophobic compartment and an outer hydrophilic compartment that renders it highly soluble in water. The design is general, capable of carrying small peptides [348-349]. Though we test this proof of concept in ocular cell lines for octreotide delivery, a wide range of human diseases could be treated with intracellular biologic administered by an effective nanocarrier system.

(ii) Physicochemical properties, *in vitro* release and drug entrapment and loading capacities of organo and multi-layered nanomicelles were evaluated utilizing dynamic light scattering (DLS) and ultra-fast liquid chromatography (UFLC).

(iii) The cytotoxicity of multi-layered nanomicelles was studied in HRPE (Human retinal pigment epithelial, D407), CCL 20.2 (Human conjunctival epithelial) and RF/6A (rhesus

choroid-retinal endothelial) cells by the 3-(4,5-dimethylthiazol-2-yl)-2,5-diphenyltetrazolium bromide (MTT) assay.

(iv) The uptake behavior and permeability of coumarin-6, coumarin-6-loaded nanomicelles, rhodamine and rhodamine-loaded multi-layered nanomicelles were demonstrated in D407, CCL 20.2 and RF/6A cells using flow cytometry (FCM).

7.3. Experimental

7.3.1. Materials

Dipeptide (Gly-Sar) was purchased from Bachem (Bubendorf, Switzerland). Tripeptide (Gly-Gly-Gly) and Tetrapeptide (Gly-Gly-Gly-Gly) were obtained from Sigma-Aldrich (St. Louis, MO). Octreotide, Human recombinant insulin, and Immunoglobulin G (IgG) were procured from ChinaPeptides Co., Ltd. (Shanghai, China), MP Biomedicals (Santa Ana, CA) and LEE BioSolutions, Inc. (St. Louis, MO) respectively. Hydrogenated castor oil-40 (HCO-40) of pharmaceutical grade was procured from Barnet Products, USA and octoxynol-40 (OC-40 or Igepal CA-897) was purchased from Rhodia Inc., New Jersey, USA. For buffer and formulation preparation double distilled deionized water was utilized. HPLC grade DMSO and methanol were purchased from Fisher Scientific Co. (Pittsburgh, PA, USA). TrypLETM Express Stable trypsin solution, Dulbecco's modified Eagle's medium (DMEM) were received from Invitrogen (Carlsbad, CA, USA). Fetal bovine serum (FBS) was obtained from Atlanta Biologics (Lawrenceville, GA, USA). Micro-BCA assay kit was obtained from Fisher Scientific Inc., (Rockford, IL). All other chemicals were of analytical reagent grade procured from Thermo Fischer Scientific or Sigma Aldrich and were utilized without any further purification.

7.3.2. Cell culture

Human retinal pigment epithelial cell line D407 was kindly provided by Dr. Richard Hunt (University of South Carolina, Columbia, SC, USA). Human conjunctival CCL 20.2 and rhesus choroid-retinal endothelial RF/6A cell lines were obtained from the American Type Culture Collection (ATCC, Manassas, VA). D407 and CCL 20.2 cell lines were cultured in T75 flasks in DMEM medium containing high glucose and glutamine concentration, 1%

nonessential amino acids and 10% FBS (heat-inactivated). RF/6A cells were cultured in RPMI-1640 medium containing sodium bicarbonate and 15% FBS (non heat-inactivated). All the culture mediums contained 100 IU/ml streptomycin and 100 IU/ml penicillin. The pH of the mediums were maintained at 7.4. Cells were maintained at 37ºC in an atmosphere containing 5% CO2 and 90% relative humidity. The mediums were replaced every alternate day until cells reached 80-90% confluency (5-7 days for D407, CCL 20.2 and 19-21 days for RF/6A cells).

7.3.3. Preparation of multi-layered nanomicelles

The multi-layered nanomicellar formulation was prepared following a 2-step process. The first step involved the solvent-induced encapsulation of various agents used herein in terms of organo-nanomicelle formation. To encapsulate a macromolecule, 2.5 wt. % HCO-40 and 1.005 wt. % OC-40, were dissolved separately in ethanol and mixed to generate a homogenous solution. Macromolecule, 0.1 wt. % was dissolved in ethanol/DI water and added to polymer-ethanol solution drop-wise. The resulting transparent solution containing the organo-nanomicelle was evaporated under high-speed vacuum (Genevac, Ipswich, Suffolk, UK) overnight (~10 h) to obtain a solid thin film. The solid thin film was dissolved in chloroform and filtered with a 0.2 μm nylon membrane filter to remove unentrapped drug aggregates and other foreign particulates. The transparent solution was characterized for size, polydispersity index (PDI) and zeta potential.

The second step in the overall nanomicelle preparation process is the formation of highly stable and aqueous soluble three-layered nanomicelle incorporating the macromolecule/polymer complex (organo-nanomicelle). For this step, 5.0 wt. % HCO-40 and 2.01 wt. % OC-40 were separately dissolved in ethanol and mixed in a vial. The polymer ethanol solution was added dropwise to the vial containing organo-nanomicelle chloroform

solution and mixed thoroughly. The solvent was then removed by evaporation under high-speed vacuum and subsequently rehydrated in DI water to the desired volume. The resulting viscous multi-layered nanomicelle solution was filtered through 0.2 μm nylon membrane filter and characterized for size, PDI and zeta potential using DLS.

7.3.4. Characterization

Hydrodynamic diameter, PDI and zeta potential of both organo-nanomicelles and milti-layered nanomicelles were determined with Zeta Sizer (Zetasizer Nano ZS, Malvern Instruments Ltd, Worcestershire, UK) at RT. Briefly, 1ml of nanomicellar solution (2 mg/mL) was placed into a glass cuvette. The samples were measured at a scattering angle of 173 º and 25 ºC. Average values were calculated from three replicate measurements of each sample.

7.3.5. ^{1}H-NMR spectroscopy

To perform ^{1}H-NMR spectroscopy, Octreotide, Blank and Octreotide-loaded multi-layered nanomicelles were prepared in D_2O for NMR analysis. Spectra were recorded with Varian-400 NMR instrument. NMR data was processed using VNMRJ or ACD labs software.

7.3.6. Entrapment and loading efficiency

The total amount of macromolecule entrapped in the formulation was determined by bicinchoninic acid assay (BCA). Ten milliliters of each organo-nanomicellar formulation was collected and centrifuged at 10,000 rpm for 10 min at 4 ºC. One milliliter of supernatant was carefully collected from each centrifuge tube and transferred into fresh vials and lyophilized to obtain a solid pellet. Five hundred microliter of DI water was added to each vial in order to reverse the organo-nanomicelles and release the macromolecule in the surrounding aqueous solvent. Micro BCA protein estimation kit (Thermo Scientific, IL) was employed for the

estimation of total protein/peptide content. The percent entrapment and loading efficiency of peptides and proteins were calculated according to the following formula:

Percent entrapment = (mass of a macromolecule in organo-nanomicelles)/ (mass of a macromolecule added in formulation) x 100 **[Eq. 14]**

Loading efficiency = (mass of a macromolecule in organo-nanomicelles)/ (mass of a macromolecule added + mass of polymers used) x 100 **[Eq. 15]**

7.3.7. In vitro cytotoxicity: MTT assay

Cytotoxicity of HCO-40, OC-40 and multi-layered nanomicelles against D407, CCL 20.2 and RF/6A cells were assessed in vitro by MTT assay. All the three cell lines were seeded into a 96-well plate at a density of 1x104 cells/well in 100 µL complete DMEM solution containing 10% FBS. Cells were cultured for 1 day at 37 ºC in 5% CO2 atmosphere. Different concentrations of HCO-40, OC-40 and multi-layered nanomicelles were prepared in serum free medium and filtered with 0.22 um sterile nylon membrane filters under laminar flow hood. Afterwards, the media were replaced with 100 µl of different treatment groups and incubated for 24 h at 37 ºC. After 24 h of incubation, MTT stock solution (5 mg/mL in potassium phosphate buffer, PBS 20 µL) was added to each well and incubated for 2.5 h. The absorbance was measured with a microplate reader (BioRad Hercules, CA, USA) at 450 nm. Cell viability was expressed according to the following formula:

Cell viability (%) = (Abs of sample- Abs of negative control)/ (Abs of positive control- Abs of negative control) * 100 **[Eq. 16]**

7.3.8. In vitro release of octreotide from octreotide-loaded multi-layered nanomicelles

A fixed volume (1 mg/mL) of octreotide-loaded multi-layered nanomicelles was transferred to a membrane tubing (MWCO 8000-10000 Da, Spectrum labs, CA, USA). The tubing was subsequently immersed in 5 mL PBST (PBS-Tween, pH 7.4) or STF (simulated tear fluid) solution in a shaking water bath fixed at 60 rpm and 37 ºC to maintain sink condition. At predetermined time points, entire 5 mL of external buffer was withdrawn and replaced with 5 mL of fresh buffer solution. The amount of octreotide released was determined by a RP-HPLC method. Release study was performed in triplicates. The results were plotted as mean±SD. The release data was fitted for zero order, first order, Higuchi and Korsmeyer-Peppas model to determine the kinetics of DEX release.

7.3.9. Evaluation of cellular uptake by flow cytometry (FCM)

D407, CCL 20.2 and RF/6A cells were seeded into 12-well plates at a density of 2.5x104 cells/well in 24 mL complete DMEM/RPMI containing 10% FBS, and maintained until they achieved 80-90% confluency (6-7 days) at 37 ºC in 5% CO2 atmosphere. Afterwards, cells were incubated with coumarin-6, coumarin-6 loaded nanomicelles, rhodamine and rhodamine-loaded multi-layered nanomicelles at a final coumarin-6/rhodamine concentration of 50 µg/mL in serum free medium for predetermined time points at 37 ºC. At each time point, the culture medium was removed and cells were washed twice with DPBS to remove the various treatment groups that were not ingested by the cells. Cells were detached with trypsin for 10 min, and then centrifuged at 1550 rpm for 10 min to obtain a solid pellet. The solid cell pellet was washed twice with DPBS. After removal of the supernatant, the cells were resuspended in 500 µL of 4% (w/v) paraformaldehyde aqueous solution and stored at 4 ºC. The mean fluorescence intensity of coumarin-6, coumarin-6 loaded nanomicelles, rhodamine

and rhodamine-loaded multi-layered nanomicelles in cells were analyzed by FCM (Becton Dickinson, Franklin Lakes, NJ, USA) with an excitation wavelength of 490 nm (coumarin-6) and 660 nm (rhodamine) for comparative studies.

7.4. Sample and Data Analysis

7.4.1. Ultra-fast liquid chromatography (UFLC) analysis

The octreotide concentration in released media was quantified by UFLC assay. A Shimadhu (Shimadzu Scientific Instruments, Columbia, MD, USA) HPLC system coupled with pumps having built-in system controller (LC-20AT), degasser (DGU-20A3R), DAD detector (SPD-20AV) and autosampler (SIL-20AHT) were employed. Phenomenax column (Phenomenex C18 kinetex column 100 x 4.6 mm, 5 mm) along with a guard column (Phenomenex SecuritGuard Catridges, C18, 4 x 2 mm) was used at a flow rate of 0.5 mL/min. A gradient elution method was employed. Mobile Phase A (HPLC water with 0.1% formic acid) at 10% and mobile phase B (ACN with 0.1% formic acid) at 90% were ran for first 2 min followed by a linear gradient to reach 100% of Phase B at 18 min. Standards were prepared in PBS buffer ranging from 3.1 to 100 mg/ml. DAD detector was set at 280 nm to determine UV absorbance. Injection volumes was 50 µl.

7.4.2. HPLC–MS analysis

HPLC–MS analysis was performed with electrospray ionization (ESI) in a positive ion mode on QTrap® API-3200 mass spectrometer equipped with Shimadzu quaternary pump, vacuum degasser, DAD detector and autosampler (Shimadzu Scientific Instruments, Columbia, MD, USA). Data acquisition and data processing were performed by Analyst 1.4.2 software package (Applied Biosystems, Foster City, CA, USA). LC conditions including

column and gradient composition remains same as explained in the earlier UFLC assay. Injection volumes were 30 µL for all samples. UV detector was set on 280 nm and MS was set in a range of 200–1700 amu. The extracted ion chromatogram (EIC) from the total ion current (TIC) chromatogram was compared with UV chromatogram to identify the native octreotide and confirm absence of any acylated adducts.

7.5. Statistical analysis

All experiments were conducted at least in triplicate and results were expressed as mean ± S.D. Student t-test was employed to determine statistical significance among groups. A value of $p \leq 0.05$ was considered to be statistically significant.

7.6. Results and Discussion

7.6.1. Preparation of multi-layered nanomicelles

The process of a peptides and proteins encapsulation and formation of a stable multi-layered nanomicellar formulation is shown in Figure 7-1 A. The overall process was accomplished in two steps. The first step involves the process of peptide encapsulation, achieved via formation of an organo-nanomicelle or reverse nanomicelle. Self-assembly of the organo-nanomicelle occurs spontaneously as the polar ethanol/water mixture is replaced with the organic or less-polar chloroform. This allows water soluble peptide to get entrapped into the hydrophilic core of the organo-nanomicelles and thus reduces interaction with the organic solvent. The organo-nanomicelle can be described as a core-shell structure, where the core is composed of polymer/peptide complex with chloroform as a dispersant. In the conventional aqueous system, encapsulation of hydrophilic peptides and proteins within hydrophobic compartment suffer from low loading efficiency due to the high solubility of these molecules

in aqueous solutions. Thus, we performed the encapsulation step in organic solvent (chloroform) which is a non-solvent for peptides and proteins. The drastic change in solubility drives the aggregation of the organo-nanomicelle and preferential fractionation of peptide into the nanomicelle core. Using this method, we were able to achieve an encapsulation efficiency of approximately 76% for a peptide (octreotide). The loading results of various other peptides and proteins have been shown in the Table 7-1.

The peptide-loaded organo-nanomicelles were then formulated into a stable aqueous solution in the second step shown in Figure 7-1 A. We used the same polymers, HCO-40/OC-40 (double concentration), to form a protective aqueous solubilizing layer on the surface of the organo-nanomicelles. The resulting nanomicelle is a multi-layered system comprising of three regions: hydrophilic core: peptide/polymer; intermediate hydrophobic layer, and outer hydrophilic shell (Figure 7-1 B). Appearance of the nanomicelle solution at different settings are shown in Figure 7-2. In the first step, the peptide loaded organo-nanomicelle solution was obtained in chloroform without any precipitation. The formation of stable aqueous multi-layered nanomicelle in the second step was evident by the absence of precipitation when HCO-40/OC-40 outer layer was added (Figure 7-1 D). In contrast, when the stabilizing outer layer is not included in the formulation, we observed immediate precipitation of the peptide loaded organo-nanomicelle in the aqueous environment (Figure 7-2 C).

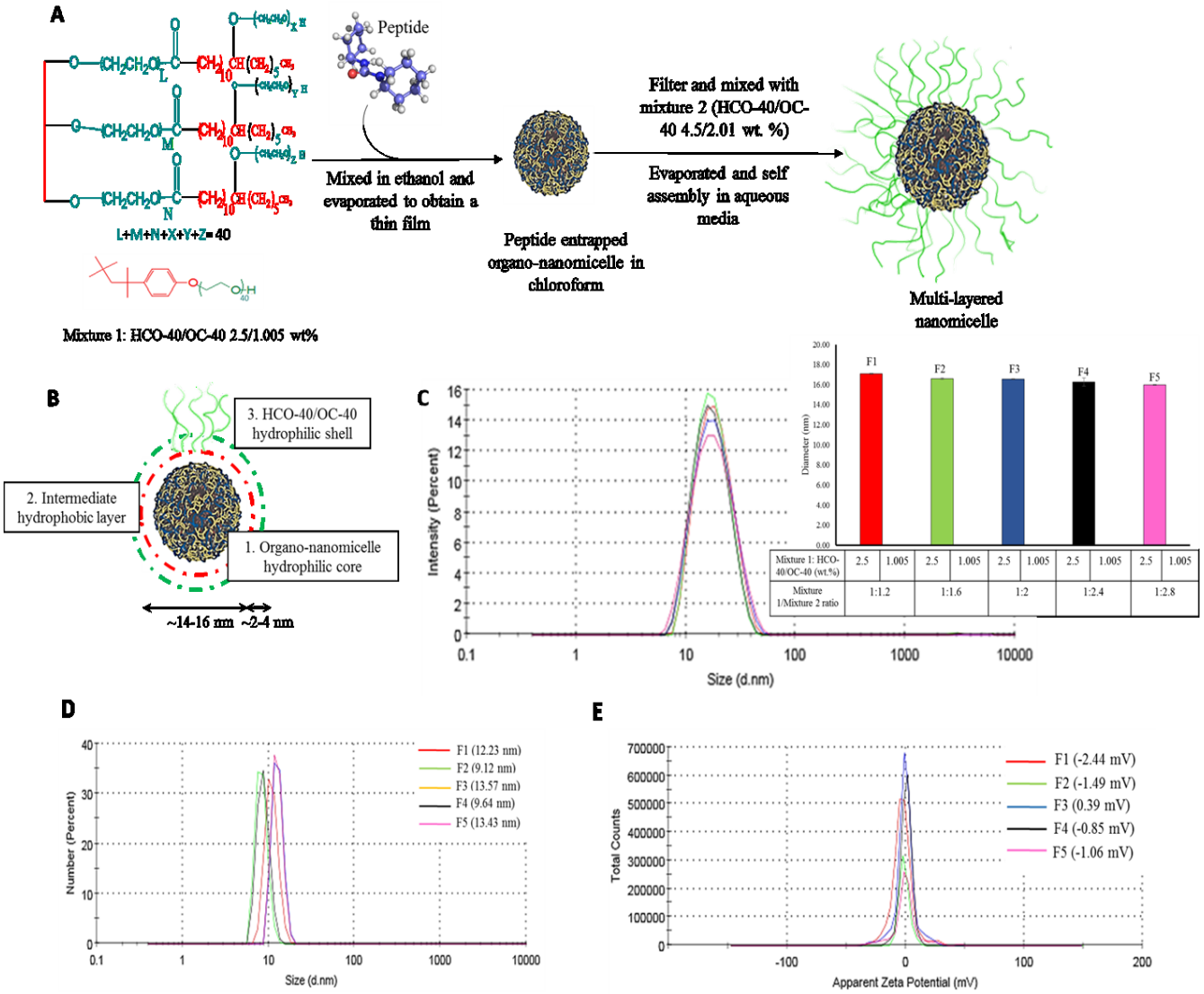

Figure 7-1 Synthesis of multi-layered nanomicelles: (A) A schematic illustration shows the processes of preparing multi-layered nanomicelles by a modified multi-step solvent evaporation/rehydration method. (B) The multi-layered nanomicelles are comprised of a hydrophilic organ-nanomicelle core, a hydrophilic HCO-40/OC-40 shell and an intermediate hydrophobic layer between hydrophilic core and shell. (C) By varying the mixture 1/mixture 2 ratio, we can tune the multi-layered nanomicelles size in a physiological environment. The effect of formulation parameters on the (D) size of orgno-nanomicelles and (E) zeta potential of multi-layered nanomicelles. Data represent mean ± S.D (n= 3-4)

Table 7-1 Loading and entrapment efficiency of multi-layered nanomicelles for a series of peptides and proteins with varying molecular weights. Data represent mean ± S.D (n= 3-4)

Drug	MW (Da)	Loading efficiency (%)	Entrapment efficiency (%)
Gly-Sar	146.15	0.99±0.12	70.77±0.93
Gly-Gly-Gly	189.2	1.39±0.23	99.18±0.66
Gly-Gly-Gly-Gly	246.23	1.41±0.37	100.41±1.84
Octreotide	**1013.24**	**1.10±0.22**	**78.52±2.01**
Insulin	5733.55	0.17±0.08	12.48±0.67
IgG	150,000	0.16±0.06	11.60±0.49

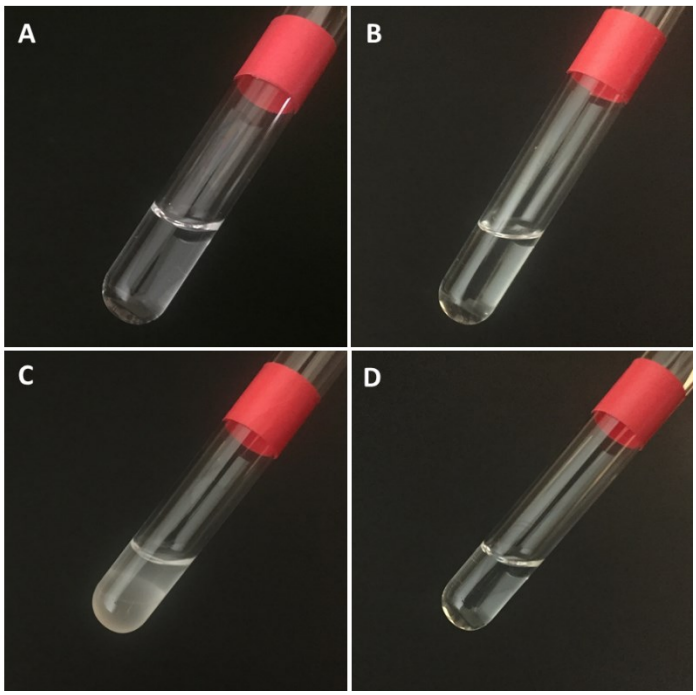

Figure 7-2 The images of various nanomicellar formulations: (A) Deionized (DI)-water, (B) Octreotide-loaded organo-nanomicelles in chloroform, (C) Precipitated octreotide-loaded organo-nanomicelles after adding to an aqueous solution, (D) Octreotide-loaded multi-layered nanomicelles

7.6.2. Characterization of organo and multi-layered nanomicelles

The ability of an amphiphilic polymer to condense a peptide or macromolecule is primarily influenced by the hydrophilic interactions of hydrophilic groups (i.e. oxyethylene) and flexibility of the molecular structure[359]. Nanomicellar constructs from a single amphiphilic polymer are not very thermodynamically stable[360]. The inclusion of a second polymer can cause interlock hydrogen bonding with the primary polymer to generate very stable nanomicelles up to 65 ˚C. Moreover, the oxygen and hydrogen atoms of hydroxyl groups may form intramolecular hydrogen bonding with adjacent polymer chain affording some degree of stability, and control the release behavior. We have screened different combinations of HCO-40 and OC-40 for use in the preparation of organo-nanomicelles. No significant difference in nanomicellar size was observed (Figure 7-1 D). Thus, HCO-40/OC-40 combination which demonstrated the highest entrapment and loading efficiency (Table 7-2) was used for the inner core of the multi-layered nanomicelle formulations evaluated in this study. Table 7-3 shows the DLS measurements of hydrodynamic diameters, PDI and zeta potential obtained for the HCO-40/OC-40 derived multi-layered nanomicelles. For organo-nanomicelles, variation in polymer concentration significantly affected the entrapment efficiency (Table 7-2).

For the octreotide encapsulated multi-layered nanomicelles consisting of 2.5 wt. % HCO-40 and 1.005 wt. % OC-40 as inner core and 5.0 wt. % HCO-40 and 2.01 wt. % OC-40 as outer layer, the expected increase in multi-layered nanomicelle diameter from organo-nanomicelle was observed (Figure 7-1 C). The obtained hydrodynamic diameters were in the range ca. 17 nm for all multi-layered nanomicellar formulations (Figure 7-8). This is particularly important as the lower size of the nanomicelles would promote passive diffusion of the nanoconstructs into the scleral aqueous channels (size ranging from 20-80 nm) to reach

back of the eye. More importantly, Cequa®, Sun Pharmaceuticals, a nanomicellar formulation of cyclosporine (~15-20 nm) was recently approved by the US FDA for the treatment of dry eye syndrome and has demonstrated improved drug absorption into human ocular tissues. We also characterized the zeta potential of multi-layered nanomicelles using electrophoretic light scattering. The zeta potential was shown to have a value close to zero (neutral) (Figure 7-1 E). Additionally, continuous dilution by the tear fluids in the cul de sac and the limited capacity of the precorneal pocket leads to poor drug concentrations after topical application. In this regard, PVP K90 has been employed in order to enhance the viscosity of the nanomicellar formulation resulting in improved retention at the site of administration and/or ocular tissues.

Table 7-2 Loading and entrapment efficiency of organo-nanomicelles for octreotide at varying wt. % ratio of polymers, HCO-40 and OC-40. Data represent mean ± S.D (n= 3-4)

Organo-nanomicelle	**Composition (HCO-40: OC-40) (wt. %)**	**Loading efficiency (%)**	**Entrapment efficiency (%)**
F1	0.5:2	0.90 ± 0.02	61.86 ± 1.03
F2	1.68:0.75	0.99 ± 0.06	71.07 ± 0.62
F3	**2.5:1.005**	**1.08 ± 0.02**	**78.52 ± 2.01**
F4	0.5:0.01	0.86 ± 0.05	58.21 ± 0.57
F5	2.5:0.01	1.01 ± 0.03	76.36 ± 1.56

Table 7-3 Changes in average diameter, zeta potential and polydispersity of octreotide-loaded multi-layered nanomicelles by varying the layer 1/layer 2 polymer ratio. Data represent mean ± S.D (n= 3-4)

Multi-layered nanomicelles	Z-Ave Diameter (nm)	Zeta-potential (mV)	Polydispersity
F1	17.07 ± 0.05	-2.44 ± 0.52	0.16 ± 0.01
F2	16.59 ± 0.08	-1.49 ± 0.18	0.15 ± 0.01
F3	**16.56 ± 0.04**	**0.39 ± 0.18**	**0.14 ± 0.01**
F4	16.26 ± 0.41	-0.85 ± 0.26	0.17 ± 0.02
F5	15.97 ± 0.04	-1.06 ± 0.67	0.15 ± 0.01

7.6.3. 1H-NMR spectroscopy of multi-layered nanomicelles

The process of multi-layered nanomicelle formation and octreotide encapsulation in multi-layered nanomicelle core were studied with proton NMR spectroscopy. 1H-NMR spectra for blank and octreotide-loaded multi-layered nanomicelles were recorded and compared. Sharp 1H-NMR signals from oxyethylene (-CH2-CH2-O) (δ=3.8 ppm) protons and weak signals from methyl (δ=0.9 ppm) and methylene (δ=1.3 ppm) protons of the hydrophobic chains were recorded. In addition, very weak signals from aromatic protons (δ=7.3 ppm) on phenyl ring were also recorded. Moreover, there was no significant difference observed in the spectra for blank and octreotide-loaded multi-layered nanomicelles (Figures 7-3 and 7-4). No characteristic peaks from octreotide were observed in octreotide-loaded multi-layered nanomicelles implying that the drug was molecularly dispersed in the nanomicellar core (Figures 7-5 and 7-6).

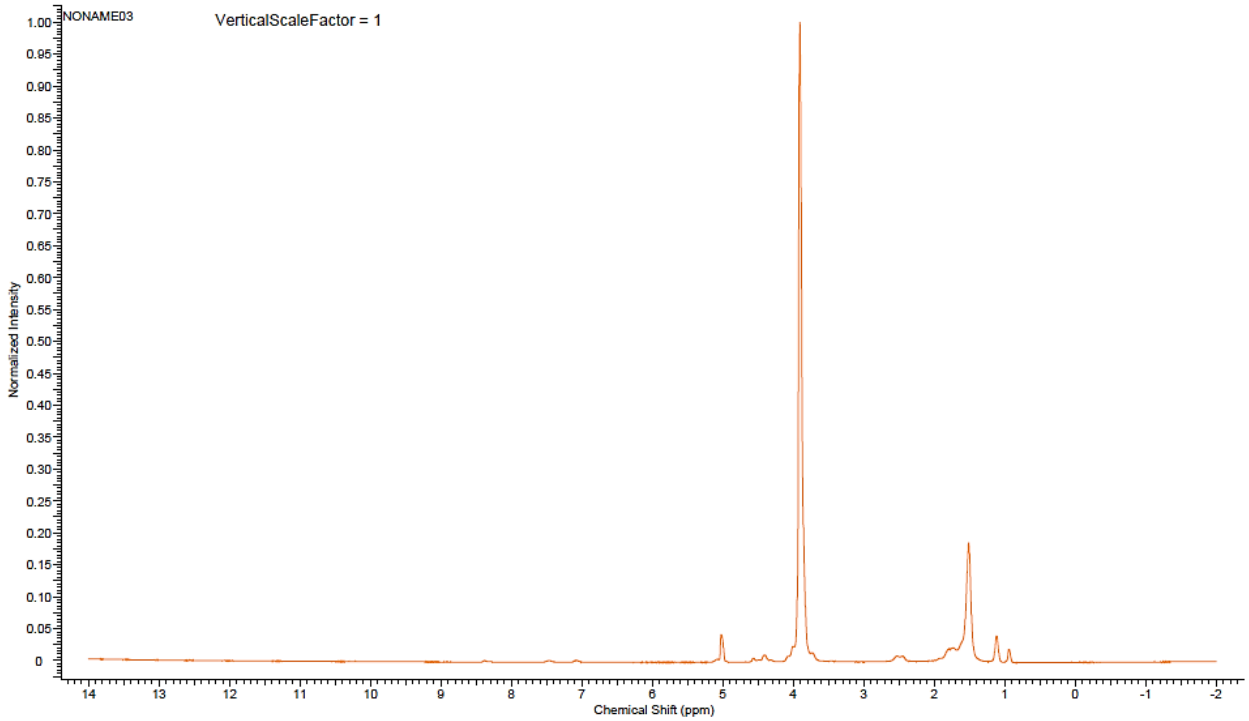

Figure 7-3 ^{1}H-NMR spectra for Blank multi-layered nanomicelles in D_20

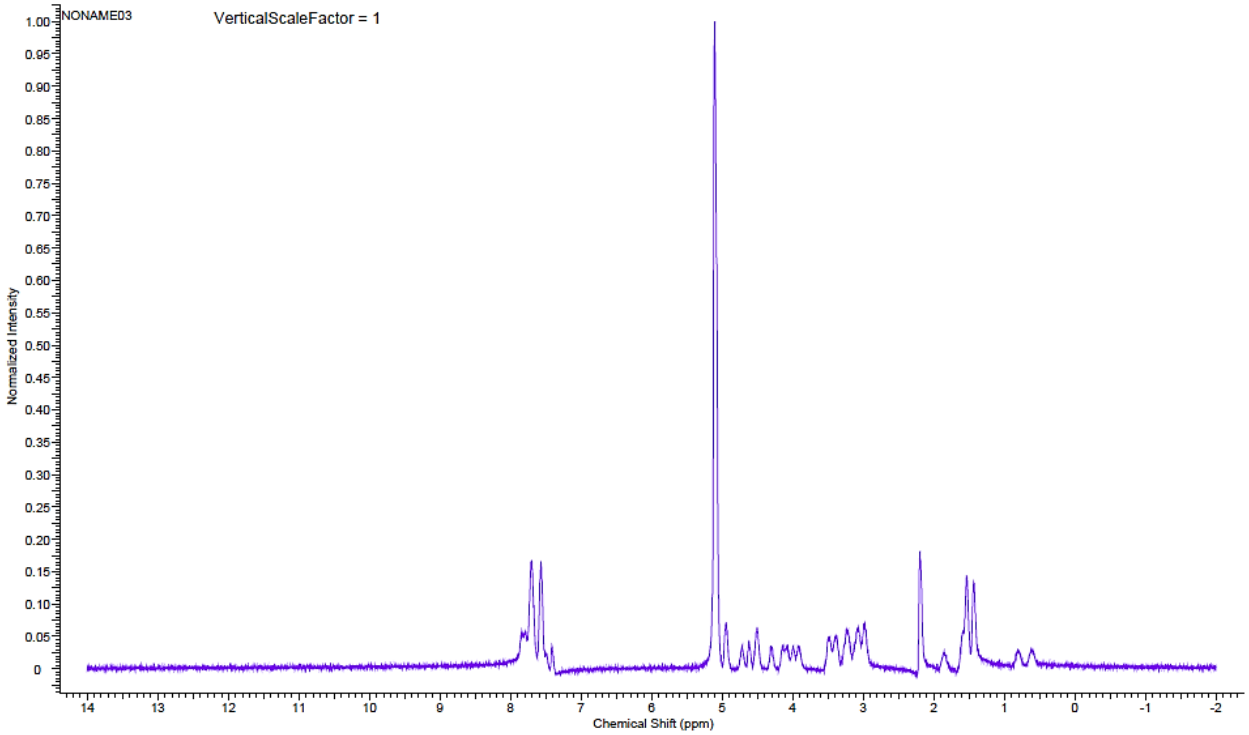

Figure 7-4 ^{1}H-NMR spectra for Octreotide in D_20

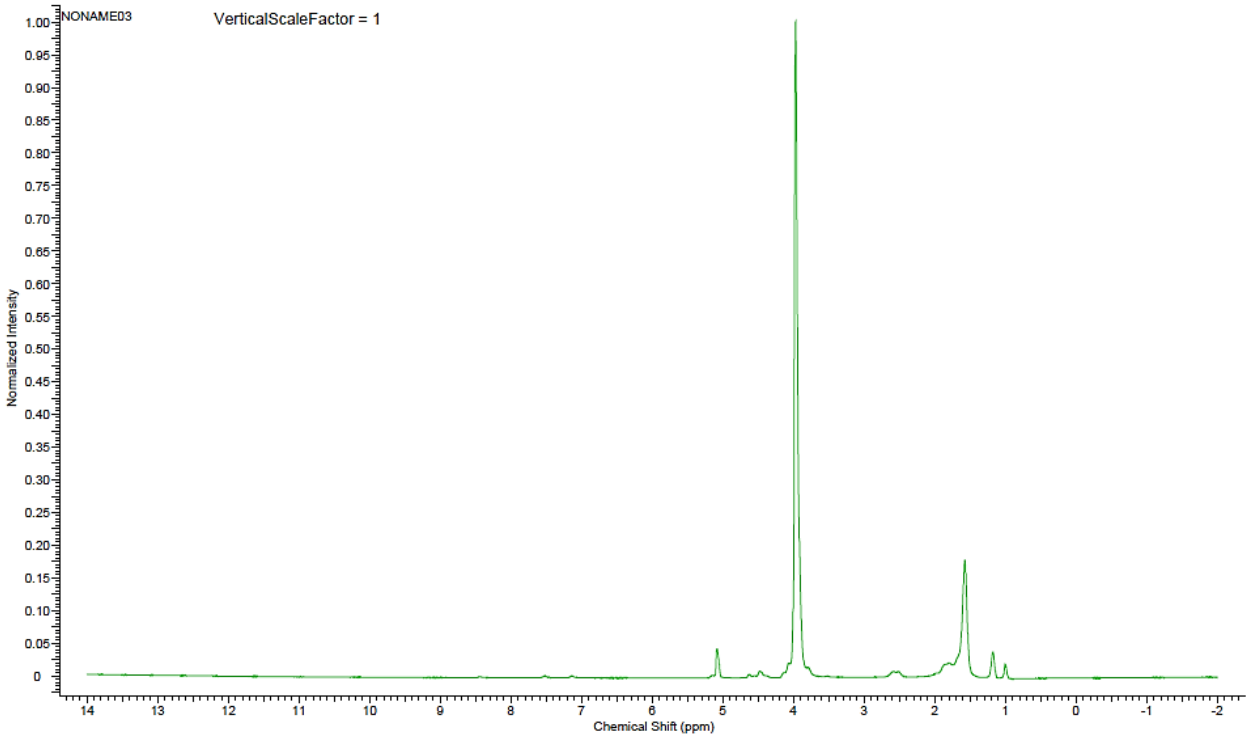

Figure 7-6 ^{1}H-NMR spectra for Octreotide-loaded multi-layered nanomicelles in D_20

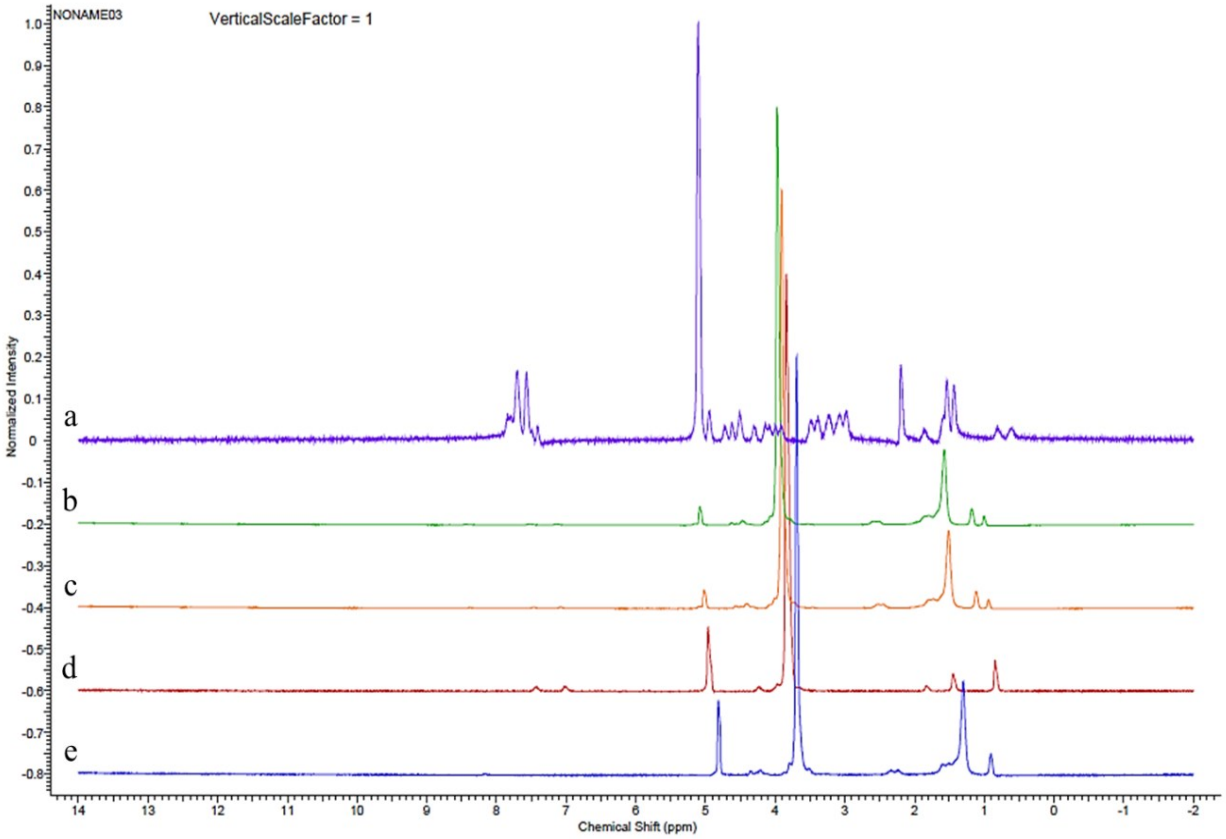

Figure 7-5 ^{1}H-NMR spectroscopies for (a) Octreotide; (b) Octreotide-loaded multi-layered nanomicelles; (c) Blank multi-layered nanomicelles; (d) OC-40 and (e) HCO-40 in D_20

7.6.4. Encapsulation efficiency

Entrapment of hydrophilic peptides and proteins within the hydrophobic core of polymeric nanocarriers typically leads to poor encapsulation efficiency. In aqueous solutions, a vast majority of amphiphilic polymers utilized as delivery vehicles exhibit low CMC and fast micellization kinetics[183]. Although these nanomicelles are highly stable and allow for prolonged circulation lifetime, the fast micellization kinetics may limit the amount of hydrophilic peptides and proteins getting entrapped[159]. Additionally, hydrophilic peptides and proteins often exist as water-soluble ionic species. Accumulation of such species into the hydrophobic core is thermodynamically unfavorable. A common approach to achieve higher encapsulation efficiency is the use of double emulsion technique[361]. However, this method requires precise control to obtain uniform sized particles. The method we report here is a highly robust method for the encapsulation of highly water-soluble small peptides within the multi-layered nanomicelle. Our method is unique in its approach and tries to overcome the problems associated with poor encapsulation efficiency of hydrophilic molecules. In principal, the core-shell structure of our organo-nanomicelles contains a hydrophilic core and a hydrophobic shell. The incorporation of the peptide within the hydrophilic core is thermodynamically favorable. Second, micellization of the organo-nanomicelles occurs via chain reorganization as the water-insoluble polymer/peptide complex aggregate and further solvent-induced condensation of peptide occurs. Although we have not yet studied the micellization kinetics, we anticipate chain reorganization to occur on a timescale long enough to allow internalization of the water-insoluble polymer/peptide complex into the core.

The encapsulation efficiency of the multi-layered nanomicelle was investigated as described above. The amount of entrapped macromolecule was compared to the initial added

amount to determine the encapsulation efficiency. We investigated the encapsulation efficiency as a function of differing polymer concentrations. Figure 7-7 show the percentage of various peptides and proteins entrapped in the multi-layered nanomicelles at polymer concentrations of 2.5 wt. % HCO-40 and 1.005 wt. % OC-40 and 2 mg of peptides and proteins. We observed a decrease in percentage of macromolecule encapsulated as the molecular weights increased. However, the percentage of dipeptide (Gly-Sar) encapsulated in the nanomicelles was just 70%. This may be due to the lower hydrophilicity of dipeptide in comparison to tri- and tetra- peptides. In contrast, higher amounts of octreotide, insulin, and IgG resulted in diminished encapsulation efficiency of the multi-layered nanomicelles. Consequently, higher hydrophilicity and lower molecular weight may increase the possibility of hydrophilic interactions in the hydrophilic core of the multi-layered nanomicelles and thus may enhance the encapsulation efficiency. Detailed investigation on the solvent-induced self-assembly is needed to fully understand the micellization process and encapsulation of peptides and proteins within the core.

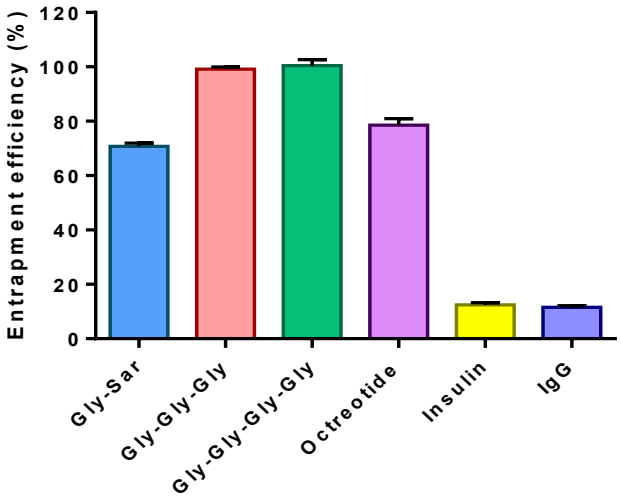

Figure 7-7 Encapsulation or entrapment efficiency of multi-layered nanomicelles for various macromolecules or biologic. Data represent mean ± S.D (n= 3-4)

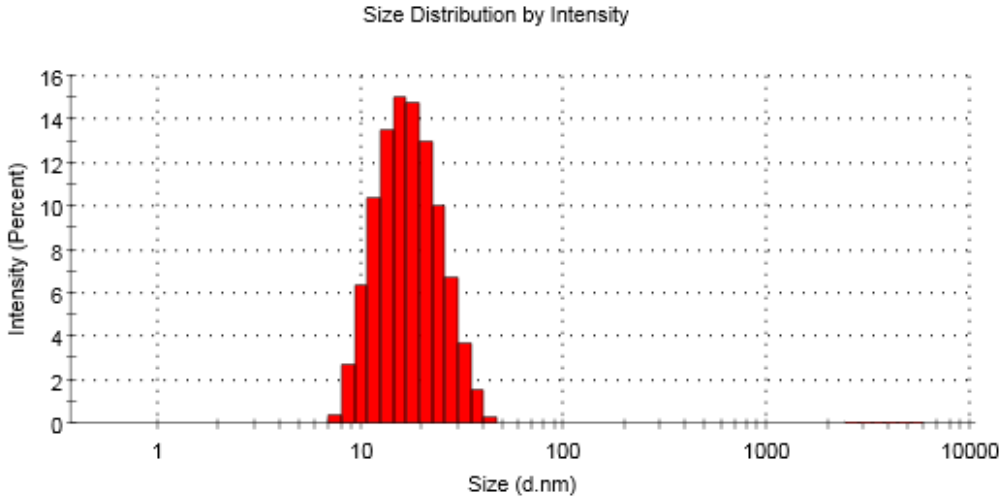

Figure 7-8 Size distribution from DLS measurements of multi-layered nanomicelles (F3, Z-Ave Diameter 16.56±0.04 nm). Data represent mean ± S.D (n= 3-4)

7.6.5. Release kinetics

Once circulating, multi-layered nanomicelles are internalized by target cells, the payload is released from the endosome and merges with lysosome and finally reaches the nucleus. We examined the release profile of multi-layered nanomicelles using PBST and STF at 37°C to simulate the environment of a human eye. The release profile as a function of time is shown in Figure 7-9. Previously, we have shown that HCO-40/OC-40 nanomicelles could sustain the release of hydrophobic drugs for more than a month. In this study, octreotide was used as a model large molecule drug. We observed excellent octreotide release of up to 100% from the multi-layered nanomicelles in 264 h (11 days) and 648 h (27 days) in PBST (Figure 7-9 A) and STF (Figure 7-9 B) respectively. A sustained release of octreotide from the hydrophilic core of the multi-layered nanomicelles was achieved without any significant burst release. Unlike hydrophobic drugs, where the higher concentration of surfactant in STF improved the release rate, the octreotide release was delayed in this case compared to PBST. In addition, the faster release of octreotide from the multi-layered nanomicelles could be explained by the weak hydrophilic interactions between octreotide and hydrophilic segments of polymers in comparison to much stronger interactions of hydrophobic drugs at the hydrophobic nanomicellar core.

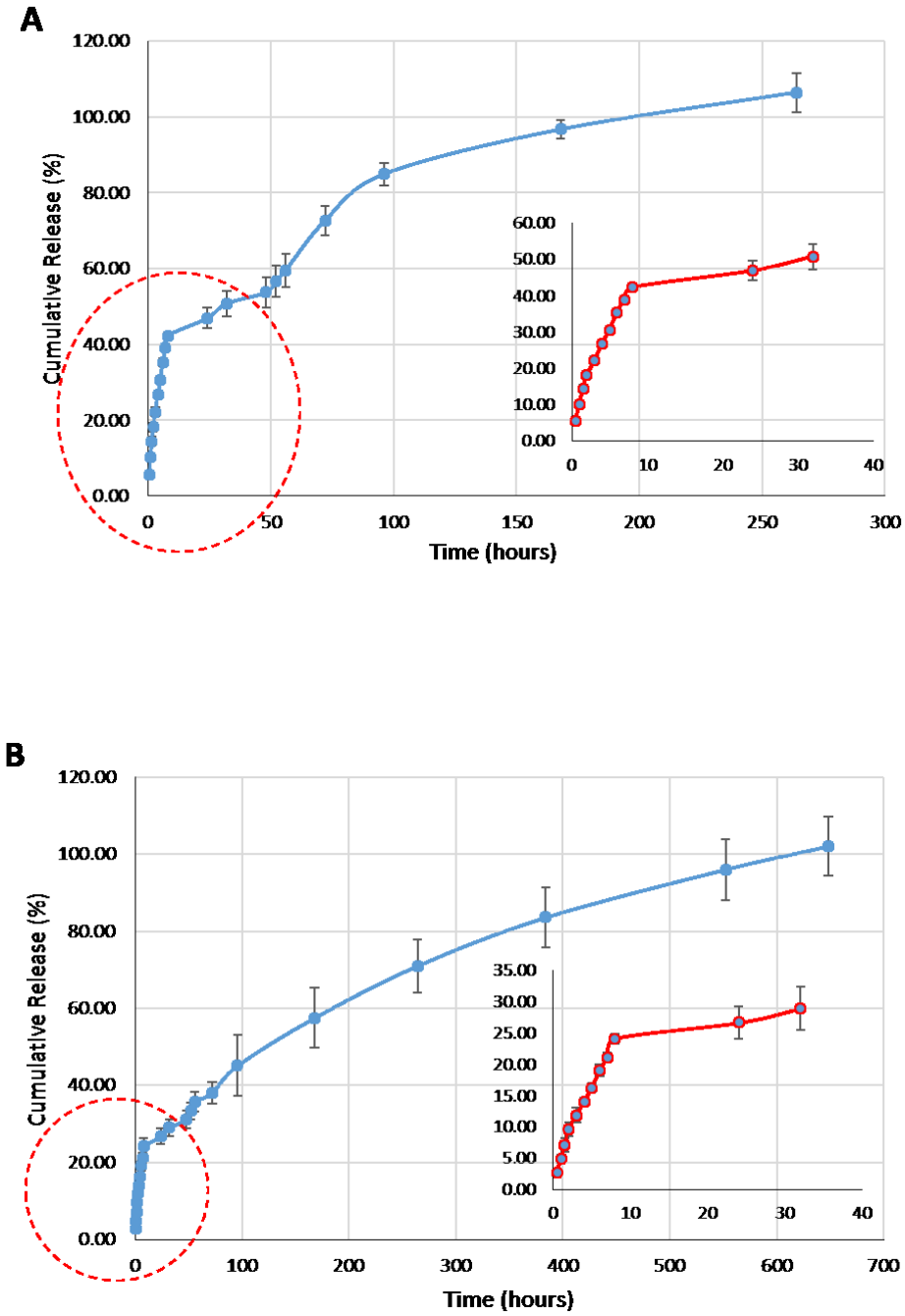

Figure 7-9 Octreotide release profiles of multi-layered nanomicelles: A) in PBST, pH 7.4 and B) in STF, pH 7.4 with circled region showing the release pattern for first 32 hours. Data represent mean ± S.D (n= 3-4)

Table 7-4 Summary of fit for kinetic models and associated parameters for release of octreotide from multi-layered nanomicelles. Data represent mean ± S.D (n= 3-4)

Release medium	Kinetic and Mechanistic Models						
	Higuchi Model	Korsmeyer-Peppas model		Hixson-Crowell model	Zero Order	First order	
	R^2	R^2	n	R^2	R^2	R^2	Rate constant k ($Hour^{-1}$)
PBST	0.8169	0.9483	0.3450	0.7854	-0.2180	0.8731	0.4810
STF	0.9675	0.9708	0.3892	0.8892	0.5540	0.9105	0.1599

Further, the release data was fitted to various mechanistic models including Higuchi, Hixson-Crowell and Korsmeyer-Peppas models to determine the kinetics of octreotide release (Table 7-4). The best fit was found with the Korsmeyer-Peppas model with R^2 of 0.9483 and 0.9708 compared to other models for PBST and STF respectively. The n value was found to be 0.3450 and 0.3892 for PBST and STF respectively. Value of diffusion exponent $n < 0.5$ suggests that mechanism of release was pseudo-Fickian diffusion. In both pseudo- and non-Fickian diffusion mechanisms, drug release is controlled by the thickness of the polymer. Data was also fitted to zero- and first- order equations to determine the order of release. Process of release followed first order kinetics with R^2 values of 0.8731 and 0.9105 for PBST and STF respectively indicating release rate is proportional to the drug concentration. Compared to PBST, release rate was slower in STF, as indicted by first order rate constant which can be attributed to the higher concentration of surfactant in STF impeding the drug release.

Moreover, the released octreotide from the multi-layered nanomicelles in PBST and STF was analyzed in HPLC-MS for native and acylated forms. In contrast to marketed PLGA formulation of octreotide (Sandostatin LAR® depot) where >60% of octreotide is acylated during in vitro release over a 3 months period, no acylation was observed in our case. Such

impediment of acylation may be explained by absence of acidic pH conditions and faster release or low incubation time of octreotide with the polymers. One hundred percent (100%) of octreotide was chemically intact following the release relative to Sandostatin LAR® depot where <20% was released in native form. HPLC–MS analysis was performed to identify the peaks associated with native and/or acylated peptide in the LC chromatogram. HPLC–MS profile for release samples on day 11 and 27 from PBST and STF are represented in Figures 7-11 and 7-12 respectively in comparison to blank (Figure 7-10). Native octreotide eluted at 8.29 min in extracted ion-chromatogram as m/z of 1020.1 corresponding to peak at 8.28 min in UV chromatogram. Presence of 1020.1 m/z suggest that the peptide maintained its native cyclic chemical structure.

Several groups have investigated the use of delivery systems to deliver biologics for the treatment of back of the eye diseases such as age-related macular degeneration (AMD), diabetic retinopathy (DR)[362]. Intravitreal administration of such delivery systems has been shown to greatly sustain biologic release abilities for longer period[363]. Consequently, our unique multi-layered nanomicelles proved the hypothesis based on those references for the effective topical peptide delivery.

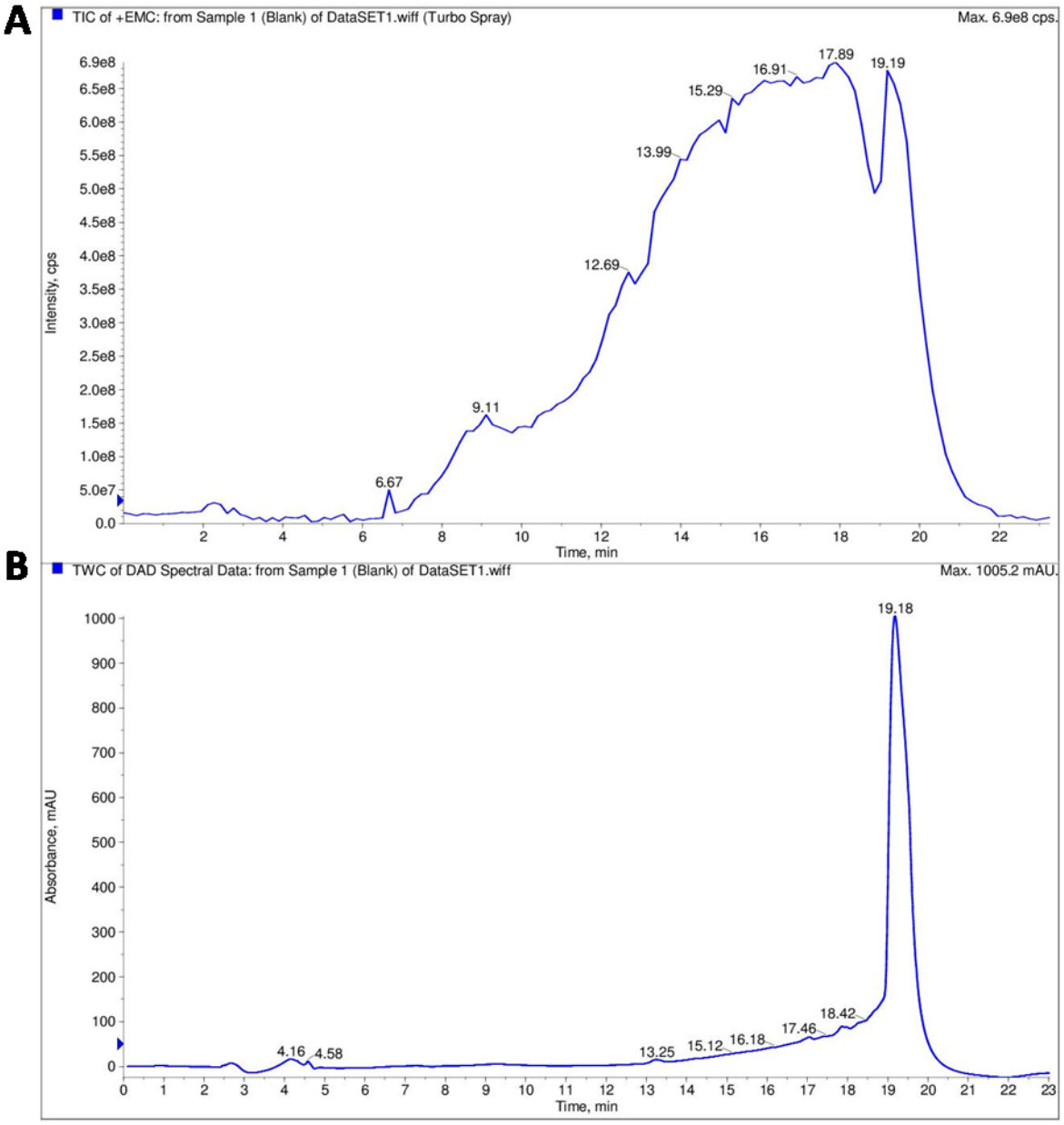

Figure 7-10 HPLC-MS spectrum of blank: A) total ion current (TIC) chromatogram for the enhanced multiply charged (EMC) scan and B) UV chromatogram

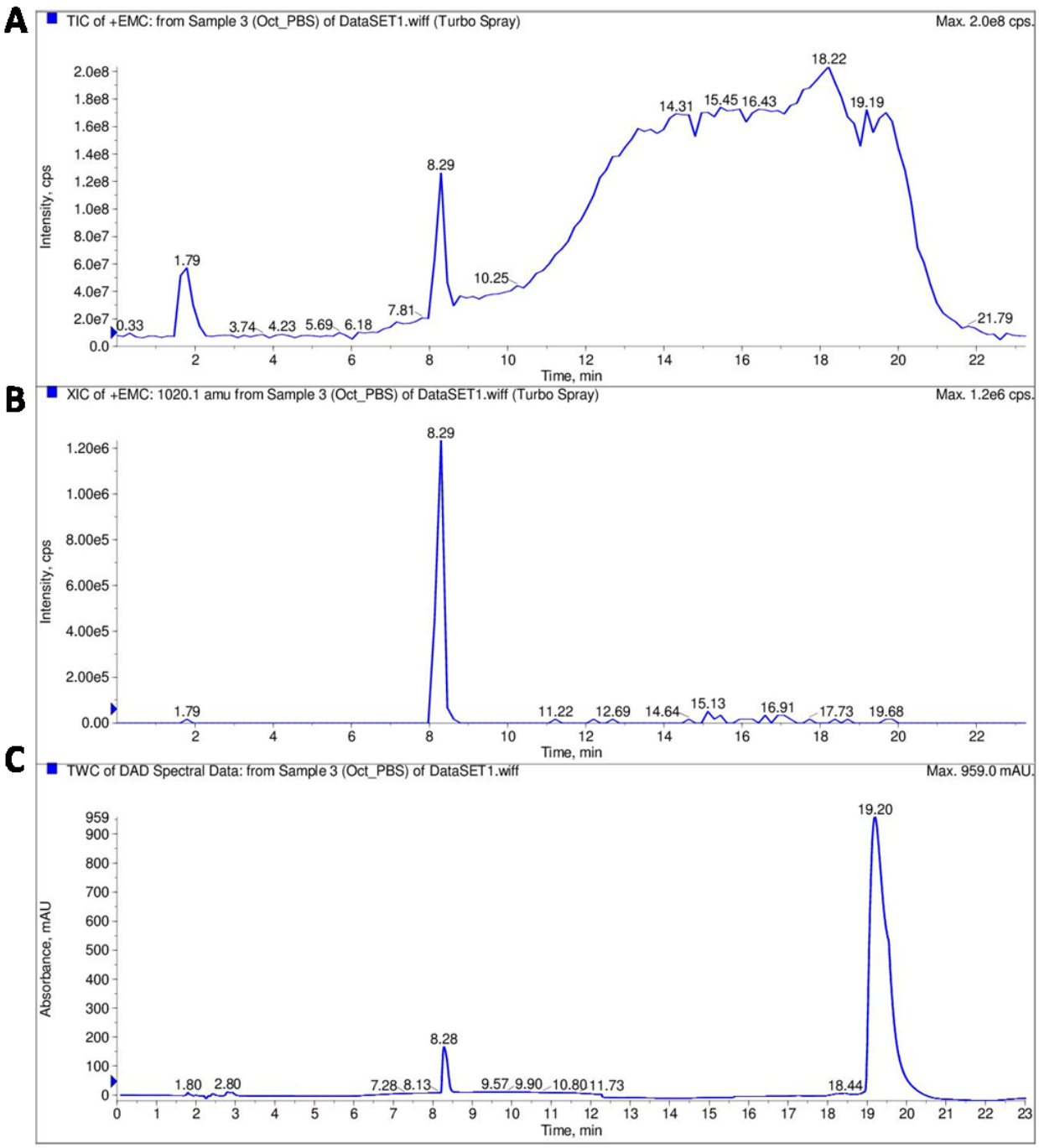

Figure 7-11 HPLC-MS spectrum of release sample (Day 11) from multi-layered nanomicelles in PBST: A) total ion current (TIC) chromatogram for the enhanced multiply charged (EMC) scan, B) extracted ion chromatogram (EIC) for octreotide, m/z 1020.1 and C) UV chromatogram

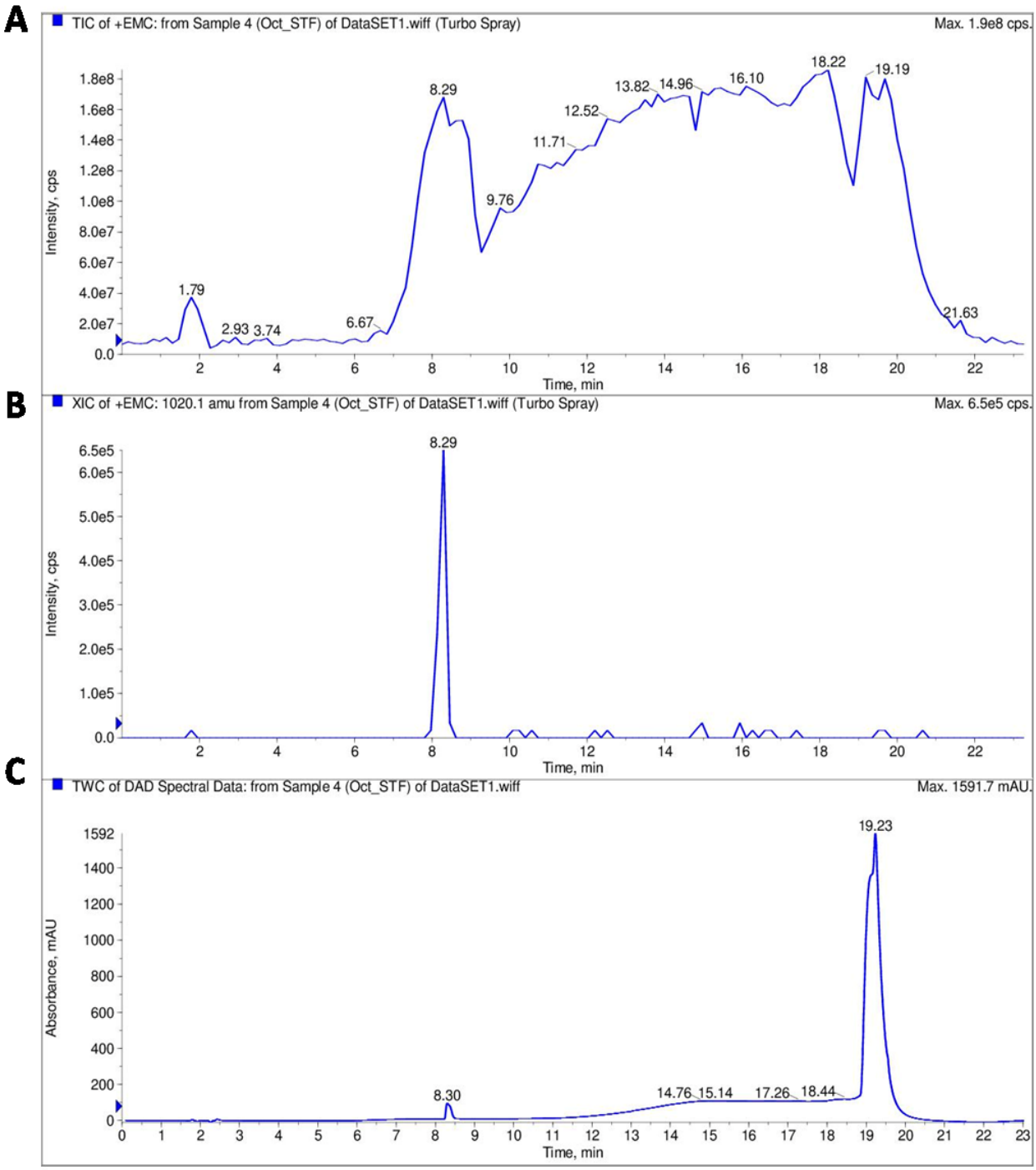

Figure 7-12 HPLC-MS spectrum of release sample (Day 27) from multi-layered nanomicelles in STF: A) total ion current (TIC) chromatogram for the enhanced multiply charged (EMC) scan, B) extracted ion chromatogram (EIC) for octreotide, m/z 1020.1 and C) UV chromatogram

7.6.6. Effect of release media on drug release

In addition to the development of suitable apparatus to assess in vitro drug release, selection of an appropriate release media cannot be overlooked. In contrast to oral dosage forms where release media typically mimics pH of the gastrointestinal tract, release media selection for nano-sized dosage forms vary depending on the site of administration and site of action of the formulation. We have utilized two released media in here: PBST i.e. PBST containing 0.002 wt. % Tween 20 in order to solubilize the hydrophobic prodrug and STF containing 0.5 wt. % Tween-80 which closely mimics the tear fluid i.e. the site of administration. Results from *in vitro* release studies indicated significantly higher rate of prodrug release in STF ($k=0.1239\ hr^{-1}$) in comparison to PBST ($k=0.1045\ hr^{-1}$). Such behavior could be attributed to improved solubilization of the hydrophobic prodrug resulting from higher concentration of surfactant (Tween-80) in the release media, STF. In contrary, the higher concentration of Tween-80 in STF interfered with the hydrophilic drug release and thus significantly lowered the release rate in STF ($k=0.1599\ hr^{-1}$) in comparison to PBST ($k=0.4810\ hr^{-1}$).

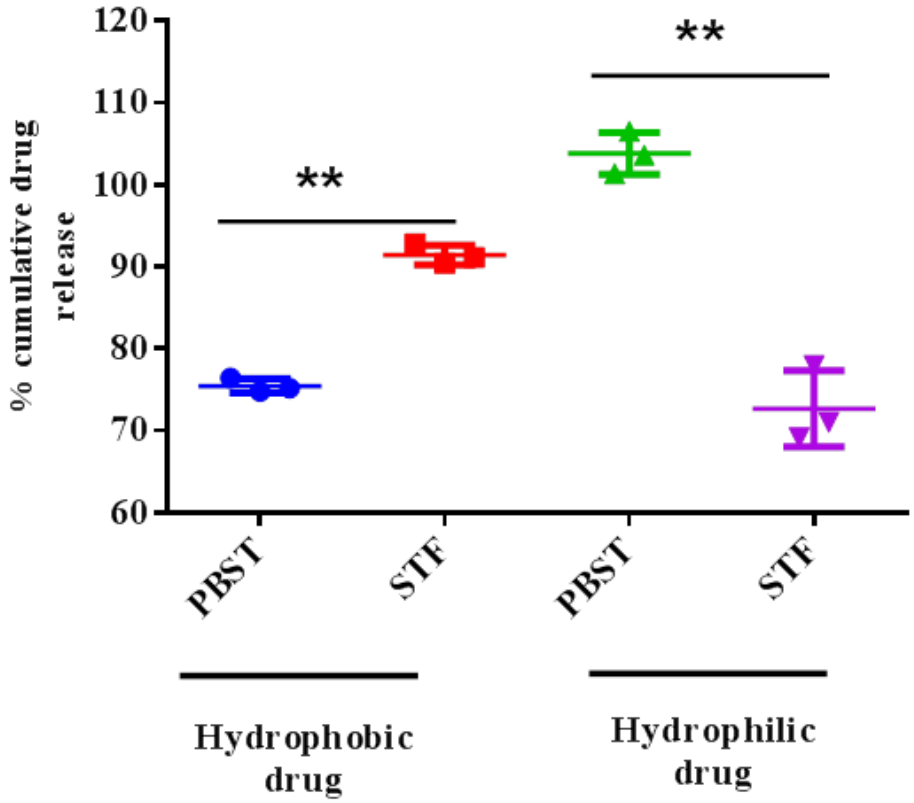

Figure 7-13 Cumulative drug release (percentage) in PBST and STF (pH 7.4) from hydrophobic (B-C12-cCDF) and hydrophilic (octreotide)-loaded nanomicelles for 34 and 11 days respectively using dialysis membrane with molecular weight 2kDa. The standard deviation for each data point was averaged over three samples (n=3)

7.6.7. Cell cytotoxicity

A major drawback of polymer based delivery vehicles is the often observed high cell toxicity. Polymer toxicity increases with increasing cationic charge density and flexibility[364]. Cell toxicity is caused when normal cell activities are constrained by accumulation of cationic charges at cell surface or internal compartments thus leading to high osmotic pressure. We investigated the potential toxicity of the multi-layered nanomicelles using a cell viability assay. At the lowest tested concentrations, we observed 100% cell viability for the multi-layered nanomicelles as well as for the individual polymers in all the three cell lines. While, OC-40 did not exhibit any toxicity in D407 and CCL 20.2 cells, a slight decrease in cell viability was observed in RF/6A endothelial cells. Increase in HCO-40 concentration led to decrease in cell viability as expected. The multi-layered nanomicelles gradually lowered cell viability, while HCO-40 at higher concentrations reached a minimum plateau of ~15% and ~25% cell viability in D407 and CCL 20.2 cells respectively. The toxicity results can also be explained in terms of IC50 values, which is the concentration required to cause toxicity in the 50% of the cells measured. As shown in Figure 7-14 the multi-layered nanomicelles showed IC50 larger than the individual polymer, HCO-40 in D407 cells. However, highest concentrations of OC-40 and the multi-layered nanomicelles did not reach IC50 values in CCL 20.2 and RF/6A cells. The lower toxicity in RF/6A endothelial cells in contrast to D407 and CCL 20.2 epithelial cells could be attributed to low paracellular permeability of endothelial cells. In fact, the residues generated from the nanomicellar formulation following a slower release pattern and increased residence time might generate limited toxicity to other ocular tissues due to the biocompatible nature of the surfactants/polymers at lower concentrations. Additionally, utilization of these

surfactants/polymers has recently demonstrated improved biocompatibility in Phase 3 human clinical trials (NCT02845674).

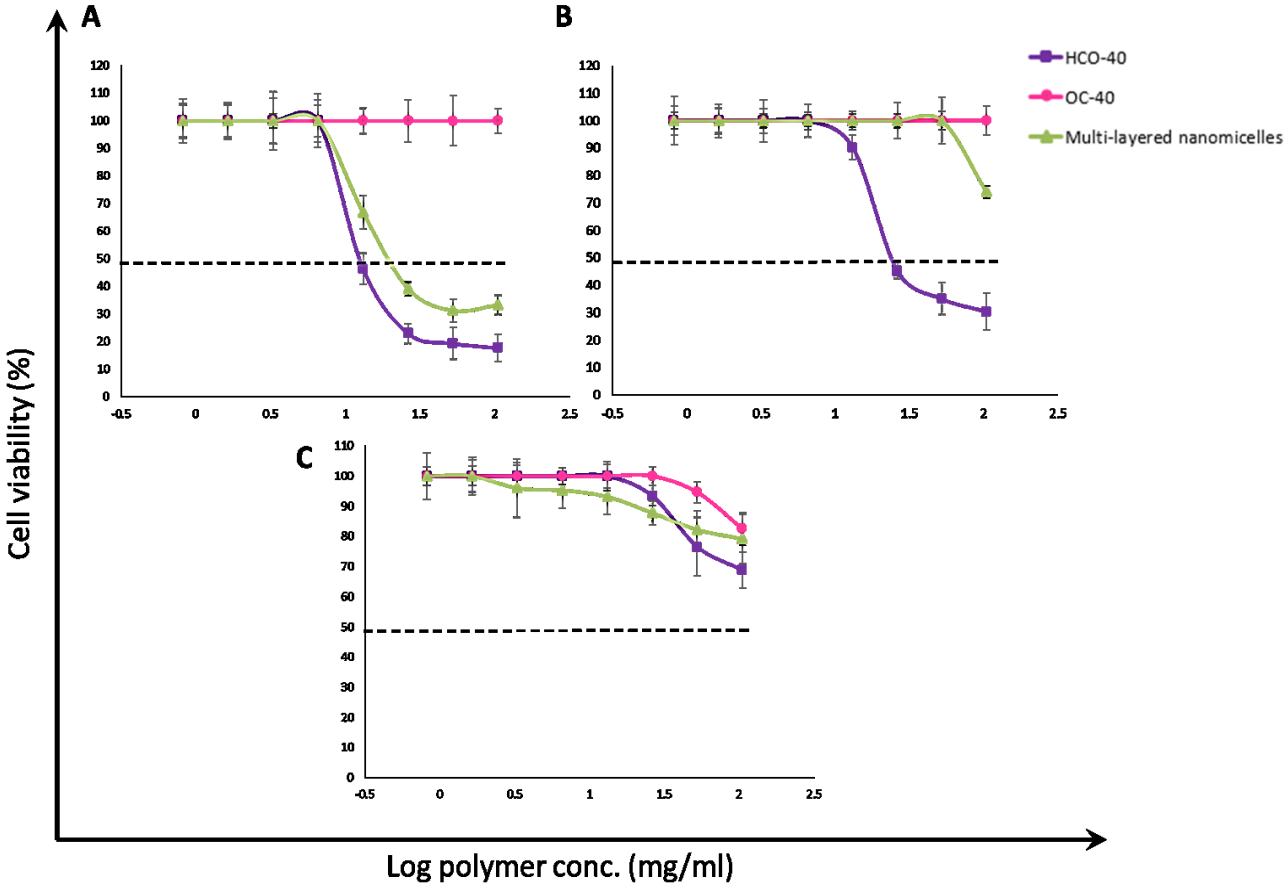

Figure 7-14 MTT assay of multi-layered nanomicelles prepared with HCO-40/OC-40 polymers to evaluate the toxicity in A) D407, B) CCL 20.2 and C) RF/6A cell lines. Data represent mean ± S.D (n= 8)

7.6.8. Intracellular accumulation of multi-layered nanomicelles

To exploit the potential of multi-layered nanomicelles, cellular uptake of a hydrophilic dye, rhodamine and rhodamine loaded multi-layered nanomicelles were compared with the hydrophobic dye, coumarin-6 loaded nanomicelles by FCM (Figure 7-15). The cellular uptake in D407, CCL 20.2 and RF/6A cells was validated by incubating the cell lines with various treatment groups for 0.5, 2, 6, 12 and 24 h (Table 7-5). Coumarin-6 and coumarin-6 loaded nanomicelles generated ~15-20 fold higher accumulation compared to rhodamine and rhodamine loaded multi-layered nanomicelles in D407 and CCL 20.2 cell lines. The difference in cell accumulation of coumarin-6 and coumarin-6-loaded nanomicelles was much higher (~100 fold) in RF/6A cell line in comparison to rhodamine and rhodamine loaded multi-layered nanomicelles (Figure 7-16). Coumarin-6 being hydrophobic in nature generated much higher loading into the hydrophobic core of nanomicelles and permeated effectively into the cells in comparison to rhodamine. The lower intracellular accumulation of rhodamine could be attributed to lower loading in the hydrophilic core of multi-layered nanomicelles and loss of drug during cell processing. The massive difference in accumulation of rhodamine and coumarin-6 in RF/6A is due to low paracellular permeability of the endothelial cells, which is in accordance with the in vitro cytotoxicity results. Most importantly, since octreotide, is 20 times more effective than the native somatostatin in suppressing growth hormone (GH) release, even lower concentrations of octreotide generated from the multi-layered nanomicellar formulation (0.078% octreotide) is anticipated to induce significant therapeutic effects in the back of the eye. In addition, lower concentrations of octreotide (0.40 mg/kg*h) following continuous subcutaneous (sc) infusion have shown to reduce serum GH levels by 3.5-fold in patients[156]. Considering the improved in-vivo cyclosporine (CsA) concentrations generated in

the retina (13.03 ng/ml) by the nanomicellar formulations (0.1% CsA) developed in our laboratory[248] and the tremendous potency of octreotide in reducing GH levels, this octreotide-loaded nanomicellar constructs presents a novel approach for delivering therapeutic peptides and thus holds remarkable potential in impeding the progression of PDR.

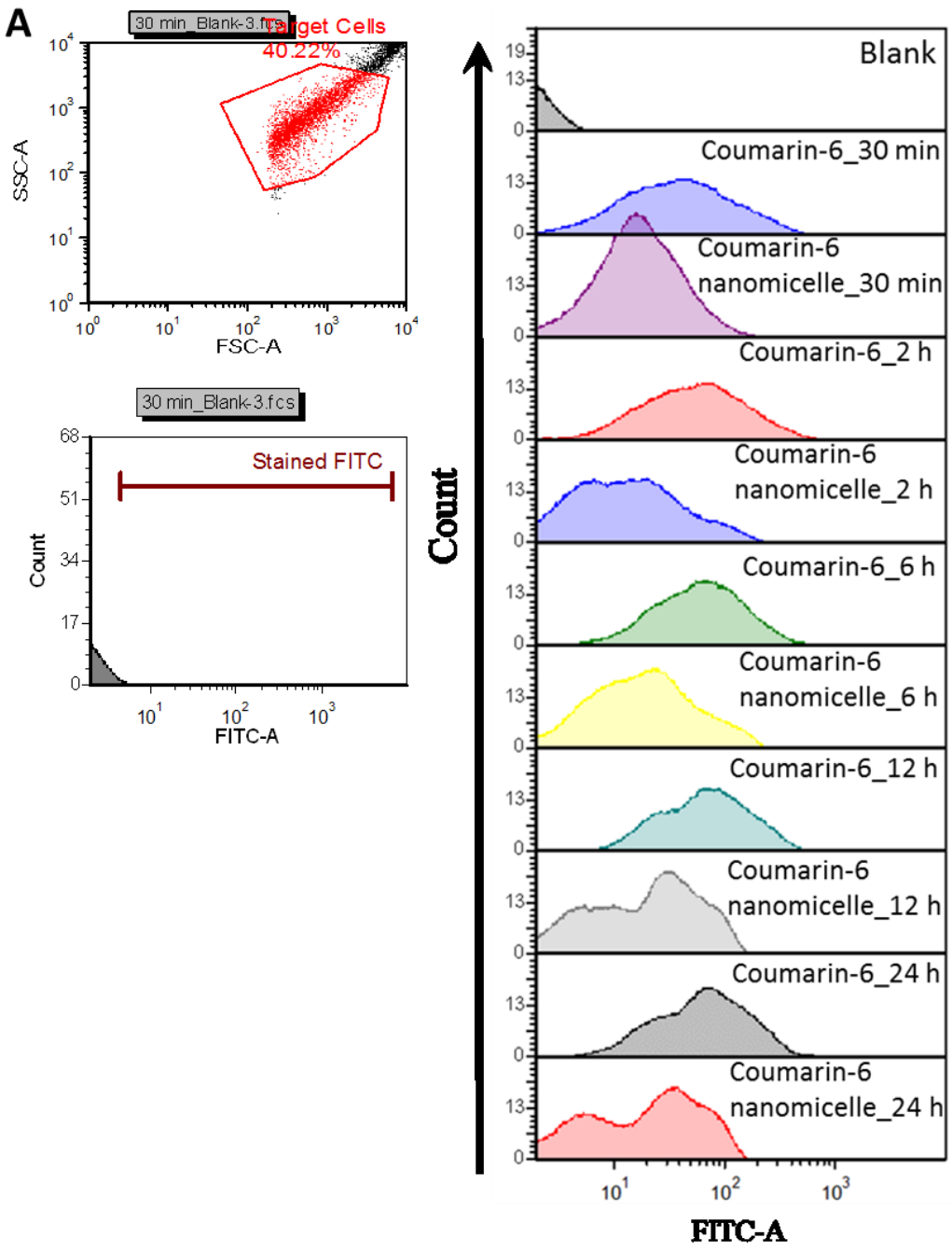
A
30 min_Blank-3.fcs
Target Cells
40.22%
SSC-A
FSC-A
30 min_Blank-3.fcs
Stained FITC
Count
FITC-A
Count
Blank
Coumarin-6_30 min
Coumarin-6 nanomicelle_30 min
Coumarin-6_2 h
Coumarin-6 nanomicelle_2 h
Coumarin-6_6 h
Coumarin-6 nanomicelle_6 h
Coumarin-6_12 h
Coumarin-6 nanomicelle_12 h
Coumarin-6_24 h
Coumarin-6 nanomicelle_24 h
FITC-A

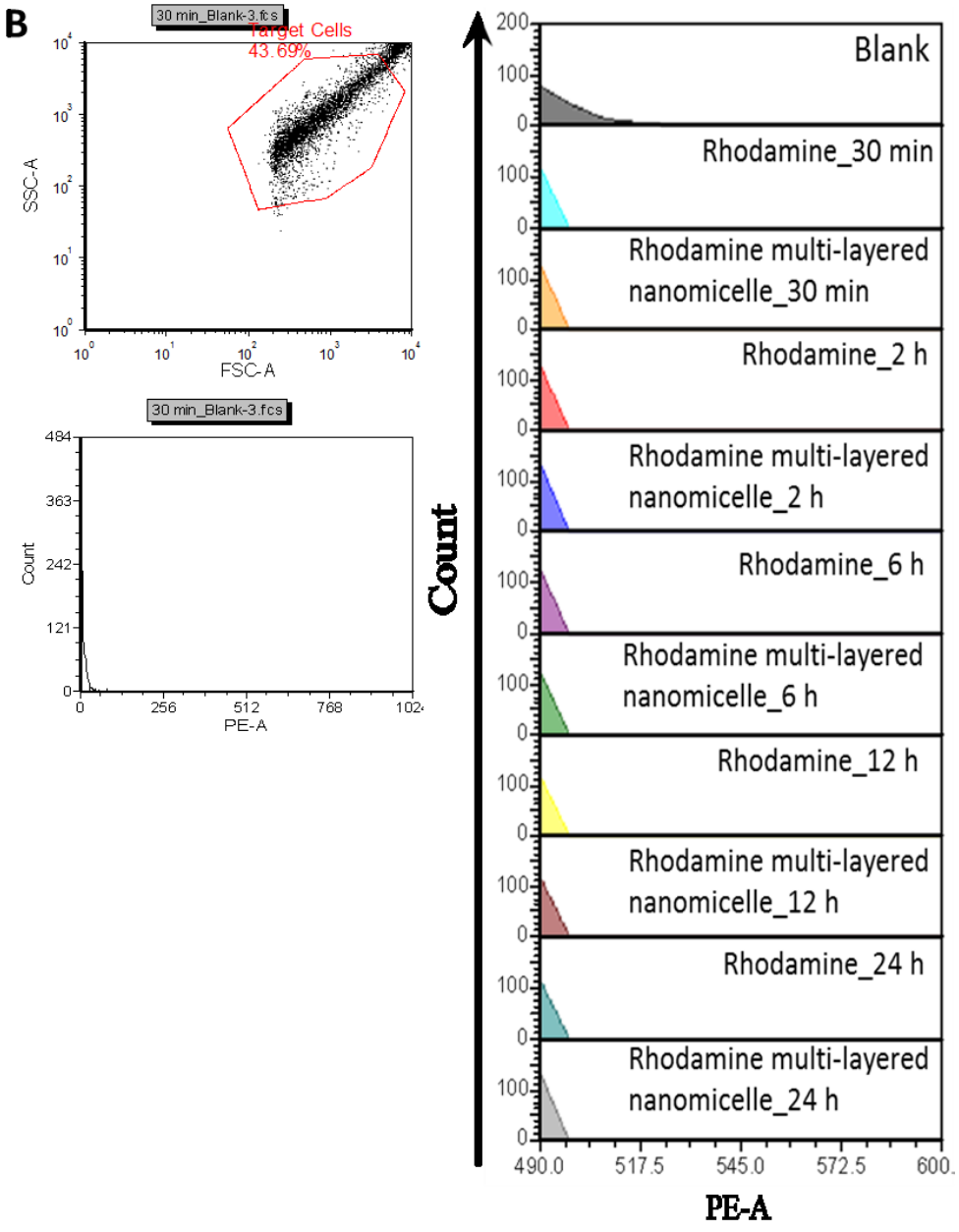

Figure 7-15 FACS histogram for A) coumarin-6, coumarin-6-loaded nanomicelles and B) rhodamine, rhodamine-loaded multi-layered nanomicelles in CCL 20.2 cells. Data represent mean ± S.D (n= 3-4)

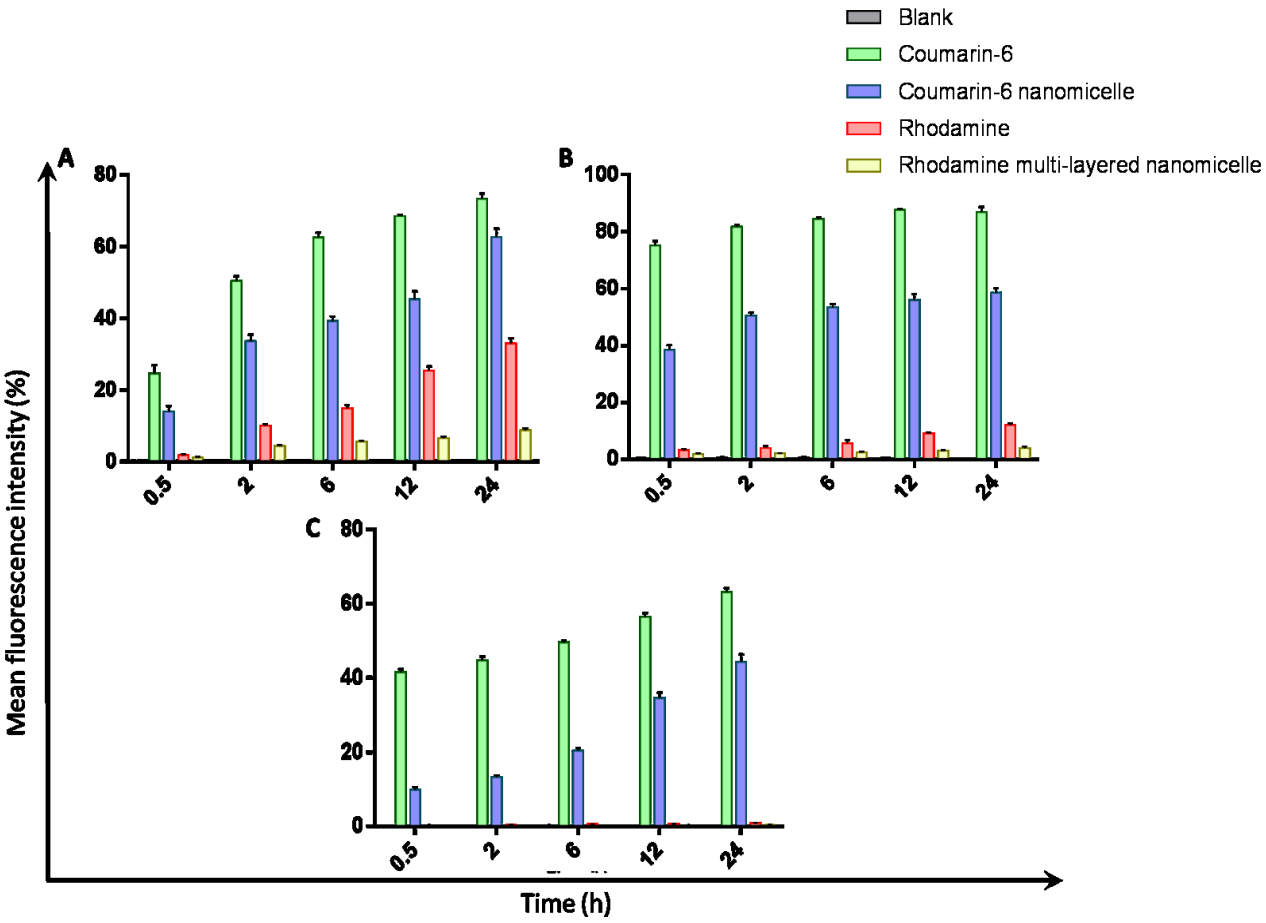

Figure 7-16 Intracellular accumulation of multi-layered nanomicelles: FACS analysis of rhodamine and rhodamine-loaded multi-layered nanomicelles in comparison to coumarin-6 and coumarin-6-loaded nanomicelles in A) D407, B) CCL 20.2 and C) RF/6A cell lines. Data represent mean ± S.D (n= 3-4)

Table 7-5 Time dependent uptake of coumarin-6, coumarin-6-loaded nanomicelles, rhodamine and rhodamine-loaded multi-layered nanomicelles in A) D407, B) CCL 20.2 and C) RF/6A cell lines. Data represent mean ± S.D (n= 3-4)

Treatment groups	**D407**					**CCL 20.2**					**RF/6A**				
	0.5 h	2 h	6 h	12 h	24 h	0.5 h	2 h	6 h	12 h	24 h	0.5 h	2 h	6 h	12 h	24 h
Coumarin-6	24.53 ± 2.09	50.35 ± 1.25	62.53 ± 1.18	68.50 ± 0.34	73.33 ± 1.38	75.13 ± 1.33	81.60 ± 0.83	84.40 ± 0.43	87.55 ± 0.38	86.78 ± 1.60	41.53 ± 0.70	44.68 ± 0.95	49.50 ± 0.47	56.40 ± 0.92	63.08 ± 1.00
Coumarin-6 loaded nanomicelles	13.98 ± 1.34	33.58 ± 1.61	39.20 ± 1.12	45.20 ± 2.13	62.63 ± 2.00	38.45 ± 1.53	50.45 ± 0.96	53.40 ± 0.98	55.88 ± 1.98	58.45 ± 1.54	9.85 ± 0.63	13.25 ± 0.47	20.35 ± 0.72	34.53 ± 1.31	44.30 ± 1.78
Rhodamine	1.78 ± 0.26	10.05 ± 0.35	14.85 ± 0.80	25.38 ± 1.01	32.90 ± 1.33	3.18 ± 0.41	4.05 ± 0.50	5.65 ± 1.04	9.13 ± 0.19	12.05 ± 0.47	0.25 ± 0.05	0.38 ± 0.04	0.48 ± 0.04	0.58 ± 0.04	0.85 ± 0.05
Rhodamine loaded multi-layered nanomicelles	1.08 ± 0.18	4.28 ± 0.33	5.58 ± 0.20	6.60 ± 0.34	8.70 ± 0.44	1.85 ± 0.27	2.15 ± 0.05	2.48 ± 0.18	3.05 ± 0.11	3.98 ± 0.46	0.08 ± 0.04	0.08 ± 0.04	0.18 ± 0.04	0.25 ± 0.05	0.38 ± 0.04

7.7. Conclusion

For the first time, a combination of two polymers, HCO-40 and OC-40 was utilized to develop self-assembling multi-layered nanomicelles for sustained delivery of small peptides to back of the eye following topical application. The encapsulation method utilized a combination of hydrophilic interaction and solvent induced encapsulation to entrap high concentrations of octreotide within the hydrophilic core of the multi-layered nanomicelles. The compact micellar nanoconstructs sustained and prevented the degradation of octreotide over a long period. This is considered to be an important feature of the multi-layered nanomicelles, which can enhance long-term delivery of small peptides after topical administration. Additionally, easy and reproducible preparation steps, visual clarity, nanosize, improved loading capacity, stability and biocompatibility are requisite that render these self-assembling nanoconstructs an appealing delivery system for topical application of small peptides. The future modifications to the modular design may include extracellular targeting ligands to concentrate peptide-loaded multi-layered nanomicelles to a specific cell type or tissue. This study suggests a biocompatible and easy to fabricate small peptide vehicle and future in vivo studies will further establish feasibility of therapeutic peptides to treat various deadly “undruggable” diseases.

CHAPTER 8

8. SUMMARY AND RECOMMENDATIONS

8.1. Summary

Higher expression of efflux pumps on the human epithelial and brain capillary endothelial cells plays a significant role in the disposition of a wide range of therapeutics including HIV agents such as LPV. Poor aqueous solubility and higher affinity towards drug efflux pumps and metabolizing enzymes (CYP3A4) pose a major challenge to LPV delivery. This dissertation project provides an expedient strategy to improve oral and possibly brain absorption of LPV using a prodrug approach. Chemical modifications of LPV by conjugating amino acid or peptide moieties resulted in significant uptake and evasion of efflux pumps such as P-gp and MRP2. In addition, these chemically modified prodrugs were recognized by more than one influx or nutrient transport systems at a time, highly expressed on the intestinal epithelial and brain capillary endothelial cells. Interestingly, prodrugs generated superior aqueous solubility relative to LPV. Leu-LPV and His-Leu-LPV prodrugs demonstrated lower affinity towards P-gp and MRP2 relative to LPV. Both the prodrugs were found to be highly stable at lower pHs but hydrolyzed rapidly at pH 7.4 relative to pH 4. His-Leu-LPV exhibited both PepT1 and PHT1 transporter-mediated cellular uptake. Enzymatic hydrolysis studies revealed a steady regeneration of Leu-LPV and LPV from His-Leu-LPV with significant contribution by esterases in comparison to peptidases. Overall, histidine based peptide prodrug of LPV with dual targeting properties is a state-of-the-art strategy to ameliorate oral and possibly brain absorption of LPV.

Such strategy of targeting influx or nutrient transport systems has further led to development of a topical self-assembling nanomicellar formulation of a highly potent

transporter targeted prodrug of cyclic cidofovir for cytomegalovirus retinitis (CMV, an infection of retina in AIDS patients).

In contrast to numerous examples of successful ocular drug delivery (ODD) systems, nanomicelles have gained significant interest in the past decade for back of the eye delivery. Drug delivery especially to the intraocular tissues following topical administration is highly challenging due to the complex structure of the eye. The high aqueous solubility of nanomicellar formulations allows them to traverse through trans-scleral pathway rather than trans-corneal route to deliver drugs to the intraocular tissues. B-C12-cCDF, prodrug although being highly potent, has low aqueous solubility and faces the wrath of being detected by RES and efflux pumps. In order to overcome such shortcomings, a nanomicellar formulation of B-C12-cCDF was developed using solvent evaporation-rehydration method. Statistical DOE was utilized to screen and achieve desired formulation with highest loading and entrapment and minimal micellar size and PDI. Biocompatibility of the polymers and prodrug-loaded nanomicelles by in vitro cell cytotoxicity (MTT, LDH and ELISA) in ocular cell lines suggests that the prodrug-loaded nanomicelle might be safe for ODD. Interestingly, B-C12-cCDF-loaded nanomicelles efficiently internalized into D407 and HCE-T cells in 24 h. Significant transport across in-vitro corneal-retinal model with a release period of ~33 days indicated the potential of nanomicelles in delivering anti-viral prodrugs for prolonged periods to the back of the eye.

Exploiting the nature of such a promising delivery systems, nanomicelles have allowed us to explore their potential in entrapping hydrophilic peptides and proteins. Poor chemical and physical stability and short circulating plasma half-lives are major challenges in biologic or macromolecule delivery. Additionally, acylation at the lysine residue by degraded products of

PLGA polymers further impede delivery of proteins and peptides in their native forms. Therefore, self-assembling multi-layered nanomicelles were generated to entrap octreotide using a combination of hydrophilic interaction and solvent-induced encapsulation. In the first step, entrapment of the octreotide in the hydrophilic core of the organo-nanomicelle was achieved in chloroform followed by addition of a protective aqueous solubilizing layer on the surface of the organo-nanomicelle. The resulting multi-layered nanomicellar system comprised of three regions: hydrophilic core: peptide/polymer, intermediate hydrophobic layer, and outer hydrophilic shell. The multi-layered nanomicelle displayed a size range of ~16-20 nm with zeta potential close to neutral (~-2.44-0.39 mV) at different polymer concentrations. Negligible toxicity was observed at lower concentrations in various ocular cell lines with sustained release of octreotide for 27 and 11 days in STF and PBST respectively in native form. This work demonstrated an all-biologic nanocarrier capable of delivering functional native biologic for the treatment of a wide variety of diseases.

8.2. Recommendations

For improving oral absorption: In the present study, histidine based peptide prodrug was developed to improve oral and possibly brain absorption of LPV. Although, the dual targeted approach is promising, certain modifications or strategies may be employed to facilitate drug penetration into HIV reservoirs and reduce systemic toxicities.

L-enantiomers of histidine and leucine were utilized herein. Although, L-forms are associated with improved affinity towards influx transporters, D-stereo isomeric prodrugs can be synthesized to improve the stability of the prodrugs. For instance, D-histidine-L-leuine-

LPV (DL-LPV) and L-histidine-D-leucine-LPV (LDLPV) can be developed to promote metabolic as well as enzymatic stability of prodrugs.

For long-term prodrug delivery: With the advent of long-acting parenteral (LAP) antiretroviral (ARV) drugs, ARV prodrugs may be nanoformulated (e.g. Poloxamer 407) to facilitate monocyte-macrophage entry, retention and intracellular drug-depot formation. This strategy may not only provide long-term protection against HIV challenge, but also serve to extend viral restriction in other HIV residing tissues including lymph nodes and gut associated lymphoid tissues and spleen (peptide/histidine transporter, PHT2 is localized in the lymphatic system as well).

For both receptor and transporter mediated prodrug delivery: TAT peptide, a small polypeptide of 86 amino acids derived from HIV-1 may be used as a targeting ligand for ARV prodrug nanoformulations. TAT peptide will allow receptor-mediated permeation of the nanoformulation into the cell membrane while the released prodrug will traverse through transporter-mediated mechanism, allowing much higher concentrations across the BBB in HIV residing tissues.

For topical ocular hydrophobic molecule delivery: In this project, biotin receptors targeted prodrug of cidofovir (B-C12-cCDF) was encapsulated into nanomicelles for retinal drug delivery. The available free hydroxyl group of one of the polymers, OC-40 may be conjugated to ascorbic acid to target the high-affinity ascorbate transporters expressed on the retina for drug delivery.

For topical ocular biologic delivery: Hydrophobic-ion pairing (HIP) complexation can help in neutralizing the charges on proteins and peptides rendering them insoluble in aqueous solvents. Such an approach may help in improving the loading capacity of proteins and peptides and further delaying the release to more than a month from nanomicelles.

Another alternative approach may be to suspend the multi-layered nanomicelles in a clear thermoresponsive gel. This strategy may allow better retention, minimization of precorneal loss and sustained release of hydrophilic peptides and proteins from the multi-layered nanomicelles in gel to the back of the eye.

Evaluation of efficacy of octreotide-loaded multi-layered micelles using choroid sprouting assay: Choroid sprouting assay is highly reproducible and pertinent to angiogenesis research, particularly in the neovascular AMD field. The choroid sprouting assay can be used to evaluate pro- and anti-angiogenic pharmacological interventions. Importantly, the choroid sprouting assay allows for analysis of the interaction between choroidal endothelial cells and their adjacent cells (e.g. RPE cells) to uncover mechanisms that control choroidal vascular growth of specific relevance (but not exclusively) to sub-retinal proliferative disorders. RPE/choroid/sclera complex obtained from enucleated eyes from mice can be embedded in matrigel and evaluated for microvascular sprouts after pretreatment with octreotide and octreotide-loaded multi-layered nanomicelles.

APPENDIX

SPRINGER NATURE LICENSE TERMS AND CONDITIONS

Jun 26, 2018

This Agreement between Abhirup Mandal ("You") and Springer Nature ("Springer Nature") consists of your license details and the terms and conditions provided by Springer Nature and Copyright Clearance Center.

License Number	4376570300049
License date	Jun 26, 2018
Licensed Content Publisher	Springer Nature
Licensed Content Publication	Nature Reviews Immunology
Licensed Content Title	Vaccines: New hope for an aids vaccine
Licensed Content Author	Harriet L. Robinson
Licensed Content Date	Apr 1, 2002
Licensed Content Volume	2
Licensed Content Issue	4
Type of Use	Thesis/Dissertation
Requestor type	academic/university or research institute
Format	print and electronic
Portion	figures/tables/illustrations
Number of figures/tables/illustrations	1
High-res required	no
Will you be translating?	no
Circulation/distribution	>50,000
Author of this Springer Nature content	no
Title	NOVEL PRODRUGS AND SELF-ASSEMBLING NANOCARRIERS TO IMPROVE DRUG DELIVERY
Instructor name	Ashim K. Mitra
Institution name	University of Missouri-Kansas City
Expected presentation date	Oct 2018
Portions	Figure 1A
Requestor Location	Abhirup Mandal 2464 Charlotte Street (HSB-5258) UMKC School of Pharmacy Division of Pharmaceutical Sciences KANSAS CITY, MO 64108 United States Attn: Abhirup Mandal
Billing Type	Invoice
Billing Address	Abhirup Mandal 2464 Charlotte Street (HSB-5258) UMKC School of Pharmacy Division of Pharmaceutical Sciences

SPRINGER NATURE LICENSE TERMS AND CONDITIONS

Jun 26, 2018

This Agreement between Abhirup Mandal ("You") and Springer Nature ("Springer Nature") consists of your license details and the terms and conditions provided by Springer Nature and Copyright Clearance Center.

License Number	4376570645130
License date	Jun 26, 2018
Licensed Content Publisher	Springer Nature
Licensed Content Publication	Nature Reviews Microbiology
Licensed Content Title	A mechanistic theory to explain the efficacy of antiretroviral therapy
Licensed Content Author	Sarah B. Laskey, Robert F. Siliciano
Licensed Content Date	Sep 29, 2014
Licensed Content Volume	12
Licensed Content Issue	11
Type of Use	Thesis/Dissertation
Requestor type	academic/university or research institute
Format	print and electronic
Portion	figures/tables/illustrations
Number of figures/tables/illustrations	1
High-res required	no
Will you be translating?	no
Circulation/distribution	>50,000
Author of this Springer Nature content	no
Title	NOVEL PRODRUGS AND SELF-ASSEMBLING NANOCARRIERS TO IMPROVE DRUG DELIVERY
Instructor name	Ashim K. Mitra
Institution name	University of Missouri-Kansas City
Expected presentation date	Oct 2018
Portions	Figure 1
Requestor Location	Abhirup Mandal 2464 Charlotte Street (HSB-5258) UMKC School of Pharmacy Division of Pharmaceutical Sciences KANSAS CITY, MO 64108 United States Attn: Abhirup Mandal
Billing Type	Invoice
Billing Address	Abhirup Mandal 2464 Charlotte Street (HSB-5258) UMKC School of Pharmacy Division of Pharmaceutical Sciences

SPRINGER NATURE LICENSE TERMS AND CONDITIONS

Jun 26, 2018

This Agreement between Abhirup Mandal ("You") and Springer Nature ("Springer Nature") consists of your license details and the terms and conditions provided by Springer Nature and Copyright Clearance Center.

License Number	4376580091984
License date	Jun 26, 2018
Licensed Content Publisher	Springer Nature
Licensed Content Publication	Nature Reviews Drug Discovery
Licensed Content Title	Strategies in the design of antiviral drugs
Licensed Content Author	Erik De Clercq
Licensed Content Date	Jan 1, 2002
Licensed Content Volume	1
Licensed Content Issue	1
Type of Use	Thesis/Dissertation
Requestor type	academic/university or research institute
Format	print and electronic
Portion	figures/tables/illustrations
Number of figures/tables/illustrations	1
High-res required	no
Will you be translating?	no
Circulation/distribution	>50,000
Author of this Springer Nature content	no
Title	NOVEL PRODRUGS AND SELF-ASSEMBLING NANOCARRIERS TO IMPROVE DRUG DELIVERY
Instructor name	Ashim K. Mitra
Institution name	University of Missouri-Kansas City
Expected presentation date	Oct 2018
Portions	Figure 4C
Requestor Location	Abhirup Mandal 2464 Charlotte Street (HSB-5258) UMKC School of Pharmacy Division of Pharmaceutical Sciences KANSAS CITY, MO 64108 United States Attn: Abhirup Mandal
Billing Type	Invoice
Billing Address	Abhirup Mandal 2464 Charlotte Street (HSB-5258) UMKC School of Pharmacy Division of Pharmaceutical Sciences

SPRINGER NATURE LICENSE TERMS AND CONDITIONS

Jun 26, 2018

This Agreement between Abhirup Mandal ("You") and Springer Nature ("Springer Nature") consists of your license details and the terms and conditions provided by Springer Nature and Copyright Clearance Center.

License Number	4376581442447
License date	Jun 26, 2018
Licensed Content Publisher	Springer Nature
Licensed Content Publication	Treatments in Endocrinology
Licensed Content Title	The Potential Role of Octreotide in the Treatment of Diabetic Retinopathy
Licensed Content Author	Maria B. Grant, Sergio Caballero
Licensed Content Date	Jan 1, 2005
Licensed Content Volume	4
Licensed Content Issue	4
Type of Use	Thesis/Dissertation
Requestor type	academic/university or research institute
Format	print and electronic
Portion	figures/tables/illustrations
Number of figures/tables/illustrations	1
Will you be translating?	no
Circulation/distribution	>50,000
Author of this Springer Nature content	no
Title	NOVEL PRODRUGS AND SELF-ASSEMBLING NANOCARRIERS TO IMPROVE DRUG DELIVERY
Instructor name	Ashim K. Mitra
Institution name	University of Missouri-Kansas City
Expected presentation date	Oct 2018
Portions	Figure 2
Requestor Location	Abhirup Mandal 2464 Charlotte Street (HSB-5258) UMKC School of Pharmacy Division of Pharmaceutical Sciences KANSAS CITY, MO 64108 United States Attn: Abhirup Mandal
Billing Type	Invoice
Billing Address	Abhirup Mandal 2464 Charlotte Street (HSB-5258) UMKC School of Pharmacy Division of Pharmaceutical Sciences

BENTHAM SCIENCE PUBLISHERS LTD. ORDER DETAILS

May 29, 2018

Order Number	501401106
Order date	May 16, 2018
Licensed content publisher	Bentham Science Publishers Ltd.
Licensed content title	CURRENT DRUG TARGETS
Licensed content date	Jan 1, 2000
Type of Use	Thesis/Dissertation
Requestor type	Academic institution
Format	Print, Electronic
Portion	chapter/article
The requesting person/organization is:	Abhirup Mandal/University of Missouri-Kansas City
Title or numeric reference of the portion(s)	Full article
Title of the article or chapter the portion is from	Design of Lipophilic Prodrugs to Improve Drug Delivery and Efficacy
Editor of portion(s)	N/A
Author of portion(s)	Abhirup Mandal, Mitesh Patel, Ye Sheng, Ashim K. Mitra
Volume of serial or monograph.	17
Issue, if republishing an article from a serial	15
Page range of the portion	
Publication date of portion	Dec 1, 2016
Rights for	Main Product, any product related to main product, and other compilations/derivative products
Duration of use	Life of current and all future editions
Creation of copies for the disabled	yes
With minor editing privileges	yes
For distribution to	Worldwide
In the following language(s)	Original language of publication
With incidental promotional use	yes
The lifetime unit quantity of new product	More than 2,000,000
Title	DECIPHERING NOVEL PRODRUGS AND SELF-ASSEMBLING NANOCARRIERS FOR HIV AND OCULAR COMPLICATIONS
Instructor name	Ashim K. Mitra
Institution name	University of Missouri-Kansas City
Expected presentation date	Oct 2018
Total (may include CCC user fee)	0.00 USD

American Society for Clinical Investigation LICENSE TERMS AND CONDITIONS

Jul 02, 2018

This is a License Agreement between Abhirup Mandal ("You") and American Society for Clinical Investigation ("American Society for Clinical Investigation") provided by Copyright Clearance Center ("CCC"). The license consists of your order details, the terms and conditions provided by American Society for Clinical Investigation, and the payment terms and conditions.

All payments must be made in full to CCC. For payment instructions, please see information listed at the bottom of this form.

License Number	4380880348943
License date	Jun 26, 2018
Licensed content publisher	American Society for Clinical Investigation
Licensed content title	JOURNAL OF CLINICAL INVESTIGATION. ONLINE
Licensed content date	Dec 31, 1969
Type of Use	Thesis/Dissertation
Requestor type	Academic institution
Format	Print, Electronic
Portion	image/photo
Number of images/photos requested	1
The requesting person/organization is:	Abhirup Mandal/University of Missouri-Kansas City
Title or numeric reference of the portion(s)	Figure 1A
Title of the article or chapter the portion is from	Diabetic retinopathy: current understanding, mechanisms, and treatment strategies.
Editor of portion(s)	N/A
Author of portion(s)	Duh EJ, Sun JK, Stitt AW
Volume of serial or monograph.	Volume 2
Issue, if republishing an article from a serial	Issue 14
Page range of the portion	Page 3
Publication date of portion	July 20, 2017
Rights for	Main product
Duration of use	Life of current and all future editions
Creation of copies for the disabled	no
With minor editing privileges	yes
For distribution to	Worldwide
In the following language(s)	Original language of publication

With incidental promotional use	no
The lifetime unit quantity of new product	More than 2,000,000
Title	NOVEL PRODRUGS AND SELF-ASSEMBLING NANOCARRIERS TO IMPROVE DRUG DELIVERY
Instructor name	Ashim K. Mitra
Institution name	University of Missouri-Kansas City
Expected presentation date	Oct 2018
Billing Type	Invoice
Billing Address	Abhirup Mandal 2464 Charlotte Street (HSB-5258) UMKC School of Pharmacy Division of Pharmaceutical Sciences KANSAS CITY, MO 64108 United States Attn: Abhirup Mandal
Total (may include CCC user fee)	0.00 USD

SPRINGER SCIENCE AND BUS MEDIA B V ORDER DETAILS

Dec 06, 2018

Order Number	501448934
Order date	Dec 05, 2018
Licensed content publisher	Springer Science and Bus Media B V
Licensed content title	AAPS PharmSciTech
Licensed content date	Jan 1, 2000
Type of Use	Thesis/Dissertation
Requestor type	Academic institution
Format	Print, Electronic
Portion	chapter/article
The requesting person/organization is:	Abhirup Mandal/UMKC
Title or numeric reference of the portion(s)	Complete article
Title of the article or chapter the portion is from	Multi-layered nanomicelles as self-assembled nanocarrier systems for ocular peptide delivery
Editor of portion(s)	Robert O. Williams III
Author of portion(s)	Abhirup Mandal
Volume of serial or monograph.	N/A
Page range of the portion	
Publication date of portion	2018
Rights for	Main product
Duration of use	Life of current and all future editions
Creation of copies for the disabled	no
With minor editing privileges	yes
For distribution to	Worldwide
In the following language(s)	Original language of publication
With incidental promotional use	no
The lifetime unit quantity of new product	More than 2,000,000
Title	NOVEL PRODRUGS AND SELF-ASSEMBLING NANOCARRIERS TO IMPROVE DRUG DELIVERY
Institution name	University of Missouri-Kansas City
Expected presentation date	Dec 2018
Total (may include CCC user fee)	Not Available

REFERENCES

1. Duh, E. J.; Sun, J. K.; Stitt, A. W., Diabetic retinopathy: Current understanding, mechanisms, and treatment strategies. *JCI Insight* **2017,** *2* (14).

2. Keunen, J. E.; Rothova, A., Images in clinical medicine. Cytomegalovirus retinitis in aids. *N Engl J Med* **1995,** *333* (10), 637.

3. Grant, M. B.; Caballero, S., Jr., The potential role of octreotide in the treatment of diabetic retinopathy. *Treat Endocrinol* **2005,** *4* (4), 199-203.

4. Robinson, H. L., New hope for an aids vaccine. *Nat Rev Immunol* **2002,** *2* (4), 239-50.

5. Laskey, S. B.; Siliciano, R. F., A mechanistic theory to explain the efficacy of antiretroviral therapy. *Nat Rev Microbiol* **2014,** *12* (11), 772-80.

6. De Clercq, E., Strategies in the design of antiviral drugs. *Nat Rev Drug Discov* **2002,** *1* (1), 13-25.

7. Mahato, R.; Tai, W.; Cheng, K., Prodrugs for improving tumor targetability and efficiency. *Adv Drug Deliv Rev* **2011,** *63* (8), 659-70.

8. Rautio, J.; Kumpulainen, H.; Heimbach, T.; Oliyai, R.; Oh, D.; Jarvinen, T.; Savolainen, J., Prodrugs: Design and clinical applications. *Nat Rev Drug Discov* **2008,** *7* (3), 255-70.

9. Huttunen, K. M.; Raunio, H.; Rautio, J., Prodrugs--from serendipity to rational design. *Pharmacol Rev* **2011,** *63* (3), 750-71.

10. Al-Jabri, A. A., Mechanisms of host resistance against hiv infection and progression to aids. *Sultan Qaboos Univ Med J* **2007,** *7* (2), 82-96.

11. Deeks, S. G.; Lewin, S. R.; Havlir, D. V., The end of aids: Hiv infection as a chronic disease. *Lancet* **2013,** *382* (9903), 1525-33.

12. Eisinger, R. W.; Fauci, A. S., Ending the hiv/aids pandemic(1). *Emerg Infect Dis* **2018,** *24* (3), 413-416.

13. Corey, L.; Gray, G. E., Preventing acquisition of hiv is the only path to an aids-free generation. *Proc Natl Acad Sci U S A* **2017,** *114* (15), 3798-3800.

14. German Advisory Committee Blood, Human immunodeficiency virus (hiv). *Transfus Med Hemother* **2016,** *43* (3), 203-22.

15. Gamble, T. R.; Yoo, S.; Vajdos, F. F.; von Schwedler, U. K.; Worthylake, D. K.; Wang, H.; McCutcheon, J. P.; Sundquist, W. I.; Hill, C. P., Structure of the carboxyl-terminal dimerization domain of the hiv-1 capsid protein. *Science* **1997,** *278* (5339), 849-53.

16. Huang, M.; Orenstein, J. M.; Martin, M. A.; Freed, E. O., P6gag is required for particle production from full-length human immunodeficiency virus type 1 molecular clones expressing protease. *J Virol* **1995,** *69* (11), 6810-8.

17. Karn, J.; Stoltzfus, C. M., Transcriptional and posttranscriptional regulation of hiv-1 gene expression. *Cold Spring Harb Perspect Med* **2012,** *2* (2), a006916.

18. Malim, M. H.; Emerman, M., Hiv-1 accessory proteins--ensuring viral survival in a hostile environment. *Cell Host Microbe* **2008,** *3* (6), 388-98.

19. Dube, M.; Bego, M. G.; Paquay, C.; Cohen, E. A., Modulation of hiv-1-host interaction: Role of the vpu accessory protein. *Retrovirology* **2010,** *7*, 114.

20. Luban, J., Absconding with the chaperone: Essential cyclophilin-gag interaction in hiv-1 virions. *Cell* **1996,** *87* (7), 1157-9.

21. Sutton, J.; Dotson, D.; Dong, X., Molecular events in late stages of hiv-1 replication. *JSM Microbiol* **2013,** *1* (1).

22. Nisole, S.; Saib, A., Early steps of retrovirus replicative cycle. *Retrovirology* **2004,** *1*, 9.

23. Kumar, G. N.; Jayanti, V. K.; Johnson, M. K.; Uchic, J.; Thomas, S.; Lee, R. D.; Grabowski, B. A.; Sham, H. L.; Kempf, D. J.; Denissen, J. F.; Marsh, K. C.; Sun, E.; Roberts, S. A., Metabolism and disposition of the hiv-1 protease inhibitor lopinavir (abt-378) given in combination with ritonavir in rats, dogs, and humans. *Pharm Res* **2004,** *21* (9), 1622-30.

24. Mallick, P.; Taneja, G.; Moorthy, B.; Ghose, R., Regulation of drug-metabolizing enzymes in infectious and inflammatory disease: Implications for biologics-small molecule drug interactions. *Expert Opin Drug Metab Toxicol* **2017,** *13* (6), 605-616.

25. Patel, M.; Mandava, N.; Gokulgandhi, M.; Pal, D.; Mitra, A. K., Amino acid prodrugs: An approach to improve the absorption of hiv-1 protease inhibitor, lopinavir. *Pharmaceuticals (Basel)* **2014,** *7* (4), 433-52.

26. Miller, D. S.; Bauer, B.; Hartz, A. M., Modulation of p-glycoprotein at the blood-brain barrier: Opportunities to improve central nervous system pharmacotherapy. *Pharmacol Rev* **2008,** *60* (2), 196-209.

27. Loscher, W.; Potschka, H., Blood-brain barrier active efflux transporters: Atp-binding cassette gene family. *NeuroRx* **2005,** *2* (1), 86-98.

28. Vasiliou, V.; Vasiliou, K.; Nebert, D. W., Human atp-binding cassette (abc) transporter family. *Hum Genomics* **2009,** *3* (3), 281-90.

29. Dubrovskyi, O.; Birukova, A. A.; Birukov, K. G., Measurement of local permeability at subcellular level in cell models of agonist- and ventilator-induced lung injury. *Lab Invest* **2013,** *93* (2), 254-63.

30. Zhang, M. Q.; Wilkinson, B., Drug discovery beyond the 'rule-of-five'. *Curr Opin Biotechnol* **2007,** *18* (6), 478-88.

31. Matsson, P.; Doak, B. C.; Over, B.; Kihlberg, J., Cell permeability beyond the rule of 5. *Adv Drug Deliv Rev* **2016**.

32. Dobson, P. D.; Kell, D. B., Carrier-mediated cellular uptake of pharmaceutical drugs: An exception or the rule? *Nat Rev Drug Discov* **2008,** *7* (3), 205-20.

33. Mandal, A.; Patel, M.; Sheng, Y.; Mitra, A. K., Design of lipophilic prodrugs to improve drug delivery and efficacy. *Curr Drug Targets* **2015**.

34. Vadlapudi, A. D.; Vadlapatla, R. K.; Earla, R.; Sirimulla, S.; Bailey, J. B.; Pal, D.; Mitra, A. K., Novel biotinylated lipid prodrugs of acyclovir for the treatment of herpetic keratitis (hk): Transporter recognition, tissue stability and antiviral activity. *Pharm Res* **2013,** *30* (8), 2063-76.

35. Estudante, M.; Morais, J. G.; Soveral, G.; Benet, L. Z., Intestinal drug transporters: An overview. *Adv Drug Deliv Rev* **2013,** *65* (10), 1340-56.

36. Tucker, G. T.; Houston, J. B.; Huang, S. M., Optimizing drug development: Strategies to assess drug metabolism/transporter interaction potential--toward a consensus. *Pharm Res* **2001,** *18* (8), 1071-80.

37. Klaassen, C. D.; Aleksunes, L. M., Xenobiotic, bile acid, and cholesterol transporters: Function and regulation. *Pharmacol Rev* **2010,** *62* (1), 1-96.

38. Pardridge, W. M., The blood-brain barrier: Bottleneck in brain drug development. *NeuroRx* **2005,** *2* (1), 3-14.

39. Di, L.; Artursson, P.; Avdeef, A.; Ecker, G. F.; Faller, B.; Fischer, H.; Houston, J. B.; Kansy, M.; Kerns, E. H.; Kramer, S. D.; Lennernas, H.; Sugano, K., Evidence-based approach to assess passive diffusion and carrier-mediated drug transport. *Drug Discov Today* **2012,** *17* (15-16), 905-12.

40. Prime-Chapman, H. M.; Fearn, R. A.; Cooper, A. E.; Moore, V.; Hirst, B. H., Differential multidrug resistance-associated protein 1 through 6 isoform expression and function in human intestinal epithelial caco-2 cells. *J Pharmacol Exp Ther* **2004,** *311* (2), 476-84.

41. Shugarts, S.; Benet, L. Z., The role of transporters in the pharmacokinetics of orally administered drugs. *Pharm Res* **2009,** *26* (9), 2039-54.

42. Minocha, M.; Khurana, V.; Qin, B.; Pal, D.; Mitra, A. K., Enhanced brain accumulation of pazopanib by modulating p-gp and bcrp1 mediated efflux with canertinib or erlotinib. *Int J Pharm* **2012,** *436* (1-2), 127-34.

43. Minocha, M.; Khurana, V.; Qin, B.; Pal, D.; Mitra, A. K., Co-administration strategy to enhance brain accumulation of vandetanib by modulating p-glycoprotein (p-gp/abcb1) and breast cancer resistance protein (bcrp1/abcg2) mediated efflux with m-tor inhibitors. *Int J Pharm* **2012,** *434* (1-2), 306-14.

44. Dean, M.; Rzhetsky, A.; Allikmets, R., The human atp-binding cassette (abc) transporter superfamily. *Genome Res* **2001,** *11* (7), 1156-66.

45. Joseph, S.; Nicolson, T. J.; Hammons, G.; Word, B.; Green-Knox, B.; Lyn-Cook, B., Expression of drug transporters in human kidney: Impact of sex, age, and ethnicity. *Biol Sex Differ* **2015,** *6*, 4.

46. Tamai, I.; Saheki, A.; Saitoh, R.; Sai, Y.; Yamada, I.; Tsuji, A., Nonlinear intestinal absorption of 5-hydroxytryptamine receptor antagonist caused by absorptive and secretory transporters. *J Pharmacol Exp Ther* **1997,** *283* (1), 108-15.

47. Sjostedt, N.; Deng, F.; Rauvala, O.; Tepponen, T.; Kidron, H., Interaction of food additives with intestinal efflux transporters. *Mol Pharm* **2017,** *14* (11), 3824-3833.

48. Amin, M. L., P-glycoprotein inhibition for optimal drug delivery. *Drug Target Insights* **2013,** *7*, 27-34.

49. Kimura, Y.; Morita, S. Y.; Matsuo, M.; Ueda, K., Mechanism of multidrug recognition by mdr1/abcb1. *Cancer Sci* **2007,** *98* (9), 1303-10.

50. Schinkel, A. H., P-glycoprotein, a gatekeeper in the blood-brain barrier. *Adv Drug Deliv Rev* **1999,** *36* (2-3), 179-194.

51. Seelig, A., A general pattern for substrate recognition by p-glycoprotein. *Eur J Biochem* **1998,** *251* (1-2), 252-61.

52. Greiner, B.; Eichelbaum, M.; Fritz, P.; Kreichgauer, H. P.; von Richter, O.; Zundler, J.; Kroemer, H. K., The role of intestinal p-glycoprotein in the interaction of digoxin and rifampin. *J Clin Invest* **1999,** *104* (2), 147-53.

53. Hendrikse, N. H.; Schinkel, A. H.; de Vries, E. G.; Fluks, E.; Van der Graaf, W. T.; Willemsen, A. T.; Vaalburg, W.; Franssen, E. J., Complete in vivo reversal of p-glycoprotein pump function in the blood-brain barrier visualized with positron emission tomography. *Br J Pharmacol* **1998,** *124* (7), 1413-8.

54. Sasongko, L.; Link, J. M.; Muzi, M.; Mankoff, D. A.; Yang, X.; Collier, A. C.; Shoner, S. C.; Unadkat, J. D., Imaging p-glycoprotein transport activity at the human blood-brain barrier with positron emission tomography. *Clin Pharmacol Ther* **2005,** *77* (6), 503-14.

55. Dahan, A.; Amidon, G. L., Small intestinal efflux mediated by mrp2 and bcrp shifts sulfasalazine intestinal permeability from high to low, enabling its colonic targeting. *Am J Physiol Gastrointest Liver Physiol* **2009,** *297* (2), G371-7.

56. Leslie, E. M.; Deeley, R. G.; Cole, S. P., Multidrug resistance proteins: Role of p-glycoprotein, mrp1, mrp2, and bcrp (abcg2) in tissue defense. *Toxicol Appl Pharmacol* **2005,** *204* (3), 216-37.

57. Homolya, L.; Varadi, A.; Sarkadi, B., Multidrug resistance-associated proteins: Export pumps for conjugates with glutathione, glucuronate or sulfate. *Biofactors* **2003,** *17* (1-4), 103-14.

58. Schwenk, M. H.; Pai, A. B., Drug transporter function--implications in ckd. *Adv Chronic Kidney Dis* **2016,** *23* (2), 76-81.

59. Shibayama, Y.; Iwashita, Y.; Yoshikawa, Y.; Kondo, T.; Ikeda, R.; Takeda, Y.; Osada, T.; Sugawara, M.; Yamada, K.; Iseki, K., Effect of 5-fluorouracil treatment on sn-38 absorption from intestine in rats. *Biol Pharm Bull* **2011,** *34* (9), 1418-25.

60. Vlaming, M. L.; Mohrmann, K.; Wagenaar, E.; de Waart, D. R.; Elferink, R. P.; Lagas, J. S.; van Tellingen, O.; Vainchtein, L. D.; Rosing, H.; Beijnen, J. H.; Schellens, J. H.; Schinkel, A. H., Carcinogen and anticancer drug transport by mrp2 in vivo: Studies using mrp2 (abcc2) knockout mice. *J Pharmacol Exp Ther* **2006,** *318* (1), 319-27.

61. Ruiz, M. L.; Villanueva, S. S.; Luquita, M. G.; Pellegrino, J. M.; Rigalli, J. P.; Arias, A.; Sanchez Pozzi, E. J.; Mottino, A. D.; Catania, V. A., Induction of intestinal multidrug resistance-associated protein 2 (mrp2) by spironolactone in rats. *Eur J Pharmacol* **2009,** *623* (1-3), 103-6.

62. Ni, Z.; Bikadi, Z.; Rosenberg, M. F.; Mao, Q., Structure and function of the human breast cancer resistance protein (bcrp/abcg2). *Curr Drug Metab* **2010,** *11* (7), 603-17.

63. International Transporter, C.; Giacomini, K. M.; Huang, S. M.; Tweedie, D. J.; Benet, L. Z.; Brouwer, K. L.; Chu, X.; Dahlin, A.; Evers, R.; Fischer, V.; Hillgren, K. M.; Hoffmaster, K. A.; Ishikawa, T.; Keppler, D.; Kim, R. B.; Lee, C. A.; Niemi, M.; Polli, J. W.; Sugiyama, Y.; Swaan, P. W.; Ware, J. A.; Wright, S. H.; Yee, S. W.; Zamek-Gliszczynski, M. J.; Zhang, L., Membrane transporters in drug development. *Nat Rev Drug Discov* **2010,** *9* (3), 215-36.

64. Peroni, R. N.; Di Gennaro, S. S.; Hocht, C.; Chiappetta, D. A.; Rubio, M. C.; Sosnik, A.; Bramuglia, G. F., Efavirenz is a substrate and in turn modulates the expression of the efflux transporter abcg2/bcrp in the gastrointestinal tract of the rat. *Biochem Pharmacol* **2011,** *82* (9), 1227-33.

65. Johnston, R. A.; Rawling, T.; Chan, T.; Zhou, F.; Murray, M., Selective inhibition of human solute carrier transporters by multikinase inhibitors. *Drug Metab Dispos* **2014,** *42* (11), 1851-7.

66. Roth, M.; Obaidat, A.; Hagenbuch, B., Oatps, oats and octs: The organic anion and cation transporters of the slco and slc22a gene superfamilies. *Br J Pharmacol* **2012,** *165* (5), 1260-87.

67. Pelis, R. M.; Wright, S. H., Slc22, slc44, and slc47 transporters--organic anion and cation transporters: Molecular and cellular properties. *Curr Top Membr* **2014,** *73*, 233-61.

68. Smith, D. E.; Clemencon, B.; Hediger, M. A., Proton-coupled oligopeptide transporter family slc15: Physiological, pharmacological and pathological implications. *Mol Aspects Med* **2013,** *34* (2-3), 323-36.

69. Agu, R.; Cowley, E.; Shao, D.; Macdonald, C.; Kirkpatrick, D.; Renton, K.; Massoud, E., Proton-coupled oligopeptide transporter (pot) family expression in human nasal epithelium and their drug transport potential. *Mol Pharm* **2011,** *8* (3), 664-72.

70. Zwarycz, B.; Wong, E. A., Expression of the peptide transporters pept1, pept2, and pht1 in the embryonic and posthatch chick. *Poult Sci* **2013,** *92* (5), 1314-21.

71. Jain, R.; Duvvuri, S.; Kansara, V.; Mandava, N. K.; Mitra, A. K., Intestinal absorption of novel-dipeptide prodrugs of saquinavir in rats. *Int J Pharm* **2007,** *336* (2), 233-40.

72. Lindley, D. J.; Carl, S. M.; Mowery, S. A.; Knipp, G. T., The evaluation of peptide/histidine transporter 1 (pht1) function: Uptake kinetics utilizing a cos-7 stably transfected cell line. *Rev Mex Cienc Farm* **2011,** *42* (4), 57-65.

73. Wang, X. X.; Hu, Y.; Keep, R. F.; Toyama-Sorimachi, N.; Smith, D. E., A novel role for pht1 in the disposition of l-histidine in brain: In vitro slice and in vivo pharmacokinetic studies in wildtype and pht1 null mice. *Biochem Pharmacol* **2017,** *124*, 94-102.

74. Song, F.; Hu, Y.; Wang, Y.; Smith, D. E.; Jiang, H., Functional characterization of human peptide/histidine transporter 1 in stably transfected mdck cells. *Mol Pharm* **2018,** *15* (2), 385-393.

75. Yamashita, T.; Shimada, S.; Guo, W.; Sato, K.; Kohmura, E.; Hayakawa, T.; Takagi, T.; Tohyama, M., Cloning and functional expression of a brain peptide/histidine transporter. *J Biol Chem* **1997,** *272* (15), 10205-11.

76. Yanagida, O.; Kanai, Y.; Chairoungdua, A.; Kim, D. K.; Segawa, H.; Nii, T.; Cha, S. H.; Matsuo, H.; Fukushima, J.; Fukasawa, Y.; Tani, Y.; Taketani, Y.; Uchino, H.; Kim, J. Y.; Inatomi, J.; Okayasu, I.; Miyamoto, K.; Takeda, E.; Goya, T.; Endou, H., Human l-type amino acid transporter 1 (lat1): Characterization of function and expression in tumor cell lines. *Biochim Biophys Acta* **2001,** *1514* (2), 291-302.

77. Geier, E. G.; Schlessinger, A.; Fan, H.; Gable, J. E.; Irwin, J. J.; Sali, A.; Giacomini, K. M., Structure-based ligand discovery for the large-neutral amino acid transporter 1, lat-1. *Proc Natl Acad Sci U S A* **2013,** *110* (14), 5480-5.

78. Hughes, P. J.; Cretton-Scott, E.; Teague, A.; Wensel, T. M., Protease inhibitors for patients with hiv-1 infection: A comparative overview. *P T* **2011,** *36* (6), 332-45.

79. Kis, O.; Robillard, K.; Chan, G. N.; Bendayan, R., The complexities of antiretroviral drug-drug interactions: Role of abc and slc transporters. *Trends Pharmacol Sci* **2010,** *31* (1), 22-35.

80. Christians, U., Transport proteins and intestinal metabolism: P-glycoprotein and cytochrome p4503a. *Ther Drug Monit* **2004,** *26* (2), 104-6.

81. Cvetkovic, R. S.; Goa, K. L., Lopinavir/ritonavir: A review of its use in the management of hiv infection. *Drugs* **2003,** *63* (8), 769-802.

82. Luo, S.; Wang, Z.; Patel, M.; Khurana, V.; Zhu, X.; Pal, D.; Mitra, A. K., Targeting svct for enhanced drug absorption: Synthesis and in vitro evaluation of a novel vitamin c conjugated prodrug of saquinavir. *Int J Pharm* **2011,** *414* (1-2), 77-85.

83. Chandwani, A.; Shuter, J., Lopinavir/ritonavir in the treatment of hiv-1 infection: A review. *Ther Clin Risk Manag* **2008,** *4* (5), 1023-33.

84. Senise, J. F.; Castelo, A.; Martinez, M., Current treatment strategies, complications and considerations for the use of hiv antiretroviral therapy during pregnancy. *AIDS Rev* **2011,** *13* (4), 198-213.

85. Bertrand, Y.; Capdeville, R.; Balduck, N.; Philippe, N., Cyclosporin a used to reverse drug resistance increases vincristine neurotoxicity. *Am J Hematol* **1992,** *40* (2), 158-9.

86. Kerr, D. J.; Graham, J.; Cummings, J.; Morrison, J. G.; Thompson, G. G.; Brodie, M. J.; Kaye, S. B., The effect of verapamil on the pharmacokinetics of adriamycin. *Cancer Chemother Pharmacol* **1986,** *18* (3), 239-42.

87. Wang, Z.; Pal, D.; Mitra, A. K., Stereoselective evasion of p-glycoprotein, cytochrome p450 3a, and hydrolases by peptide prodrug modification of saquinavir. *J Pharm Sci* **2012,** *101* (9), 3199-213.

88. Patel, M.; Sheng, Y.; Mandava, N. K.; Pal, D.; Mitra, A. K., Dipeptide prodrug approach to evade efflux pumps and cyp3a4 metabolism of lopinavir. *Int J Pharm* **2014,** *476* (1-2), 99-107.

89. Agarwal, S.; Boddu, S. H.; Jain, R.; Samanta, S.; Pal, D.; Mitra, A. K., Peptide prodrugs: Improved oral absorption of lopinavir, a hiv protease inhibitor. *Int J Pharm* **2008,** *359* (1-2), 7-14.

90. Talluri, R. S.; Gaudana, R.; Hariharan, S.; Mitra, A. K., Pharmacokinetics of stereoisomeric dipeptide prodrugs of acyclovir following intravenous and oral administrations in rats: A study involving in vivo corneal uptake of acyclovir following oral dosing. *Ophthalmol Eye Dis* **2009,** *1*, 21-31.

91. Anand, B. S.; Hill, J. M.; Dey, S.; Maruyama, K.; Bhattacharjee, P. S.; Myles, M. E.; Nashed, Y. E.; Mitra, A. K., In vivo antiviral efficacy of a dipeptide acyclovir prodrug, val-

val-acyclovir, against hsv-1 epithelial and stromal keratitis in the rabbit eye model. *Invest Ophthalmol Vis Sci* **2003,** *44* (6), 2529-34.

92. Kansara, V.; Hao, Y.; Mitra, A. K., Dipeptide monoester ganciclovir prodrugs for transscleral drug delivery: Targeting the oligopeptide transporter on rabbit retina. *J Ocul Pharmacol Ther* **2007,** *23* (4), 321-34.

93. Bhardwaj, R. K.; Herrera-Ruiz, D.; Eltoukhy, N.; Saad, M.; Knipp, G. T., The functional evaluation of human peptide/histidine transporter 1 (hpht1) in transiently transfected cos-7 cells. *Eur J Pharm Sci* **2006,** *27* (5), 533-42.

94. Hu, Y.; Xie, Y.; Keep, R. F.; Smith, D. E., Divergent developmental expression and function of the proton-coupled oligopeptide transporters pept2 and pht1 in regional brain slices of mouse and rat. *J Neurochem* **2014,** *129* (6), 955-65.

95. Herrera-Ruiz, D.; Wang, Q.; Gudmundsson, O. S.; Cook, T. J.; Smith, R. L.; Faria, T. N.; Knipp, G. T., Spatial expression patterns of peptide transporters in the human and rat gastrointestinal tracts, caco-2 in vitro cell culture model, and multiple human tissues. *AAPS PharmSci* **2001,** *3* (1), E9.

96. Patel, M.; Vadlapatla, R. K.; Shah, S.; Mitra, A. K., Molecular expression and functional activity of sodium dependent multivitamin transporter in human prostate cancer cells. *Int J Pharm* **2012,** *436* (1-2), 324-31.

97. Sahoo, S. K.; Dilnawaz, F.; Krishnakumar, S., Nanotechnology in ocular drug delivery. *Drug Discov Today* **2008,** *13* (3-4), 144-51.

98. Sengupta, S.; Kulkarni, A., Design principles for clinical efficacy of cancer nanomedicine: A look into the basics. *ACS Nano* **2013,** *7* (4), 2878-82.

99. De Jong, W. H.; Borm, P. J. A., Drug delivery and nanoparticles: Applications and hazards. *International Journal of Nanomedicine* **2008,** *3* (2), 133-149.

100. Edelhauser, H. F.; Rowe-Rendleman, C. L.; Robinson, M. R.; Dawson, D. G.; Chader, G. J.; Grossniklaus, H. E.; Rittenhouse, K. D.; Wilson, C. G.; Weber, D. A.; Kuppermann, B. D.; Csaky, K. G.; Olsen, T. W.; Kompella, U. B.; Holers, V. M.; Hageman, G. S.; Gilger, B. C.; Campochiaro, P. A.; Whitcup, S. M.; Wong, W. T., Ophthalmic drug delivery systems for the treatment of retinal diseases: Basic research to clinical applications. *Invest Ophthalmol Vis Sci* **2010,** *51* (11), 5403-5420.

101. Ahuja, M.; Dhake, A. S.; Sharma, S. K.; Majumdar, D. K., Topical ocular delivery of nsaids. *The AAPS Journal* **2008,** *10* (2), 229.

102. Gaynes, B. I.; Onyekwuluje, A., Topical ophthalmic nsaids: A discussion with focus on nepafenac ophthalmic suspension. *Clinical ophthalmology (Auckland, N.Z.)* **2008,** *2* (2), 355-368.

103. Mao, Y.; Kiss, S.; Boyer, J. L.; Hackett, N. R.; Qiu, J.; Carbone, A.; Mezey, J. G.; Kaminsky, S. M.; D'Amico, D. J.; Crystal, R. G., Persistent suppression of ocular neovascularization with intravitreal administration of aavrh.10 coding for bevacizumab. *Human Gene Therapy* **2011,** *22* (12), 1525-1535.

104. Jaissle, G. B.; Szurman, P.; Bartz-Schmidt, K. U., [ocular side effects and complications of intravitreal triamcinolone acetonide injection]. *Ophthalmologe* **2004,** *101* (2), 121-8.

105. Rotsos, T. G.; Moschos, M. M., Cystoid macular edema. *Clinical ophthalmology (Auckland, N.Z.)* **2008,** *2* (4), 919-930.

106. Han, S.; Shen, J.-q.; Gan, Y.; Geng, H.-m.; Zhang, X.-x.; Zhu, C.-l.; Gan, L., Novel vehicle based on cubosomes for ophthalmic delivery of flurbiprofen with low irritancy and high bioavailability. *Acta Pharmacologica Sinica* **2010,** *31* (8), 990-998.

107. Ahuja, M.; Dhake, A. S.; Sharma, S. K.; Majumdar, D. K., Topical ocular delivery of nsaids. *AAPS J* **2008,** *10* (2), 229-41.

108. Tiwari, G.; Tiwari, R.; Rai, A. K., Cyclodextrins in delivery systems: Applications. *J Pharm Bioallied Sci* **2010,** *2* (2), 72-9.

109. Kaur, I. P.; Kanwar, M., Ocular preparations: The formulation approach. *Drug Dev Ind Pharm* **2002,** *28* (5), 473-93.

110. Cabrera, M.; Yeh, S.; Albini, T. A., Sustained-release corticosteroid options. *J Ophthalmol* **2014,** *2014*, 164692.

111. Kempen, J. H.; Min, Y. I.; Freeman, W. R.; Holland, G. N.; Friedberg, D. N.; Dieterich, D. T.; Jabs, D. A.; Studies of Ocular Complications of, A. R. G., Risk of immune recovery uveitis in patients with aids and cytomegalovirus retinitis. *Ophthalmology* **2006,** *113* (4), 684-94.

112. Port, A. D.; Orlin, A.; Kiss, S.; Patel, S.; D'Amico, D. J.; Gupta, M. P., Cytomegalovirus retinitis: A review. *J Ocul Pharmacol Ther* **2017,** *33* (4), 224-234.

113. Stewart, M. W., Optimal management of cytomegalovirus retinitis in patients with aids. *Clin Ophthalmol* **2010,** *4*, 285-99.

114. Chamberlain, C. E.; Penzak, S. R.; Alfaro, R. M.; Wesley, R.; Daniels, C. E.; Hale, D.; Kirk, A. D.; Mannon, R. B., Pharmacokinetics of low and maintenance dose valganciclovir in kidney transplant recipients. *Am J Transplant* **2008,** *8* (6), 1297-302.

115. Pescovitz, M. D.; Rabkin, J.; Merion, R. M.; Paya, C. V.; Pirsch, J.; Freeman, R. B.; O'Grady, J.; Robinson, C.; To, Z.; Wren, K.; Banken, L.; Buhles, W.; Brown, F., Valganciclovir results in improved oral absorption of ganciclovir in liver transplant recipients. *Antimicrob Agents Chemother* **2000,** *44* (10), 2811-5.

116. Plosker, G. L.; Noble, S., Cidofovir: A review of its use in cytomegalovirus retinitis in patients with aids. *Drugs* **1999,** *58* (2), 325-45.

117. Xu, Y.; Johansson, M.; Karlsson, A., Human ump-cmp kinase 2, a novel nucleoside monophosphate kinase localized in mitochondria. *J Biol Chem* **2008,** *283* (3), 1563-71.

118. Squires, K. E., Oral ganciclovir for cytomegalovirus retinitis in patients with aids: Results of two randomized studies. *AIDS* **1996,** *10 Suppl 4*, S13-8.

119. Caruso Brown, A. E.; Cohen, M. N.; Tong, S.; Braverman, R. S.; Rooney, J. F.; Giller, R.; Levin, M. J., Pharmacokinetics and safety of intravenous cidofovir for life-threatening viral infections in pediatric hematopoietic stem cell transplant recipients. *Antimicrob Agents Chemother* **2015,** *59* (7), 3718-25.

120. Ray, A. S.; Cihlar, T.; Robinson, K. L.; Tong, L.; Vela, J. E.; Fuller, M. D.; Wieman, L. M.; Eisenberg, E. J.; Rhodes, G. R., Mechanism of active renal tubular efflux of tenofovir. *Antimicrob Agents Chemother* **2006,** *50* (10), 3297-304.

121. Patel, A.; Cholkar, K.; Agrahari, V.; Mitra, A. K., Ocular drug delivery systems: An overview. *World J Pharmacol* **2013,** *2* (2), 47-64.

122. Zhang, W.; Prausnitz, M. R.; Edwards, A., Model of transient drug diffusion across cornea. *J Control Release* **2004,** *99* (2), 241-58.

123. Tiffany, J. M., Tears in health and disease. *Eye (Lond)* **2003,** *17* (8), 923-6.

124. Reichl, S.; Kolln, C.; Hahne, M.; Verstraelen, J., In vitro cell culture models to study the corneal drug absorption. *Expert Opin Drug Metab Toxicol* **2011,** *7* (5), 559-78.

125. Urtti, A., Challenges and obstacles of ocular pharmacokinetics and drug delivery. *Adv Drug Deliv Rev* **2006,** *58* (11), 1131-5.

126. Mannermaa, E.; Vellonen, K. S.; Urtti, A., Drug transport in corneal epithelium and blood-retina barrier: Emerging role of transporters in ocular pharmacokinetics. *Adv Drug Deliv Rev* **2006,** *58* (11), 1136-63.

127. Liaw, J.; Robinson, J. R., The effect of polyethylene-glycol molecular-weight on corneal transport and the related influence of penetration enhancers. *Int J Pharm* **1992,** *88* (1-3), 125-140.

128. Barar, J.; Asadi, M.; Mortazavi-Tabatabaei, S. A.; Omidi, Y., Ocular drug delivery; impact of in vitro cell culture models. *J Ophthalmic Vis Res* **2009,** *4* (4), 238-52.

129. Hamalainen, K. M.; Kananen, K.; Auriola, S.; Kontturi, K.; Urtti, A., Characterization of paracellular and aqueous penetration routes in cornea, conjunctiva, and sclera. *Invest Ophthalmol Vis Sci* **1997,** *38* (3), 627-34.

130. Kim, Y. C.; Chiang, B.; Wu, X.; Prausnitz, M. R., Ocular delivery of macromolecules. *J Control Release* **2014,** *190*, 172-81.

131. Lee, J.; Pelis, R. M., Drug transport by the blood-aqueous humor barrier of the eye. *Drug Metab Dispos* **2016,** *44* (10), 1675-81.

132. Cunha-Vaz, J., The blood-ocular barriers. *Surv Ophthalmol* **1979,** *23* (5), 279-96.

133. van Bekkum, D. W., Use of ionizing radiation in transplantation. *Transplant Proc* **1974,** *6* (4 Suppl 1), 59-65.

134. Wu, K. M., A new classification of prodrugs: Regulatory perspectives. *Pharmaceuticals* **2009,** *2* (3), 77-81.

135. Zawilska, J. B.; Wojcieszak, J.; Olejniczak, A. B., Prodrugs: A challenge for the drug development. *Pharmacol Rep* **2013,** *65* (1), 1-14.

136. Li, F.; Maag, H.; Alfredson, T., Prodrugs of nucleoside analogues for improved oral absorption and tissue targeting. *J Pharm Sci* **2008,** *97* (3), 1109-34.

137. Liederer, B. M.; Borchardt, R. T., Enzymes involved in the bioconversion of ester-based prodrugs. *J Pharm Sci* **2006,** *95* (6), 1177-95.

138. Srinivas, N. R., The rationality for using prodrug approach in drug discovery programs for new xenobiotics: Opportunities and challenges. *Eur J Drug Metab Pharmacokinet* **2011,** *36* (2), 49-59.

139. Li, C.; Wallace, S., Polymer-drug conjugates: Recent development in clinical oncology. *Adv Drug Deliv Rev* **2008,** *60* (8), 886-98.

140. DeFeo-Jones, D.; Garsky, V. M.; Wong, B. K.; Feng, D. M.; Bolyar, T.; Haskell, K.; Kiefer, D. M.; Leander, K.; McAvoy, E.; Lumma, P.; Wai, J.; Senderak, E. T.; Motzel, S. L.; Keenan, K.; Van Zwieten, M.; Lin, J. H.; Freidinger, R.; Huff, J.; Oliff, A.; Jones, R. E., A peptide-doxorubicin 'prodrug' activated by prostate-specific antigen selectively kills prostate tumor cells positive for prostate-specific antigen in vivo. *Nat Med* **2000,** *6* (11), 1248-52.

141. Simplicio, A. L.; Clancy, J. M.; Gilmer, J. F., Beta-aminoketones as prodrugs with ph-controlled activation. *Int J Pharm* **2007,** *336* (2), 208-14.

142. Majumdar, S.; Sloan, K. B., Synthesis, hydrolyses and dermal delivery of n-alkyl-n-alkyloxycarbonylaminomethyl (nanaocam) derivatives of phenol, imide and thiol containing drugs. *Bioorg Med Chem Lett* **2006,** *16* (13), 3590-4.

143. Rouleau, A.; Garbarg, M.; Ligneau, X.; Mantion, C.; Lavie, P.; Advenier, C.; Lecomte, J. M.; Krause, M.; Stark, H.; Schunack, W.; Schwartz, J. C., Bioavailability, antinociceptive and antiinflammatory properties of bp 2-94, a histamine h3 receptor agonist prodrug. *J Pharmacol Exp Ther* **1997,** *281* (3), 1085-94.

144. Vadlapudi, A. D.; Vadlapatla, R. K.; Kwatra, D.; Earla, R.; Samanta, S. K.; Pal, D.; Mitra, A. K., Targeted lipid based drug conjugates: A novel strategy for drug delivery. *Int J Pharm* **2012,** *434* (1-2), 315-24.

145. Gokulgandhi, M. R.; Barot, M.; Bagui, M.; Pal, D.; Mitra, A. K., Transporter-targeted lipid prodrugs of cyclic cidofovir: A potential approach for the treatment of cytomegalovirus retinitis. *J Pharm Sci* **2012,** *101* (9), 3249-63.

146. Khurana, V.; Vadlapudi, A. D.; Vadlapatla, R. K.; Pal, D.; Mitra, A. K., Functional characterization and molecular identification of vitamin c transporter (svct2) in human corneal epithelial (hcec) and retinal pigment epithelial (d407) cells. *Curr Eye Res* **2015,** *40* (5), 457-69.

147. Khurana, V.; Kwatra, D.; Pal, D.; Mitra, A. K., Molecular expression and functional activity of vitamin c specific transport system (svct2) in human breast cancer cells. *Int J Pharm* **2014,** *474* (1-2), 14-24.

148. Khurana, V.; Minocha, M.; Pal, D.; Mitra, A. K., Role of oatp-1b1 and/or oatp-1b3 in hepatic disposition of tyrosine kinase inhibitors. *Drug Metabol Drug Interact* **2014,** *29* (3), 179-90.

149. Khurana, V.; Minocha, M.; Pal, D.; Mitra, A. K., Inhibition of oatp-1b1 and oatp-1b3 by tyrosine kinase inhibitors. *Drug Metabol Drug Interact* **2014,** *29* (4), 249-59.

150. Vadlapudi, A. D.; Vadlapatla, R. K.; Pal, D.; Mitra, A. K., Functional and molecular aspects of biotin uptake via smvt in human corneal epithelial (hcec) and retinal pigment epithelial (d407) cells. *AAPS J* **2012,** *14* (4), 832-42.

151. Vadlapudi, A. D.; Vadlapatla, R. K.; Mitra, A. K., Sodium dependent multivitamin transporter (smvt): A potential target for drug delivery. *Curr Drug Targets* **2012,** *13* (7), 994-1003.

152. Luo, S.; Kansara, V. S.; Zhu, X.; Mandava, N. K.; Pal, D.; Mitra, A. K., Functional characterization of sodium-dependent multivitamin transporter in mdck-mdr1 cells and its utilization as a target for drug delivery. *Mol Pharm* **2006,** *3* (3), 329-39.

153. Kansara, V.; Luo, S.; Balasubrahmanyam, B.; Pal, D.; Mitra, A. K., Biotin uptake and cellular translocation in human derived retinoblastoma cell line (y-79): A role of hsmvt system. *Int J Pharm* **2006,** *312* (1-2), 43-52.

154. Balamurugan, K.; Ortiz, A.; Said, H. M., Biotin uptake by human intestinal and liver epithelial cells: Role of the smvt system. *Am J Physiol Gastrointest Liver Physiol* **2003,** *285* (1), G73-7.

155. Janoria, K. G.; Hariharan, S.; Paturi, D.; Pal, D.; Mitra, A. K., Biotin uptake by rabbit corneal epithelial cells: Role of sodium-dependent multivitamin transporter (smvt). *Curr Eye Res* **2006,** *31* (10), 797-809.

156. Moller, D. E.; Moses, A. C.; Jones, K.; Thorner, M. O.; Vance, M. L., Octreotide suppresses both growth hormone (gh) and gh-releasing hormone (ghrh) in acromegaly due to ectopic ghrh secretion. *J Clin Endocrinol Metab* **1989,** *68* (2), 499-504.

157. Chatterjee, N. S.; Kumar, C. K.; Ortiz, A.; Rubin, S. A.; Said, H. M., Molecular mechanism of the intestinal biotin transport process. *Am J Physiol* **1999,** *277* (4 Pt 1), C605-13.

158. Prasad, P. D.; Wang, H.; Huang, W.; Fei, Y. J.; Leibach, F. H.; Devoe, L. D.; Ganapathy, V., Molecular and functional characterization of the intestinal na+-dependent multivitamin transporter. *Arch Biochem Biophys* **1999,** *366* (1), 95-106.

159. Lu, Y.; Park, K., Polymeric micelles and alternative nanonized delivery vehicles for poorly soluble drugs. *Int J Pharm* **2013,** *453* (1), 198-214.

160. Arnarson, T.; Elworthy, P. H., Effects of structural variations of non-ionic surfactants on micellar properties and solubilization: Surfactants based on erucyl and behenyl (c22) alcohols. *J Pharm Pharmacol* **1980,** *32* (6), 381-5.

161. Trivedi, R.; Kompella, U. B., Nanomicellar formulations for sustained drug delivery: Strategies and underlying principles. *Nanomedicine (Lond)* **2010,** *5* (3), 485-505.

162. Rios-Doria, J.; Carie, A.; Costich, T.; Burke, B.; Skaff, H.; Panicucci, R.; Sill, K., A versatile polymer micelle drug delivery system for encapsulation and in vivo stabilization of hydrophobic anticancer drugs. *J Drug Deliv* **2012,** *2012*, 951741.

163. Tadros, T. F., Microemulsions. In *Applied surfactants*, Wiley-VCH Verlag GmbH & Co. KGaA: 2005; pp 309-334.

164. Aliabadi, H. M.; Lavasanifar, A., Polymeric micelles for drug delivery. *Expert Opin Drug Deliv* **2006,** *3* (1), 139-62.

165. Owen, S. C.; Chan, D. P. Y.; Shoichet, M. S., Polymeric micelle stability. *Nano Today* **2012,** *7* (1), 53-65.

166. Torchilin, V. P., Structure and design of polymeric surfactant-based drug delivery systems. *J Control Release* **2001,** *73* (2-3), 137-72.

167. Deng, C.; Jiang, Y.; Cheng, R.; Meng, F.; Zhong, Z., Biodegradable polymeric micelles for targeted and controlled anticancer drug delivery: Promises, progress and prospects. *Nano Today* **2012,** *7* (5), 467-480.

168. Salvage, J. P.; Thom, C.; Lewis, A. L.; Phillips, G. J.; Lloyd, A. W., Nanoprecipitation of polymeric nanoparticle micelles based on 2-methacryloyloxyethyl phosphorylcholine (mpc) with 2-(diisopropylamino)ethyl methacrylate (dpa), for intracellular delivery applications. *J Mater Sci Mater Med* **2015,** *26* (3), 150.

169. Kwon, G. S.; Okano, T., Polymeric micelles as new drug carriers. *Adv Drug Deliver Rev* **1996,** *21* (2), 107-116.

170. Kedar, U.; Phutane, P.; Shidhaye, S.; Kadam, V., Advances in polymeric micelles for drug delivery and tumor targeting. *Nanomedicine* **2010,** *6* (6), 714-29.

171. Adams, M. L.; Lavasanifar, A.; Kwon, G. S., Amphiphilic block copolymers for drug delivery. *J Pharm Sci* **2003,** *92* (7), 1343-55.

172. Lin, J.; Zhu, J.; Chen, T.; Lin, S.; Cai, C.; Zhang, L.; Zhuang, Y.; Wang, X. S., Drug releasing behavior of hybrid micelles containing polypeptide triblock copolymer. *Biomaterials* **2009,** *30* (1), 108-17.

173. Bachu, R. D.; Chowdhury, P.; Al-Saedi, Z. H. F.; Karla, P. K.; Boddu, S. H. S., Ocular drug delivery barriers-role of nanocarriers in the treatment of anterior segment ocular diseases. *Pharmaceutics* **2018,** *10* (1).

174. Zhang, Y.; Li, Q.; Welsh, W. J.; Moghe, P. V.; Uhrich, K. E., Micellar and structural stability of nanoscale amphiphilic polymers: Implications for anti-atherosclerotic bioactivity. *Biomaterials* **2016,** *84*, 230-240.

175. Barz, M.; Luxenhofer, R.; Zentel, R.; Vicent, M. J., Overcoming the peg-addiction: Well-defined alternatives to peg, from structure-property relationships to better defined therapeutics. *Poly Chem* **2011,** *2* (9), 1900-1918.

176. Lu, J.; Choi, S.; Bates, F. S.; Lodge, T. P., Molecular exchange in diblock copolymer micelles: Bimodal distribution in core-block molecular weights. *ACS Macro Letters* **2012,** *1* (8), 982-985.

177. Kwon, G.; Suwa, S.; Yokoyama, M.; Okano, T.; Sakurai, Y.; Kataoka, K., Enhanced tumor accumulation and prolonged circulation times of micelle-forming poly (ethylene oxide-aspartate) block copolymer-adriamycin conjugates. *J Control Release* **1994,** *29* (1-2), 17-23.

178. Masayuki, Y.; Kwon, G. S.; Teruo, O.; Yasuhisa, S.; Mayumi, N.; Kazunori, K., Influencing factors on in vitro micelle stability of adriamycin-block copolymer conjugates. *Journal of Controlled Release* **1994,** *28* (1), 59-65.

179. Kwon, G. S.; Yokoyama, M.; Okano, T.; Sakurai, Y.; Kataoka, K., Biodistribution of micelle-forming polymer-drug conjugates. *Pharm Res* **1993,** *10* (7), 970-4.

180. Yokoyama, M.; Sugiyama, T.; Okano, T.; Sakurai, Y.; Naito, M.; Kataoka, K., Analysis of micelle formation of an adriamycin-conjugated poly(ethylene glycol)-poly(aspartic acid) block copolymer by gel permeation chromatography. *Pharm Res* **1993,** *10* (6), 895-9.

181. Yokoyama, M.; Miyauchi, M.; Yamada, N.; Okano, T.; Sakurai, Y.; Kataoka, K.; Inoue, S., Characterization and anticancer activity of the micelle-forming polymeric anticancer drug adriamycin-conjugated poly(ethylene glycol)-poly(aspartic acid) block copolymer. *Cancer Res* **1990,** *50* (6), 1693-700.

182. Talelli, M.; Barz, M.; Rijcken, C. J.; Kiessling, F.; Hennink, W. E.; Lammers, T., Core-crosslinked polymeric micelles: Principles, preparation, biomedical applications and clinical translation. *Nano Today* **2015,** *10* (1), 93-117.

183. Xu, W.; Ling, P.; Zhang, T., Polymeric micelles, a promising drug delivery system to enhance bioavailability of poorly water-soluble drugs. *J Drug Deliv* **2013,** *2013*, 340315.

184. Lu, Y.; Chowdhury, D.; Vladisavljevic, G. T.; Koutroumanis, K.; Georgiadou, S., Production of fluconazole-loaded polymeric micelles using membrane and microfluidic dispersion devices. *Membranes (Basel)* **2016,** *6* (2).

185. Yokoyama, M., Polymeric micelles as a new drug carrier system and their required considerations for clinical trials. *Expert Opin Drug Deliv* **2010,** *7* (2), 145-58.

186. Rapoport, N. Y.; Herron, J. N.; Pitt, W. G.; Pitina, L., Micellar delivery of doxorubicin and its paramagnetic analog, ruboxyl, to hl-60 cells: Effect of micelle structure and ultrasound on the intracellular drug uptake. *J Control Release* **1999,** *58* (2), 153-62.

187. Zhao, Y.; Liu, G.; Shen, J. X.; Aubry, A.-F., Reasons for calibration standard curve slope variation in lc–ms assays and how to address it. *Bioanalysis* **2014,** *6* (11), 1439-1443.

188. Kwon, G. S.; Naito, M.; Yokoyama, M.; Okano, T.; Sakurai, Y.; Kataoka, K., Physical entrapment of adriamycin in ab block copolymer micelles. *Pharm Res* **1995,** *12* (2), 192-5.

189. Yu, B. G.; Okano, T.; Kataoka, K.; Kwon, G., Polymeric micelles for drug delivery: Solubilization and haemolytic activity of amphotericin b. *J Control Release* **1998,** *53* (1-3), 131-6.

190. Lavasanifar, A.; Samuel, J.; Kwon, G. S., Micelles of poly(ethylene oxide)-block-poly(n-alkyl stearate l-aspartamide): Synthetic analogues of lipoproteins for drug delivery. *J Biomed Mater Res* **2000,** *52* (4), 831-5.

191. Kulthe, S. S.; Choudhari, Y. M.; Inamdar, N. N.; Mourya, V., Polymeric micelles: Authoritative aspects for drug delivery. *Designed Monomers and Polymers* **2012,** *15* (5), 465-521.

192. Dalwadi, G.; Benson, H. A.; Chen, Y., Comparison of diafiltration and tangential flow filtration for purification of nanoparticle suspensions. *Pharm Res* **2005,** *22* (12), 2152-62.

193. La, S. B.; Okano, T.; Kataoka, K., Preparation and characterization of the micelle-forming polymeric drug indomethacin-incorporated poly(ethylene oxide)-poly(beta-benzyl l-aspartate) block copolymer micelles. *J Pharm Sci* **1996,** *85* (1), 85-90.

194. Kataoka, K.; Matsumoto, T.; Yokoyama, M.; Okano, T.; Sakurai, Y.; Fukushima, S.; Okamoto, K.; Kwon, G. S., Doxorubicin-loaded poly(ethylene glycol)-poly(beta-benzyl-l-aspartate) copolymer micelles: Their pharmaceutical characteristics and biological significance. *J Control Release* **2000,** *64* (1-3), 143-53.

195. Djordjevic, J.; Michniak, B.; Uhrich, K. E., Amphiphilic star-like macromolecules as novel carriers for topical delivery of nonsteroidal anti-inflammatory drugs. *AAPS PharmSci* **2003,** *5* (4), 1-12.

196. Lavasanifar, A.; Samuel, J.; Kwon, G. S., The effect of fatty acid substitution on the in vitro release of amphotericin b from micelles composed of poly(ethylene oxide)-block-poly(n-hexyl stearate-l-aspartamide). *J Control Release* **2002,** *79* (1-3), 165-72.

197. Zhang, X.; Burt, H. M.; Von Hoff, D.; Dexter, D.; Mangold, G.; Degen, D.; Oktaba, A. M.; Hunter, W. L., An investigation of the antitumour activity and biodistribution of polymeric micellar paclitaxel. *Cancer Chemother Pharmacol* **1997,** *40* (1), 81-6.

198. Zhang, X. C.; Jackson, J. K.; Burt, H. M., Development of amphiphilic diblock copolymers as micellar carriers of taxol. *International Journal of Pharmaceutics* **1996,** *132* (1-2), 195-206.

199. Shuai, X.; Merdan, T.; Schaper, A. K.; Xi, F.; Kissel, T., Core-cross-linked polymeric micelles as paclitaxel carriers. *Bioconjug Chem* **2004,** *15* (3), 441-8.

200. Shuai, X.; Ai, H.; Nasongkla, N.; Kim, S.; Gao, J., Micellar carriers based on block copolymers of poly(epsilon-caprolactone) and poly(ethylene glycol) for doxorubicin delivery. *J Control Release* **2004,** *98* (3), 415-26.

201. Song, R.; Zhou, Y.; Li, Y.; Yang, Z.; Li, F.; Huang, Q.; Shi, T.; Zhang, G., Preparation and characterization of mpeg-g-α-zein biohybrid micelles as a nano-carrier. *Journal of Applied Polymer Science* **2015,** *132* (38), n/a-n/a.

202. Jette, K. K.; Law, D.; Schmitt, E. A.; Kwon, G. S., Preparation and drug loading of poly(ethylene glycol)-block-poly(epsilon-caprolactone) micelles through the evaporation of a cosolvent azeotrope. *Pharm Res* **2004,** *21* (7), 1184-91.

203. Le Garrec, D.; Gori, S.; Luo, L.; Lessard, D.; Smith, D. C.; Yessine, M. A.; Ranger, M.; Leroux, J. C., Poly(n-vinylpyrrolidone)-block-poly(d,l-lactide) as a new polymeric solubilizer for hydrophobic anticancer drugs: In vitro and in vivo evaluation. *J Control Release* **2004,** *99* (1), 83-101.

204. Nishiyama, N.; Yokoyama, M.; Aoyagi, T.; Okano, T.; Sakurai, Y.; Kataoka, K., Preparation and characterization of self-assembled polymer−metal complex micelle from cis-dichlorodiammineplatinum(ii) and poly(ethylene glycol)−poly(α,β-aspartic acid) block copolymer in an aqueous medium. *Langmuir* **1999,** *15* (2), 377-383.

205. Nishiyama, N.; Okazaki, S.; Cabral, H.; Miyamoto, M.; Kato, Y.; Sugiyama, Y.; Nishio, K.; Matsumura, Y.; Kataoka, K., Novel cisplatin-incorporated polymeric micelles can eradicate solid tumors in mice. *Cancer Res* **2003,** *63* (24), 8977-83.

206. Yuan, X.; Harada, A.; Yamasaki, Y.; Kataoka, K., Stabilization of lysozyme-incorporated polyion complex micelles by the omega-end derivatization of poly(ethylene

glycol)-poly(alpha,beta-aspartic acid) block copolymers with hydrophobic groups. *Langmuir* **2005,** *21* (7), 2668-74.

207. Wakebayashi, D.; Nishiyama, N.; Itaka, K.; Miyata, K.; Yamasaki, Y.; Harada, A.; Koyama, H.; Nagasaki, Y.; Kataoka, K., Polyion complex micelles of pdna with acetal-poly(ethylene glycol)-poly(2-(dimethylamino)ethyl methacrylate) block copolymer as the gene carrier system: Physicochemical properties of micelles relevant to gene transfection efficacy. *Biomacromolecules* **2004,** *5* (6), 2128-2136.

208. Hughes, P. M.; Olejnik, O.; Chang-Lin, J. E.; Wilson, C. G., Topical and systemic drug delivery to the posterior segments. *Adv Drug Deliv Rev* **2005,** *57* (14), 2010-32.

209. Lee, V. H.; Robinson, J. R., Topical ocular drug delivery: Recent developments and future challenges. *J Ocul Pharmacol* **1986,** *2* (1), 67-108.

210. Di Tommaso, C.; Bourges, J. L.; Valamanesh, F.; Trubitsyn, G.; Torriglia, A.; Jeanny, J. C.; Behar-Cohen, F.; Gurny, R.; Moller, M., Novel micelle carriers for cyclosporin a topical ocular delivery: In vivo cornea penetration, ocular distribution and efficacy studies. *Eur J Pharm Biopharm* **2012,** *81* (2), 257-64.

211. Luo, L.; Tam, J.; Maysinger, D.; Eisenberg, A., Cellular internalization of poly(ethylene oxide)-b-poly(epsilon-caprolactone) diblock copolymer micelles. *Bioconjug Chem* **2002,** *13* (6), 1259-65.

212. Allen, C.; Yu, Y.; Eisenberg, A.; Maysinger, D., Cellular internalization of pcl(20)-b-peo(44) block copolymer micelles. *Biochim Biophys Acta* **1999,** *1421* (1), 32-8.

213. Savic, R.; Luo, L.; Eisenberg, A.; Maysinger, D., Micellar nanocontainers distribute to defined cytoplasmic organelles. *Science* **2003,** *300* (5619), 615-8.

214. Li, J.; Li, Z.; Zhou, T.; Zhang, J.; Xia, H.; Li, H.; He, J.; He, S.; Wang, L., Positively charged micelles based on a triblock copolymer demonstrate enhanced corneal penetration. *Int J Nanomedicine* **2015,** *10*, 6027-37.

215. Cabral, H.; Miyata, K.; Osada, K.; Kataoka, K., Block copolymer micelles in nanomedicine applications. *Chem Rev* **2018,** *118* (14), 6844-6892.

216. Li, Y.; Kwon, G. S., Methotrexate esters of poly(ethylene oxide)-block-poly(2-hydroxyethyl-l-aspartamide). Part i: Effects of the level of methotrexate conjugation on the stability of micelles and on drug release. *Pharm Res* **2000,** *17* (5), 607-11.

217. Nishiyama, N.; Koizumi, F.; Okazaki, S.; Matsumura, Y.; Nishio, K.; Kataoka, K., Differential gene expression profile between pc-14 cells treated with free cisplatin and cisplatin-incorporated polymeric micelles. *Bioconjug Chem* **2003,** *14* (2), 449-57.

218. Matsuya, T.; Tashiro, S.; Hoshino, N.; Shibata, N.; Nagasaki, Y.; Kataoka, K., A core-shell-type fluorescent nanosphere possessing reactive poly(ethylene glycol) tethered chains on

the surface for zeptomole detection of protein in time-resolved fluorometric immunoassay. *Anal Chem* **2003,** *75* (22), 6124-32.

219. Lee, J.; Cho, E. C.; Cho, K., Incorporation and release behavior of hydrophobic drug in functionalized poly(d,l-lactide)-block-poly(ethylene oxide) micelles. *J Control Release* **2004,** *94* (2-3), 323-35.

220. Rapoport, N., Stabilization and activation of pluronic micelles for tumor-targeted drug delivery. *Colloids and Surfaces B-Biointerfaces* **1999,** *16* (1-4), 93-111.

221. Son, S.; Shin, E.; Kim, B. S., Light-responsive micelles of spiropyran initiated hyperbranched polyglycerol for smart drug delivery. *Biomacromolecules* **2014,** *15* (2), 628-34.

222. Yu, H. J.; Cui, Z. R.; Yu, P. C.; Guo, C. Y.; Feng, B.; Jiang, T. Y.; Wang, S. L.; Yin, Q.; Zhong, D. F.; Yang, X. L.; Zhang, Z. W.; Li, Y. P., Ph- and nir light-responsive micelles with hyperthermia-triggered tumor penetration and cytoplasm drug release to reverse doxorubicin resistance in breast cancer. *Adv Funct Mater* **2015,** *25* (17), 2489-2500.

223. Chen, C.-J.; Jin, Q.; Liu, G.-Y.; Li, D.-D.; Wang, J.-L.; Ji, J., Reversibly light-responsive micelles constructed via a simple modification of hyperbranched polymers with chromophores. *Polymer* **2012,** *53* (17), 3695-3703.

224. Yan, Q.; Hu, J.; Zhou, R.; Ju, Y.; Yin, Y.; Yuan, J., Visible light-responsive micelles formed from dialkoxyanthracene-containing block copolymers. *Chem Commun (Camb)* **2012,** *48* (13), 1913-5.

225. Denayer, T.; Stöhr, T.; Van Roy, M., Animal models in translational medicine: Validation and prediction. *New Horizons in Translational Medicine* **2014,** *2* (1), 5-11.

226. Bisht, R.; Jaiswal, J. K.; Chen, Y. S.; Jin, J.; Rupenthal, I. D., Light-responsive in situ forming injectable implants for effective drug delivery to the posterior segment of the eye. *Expert Opin Drug Deliv* **2016,** *13* (7), 953-62.

227. De Clercq, E., Clinical potential of the acyclic nucleoside phosphonates cidofovir, adefovir, and tenofovir in treatment of DNA virus and retrovirus infections. *Clin Microbiol Rev* **2003,** *16* (4), 569-96.

228. Chen, P.; Chen, H.; Zang, X.; Chen, M.; Jiang, H.; Han, S.; Wu, X., Expression of efflux transporters in human ocular tissues. *Drug Metab Dispos* **2013,** *41* (11), 1934-48.

229. Dahlin, A.; Geier, E.; Stocker, S. L.; Cropp, C. D.; Grigorenko, E.; Bloomer, M.; Siegenthaler, J.; Xu, L.; Basile, A. S.; Tang-Liu, D. D.; Giacomini, K. M., Gene expression profiling of transporters in the solute carrier and atp-binding cassette superfamilies in human eye substructures. *Mol Pharm* **2013,** *10* (2), 650-63.

230. Gonzalez, L.; Loza, R. J.; Han, K. Y.; Sunoqrot, S.; Cunningham, C.; Purta, P.; Drake, J.; Jain, S.; Hong, S.; Chang, J. H., Nanotechnology in corneal neovascularization therapy--a review. *J Ocul Pharmacol Ther* **2013,** *29* (2), 124-34.

231. Prokop, A.; Davidson, J. M., Nanovehicular intracellular delivery systems. *J Pharm Sci* **2008,** *97* (9), 3518-90.

232. Mandal, A.; Bisht, R.; Rupenthal, I. D.; Mitra, A. K., Polymeric micelles for ocular drug delivery: From structural frameworks to recent preclinical studies. *Journal of Controlled Release* **2017,** *248*, 96-116.

233. Jhaveri, A. M.; Torchilin, V. P., Multifunctional polymeric micelles for delivery of drugs and sirna. *Front Pharmacol* **2014,** *5*, 77.

234. Croy, S. R.; Kwon, G. S., Polymeric micelles for drug delivery. *Curr Pharm Des* **2006,** *12* (36), 4669-84.

235. Qiu, L.; Zheng, C.; Jin, Y.; Zhu, K., Polymeric micelles as nanocarriers for drug delivery. *Expert Opinion on Therapeutic Patents* **2007,** *17* (7), 819-830.

236. Suresh, P. K.; Sah, A. K., Nanocarriers for ocular delivery for possible benefits in the treatment of anterior uveitis: Focus on current paradigms and future directions. *Expert Opin Drug Deliv* **2014,** *11* (11), 1747-68.

237. Kataki, M. S.; Kakoti, B. B.; Jameson, M.; Solanki, A.; Hirani, A.; Pathak, Y., Nanoplatforms for delivery of sirna to the eye. *Curr Pharm Des* **2015,** *21* (31), 4587-93.

238. Rowe-Rendleman, C. L.; Durazo, S. A.; Kompella, U. B.; Rittenhouse, K. D.; Di Polo, A.; Weiner, A. L.; Grossniklaus, H. E.; Naash, M. I.; Lewin, A. S.; Horsager, A.; Edelhauser, H. F., Drug and gene delivery to the back of the eye: From bench to bedside. *Invest Ophthalmol Vis Sci* **2014,** *55* (4), 2714-30.

239. Edelhauser, H. F.; Rowe-Rendleman, C. L.; Robinson, M. R.; Dawson, D. G.; Chader, G. J.; Grossniklaus, H. E.; Rittenhouse, K. D.; Wilson, C. G.; Weber, D. A.; Kuppermann, B. D.; Csaky, K. G.; Olsen, T. W.; Kompella, U. B.; Holers, V. M.; Hageman, G. S.; Gilger, B. C.; Campochiaro, P. A.; Whitcup, S. M.; Wong, W. T., Ophthalmic drug delivery systems for the treatment of retinal diseases: Basic research to clinical applications. *Invest Ophthalmol Vis Sci* **2010,** *51* (11), 5403-20.

240. Alvarez-Rivera, F.; Fernandez-Villanueva, D.; Concheiro, A.; Alvarez-Lorenzo, C., Alpha-lipoic acid in soluplus((r)) polymeric nanomicelles for ocular treatment of diabetes-associated corneal diseases. *J Pharm Sci* **2016,** *105* (9), 2855-63.

241. Wang, H.; Chhablani, J.; Freeman, W. R.; Beadle, J. R.; Hostetler, K. Y.; Hartmann, K.; Conner, L.; Aldern, K. A.; Pearson, L.; Cheng, L., Intraocular safety and pharmacokinetics of hexadecyloxypropyl-cidofovir (hdp-cdv) as a long-lasting intravitreal antiviral drug. *Invest Ophthalmol Vis Sci* **2011,** *52* (13), 9391-6.

242. Ohkura, Y.; Akanuma, S.; Tachikawa, M.; Hosoya, K., Blood-to-retina transport of biotin via na+-dependent multivitamin transporter (smvt) at the inner blood-retinal barrier. *Exp Eye Res* **2010,** *91* (3), 387-92.

243. Occhiutto, M. L.; Freitas, F. R.; Maranhao, R. C.; Costa, V. P., Breakdown of the blood-ocular barrier as a strategy for the systemic use of nanosystems. *Pharmaceutics* **2012,** *4* (2), 252-75.

244. McMillan, J.; Batrakova, E.; Gendelman, H. E., Cell delivery of therapeutic nanoparticles. *Prog Mol Biol Transl Sci* **2011,** *104*, 563-601.

245. Ulbrich, W.; Lamprecht, A., Targeted drug-delivery approaches by nanoparticulate carriers in the therapy of inflammatory diseases. *J R Soc Interface* **2010,** *7 Suppl 1*, S55-66.

246. Vadlapatla, R. K.; Vadlapudi, A. D.; Pal, D.; Mitra, A. K., Role of membrane transporters and metabolizing enzymes in ocular drug delivery. *Curr Drug Metab* **2014,** *15* (7), 680-93.

247. Gaudana, R.; Ananthula, H. K.; Parenky, A.; Mitra, A. K., Ocular drug delivery. *AAPS J* **2010,** *12* (3), 348-60.

248. Cholkar, K.; Gilger, B. C.; Mitra, A. K., Topical, aqueous, clear cyclosporine formulation design for anterior and posterior ocular delivery. *Transl Vis Sci Technol* **2015,** *4* (3), 1.

249. Cholkar, K.; Gunda, S.; Earla, R.; Pal, D.; Mitra, A. K., Nanomicellar topical aqueous drop formulation of rapamycin for back-of-the-eye delivery. *AAPS PharmSciTech* **2015,** *16* (3), 610-22.

250. Guo, C.; Zhang, Y.; Yang, Z.; Li, M.; Li, F.; Cui, F.; Liu, T.; Shi, W.; Wu, X., Nanomicelle formulation for topical delivery of cyclosporine a into the cornea: In vitro mechanism and in vivo permeation evaluation. *Scientific Reports* **2015,** *5*, 12968.

251. Järvinen, K.; Järvinen, T.; Urtti, A., Ocular absorption following topical delivery. *Advanced Drug Delivery Reviews* **1995,** *16* (1), 3-19.

252. Ranta, V. P.; Urtti, A., Transscleral drug delivery to the posterior eye: Prospects of pharmacokinetic modeling. *Adv Drug Deliv Rev* **2006,** *58* (11), 1164-81.

253. Shi, S.; Zhang, Z.; Luo, Z.; Yu, J.; Liang, R.; Li, X.; Chen, H., Chitosan grafted methoxy poly(ethylene glycol)-poly(ε-caprolactone) nanosuspension for ocular delivery of hydrophobic diclofenac. *Scientific Reports* **2015,** *5*, 11337.

254. I. Pepiæ, J. L., and J. Filipoviæ-Grèiæ, Polymeric micelles in ocular drug delivery: Rationale, strategies and challenges. *Chem. Biochem. Eng. Q.* **2012,** *26* (4), 365–377.

255. Jiao, J., Polyoxyethylated nonionic surfactants and their applications in topical ocular drug delivery. *Adv Drug Deliv Rev* **2008,** *60* (15), 1663-73.

256. Snoeck, R.; Sakuma, T.; De Clercq, E.; Rosenberg, I.; Holy, A., (s)-1-(3-hydroxy-2-phosphonylmethoxypropyl)cytosine, a potent and selective inhibitor of human cytomegalovirus replication. *Antimicrob Agents Chemother* **1988,** *32* (12), 1839-44.

257. Souza, S., A review of in vitro drug release test methods for nano-sized dosage forms. *Advances in Pharmaceutics* **2014,** *2014*, 12.

258. Sahay, G.; Batrakova, E. V.; Kabanov, A. V., Different internalization pathways of polymeric micelles and unimers and their effects on vesicular transport. *Bioconjug Chem* **2008,** *19* (10), 2023-9.

259. Sahay, G.; Alakhova, D. Y.; Kabanov, A. V., Endocytosis of nanomedicines. *J Control Release* **2010,** *145* (3), 182-95.

260. Tan, S.; Duan, H.; Xun, T.; Ci, W.; Qiu, J.; Yu, F.; Zhao, X.; Wu, L.; Li, L.; Lu, L.; Jiang, S.; Liu, S., Hiv-1 impairs human retinal pigment epithelial barrier function: Possible association with the pathogenesis of hiv-associated retinopathy. *Lab Invest* **2014,** *94* (7), 777-87.

261. Reichl, S., Cell culture models of the human cornea - a comparative evaluation of their usefulness to determine ocular drug absorption in-vitro. *J Pharm Pharmacol* **2008,** *60* (3), 299-307.

262. Walsh, G., Biopharmaceutical benchmarks 2014. *Nat Biotech* **2014,** *32* (10), 992-1000.

263. Udpa, N.; Million, R. P., Monoclonal antibody biosimilars. *Nat Rev Drug Discov* **2016,** *15* (1), 13-14.

264. Syed, B. A.; Evans, J. B.; Bielory, L., Wet amd market. *Nat Rev Drug Discov* **2012,** *11* (11), 827-827.

265. Limited, S. I. P. M., The ophthalmology market **2015**, 1-46.

266. Thomas, D., Venture funding of therapeutic innovation: A comprehensive look at a decade of venture funding of drug r&d. **2015**, 1-51.

267. Walsh, G., Biopharmaceutical benchmarks 2010. *Nat Biotech* **2010,** *28* (9), 917-924.

268. Helzner, J., Fda rulings advance biosimilar drugs. *Ophthalmology Management* **2016,** *20* (July 2016), 34, 44, 45.

269. Mitragotri, S.; Burke, P. A.; Langer, R., Overcoming the challenges in administering biopharmaceuticals: Formulation and delivery strategies. *Nat Rev Drug Discov* **2014,** *13* (9), 655-72.

270. Torchilin, V., Intracellular delivery of protein and peptide therapeutics. *Drug Discov Today Technol* **2008,** *5* (2-3), e95-e103.

271. Truong-Le, V.; Lovalenti, P. M.; Abdul-Fattah, A. M., Stabilization challenges and formulation strategies associated with oral biologic drug delivery systems. *Adv Drug Deliv Rev* **2015,** *93*, 95-108.

272. Forouhi, N. G.; Wareham, N. J., Epidemiology of diabetes. *Medicine (Abingdon)* **2014,** *42* (12), 698-702.

273. Ciulla, T. A.; Amador, A. G.; Zinman, B., Diabetic retinopathy and diabetic macular edema. *Pathophysiology, screening, and novel therapies* **2003,** *26* (9), 2653-2664.

274. Tarr, J. M.; Kaul, K.; Chopra, M.; Kohner, E. M.; Chibber, R., Pathophysiology of diabetic retinopathy. *ISRN Ophthalmol* **2013,** *2013*, 343560.

275. Li, S.; Deng, G.; Liu, J.; Ma, Y.; Lu, H., The effects of a treatment combination of anti-vegf injections, laser coagulation and cryotherapy on patients with type 3 coat's disease. *BMC Ophthalmol* **2017,** *17* (1), 76.

276. Palii, S. S.; Afzal, A.; Shaw, L. C.; Pan, H.; Caballero, S.; Miller, R. C.; Jurczyk, S.; Reubi, J. C.; Tan, Y.; Hochhaus, G.; Edelhauser, H.; Geroski, D.; Shapiro, G.; Grant, M. B., Nonpeptide somatostatin receptor agonists specifically target ocular neovascularization via the somatostatin type 2 receptor. *Invest Ophthalmol Vis Sci* **2008,** *49* (11), 5094-102.

277. Scarpignato, C.; Pelosini, I., Somatostatin analogs for cancer treatment and diagnosis: An overview. *Chemotherapy* **2001,** *47 Suppl 2*, 1-29.

278. Patel, Y. C., Somatostatin and its receptor family. *Front Neuroendocrinol* **1999,** *20* (3), 157-98.

279. Grant, M. B.; Caballero, S.; Millard, W. J., Inhibition of igf-i and b-fgf stimulated growth of human retinal endothelial cells by the somatostatin analogue, octreotide: A potential treatment for ocular neovascularization. *Regul Pept* **1993,** *48* (1-2), 267-78.

280. Varma, R.; Vajaranant, T. S.; Burkemper, B.; Wu, S.; Torres, M.; Hsu, C.; Choudhury, F.; McKean-Cowdin, R., Visual impairment and blindness in adults in the united states: Demographic and geographic variations from 2015 to 2050. *JAMA Ophthalmol* **2016,** *134* (7), 802-9.

281. Zhang, K.; Zhang, L.; Weinreb, R. N., Ophthalmic drug discovery: Novel targets and mechanisms for retinal diseases and glaucoma. *Nat Rev Drug Discov* **2012,** *11* (7), 541-59.

282. Muheem, A.; Shakeel, F.; Jahangir, M. A.; Anwar, M.; Mallick, N.; Jain, G. K.; Warsi, M. H.; Ahmad, F. J., A review on the strategies for oral delivery of proteins and peptides and their clinical perspectives. *Saudi Pharm J* **2016,** *24* (4), 413-28.

283. Renukuntla, J.; Vadlapudi, A. D.; Patel, A.; Boddu, S. H.; Mitra, A. K., Approaches for enhancing oral bioavailability of peptides and proteins. *Int J Pharm* **2013,** *447* (1-2), 75-93.

284. Yi, X.; Wang, Y.; Yu, F. S., Corneal epithelial tight junctions and their response to lipopolysaccharide challenge. *Invest Ophthalmol Vis Sci* **2000,** *41* (13), 4093-100.

285. Mitic, L. L.; Van Itallie, C. M.; Anderson, J. M., Molecular physiology and pathophysiology of tight junctions i. Tight junction structure and function: Lessons from mutant animals and proteins. *Am J Physiol Gastrointest Liver Physiol* **2000,** *279* (2), G250-4.

286. Jovic, M.; Sharma, M.; Rahajeng, J.; Caplan, S., The early endosome: A busy sorting station for proteins at the crossroads. *Histol Histopathol* **2010,** *25* (1), 99-112.

287. Meacham, J. M.; Durvasula, K.; Degertekin, F. L.; Fedorov, A. G., Physical methods for intracellular delivery: Practical aspects from laboratory use to industrial-scale processing. *J Lab Autom* **2014,** *19* (1), 1-18.

288. Bruno, B. J.; Miller, G. D.; Lim, C. S., Basics and recent advances in peptide and protein drug delivery. *Ther Deliv* **2013,** *4* (11), 1443-67.

289. Pisal, D. S.; Kosloski, M. P.; Balu-Iyer, S. V., Delivery of therapeutic proteins. *J Pharm Sci* **2010,** *99* (6), 2557-75.

290. Zelikin, A. N.; Ehrhardt, C.; Healy, A. M., Materials and methods for delivery of biological drugs. *Nat Chem* **2016,** *8* (11), 997-1007.

291. Tao, Y.; Li, X. X.; Jiang, Y. R.; Bai, X. B.; Wu, B. D.; Dong, J. Q., Diffusion of macromolecule through retina after experimental branch retinal vein occlusion and estimate of intraretinal barrier. *Curr Drug Metab* **2007,** *8* (2), 151-6.

292. Jackson, T. L.; Antcliff, R. J.; Hillenkamp, J.; Marshall, J., Human retinal molecular weight exclusion limit and estimate of species variation. *Invest Ophthalmol Vis Sci* **2003,** *44* (5), 2141-6.

293. Huang, A. J.; Tseng, S. C.; Kenyon, K. R., Paracellular permeability of corneal and conjunctival epithelia. *Invest Ophthalmol Vis Sci* **1989,** *30* (4), 684-9.

294. Mandal, A.; Pal, D.; Agrahari, V.; Trinh, H. M.; Joseph, M.; Mitra, A. K., Ocular delivery of proteins and peptides: Challenges and novel formulation approaches. *Adv Drug Deliv Rev* **2018,** *126*, 67-95.

295. Bilati, U.; Allemann, E.; Doelker, E., Strategic approaches for overcoming peptide and protein instability within biodegradable nano- and microparticles. *Eur J Pharm Biopharm* **2005,** *59* (3), 375-88.

296. Meyer, C. H.; Holz, F. G., Preclinical aspects of anti-vegf agents for the treatment of wet amd: Ranibizumab and bevacizumab. *Eye (Lond)* **2011,** *25* (6), 661-72.

297. Joseph, M.; Trinh, H. M.; Cholkar, K.; Pal, D.; Mitra, A. K., Recent perspectives on the delivery of biologics to back of the eye. *Expert Opin Drug Deliv* **2016**, 1-15.

298. Xu, L.; Lu, T.; Tuomi, L.; Jumbe, N.; Lu, J.; Eppler, S.; Kuebler, P.; Damico-Beyer, L. A.; Joshi, A., Pharmacokinetics of ranibizumab in patients with neovascular age-related macular degeneration: A population approach. *Invest Ophthalmol Vis Sci* **2013,** *54* (3), 1616-24.

299. Vaishya, R. D.; Khurana, V.; Patel, S.; Mitra, A. K., Controlled ocular drug delivery with nanomicelles. *Wiley Interdiscip Rev Nanomed Nanobiotechnol* **2014,** *6* (5), 422-37.

300. Daugherty, A. L.; Mrsny, R. J., Formulation and delivery issues for monoclonal antibody therapeutics. *Adv Drug Deliv Rev* **2006,** *58* (5-6), 686-706.

301. Sasahara, K.; McPhie, P.; Minton, A. P., Effect of dextran on protein stability and conformation attributed to macromolecular crowding. *J Mol Biol* **2003,** *326* (4), 1227-37.

302. Kerwin, B. A., Polysorbates 20 and 80 used in the formulation of protein biotherapeutics: Structure and degradation pathways. *J Pharm Sci* **2008,** *97* (8), 2924-35.

303. Kompella, U. B.; Kadam, R. S.; Lee, V. H., Recent advances in ophthalmic drug delivery. *Ther Deliv* **2010,** *1* (3), 435-56.

304. Williams, K. A.; Brereton, H. M.; Farrall, A.; Standfield, S. D.; Taylor, S. D.; Kirk, L. A.; Coster, D. J., Topically applied antibody fragments penetrate into the back of the rabbit eye. *Eye (Lond)* **2005,** *19* (8), 910-3.

305. Jani, R.; Lang, J.; Rodeheaver, D.; Missel, P.; Roehrs, R.; Chowhan, M., Design and evaluation of ophthalmic pharmaceutical products. In *Modern pharmaceutics, fourth edition*, CRC Press: 2002.

306. Ali, Y.; Lehmussaari, K., Industrial perspective in ocular drug delivery. *Adv Drug Deliv Rev* **2006,** *58* (11), 1258-68.

307. Subrizi, A.; Toropainen, E.; Ramsay, E.; Airaksinen, A. J.; Kaarniranta, K.; Urtti, A., Oxidative stress protection by exogenous delivery of rhhsp70 chaperone to the retinal pigment epithelium (rpe), a possible therapeutic strategy against rpe degeneration. *Pharm Res* **2015,** *32* (1), 211-21.

308. Schymkowitz, J.; Rousseau, F., Protein aggregation: A rescue by chaperones. *Nat Chem Biol* **2016,** *12* (2), 58-59.

309. Mitragotri, S.; Burke, P. A.; Langer, R., Overcoming the challenges in administering biopharmaceuticals: Formulation and delivery strategies. *Nat Rev Drug Discov* **2014,** *13* (9), 655-672.

310. Patel, A.; Cholkar, K.; Mitra, A. K., Recent developments in protein and peptide parenteral delivery approaches. *Ther Deliv* **2014,** *5* (3), 337-65.

311. Wen, H.; Jung, H.; Li, X., Drug delivery approaches in addressing clinical pharmacology-related issues: Opportunities and challenges. *AAPS J* **2015,** *17* (6), 1327-40.

312. Moshfeghi, A. A.; Rosenfeld, P. J.; Puliafito, C. A.; Michels, S.; Marcus, E. N.; Lenchus, J. D.; Venkatraman, A. S., Systemic bevacizumab (avastin) therapy for neovascular age-related macular degeneration: Twenty-four-week results of an uncontrolled open-label clinical study. *Ophthalmology* **2006,** *113* (11), 2002 e1-12.

313. Rohrer, B.; Long, Q.; Coughlin, B.; Wilson, R. B.; Huang, Y.; Qiao, F.; Tang, P. H.; Kunchithapautham, K.; Gilkeson, G. S.; Tomlinson, S., A targeted inhibitor of the alternative complement pathway reduces angiogenesis in a mouse model of age-related macular degeneration. *Invest Ophthalmol Vis Sci* **2009,** *50* (7), 3056-64.

314. Thurman, J. M.; Renner, B.; Kunchithapautham, K.; Ferreira, V. P.; Pangburn, M. K.; Ablonczy, Z.; Tomlinson, S.; Holers, V. M.; Rohrer, B., Oxidative stress renders retinal pigment epithelial cells susceptible to complement-mediated injury. *J Biol Chem* **2009,** *284* (25), 16939-47.

315. Savini, G.; Prabhawasat, P.; Kojima, T.; Grueterich, M.; Espana, E.; Goto, E., The challenge of dry eye diagnosis. *Clin Ophthalmol* **2008,** *2* (1), 31-55.

316. Nomoto, H.; Shiraga, F.; Kuno, N.; Kimura, E.; Fujii, S.; Shinomiya, K.; Nugent, A. K.; Hirooka, K.; Baba, T., Pharmacokinetics of bevacizumab after topical, subconjunctival, and intravitreal administration in rabbits. *Invest Ophthalmol Vis Sci* **2009,** *50* (10), 4807-13.

317. Dastjerdi, M. H.; Sadrai, Z.; Saban, D. R.; Zhang, Q.; Dana, R., Corneal penetration of topical and subconjunctival bevacizumab. *Invest Ophthalmol Vis Sci* **2011,** *52* (12), 8718-23.

318. Moisseiev, E.; Waisbourd, M.; Ben-Artsi, E.; Levinger, E.; Barak, A.; Daniels, T.; Csaky, K.; Loewenstein, A.; Barequet, I. S., Pharmacokinetics of bevacizumab after topical and intravitreal administration in human eyes. *Graefes Arch Clin Exp Ophthalmol* **2014,** *252* (2), 331-7.

319. Hernandez, C.; Garcia-Ramirez, M.; Corraliza, L.; Fernandez-Carneado, J.; Farrera-Sinfreu, J.; Ponsati, B.; Gonzalez-Rodriguez, A.; Valverde, A. M.; Simo, R., Topical administration of somatostatin prevents retinal neurodegeneration in experimental diabetes. *Diabetes* **2013,** *62* (7), 2569-78.

320. Eljarrat-Binstock, E.; Orucov, F.; Aldouby, Y.; Frucht-Pery, J.; Domb, A. J., Charged nanoparticles delivery to the eye using hydrogel iontophoresis. *J Control Release* **2008,** *126* (2), 156-61.

321. Peeters, L.; Lentacker, I.; Vandenbroucke, R. E.; Lucas, B.; Demeester, J.; Sanders, N. N.; De Smedt, S. C., Can ultrasound solve the transport barrier of the neural retina? *Pharm Res* **2008,** *25* (11), 2657-65.

322. Kumar, C. M.; Eid, H.; Dodds, C., Sub-tenon's anaesthesia: Complications and their prevention. *Eye (Lond)* **2011,** *25* (6), 694-703.

323. Mather, C. M.; Kirkpatrick, J. N., Sub-tenon's administration of local anaesthetic: A review of the technique. *Br J Anaesth* **2003,** *91* (6), 922;author reply 922-3.

324. Falavarjani, K. G.; Khadamy, J.; Karimi Moghaddam, A.; Karimi, N.; Modarres, M., Posterior sub-tenon's bevacizumab injection in diabetic macular edema; a pilot study. *Saudi J Ophthalmol* **2015,** *29* (4), 270-3.

325. Hashemian, M. N.; Zare, M. A.; Rahimi, F.; Mohammadpour, M., Deep intrastromal bevacizumab injection for management of corneal stromal vascularization after deep anterior lamellar keratoplasty, a novel technique. *Cornea* **2011,** *30* (2), 215-8.

326. Kim, Y. C.; Grossniklaus, H. E.; Edelhauser, H. F.; Prausnitz, M. R., Intrastromal delivery of bevacizumab using microneedles to treat corneal neovascularization. *Invest Ophthalmol Vis Sci* **2014,** *55* (11), 7376-86.

327. Braga-Mele, R.; Chang, D. F.; Henderson, B. A.; Mamalis, N.; Talley-Rostov, A.; Vasavada, A.; Committee, A. C. C., Intracameral antibiotics: Safety, efficacy, and preparation. *J Cataract Refract Surg* **2014,** *40* (12), 2134-42.

328. Daien, V.; Papinaud, L.; Gillies, M. C.; et al., Effectiveness and safety of an intracameral injection of cefuroxime for the prevention of endophthalmitis after cataract surgery with or without perioperative capsular rupture. *JAMA Ophthalmol* **2016,** *134* (7), 810-816.

329. Kuriakose, T.; Kothari, M.; Paul, P.; Jacob, P.; Thomas, R., Intracameral amphotericin b injection in the management of deep keratomycosis. *Cornea* **2002,** *21* (7), 653-6.

330. Hu, J.; Zhang, J.; Li, Y.; Han, X.; Zheng, W.; Yang, J.; Xu, G., A combination of intrastromal and intracameral injections of amphotericin b in the treatment of severe fungal keratitis. *J Ophthalmol* **2016,** *2016*, 3436415.

331. Park, H. Y.; Kim, S. J.; Lee, H. B.; Kim, E. S.; Tchah, H., Effect of intracameral bevacizumab injection on corneal endothelium in rabbits. *Cornea* **2008,** *27* (10), 1151-5.

332. Rusovici, R.; Sakhalkar, M.; Chalam, K. V., Evaluation of cytotoxicity of bevacizumab on vegf-enriched corneal endothelial cells. *Mol Vis* **2011,** *17*, 3339-46.

333. Shin, J. P.; Lee, J. W.; Sohn, B. J.; Kim, H. K.; Kim, S. Y., In vivo corneal endothelial safety of intracameral bevacizumab and effect in neovascular glaucoma combined with ahmed valve implantation. *J Glaucoma* **2009,** *18* (8), 589-94.

334. Lim, T. H.; Bae, S. H.; Cho, Y. J.; Lee, J. H.; Kim, H. K.; Sohn, Y. H., Concentration of vascular endothelial growth factor after intracameral bevacizumab injection in eyes with neovascular glaucoma. *Korean J Ophthalmol* **2009,** *23* (3), 188-92.

335. Wolf, A.; von Jagow, B.; Ulbig, M.; Haritoglou, C., Intracameral injection of bevacizumab for the treatment of neovascular glaucoma. *Ophthalmologica* **2011,** *226* (2), 51-6.

336. Grisanti, S.; Biester, S.; Peters, S.; Tatar, O.; Ziemssen, F.; Bartz-Schmidt, K. U., Intracameral bevacizumab for iris rubeosis. *Am J Ophthalmol* **2006,** *142* (1), 158-60.

337. Han, Q.; Wang, Y.; Li, X.; Peng, R.; Li, A.; Qian, Z.; Yu, L., Effects of bevacizumab loaded peg-pcl-peg hydrogel intracameral application on intraocular pressure after glaucoma filtration surgery. *J Mater Sci Mater Med* **2015,** *26* (8), 225.

338. Fraser, S.; Steel, D., Retinal detachment. *BMJ Clin Evid* **2010,** *2010*.

339. Falavarjani, K. G.; Nguyen, Q. D., Adverse events and complications associated with intravitreal injection of anti-vegf agents: A review of literature. *Eye (Lond)* **2013,** *27* (7), 787-94.

340. Heiduschka, P.; Fietz, H.; Hofmeister, S.; Schultheiss, S.; Mack, A. F.; Peters, S.; Ziemssen, F.; Niggemann, B.; Julien, S.; Bartz-Schmidt, K. U.; Schraermeyer, U.; Tubingen Bevacizumab Study, G., Penetration of bevacizumab through the retina after intravitreal injection in the monkey. *Invest Ophthalmol Vis Sci* **2007,** *48* (6), 2814-23.

341. Seiler, G. S.; Salmon, J. H.; Mantuo, R.; Feingold, S.; Dayton, P. A.; Gilger, B. C., Effect and distribution of contrast medium after injection into the anterior suprachoroidal space in ex vivo eyes. *Invest Ophthalmol Vis Sci* **2011,** *52* (8), 5730-6.

342. Patel, S. R.; Berezovsky, D. E.; McCarey, B. E.; Zarnitsyn, V.; Edelhauser, H. F.; Prausnitz, M. R., Targeted administration into the suprachoroidal space using a microneedle for drug delivery to the posterior segment of the eye. *Invest Ophthalmol Vis Sci* **2012,** *53* (8), 4433-41.

343. Rai Udo, J.; Young, S. A.; Thrimawithana, T. R.; Abdelkader, H.; Alani, A. W.; Pierscionek, B.; Alany, R. G., The suprachoroidal pathway: A new drug delivery route to the back of the eye. *Drug Discov Today* **2015,** *20* (4), 491-5.

344. Tyagi, P.; Kadam, R. S.; Kompella, U. B., Comparison of suprachoroidal drug delivery with subconjunctival and intravitreal routes using noninvasive fluorophotometry. *PLoS One* **2012,** *7* (10), e48188.

345. Olsen, T. W.; Feng, X.; Wabner, K.; Csaky, K.; Pambuccian, S.; Cameron, J. D., Pharmacokinetics of pars plana intravitreal injections versus microcannula suprachoroidal injections of bevacizumab in a porcine model. *Invest Ophthalmol Vis Sci* **2011,** *52* (7), 4749-56.

346. Morales-Canton, V.; Fromow-Guerra, J.; Salinas Longoria, S.; Romero Vera, R.; Widmann, M.; Patel, S.; Yerxa, B., Suprachoroidal microinjection of bevacizumab is well tolerated in human patients. *Invest Ophthalmol Vis Sci* **2013,** *54* (15), 3299-3299.

347. Patel, S. R.; Lin, A. S.; Edelhauser, H. F.; Prausnitz, M. R., Suprachoroidal drug delivery to the back of the eye using hollow microneedles. *Pharm Res* **2011,** *28* (1), 166-76.

348. Nomoto, T.; Fukushima, S.; Kumagai, M.; Machitani, K.; Arnida; Matsumoto, Y.; Oba, M.; Miyata, K.; Osada, K.; Nishiyama, N.; Kataoka, K., Three-layered polyplex micelle as a multifunctional nanocarrier platform for light-induced systemic gene transfer. *Nat Commun* **2014,** *5*, 3545.

349. Abebe, D. G.; Kandil, R.; Kraus, T.; Elsayed, M.; Merkel, O. M.; Fujiwara, T., Three-layered biodegradable micelles prepared by two-step self-assembly of pla-pei-pla and pla-peg-pla triblock copolymers as efficient gene delivery system. *Macromol Biosci* **2015,** *15* (5), 698-711.

350. Nagamune, T., Biomolecular engineering for nanobio/bionanotechnology. *Nano Converg* **2017,** *4* (1), 9.

351. Leader, B.; Baca, Q. J.; Golan, D. E., Protein therapeutics: A summary and pharmacological classification. *Nat Rev Drug Discov* **2008,** *7* (1), 21-39.

352. Latham, P. W., Therapeutic peptides revisited. *Nat Biotechnol* **1999,** *17* (8), 755-7.

353. Lau, J. L.; Dunn, M. K., Therapeutic peptides: Historical perspectives, current development trends, and future directions. *Bioorg Med Chem* **2018,** *26* (10), 2700-2707.

354. Wilson, D.; Valluzzi, R.; Kaplan, D., Conformational transitions in model silk peptides. *Biophys J* **2000,** *78* (5), 2690-701.

355. Krishna, O. D.; Kiick, K. L., Protein- and peptide-modified synthetic polymeric biomaterials. *Biopolymers* **2010,** *94* (1), 32-48.

356. Ghassemi, A. H.; van Steenbergen, M. J.; Barendregt, A.; Talsma, H.; Kok, R. J.; van Nostrum, C. F.; Crommelin, D. J.; Hennink, W. E., Controlled release of octreotide and assessment of peptide acylation from poly(d,l-lactide-co-hydroxymethyl glycolide) compared to plga microspheres. *Pharm Res* **2012,** *29* (1), 110-20.

357. Vaishya, R. D.; Mandal, A.; Gokulgandhi, M.; Patel, S.; Mitra, A. K., Reversible hydrophobic ion-paring complex strategy to minimize acylation of octreotide during long-term delivery from plga microparticles. *Int J Pharm* **2015,** *489* (1-2), 237-45.

358. Vaishya, R. D.; Mandal, A.; Patel, S.; Mitra, A. K., Extended release microparticle-in-gel formulation of octreotide: Effect of polymer type on acylation of peptide during in vitro release. *Int J Pharm* **2015,** *496* (2), 676-88.

359. Yu, C.; He, B.; Xiong, M. H.; Zhang, H.; Yuan, L.; Ma, L.; Dai, W. B.; Wang, J.; Wang, X. L.; Wang, X. Q.; Zhang, Q., The effect of hydrophilic and hydrophobic structure of amphiphilic polymeric micelles on their transport in epithelial mdck cells. *Biomaterials* **2013,** *34* (26), 6284-98.

360. Mu, M.; Konno, T.; Inoue, Y.; Ishihara, K., Solubilization of poorly water-soluble compounds using amphiphilic phospholipid polymers with different molecular architectures. *Colloids Surf B Biointerfaces* **2017,** *158*, 249-256.

361. Iqbal, M.; Zafar, N.; Fessi, H.; Elaissari, A., Double emulsion solvent evaporation techniques used for drug encapsulation. *Int J Pharm* **2015,** *496* (2), 173-90.

362. Geroski, D. H.; Edelhauser, H. F., Drug delivery for posterior segment eye disease. *Invest Ophthalmol Vis Sci* **2000,** *41* (5), 961-964.

363. Hou, H.; Wang, C.; Nan, K.; Freeman, W. R.; Sailor, M. J.; Cheng, L., Controlled release of dexamethasone from an intravitreal delivery system using porous silicon dioxide. *Invest Ophthalmol Vis Sci* **2016,** *57* (2), 557-66.

364. Frohlich, E., The role of surface charge in cellular uptake and cytotoxicity of medical nanoparticles. *Int J Nanomedicine* **2012,** *7*, 5577-91.

VITA

Abhirup Mandal was born on 11th June 1991, in Vadodara, Gujarat, India. He completed his Bachelor of Science in Pharmacy from Manipal College of Pharmaceutical Sciences, Karnataka, India in 2013. After completion of his B. Pharm. degree, he joined the Interdisciplinary Ph.D. program at UMKC in the Fall 2013 to pursue a Ph.D. degree in Pharmaceutical Sciences and Chemistry. He completed his doctoral studies in October 2018 under the supervision of Dr. Ashim K. Mitra where he aimed to develop novel antiviral prodrugs and nanoformulations for ocular delivery of small molecules and peptides. Abhirup has authored/co-authored several peer reviewed publications and book chapters, and has presented his work in a number of international and national conferences. His dedication towards research has led him to achieve one of the most prestigious awards, Graduate Student Research Award in Drug Discovery and Development Interface at the American Association of Pharmaceutical Scientists (AAPS) 2016. During the course of his study at UMKC, he received the Richard and Paula Johnson Pharmacy Graduate Student Award (2015), outstanding leadership awards for serving as an officer in UMKC student chapters (2014-2017), travel grant awards from UMKC, School of Graduate Studies (2014, 2015 & 2017) and Doctoral Non-Residential Award Fellowship (2013-2018).

He is an active member of AAPS, Controlled Release Society (CRS) and Pharmaceutical Sciences Graduate Student Association (PSGSA). He served as the Chair (2018-19), Chair-Elect (2017-18) for AAPS- and Secretary (2014-16) for AAPS- and CRS-UMKC Student Chapters. He also served as the Student representative of Graduate program committee (GPC) (2016-17) and chaired the Social Media & Publications committee for Pharmaceutics Graduate Student Research Meeting (PGSRM), 2016 hosted at UMKC.